Development, Validation and Clinical Evaluation of a Subject-Specific Finite Element Model of the Vertebra with Adjacent Intervertebral Disc to Estimate Vertebral Strength

A thesis submitted to

The University of Sheffield

for the degree of

Doctor of Philosophy

by

Chu-Hee Lee

Academic Unit of Bone Metabolism

Department of Human Metabolism

Faculty of Medicine, Dentistry and Health

December 2014

Blank Page

Acknowledgements

When I started my studies at the Medical school, I hardly imagined that I would actually finish successfully with just my engineering background. There are many people who supported me to make this thesis a reality. I would like to take this opportunity to express my deepest gratitude to them.

I am deeply indebted to my supervisor Dr. Lang Yang who continuously supervised this work with endless patience. He always gave me his valuable time to discuss the project and provide thoughtful suggestions and encouragement. The invaluable discussions and the advice given during our weekly meetings accumulated stitch by stitch into what became this thesis. His organic fruits from his garden were sometimes another joy.

I am immensely grateful to Professor Richard Eastell, from the Mellanby Centre for Bone Research for giving me this opportunity to study as part of the research centre. His continuous commitment and strong expertise in the field of Osteoporosis put spurs to younger researchers and in the lead in the Mellanby Centre for Bone Research.

I would like to sincerely thank Professor Pat Lawford, from the Medical Physics group and INSIGNEO Institute for in silico Medicine. She was a great mentor who provided me with very detailed and helpful corrections to my scientific writing as well as taking care of my daily life in UK.

I would also like to express my gratitude to Dr. Andrew Narracott from the Medical Physics group, for evaluating my thesis and for his help with my ANSYS problems at times. At the same time, I would like to offer my sincere thanks to Dr. Margaret Paggiosi, from the Northern General Hospital Sheffield, who had the patience to support the bone densitometric database necessary for my thesis throughout my PhD.

I would like to thank Professor Michael Adams, Dr. Trish Dolan and Dr. Priyan Landham from the Centre for Comparative and Clinical Anatomy, from the University of Bristol for providing the valuable experimental data. My sincere

thanks go to Dr. Trish Dolan especially, for her valuable comments and guidance towards my papers and abstracts.

I also would like to offer my gratitude to my colleagues of the Medical Physics group for their friendship and daily talks with good sense of humour. Additional thanks go out to my colleagues of the Academic Unit of Bone Metabolism. I would also like to thank all my friends in South Korea and around the world.

This project was made possible through funding obtained from the award: National Institute for Health Research Biomedical Research Fellowship, NIHR-BRF-2011-013.

Lastly, I would like to express my deepest gratitude to my family members, especially my grandmother and parents who have continuously provided me with their unconditional love and unwavering support in all of life's endeavours. Without their help, the successful completion of thesis would have been impossible.

Abstract

Bone mineral density (BMD) measured by Dual-energy X-ray absorptiometry (DXA) is considered as the clinical standard for diagnosis of osteoporosis and fracture risk. Although low bone density is associated with a high fracture risk, BMD alone cannot entirely explain the occurrence of fracture. Recently, patient-specific finite element (FE) models of the vertebral body, based on quantitative computed tomography (QCT), have been used to estimate vertebral strength, and to investigate the effect of treatments.

This thesis presents an investigation of the vertebral strength and fracture risk from clinical research images. The primary aims were: i) to develop a tool using patient-specific FE model of vertebra with adjacent intervertebral disc and ii) to better understand the mechanism of vertebral fracture. This was accomplished through a number of steps. First, a program SpineVox-pro was developed in MATLAB (Mathworks Inc., Natick, MA, USA) to implement a streamlined pre/post-processing workflow for FE model generation using clinical images. Second, a FE model was developed of the Functional Spinal Unit (FSU) based on QCT and Magnetic Resonance Imaging scan sets and validated against experiment. The FSU FE model (r^2= 0.87) showed a better estimate of vertebral strength than BMD by DXA (r^2= 0.54). Finally, a new patient-specific FE model of the Disc-Vertebra-Disc unit (DVD) was proposed for clinical use. The FE strength from the DVD FE model was able to discriminate (OR 11.6, 95% CI 3.0-44.7) between women with and without vertebral fracture independent of the BMD by DXA. Furthermore, the DVD FE model was used to monitor the effect of teriparatide treatment on vertebral strength in postmenopausal women. At the Year 2 follow up, the mean percentage increases were 10% for spine areal BMD and 29% for FE predicted strength. Vertebral strength based on the DVD FE model can be additional tool in clinical trials.

Keywords: Patient-specific, Finite element model, Osteoporosis, Vertebral strength, Fracture risk

Table of Contents

TABLE OF CONTENTS

List of Figures

LIST OF FIGURES

LIST OF FIGURES

List of Tables

LIST OF TABLES

List of Abbreviations

aBMD	Areal bone mineral density
ABQ	Algorithm-Based Qualitative method
AF	Annulus fibrosus
ALL	Anterior longitudinal ligament
ALN	Alendronate
APDL	ANSYS Parametric design language
AUC	Area under the curve
BMD	Bone mineral density
BMU	Basic multicellular unit
CM SR	Coulomb-Mohr stress
CV	Coefficient of variation
D	Displacement
DDD	Disc degeneration scale
DICOM	Digital imaging and communication in medicine
DP	Drucker-Prager
DVD	Disc-vertebra-disc
DXA	Dual X-ray absorptiometry
E	Young's modulus
ECM	Extracellular matrix
EVOS	European Vertebral Osteoporosis Study
FE	Finite element
FEA	Finite element analysis
FSU	Functional spinal unit (vertebra-disc-vertebra)
GUI	Graphical user interface
HA	Hydroxyapatite
HORIZON_PFT	Zoledronic Acid Once Yearly_Pivotal Fracture Trial
HR CT	High-resolution computer tomography
HR MRI	High-resolution magnetic resonance imaging
HR-pQCT	High-resolution peripheral computer tomography
HRT	Hormone replacement therapy
HU	Hounsfield units
ISCD	International Society for Clinical Densitometry
ISL	Interspinous ligaments
IVD	Intervertebral disc
k	Kyphoplasty
L	Load
L1-L5	Lumbar vertebrae from 1 to 5
LF	Ligamentum flavum
MRI	Magnetic resonance imaging
MrOS	Osteoporotic Fractures in Men

LIST OF ABBREVIATIONS

MOS	Mechanics of the solid
MX ER	Maximum principal strain
MX SR	Maximum principal stress
NICE	National Institute of Clinical Excellence
NIH	National Institutes of Health
NMR	
NP	Nucleus pulposus
OR	Odds ratio
PA	Posterior-anterior
PaTH	Parathyroid Hormone and Alendronate for Osteoporosis
PLL	Posterior longitudinal ligament
PMMA	Polymethylmethacrylate
PTH	Parathyroid hormone
PTH 1-34	Teriparatide, FORSTEO
PTH 1-84	Intact parathyroid hormone, PREOTACT
QCT	Quantitative computer tomography
QM	Quantitative morphometry
R	Correlation coefficient
ROI	Region of interest
SD	Standard deviation
SERMs	Selective estrogen receptor modulators
SMS	Spinal motion segment
SpineVox_Pro	Developed full framework for image processing, FE mesh generation, and post-processing in this thesis
SQ	Semi-Quantitative method
SSL	Supraspinous ligament
T1-T12	Thoracic vertebrae from 1 to 12
TE	Echo time
TPTD	Teriparatide
TR	Repetition time
v	Vertebroplasty
VB	Vertebral body
VB PE	Vertebral body with posterior elements
vBMD	volumetric Bone mineral density
VCF	Vertebral compression fracture
VFA	Vertebral fracture assessment
VM SR	Von Mises Stress
VM ER	Von Mises Strain
WHO	World Health Organization

CHAPTER 1 Introduction

1.1 Motivation

Osteoporosis is a condition in which the bones become porous and weak and are more likely to fracture. The National Institute for Health and Clinical Excellence (NICE) reported, in 2009, (National Institute of Clinical Excellence, 2009) that more than 2 million women suffer from osteoporosis; there are more than 180,000 osteoporosis related fractures annually in England and Wales and the annual cost of medical and social care amounts to about £2billion. Vertebral fracture is the most common type of osteoporotic fracture and is associated with increased mortality and morbidity (Cooper et al., 1993). The European Vertebral Osteoporosis Study (EVOS) has shown that the overall age-standardised incidence of fracture was 10.7 per 1000 person-years in women and 5.7 per 1000 person-years in men (O'Neill et al., 1996).

Areal bone mineral density (aBMD) by Dual-energy X-ray absorptiometry (DXA) has been shown to have a good association with vertebral strength and fracture risk (Marshall et al., 1996, Cummings et al., 2002). Areal BMD by DXA is still the only clinical technique used to assess vertebral strength and fracture risk non-invasively. However, the use of aBMD alone has some limitations for explaining bone strength and fracture risk: aBMD accounts for approximately 70% of bone strength (NIH, 2000) and fifty percent of all patients with fractures were not diagnosed as having osteoporosis using aBMD (Schuit et al., 2004). Other factors that may affect bone quality include; bone morphology, and bone material properties as well as bone mass (Bouxsein, 2005, Hernandez and Keaveny, 2006, Reid, 2013).

Recently, finite element analysis (FEA) based on Quantitative Computed Tomography (QCT) has been adopted as an alternative non-invasive technique for assessing vertebral

strength and vertebral fracture risk, since FEA is able to integrate all the information for bone quality as well as bone density. There is some indication that QCT-based FEA has a stronger correlation with vertebral compressive strength than aBMD by DXA or vBMD by QCT alone (Crawford et al., 2003a, Melton et al., 2007). Of the many vertebral FE models described in the literature, only one-QCT-based Voxel FE model has been well used as a research tool in clinical osteoporosis studies (Keaveny et al., 2007, Mawatari et al., 2008, Melton et al., 2007, Lewiecki, 2009, Melton Iii et al., 2010, Chevalier et al., 2010, Graeff et al., 2009). In all of these papers, the FE models consider only the vertebral body without posterior elements or intervertebral discs (IVDs).

Load transfer on the vertebral column can act in two ways: the majority is done by the IVD to the vertebral body, and the remainder by the facet joints. IVD degeneration, therefore, affects the loading conditions and fracture patterns of the adjacent vertebrae (Pollintine et al., 2004a, Pollintine et al., 2004b, Adams and Dolan, 2005, Adams et al., 2006), thus an FE model that incorporates the intervertebral disc could enhance the validity of the model as a predictor of fracture. Furthermore, the posterior elements also share the load on the vertebra even though they are small in proportion to the vertebral body. The posterior elements, therefore, should also be considered when predicting realistic vertebral biomechanical characteristics *in vivo* (Imai et al., 2006). Some researchers used FE models of the functional spinal unit (FSU) that consists of two adjacent vertebrae and their IVDs, whereas others used multi-levels spinal FE models (Polikeit et al., 2004, Natarajan et al., 2003, Rohlmann et al., 2006, Schmidt et al., 2006, Noailly et al., 2005). However, none of the models were applied to the clinical studies for predicting vertebral strength as a patient-specific approach. The FSU is regarded as the smallest structural unit that has all structural components of the spine (vertebrae, IVD and ligaments) and therefore can exhibit the biomechanical behaviour which interplays between the IVD and its adjacent vertebrae. The multi-levels FE models are most physiological and complicated that consist of more than two vertebrae, multiple-IVDs, and ligaments. Another practical consideration for choosing FSU was the availability of the specimen and mechanical testing data from the University of Bristol.

There are many commercial and open-source programs for image processing of medical images (for example, Mimics, Simpleware, ImageJ, AMIRA and VTK/ITK platform) and for finite element mesh generation (for example, Hypermesh, Meshgrid, TetraGen and

CUBIT). However, these have limitations. Each of these software applications has its own data format, and the additional steps required for data format conversion may lead to loss of data quality, and importing/exporting large datasets is time-consuming. Furthermore, it is very difficult to ensure the high degree of consistency in FE model orientation, mesh density and quality, and boundary condition that is required for clinical studies involving the processing of many patient scans for the investigation of group differences or changes from baseline.

Therefore, in order to deal with the large datasets which are associated with clinical research scans, there is a clear demand for a simplified tool through a consistent full framework for generating FE model of vertebra with IVD as well as a need for further improvement of previous methods. The main work of this thesis was conducted with the overall scope of providing the best possible a framework for generating finite element model to predict vertebral strength from large clinical research data sets.

1.2 Aims and Objectives

The main aim of this thesis was to develop a diagnostic tool using finite element modelling to predict vertebral strength and fracture risk from clinical research images for large clinical studies and to better understand the mechanism of vertebral fracture. This was achieved through the following objectives:

* To develop a streamlined workflow that performs pre/post processing for the generation of a range of FE models: functional spinal unit (FSU), vertebral body with posterior elements (VB PE), vertebral body (VB), and disc-vertebra-disc unit (DVD) from medical images

* To develop a finite element model of the functional spinal unit (FSU) based on QCT and MRI scan data sets and to validate the FSU FE model using experimental data (from an *in vitro* cadaveric study)

* To compare vertebral strength predicted by the FSU model with that predicted by single vertebra and vertebral body FE models

* To apply a new patient-specific FE model of disc-vertebra-disc unit (DVD) to clinical research scans to discriminate vertebral fracture in postmenopausal women

* To apply the patient-specific DVD FE model to clinical research scans and evaluate its ability in terms of monitoring the effect of pharmacological treatment.

1.3 Outline of the thesis

The main body of this thesis is divided into seven chapters: Chapters 2 to 8.

Chapter 2 reviews a wide range of literature highlighting the basic concepts of osteoporosis and bone biomechanics whilst also covering the anatomical structure and biomechanics of lumbar spine and vertebral fractures. The state-of-the-art finite element models of lumbar spine for the vertebral strength and fracture risk assessment are reviewed together with these basic concepts in detail. Finally, the text summarises the characteristics of the current FE models and their limitations for application in clinical studies and suggests a patient-specific finite element model of vertebra for osteoporosis studies.

Chapter 3 describes the development of a full framework, SpineVox_Pro for image processing, FE mesh model generation, and post-processing, using medical research images such as QCT and MRI datasets. The SpineVox_Pro application is then used throughout the studies described in this thesis.

Chapter 4 presents the development of a new finite element model of the functional spinal unit (FSU) for predicting vertebral strength using QCT and MRI scans from sixteen cadaveric FSUs and shows the validation procedure of the FSU FE model with the experiment (the experimental work was done by Dr. Landham, University of Bristol).

Chapter 5 describes a comparative study of FE-derived vertebral strengths under pure compression and forward bending from the different FE models developed in this thesis: the vertebral body FE model, the single vertebra FE model and the FSU FE model.

Chapters 6 and 7 show the application of the full framework developed (SpineVox_Pro) to clinical research data sets. Chapter 6 proposes a new FE model of disc-vertebra-disc unit (DVD) and the study shows the application of the DVD FE model for the

discrimination power of the vertebral fracture in postmenopausal women. Chapter 7 investigates the effects of the drug teriparatide on vertebral strength in postmenopausal women using the developed DVD FE model.

Chapter 8 summarises the strengths and limitations based on each chapter and addresses the subject of future work for improvement of the models and further applications.

CHAPTER 2 Background

This literature review is preparatory to the actual work to suggest a patient-specific finite element model of vertebra and a methodology to generate the FE model for vertebral strength and fracture risk assessment clinically. Therefore, the contents of this chapter mainly have an object in view which reviews current cutting-edge finite element models of vertebra for clinical research, especially those related to osteoporosis studies. It is reached through covering the concept of osteoporosis, the basic anatomy and biomechanics of lumbar spine, and vertebral fracture assessment.

2.1 Osteoporosis

Osteoporosis was defined, in 1993, as *"a systemic skeletal disease characterized by low bone mass and micro-architectural deterioration of bone tissue, with a consequent increase in bone fragility and susceptibility to fractures"* by the World Health Organization (WHO)(ConsensusDevelopmentConference, 1993). The WHO suggested that the diagnosis of osteoporosis should be defined by a bone density of 2.5 standard deviations below the mean value for young white adult women in the lumbar spine, femoral neck or forearm i.e., T-score ≤ -2.5. The WHO T-score definition of osteoporosis is shown in Table 2.1 (Kanis and Glüer, 2000). T-scores are calculated by taking the difference between the patient's measured BMD and the young and healthy adult mean BMD divided by young adult population standard deviation (SD) as shown:

$$T-score = \frac{Subject's\ measured\ BMD - young\ adult\ normal\ Mean\ BMD}{Young\ adult\ normal\ BMD\ SD}$$

Table 2.1: WHO definition of osteoporosis and osteopenia, data taken from (WHO, 1994, Kanis and Glüer, 2000)

Terminology	T-score definition
Normal	$T \geq -1.0$
Osteopenia	$-2.5 < T < -1.0$
Osteoporosis	$T \leq -2.5$
Established osteoporosis	$T \leq -2.5$ in the presence of one or more fragility fractures

DXA is currently the most common method used to measure areal BMD. As radiation dose associated with DXA is extremely small: pencil beam DXA is from 0.1 (Lunar DPX) to 1.0 µSv and fan beam DXA is from 1.0 (Lunar Prodigy) to 10 µSv (Hologic Discovery), measurement can be repeated with minimum dose to the patients (Lewis et al., 1994, Njeh et al., 1999, Blake et al., 2006). DXA measures the extent of attenuation of the X-ray beam when two different X-ray photons, high energy and low energy beams, pass through the body. An alternative method, QCT has come into the spotlight in recent years because the geometric and structural information of bone is considered to be an important factor for the determination of bone strength. Three dimensional QCT imaging can produce volumetric BMD (g/cm³) instead of areal BMD (g/cm²) by DXA. Moreover, QCT can analyse the cortical bone and the trabecular bone separately.

A lot of literature has shown that BMD is correlated with vertebral strength and fracture risk, and thus, areal bone mineral density (BMD) by DXA is frequently used as a proxy measure of bone strength (Marshall et al., 1996, Cummings et al., 2002). However, aBMD has limitations in terms of explaining bone strength and fracture risk: aBMD alone accounts for approximately 70% of bone strength (NIH, 2000) and half of patients who have fractures were not diagnosed as having osteoporosis (Schuit et al., 2004). Due to this limitation, the National Institutes of Health Consensus Development Conference in March 2000 redefined osteoporosis more comprehensively as *"a skeletal disorder characterized by compromised bone strength predisposing to an increased risk of fracture"*. The NIH emphasised the importance of bone strength and stated that *"bone strength reflects the integration of two main features: bone density and bone quality"*. In this manner, several papers suggested that other factors associated with bone quality

such as macro- and micro-scopic architecture, and matrix and mineral composition should be considered in order to investigate bone strength and bone fracture risk as well as bone quantity (mass) for bone strength as shown in Figure 2.1 (Bouxsein, 2005, Hernandez and Keaveny, 2006, Reid, 2013).

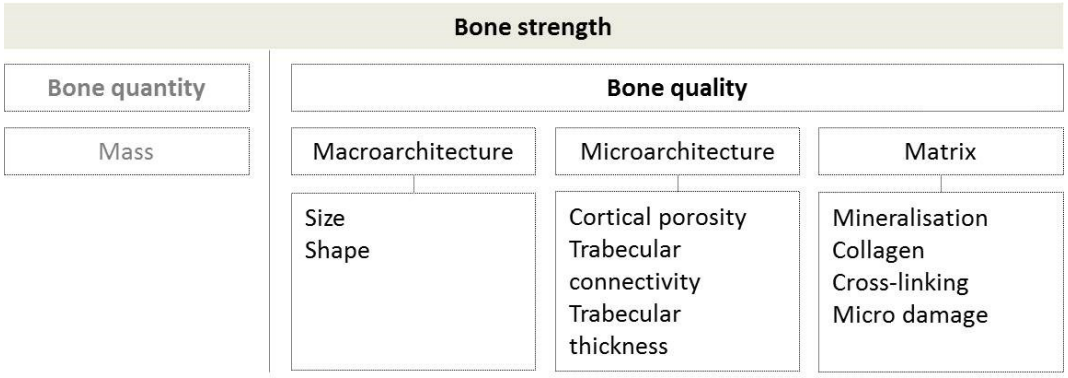

Figure 2.1: Determinants of bone strength

The general recommendation for postmenopausal osteoporosis patients is an intake of 1000 mg of calcium, 800 IU of vitamin D, and 1g/kg body weight of protein per day. General management is insufficient for reducing fracture risk, therefore, some type of pharmacological intervention is required (Tang et al., 2007). Currently available pharmacological treatments in Europe, as shown in Table 2.2, are categorised into two groups: antiresorptive agents that reduce bone resorption (bisphosphonates and selective estrogen receptor modulators: SERMs) and anabolic agents which increase bone formation (parathyroid hormone). These drugs have been shown to be efficacious in reducing the risk of vertebral fracture, non-vertebral fracture, and hip fracture (Kanis et al., 2008). In MORE study, raloxifene reduces the risk of vertebral fractures by 30 – 40% in postmenopausal women with osteoporosis (Ettinger et al., 1999). In the category of bisphosphonates, alendronate and risedronate have shown to reduce the incidence of vertebral and non-vertebral fractures by 40 – 50% and 30 – 36%, respectively (Black et al., 1996, Stevenson et al., 2005, Cranney et al., 2002, Harris et al., 1999, Reginster et al., 2000). On the other hand, Ibandronate was shown to reduce only vertebral fractures by

50 -60% (Delmas et al., 2004, Chesnut et al., 2004). HORIZON trial of Zoledronic acid that reduced vertebral fracture by 70 % and hip fracture by 40 % (Black et al., 2007).

The majority of treatments for osteoporosis work by inhibiting bone resorption (anti-resorptive treatments). However, recently treatments which stimulate bone formation (anabolic treatments) have been developed such as parathyroid hormone (PTH 1-34: Teriparatide, FORSTEO; PTH 1-84: intact PTH, PREOTACT). These treatments have been shown to be associated with a decrease in fracture risk (Neer et al., 2001, Greenspan et al., 2007).

Table 2.2: Treatments for Osteoporosis (table based on Kanis et al. (2008))

Type		Treatment	
Antiresorptive medications	Bisphosphonates	Alendronate (Fosamax)	Tablets
		Risedronate (Actonel)	Tablets
		Ibandronate (Bonviva)	Tablets
		Zoledronic acid (Aclasta)	Infusions &Injections
	Selective estrogen receptor modulators (SERMs)	Raloxifene (Evista)	Tablets
	Less commonly used drug treatments	Hormone therapy or hormone replacement therapy (HRT) for women Hormone theraphy for men Calcitriol (Rocaltrol) tablet	
Anabolic drugs	Parathyroid hormone	Teriparatide (Forsteo)	Injection
		Parathyroid hormone treatment (Preotact)	Injection

Teriparatide (PTH 1-34) is the only licensed anabolic therapy for treatment of osteoporosis in postmenopausal women in the UK. Several studies using bone-turnover markers showed that PTH increase bone formation which is greater than in bone resorption (Black et al., 2003, Chen et al., 2005, Eastell et al., 2006, Bauer et al., 2006). PTH treatment is also associated with increases in spine BMD. In women with postmenopausal osteoporosis treated with teriparatide a mean increase in spine BMD of

6% at 6 months and 13% at 24 months was observed (Obermayer-Pietsch et al., 2008). These treatment effects have been investigated using bone densitometric parameters: BMD by DXA, vBMD by QCT. However, the increases in BMD by DXA reported are not sufficient to explain the reduction in fracture risk in response to the therapy. The increase in BMD measured by DXA for the lumbar spine following TPTD treatment explains 30-41% of the vertebral fracture risk reduction whilst the remaining portion is associated with non-BMD parameters (Chen et al., 2006). Imaging parameters such as trabecular thickness, trabecular number obtained by high-resolution CT (HRCT) are also used for monitoring the treatment effect on bone. One PTH study using HRCT reported an increase in cancellous bone volumetric BMD of 13% at 6 months and showed that high resolution CT of the spine allowed the measurement of parameters of bone microstructure that increased by 16% at 6 months (Graeff et al., 2007).

Some studies here used femoral strength based on QCT femoral FE model to investigate therapeutic effects on femoral strength (Keaveny et al., 2008, Keaveny et al., 2011) and recently, some used vertebral strength derived from a QCT-based vertebral body FE model to investigate therapeutic effects on vertebral strength (Keaveny et al., 2007, Lewiecki, 2009, Imai et al., 2009, Graeff et al., 2009, Chevalier et al., 2010). These studies showed that FE-estimated strength provides a more sensitive indicator of effect of treatment on bone than densitometric variables.

2.2 Bone-mechanics

Bone has a highly hierarchical structure and consequently, the mechanical properties of bone vary with the different hierarchical structural levels, and the relationships between them. Therefore, different levels of hierarchical structure as illustrated in Figure 2.2 should be considered when investigating the properties of bone.

Some characteristics can be described from a structural viewpoint and some from the basic material properties. The structure of bone is categorised in terms of different scales: as an entire organ (femur, vertebra, tibia, etc), at the macroscale as cortical or trabecular bone, at the level of the Haversian system or single trabecula (micro: 10~500μm), lamella (submicro: 1~10 μm), fibrillar collagen, embedded mineral (nano: a

few hundred x10^{-3} µm ~1 µm), or the molecular structure of mineral, collagen, and organic proteins (subnano: < a few hundred x10^{-3} µm) (Rho et al., 1998).

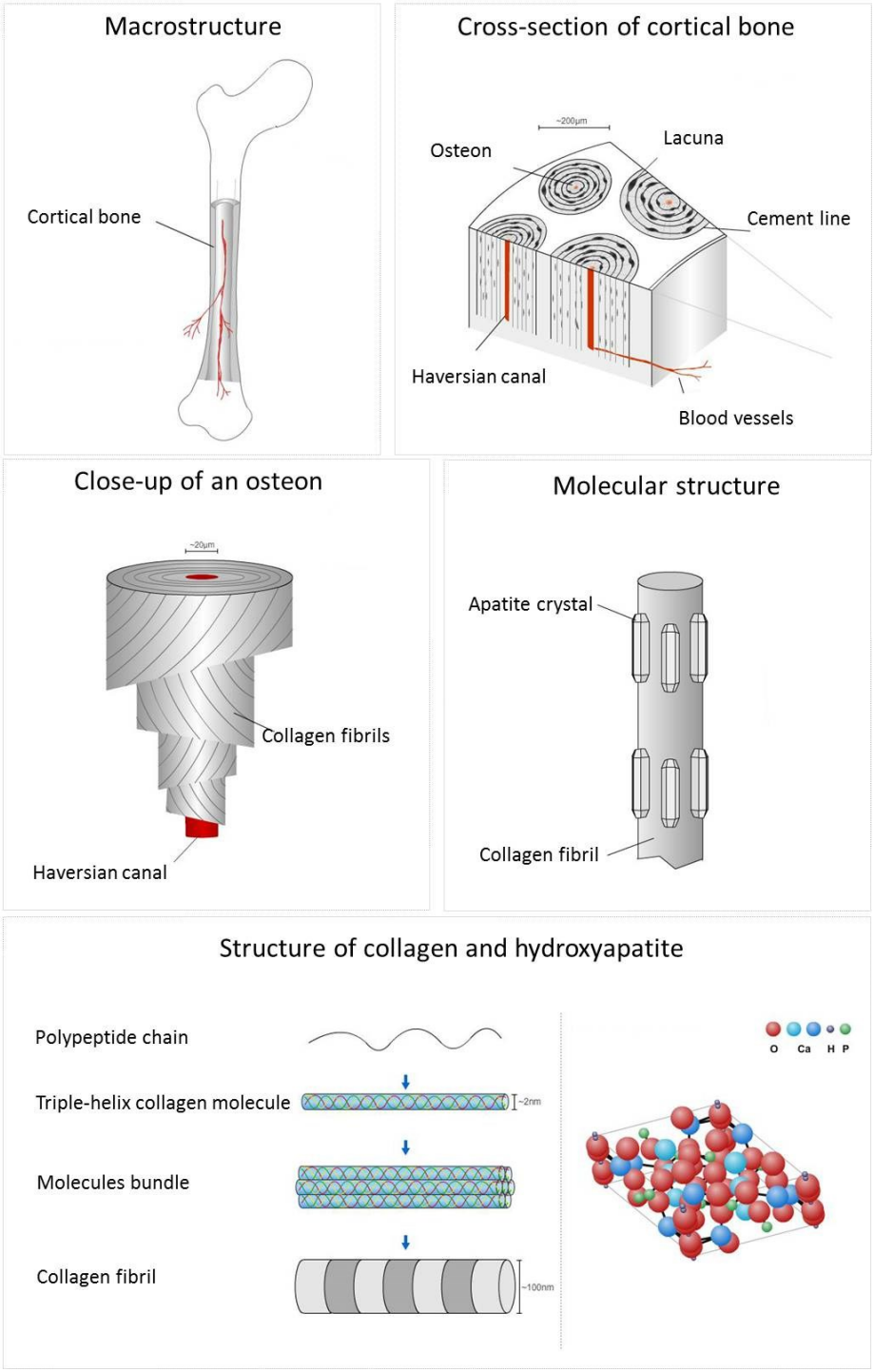

Figure 2.2: The hierarchical structural levels of cortical bone (image adapted from http://www.doitpoms.ac.uk with permission)

At the molecular level, bone can be treated as a composite material with an extracellular matrix (ECM) composed mainly of mineral, calcium phosphate (60-70%) which is approximated as hydroxyapatite ($HA: Ca_{10}(PO_4)_6(OH)_2$), collagen fibrils (5-15%), water (25-30%), and a small amount of other substances: noncollagenous proteins and inorganic salts. Collagen, with its triple helical structure, is the main fibrous protein in the body and the collagen fibres act as nucleation sites for bone mineral crystals. A higher proportion of mineral leads to an increase in bone stiffness because the mineral phase is much stiffer than the collagen phase (Renders et al., 2008).

At the macro level, bone can be categorised as one of two types, cortical or trabecular, according to porosity and location: cortical (volume fraction ≥ 0.7) and trabecular bone (0.05 ≤ volume fraction ≤ 0.3). The composition is similar whilst the structure of the two types is different. Cortical bone accounts for about 80% of the body's bone mass, forming the dense outer shell of bones and consists of osteons or Haversian systems. Each osteon comprises a Haversian canal surrounded by concentric lamellae. Between the lamellae, the bone cells or osteocytes sit within cell-sized spaces, the *lacunae*. Haversian canals contain blood vessels; these are interconnected with the other vessels on the surface of the bone. In contrast to cortical bone, trabecular bone accounts for 20 % of the total mass of skeleton and is made up of a network interconnected plate-like and rod-like elements or *trabeculae*. Spaces between the trabeculae contain bone marrow. This porous structure means that trabecular bone is lighter and less dense than cortical bone. Trabecular bone is important because osteoporotic fractures generally occur in bones, such as the vertebrae, which have a high proportion of trabecular bone. The mechanical properties of trabecular bone depend on several factors: the mineral density, volume fraction, and tissue architecture and composition. The association of these factors results in heterogeneity and anisotropy: the elastic modulus and strength of trabecular bone is primarily determined by the volume and the variations in volume fraction lead to heterogeneity (Keaveny et al., 2001, Keaveny and Buckley, 2006), whilst the different architectures within trabecular bone lead to its anisotropic characteristics (Mosekilde et al., 1987).

Bone has another unique characteristic: bone is modelled (bone formation) as the skeleton grows and continuously remodelled (bone remodelling) through a cycle of bone resorption and formation throughout the entire life of an individual. Three types of bone

cells, forming the 'basic multicellular unit (BMU)', co-operate with each other to bring about remodelling. These are; osteoblasts (bone forming cells), osteocytes (mature bone cells associated with homeostasis- maintaining oxygen and mineral levels), and osteoclasts (bone resorbing cells). In healthy bone, the balance between the work of osteoblasts and osteoclasts maintains bone tissue whereas, in osteoporotic bone, there is an imbalance of formation and resorption due to a decrease in the activity of osteoblasts. Furthermore, bone is a dynamic tissue that adapts the mass and tissue structure to the physiological loading. Bone will remodel to become stronger through trabecular architecture adaptation and following cortical bone thickening. The idea for bone adaptation from the loading was introduced by Wolff. He assumed the architecture of bone is directly related to the directions of principal stress which is known as Wolff's Law (Wolff et al., 1986). This was refined to introduce the concept of 'mechanostat' that bone adaption occurs through a mechanism known as 'mechanotransduction': the mechanical loading causes local bone deformation and the deformation stimulates bone cells. Mechanostat theory is based on the magnitude of the strain. Frost claims that there is a lower and an upper effective strain threshold to control bone remodelling process: strain between 800 and 1500 μStrain (adapted state) was reported as a balanced status which bone resorption and bone formation is in balanced; strain above the 1500 μStrain (over load) on the bone cause bone modelling to increase cortical bone mass and strength, whereas strain below 800 μStrain (disuse) cause bone remodelling because the stimuli is not sufficient to maintain bone formation and resorption is dominant resulting in reduce bone mass and strength. (Frost, 1987). This thresholds maybe relative to habitual load of individuals (Skerry, 2008).

Many different techniques can be used to assess the various factors associated with bone quality across the different scales from macro scales to nanoscales as shown in Figure 2.3.

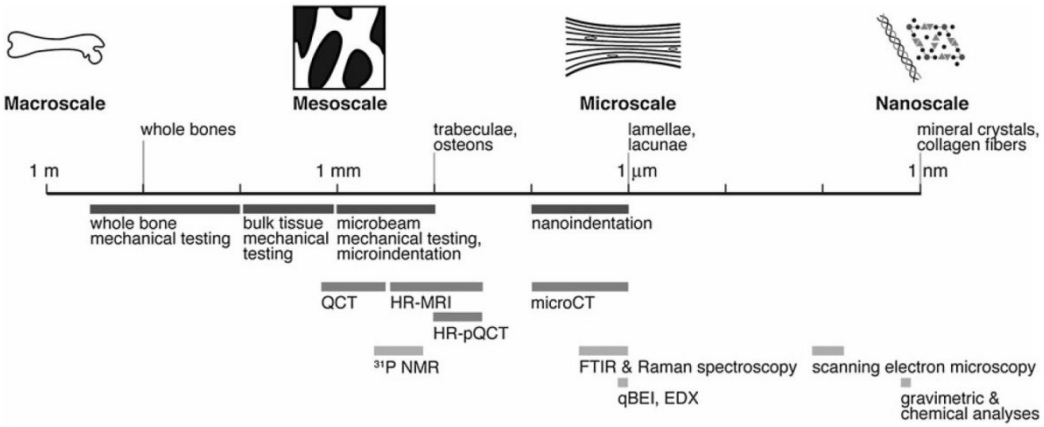

Figure 2.3: Different techniques associated with the hierarchical structural level to assess bone quality (figure with permission from (Donnelly, 2011))

Conventional densitometry such as DXA is used to measure bone mass. Bone mechanical properties are obtained from physical tests such as whole bone mechanical testing, bulk tissue specimen testing, and nano-indentation whilst bone geometry and micro-architecture are obtained from imaging techniques such as QCT, HR-pQCT, HR MRI, and micro CT. In addition, bone tissue properties, such as chemical composition, are studied by NMR imaging, vibrational spectroscopic imaging, and scanning electron microscopy (Donnelly, 2011).

Mechanical properties of bone

Despite its organic nature, bone can be treated as an engineering material. As mentioned earlier, the mechanical properties of bone can be described in terms of both structural and material properties (Table 2.3).

For trabecular bone, its structural properties are usually determined by plotting load-displacement curves as its extrinsic properties are influenced by the structure of both trabeculae and pores. This is an essential factor in carrying out a global stress analysis at the macro level. On the other hand, its material properties are defined from the stress-strain curve as the intrinsic factors are an invariant value of the material of the trabecular struts. Intrinsic factors are important properties for stress analysis at the

micro level. A typical load-displacement curve and stress-strain curve from a uniaxial tensile test is shown in Figure 2.4.

Table 2.3: Extrinsic and intrinsic factors from tensile tests

	Extrinsic from L-D curve		Intrinsic from stress-strain curve	
Strength	$\mathrm{F_u}$ Ult. Force	N	σ_u Ultimate Stress	$\mathrm{N/mm^2}$ (MPa)
Brittleness	$\mathrm{S_u}$ Ult. Displacement	mm	ε_u Ultimate Strain	-
Stiffness	K Stiffness	$\mathrm{N/mm}$	E Young's Modulus	$\mathrm{N/mm^2}$ (MPa)
Energy Absorption	U Work to Failure	$\mathrm{N-mm}$	U Toughness Modulus	$\mathrm{N/mm^2}$

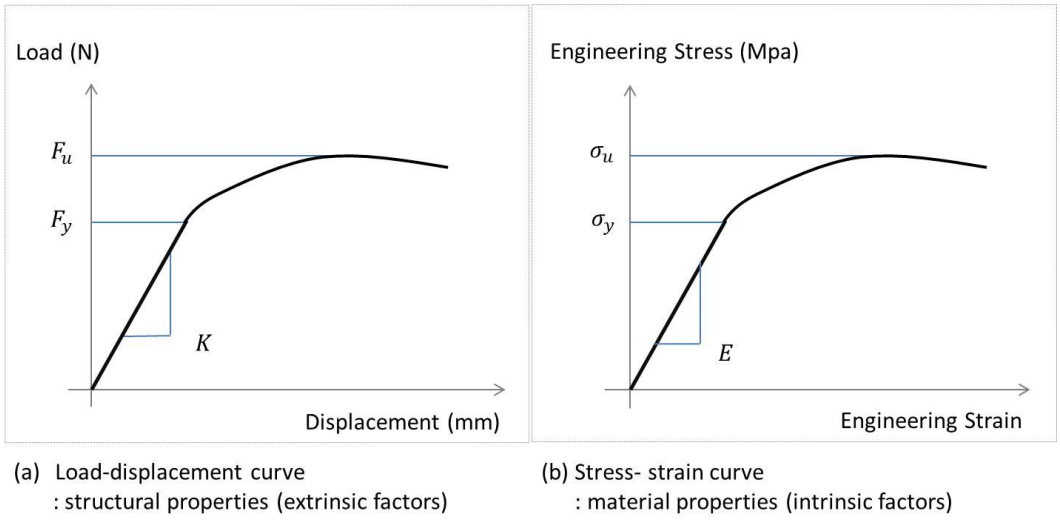

Figure 2.4: Typical load-displacement, and stress-strain curves for bone: (a) load-displacement curve, (b) Engineering stress-strain curve

Bone has a higher strength in compression than in tension. This explains why bone strength varies between anatomical sites because within the body each bone is exposed to a different stress field. In addition, bone strength varies with the loading direction. In tensile tests of cortical bone, the strength in longitudinal loading is much greater than that in the horizontal loading. For this reason, bone is described as an anisotropic

material the strength of which is dependent on loading direction. Bone is normally classified as a brittle material which shows only 0.5-3% of maximum total strain. Bone strength also changes with age: decreasing with increasing age.

Bone exhibits normal Hookean elastic behaviour to a certain extent, i.e. it has a linear stress-strain relationship. Hooke's Law for a linear elastic solid material is used to describe the mechanical properties of bone in the elastic region. Hooke's Law is generally represented in tensor form as follows:

$$[\sigma] = [S][\varepsilon] \tag{2.1}$$

$$\sigma_{ij} = S_{ijkl}\varepsilon_{ij} \tag{2.2}$$

Where, $[\sigma]$ is the stress tensor, $[\varepsilon]$ is the strain tensor, and $[S]$ is the stiffness tensor. In addition, $[C]$, the compliance tensor, can be introduced as follows:

$$[\varepsilon] = [S]^{-1}[\sigma] = [C][\sigma] \tag{2.3}$$

$$\varepsilon_{ij} = C_{ijkl}\sigma_{ij} \tag{2.4}$$

Stress and strain tensors are 2nd order tensors whilst the stiffness and compliance tensors are 4th order tensors.

The general Hooke's Law can be shown as a matrix form:

$$\begin{Bmatrix} \varepsilon_{11} \\ \varepsilon_{22} \\ \varepsilon_{33} \\ \gamma_{23} \\ \gamma_{13} \\ \gamma_{12} \end{Bmatrix} = \begin{bmatrix} C_{11} & C_{12} & C_{13} & C_{14} & C_{15} & C_{16} \\ C_{21} & C_{22} & C_{23} & C_{24} & C_{25} & C_{26} \\ C_{31} & C_{32} & C_{33} & C_{34} & C_{35} & C_{36} \\ C_{41} & C_{42} & C_{43} & C_{44} & C_{45} & C_{46} \\ C_{51} & C_{52} & C_{53} & C_{54} & C_{55} & C_{56} \\ C_{61} & C_{62} & C_{63} & C_{64} & C_{65} & C_{66} \end{bmatrix} \begin{Bmatrix} \sigma_{11} \\ \sigma_{22} \\ \sigma_{33} \\ \tau_{23} \\ \tau_{13} \\ \tau_{12} \end{Bmatrix} \tag{2.5}$$

Where, the indices refer to the anisotropic material symmetries about a point. The compliance tensors are defined by 21 independent constants. However, trabecular bone is usually treated as an orthotropic material that has 3 orthogonal planes of symmetry, where material properties are independent of direction within each plane. This leads to $C_{14} = C_{15} = C_{16} = C_{24} = C_{25} = C_{26} = C_{34} = C_{35} = C_{36} = C_{45} = C_{46} = C_{56} = 0$ and 9 independent elastic constants in the constitutive matrix:

$$C = \begin{bmatrix} C_{11} & C_{12} & C_{13} & 0 & 0 & 0 \\ C_{21} & C_{22} & C_{23} & 0 & 0 & 0 \\ C_{31} & C_{32} & C_{33} & 0 & 0 & 0 \\ 0 & 0 & 0 & C_{44} & 0 & 0 \\ 0 & 0 & 0 & 0 & C_{55} & 0 \\ 0 & 0 & 0 & 0 & 0 & C_{66} \end{bmatrix}$$

$$= \begin{bmatrix} \frac{1}{E_x} & -\frac{\nu_{yx}}{E_y} & -\frac{\nu_{zx}}{E_z} & 0 & 0 & 0 \\ -\frac{\nu_{xy}}{E_x} & \frac{1}{E_y} & -\frac{\nu_{zy}}{E_z} & 0 & 0 & 0 \\ -\frac{\nu_{xz}}{E_x} & -\frac{\nu_{yz}}{E_y} & \frac{1}{E_z} & 0 & 0 & 0 \\ 0 & 0 & 0 & \frac{1}{G_{yz}} & 0 & 0 \\ 0 & 0 & 0 & 0 & \frac{1}{G_{zx}} & 0 \\ 0 & 0 & 0 & 0 & 0 & \frac{1}{G_{xy}} \end{bmatrix} \quad (2.6)$$

Where, E_i is the Young's modulus along the axis i, G_{ij} is the shear modulus in direction j on the plane whose normal in direction i, ν_{ij} is the Poisson's ration that corresponds to a contraction in direction j when an extension is applied in direction i.

More simply, trabecular bone can be treated as a transverse isotropic material which has the same properties in one plane and different properties in the direction normal to this plane, that is, symmetrical with respect to a rotation about an axis of symmetry. Therefore, only 5 constants are independent:

$$C = \begin{bmatrix} \frac{1}{E_p} & -\frac{\nu_p}{E_p} & -\frac{\nu_{zp}}{E_z} & 0 & 0 & 0 \\ -\frac{\nu_p}{E_p} & \frac{1}{E_p} & -\frac{\nu_{zp}}{E_z} & 0 & 0 & 0 \\ -\frac{\nu_{pz}}{E_p} & -\frac{\nu_{pz}}{E_p} & \frac{1}{E_z} & 0 & 0 & 0 \\ 0 & 0 & 0 & \frac{1}{2G_{zp}} & 0 & 0 \\ 0 & 0 & 0 & 0 & \frac{1}{2G_{zp}} & 0 \\ 0 & 0 & 0 & 0 & 0 & \frac{1+\nu_p}{E_p} \end{bmatrix} \quad (2.7)$$

Where, $\frac{\nu_{pz}}{E_p} = \frac{\nu_{zp}}{E_z}$. The 5 elastic constants are the Young's modulus and poisson ratio in the x-y symmetry plane, E_p and ν_p, the Young's modulus and poisson ratio in the z-direction, E_{pz} and ν_{pz}, and the shear modulus in the z-direction G_{zp}. (Odgaard et al., 1997, Yang et al., 1998, Zysset et al., 1998). This latter case is considered to be valid since the elastic modulus and strength in the longitudinal direction are higher than those in the transverse direction in the trabecular bone of vertebra (Mosekilde et al., 1987).

2.3 Anatomical structure and biomechanics of the lumbar spine

The human spinal column is the most complex part of the musculoskeletal system. It consists of 33 vertebrae; cervical-7 (neck), thoracic-12 (chest), lumbar-5 (lower back), sacral, and coccygeal regions. The sacral and coccygeal regions are combined with the pelvis and can be considered as parts of the pelvic girdle. There are intervertebral discs between each two adjacent vertebrae and each vertebra is made up of a vertebral body and posterior elements. The spinal column has several functions; to protect the spinal cord, to support upper extremities including the head and neck, to transfer loads from the head and trunk to the pelvis, and, to allow a variety of movements such as flexion-extension, lateral flexion, and rotation. The intervertebral discs in the spinal column have a particularly important role as shock absorbers to sustain loads transmitted from the segments above, to eliminate bone-to-bone contact, and to reduce the effects of impact forces by preventing direct contact between the bony structures of the vertebrae.

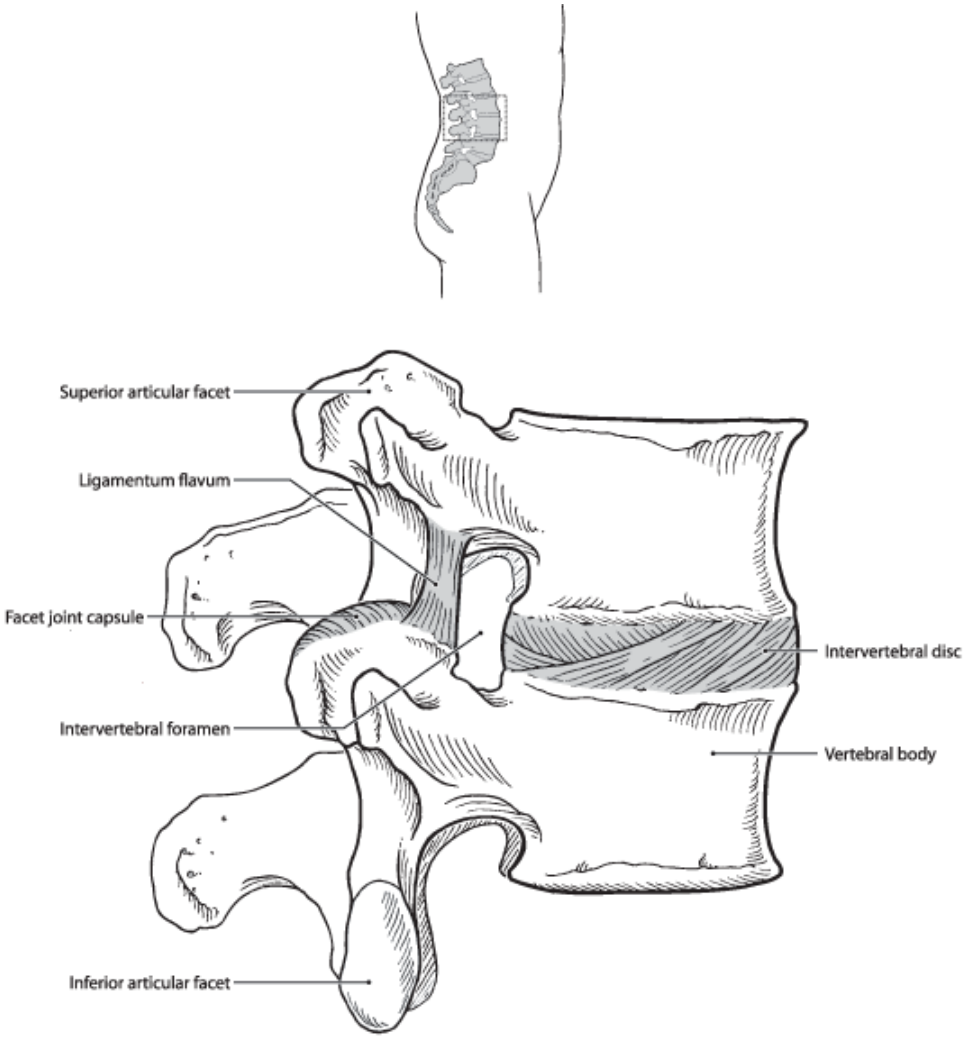

Figure 2.5: Functional spinal unit of lumbar spine (Image adapted from medical discussion paper-Back pain: http://www.wsiat.on.ca/english/mlo/back.htm with permission from Ms. Friesen)

The functional spinal unit (FSU), or spinal motion segment (SMS), consists of an intervertebral disc with two adjacent vertebrae, facet joints, and intervening ligaments as shown in Figure 2.5. It is the smallest structural unit that can exhibit the full biomechanical behaviour of the spine (Nordin and Frankel, 2012). In this study, apart from some of cadaveric specimens used for the validation work which came from T11 and 12, we limited the range to the level of the lumbar spine (L1-L5) focusing particularly on the FSU.

2.3.1 Vertebra

Each vertebra comprises a vertebral body, two pedicles, and posterior elements such as the transverse processes, articular processes, spinous process, and spinal canal as shown in Figure 2.6.

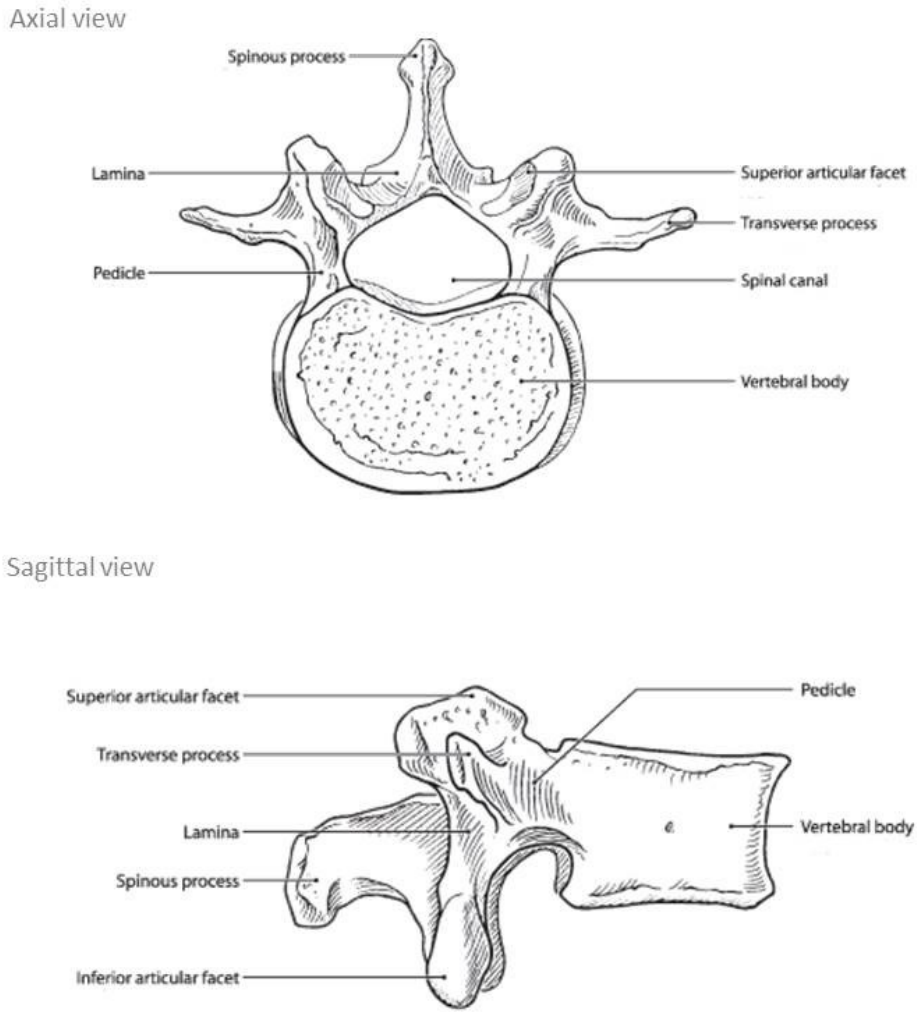

Figure 2.6: Vertebra: top) axial view; bottom) sagittal view (Image adapted from medical discussion paper-Back pain: http://www.wsiat.on.ca/english/mlo/back.htm with permission Ms. Friesen)

The vertebral body is primarily made of a trabecular bone core with a thin cortical shell. The trabecular bone comprises numerous interconnected trabecular struts surrounded by bone marrow. Trabecular architecture arises through adaptation which occurs during biological bone modelling and remodelling. Bone modelling during growth is in the form of new bone formation over existing bone with the independent activities of osteoclasts and osteoblasts leading to an increased bone mass. Bone remodelling during aging is bone formation over existing bone, achieved by 'team work' between osteoclasts and osteoblasts, resulting in maintenance at best, if not bone loss.

According to mechanical tests carried out on cadaveric specimens, in compression, the vertebral body takes 80% of the load under pure compression and the posterior elements support the remaining load which is approximately 20%. Here, the literature shows a range of values (Nachemson 1960, 18%; Adams and Hutton 1980, 16%; Lorentz 1983, 9%-25%; Yang and King 1984, 3-25%; Pal and Routal 1986, 18-22% (Nachemson, 1960, Adams and Hutton, 1980, Lorenz et al., 1983, Yang and King, 1984, Pal and Routal, 1986)). As the major load pathways through the vertebral body run in parallel to the columns of vertical trabeculae, the cortical shell and horizontal trabeculae are less important in transmitting compressive forces (Fields et al., 2011). Each individual strut of trabecular bone in the vertebral body is aligned in a vertical direction (cranio-caudal) thus the elastic modulus in the longitudinal direction is higher than that of the transverse direction. The dominant trabecular direction supports Wolff's law that bone structure is adapted to sustain habitual loads with minimum bone mass. Although bone usually shows anisotropic behaviour with a different stiffness and strength along each direction, vertebral trabecular bone is often considered as a transversely isotropic material as mentioned earlier (Mosekilde et al., 1987, Mosekilde, 1993, Ulrich et al., 1999).

Trabecular architecture changes with ageing (Boyde, 2002). The trabeculae become thinner. This is more pronounced for horizontal trabeculae in non-load bearing parts. Drug treatments may not lead to full recovery of bone strength; whilst bone mass may recover fully, connection loss between trabeculae may remain. Connections between horizontal trabeculae decrease and hence trabecular strength is decreased as demonstrated by Euler bucking theory (Guo and Kim, 2002). Consequently, fracture risk increases (Mosekilde, 1993).

2.3.2 Intervertebral disc

Intervertebral discs (IVD) are the largest avascular and aneural structures in human body. The IVD is composed of collagen fibres embedded in a highly hydrated extracellular matrix. This composition is the same irrespective of the spinal level, although the size and shape varies (Guerin and Elliott, 2006).

Each IVD has three distinct regions, as shown in Figure 2.7: the nucleus pulposus (NP: centre), the annulus fibrosus (AF: fibrous layer wrapped circumferentially on the nucleus pulposus), and two end plates (covering the inferior and superior aspects of the disc).

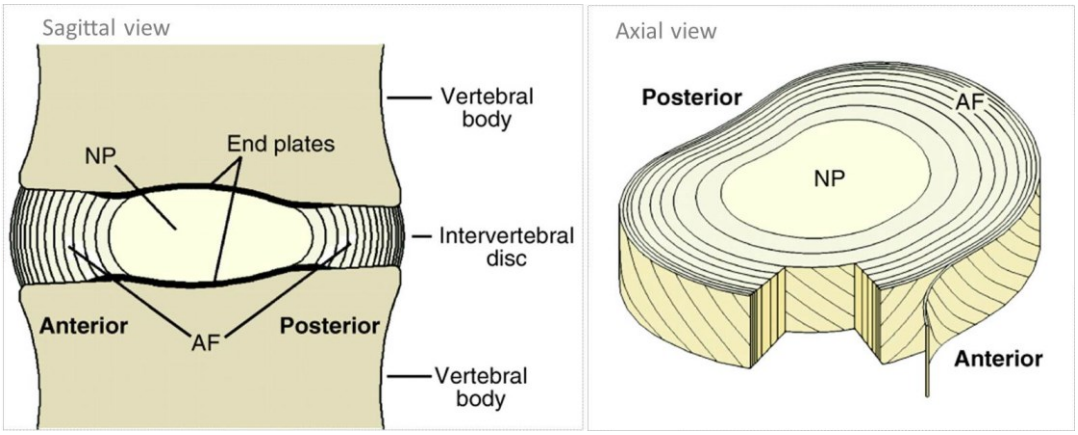

Figure 2.7: Intervertebral disc: left) sagittal view; right) axial view (Image adapted from open access journal (Smith et al., 2011))

The nucleus pulposus (NP) accounts for 30~40% of the volume fraction of the IVD and is a highly-hydrated gel, comprising 70~85% of water, with proteoglycans and collagen (50%, 15~20% of the dry weight). It acts like fluid since the NP has high water content. The water content of the NP decreases with ageing and consequently, becomes dry, and stiff. The annulus fibrosus (AF) is formed from tough, ligamentous, fibrocartilage and is composed of 50% of water, with collagen fibre bundles (10%, 70% of dry weight) embedded in proteoglycan matrix. The collagen fibres consist of around twenty layers embedded in different orientations (about 30° and 150° from the horizontal plane, in turn) and attached to the endplates. This structure is designed to avoid bulging and

support rotation. The endplates are thin plates of cortical bone perforated by many small holes, and covered by a thin layer of hyaline cartilage (Adams et al., 2002).

As IVDs degenerate with age, they experience morphological and biochemical changes. Clinical degeneration is graded *in vivo* using MRI (Pfirrmann et al., 2001). At the earliest stage of degeneration, the IVD shows increasing flexibility, but, with increased severity of degeneration the IVD becomes stiffer and shows a solid-like behaviour (Iatridis et al., 1997, Iatridis et al., 1998). The degenerative process alters the mechanical characteristics of the IVD itself and also the load distribution, thus the stress distribution on the adjacent vertebrae is affected (Adams and Roughley, 2006). In the heathy IVD load is transferred uniformly through the NP and AF whilst, for the degenerated IVD the load is transferred more through the AF (White iii and Panjabi, 1990). In severe disc degeneration, the neural arch and posterior elements of the vertebrae experienced more load-bearing. In consequence, this leads to progressive bone loss in the vertebral body which is the anterior part of vertebra and more likely to be fractured (Christiansen and Bouxsein, 2010).

2.3.3 Facet joints and Ligaments

The facet joints, the so-called *zygapophysial* joints, are the links between the inferior articular process of the upper vertebra and the superior articular process of the lower vertebra. These have an important role in limiting excessive torsion and protecting disconnection of vertebra when sliding forward (Adams et al., 2002).

The overall integrity of the spinal structure is maintained by ligaments. Many of these are connected together as shown in Figure 2.8, namely; the anterior longitudinal ligament (ALL), the posterior longitudinal ligament (PLL), the supraspinous ligament (SSL), the interspinous ligaments (ISL), and the ligamentum flavum (LF) in the lumbar spinal column. The longitudinal and supraspinous ligaments are attached to several vertebrae horizontally and the fibres of the SSL and ISL are combined together. For this reason, some loss of strength is inevitable if the spine is dissected into individual functional spinal units (Adams et al., 2002).

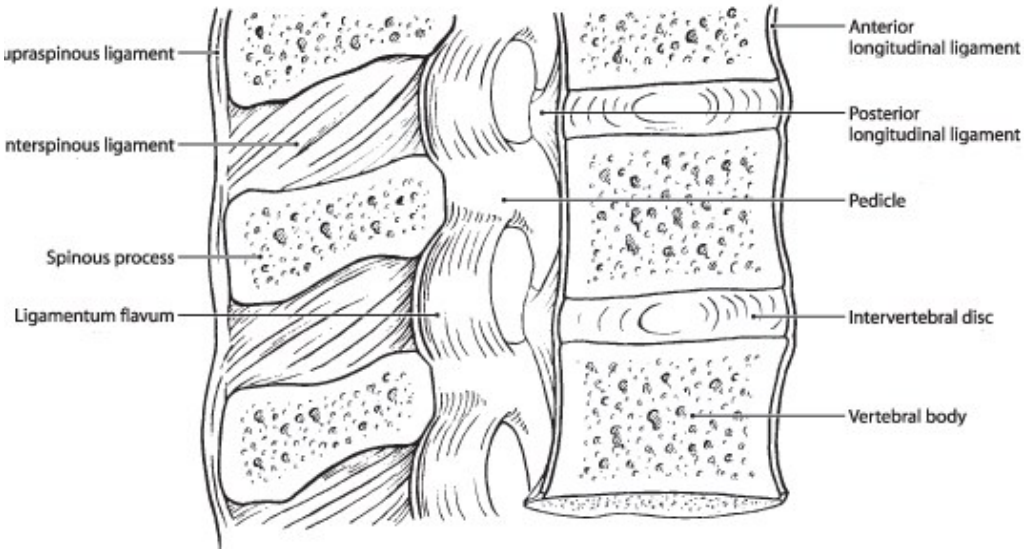

Figure 2.8: Cross-section of a sagittal view of a functional spinal unit showing the major ligaments (Image adapted from medical discussion paper-Back pain: http://www.wsiat.on.ca/english/mlo/back.htm with permission from Ms. Friesen)

2.4 Vertebral compression fracture and assessment of fracture risk

The vertebral compression fracture (VCF) is the common type of osteoporotic vertebral fracture. This commonly occurs in the levels T11 to L2 (Van Der Klift et al., 2002). An anterior wedge fracture is the most frequent type of fracture as the primary loading of the human vertebral body is asymmetrical (Wasnich RD, 1996, Jackson S.A., 2000). A vertebral fracture, in itself, can be a good predictor of future fracture risk since vertebral fractures substantially increase the risk of new fragility fractures. Women with vertebral fractures have a 5-fold increased risk of a new vertebral fracture and a 2-fold increased risk of hip fracture (Black et al., 1999, Melton Iii et al., 1999). Of those with fractures, one woman in five will suffer from a further vertebral fracture within a year (Lindsay et al., 2001).

Two imaging methods are used clinically to define vertebral fracture: vertebral fracture assessment (VFA) by DXA and conventional radiography. Conventional radiography has a superior image quality than VFA by DXA, but the effective radiation doses associated

with conventional radiography are much higher than those associated with VFA by DXA. Vertebral fracture is commonly defined as occurring in the vertebral body and several approaches for the identification of a vertebral fracture have been suggested. Conventionally, a change of 15%, or more, in the mean vertebral body height ratio assessed using quantitative morphometry (QM) is regarded as indicative of a vertebral fracture (Melton et al., 1989, Melton et al., 1993). Eastell et al. subsequently revised this definition to use standard deviations (Eastell et al., 1991). Gehlbach et al. used a similar percentage-rating system to visually grade the severity of vertebral deformity using a categorisation ranging from normal to three called the Semi-Quantitative (SQ) method (Gehlbah et al., 2000). Conventional methods are categorised into three-types: concave (collapse of the central upper endplate-leading to a reduction in the mid vertebral height), wedge (reduction of both the mid and anterior vertebral heights), and crush (collapse of the whole vertebral body). However, endplate fracture, an essential feature of typical osteoporotic vertebral fractures, is not taken into account in conventional methods. To account for the endplate the Algorithm-Based Qualitative (ABQ) Method was proposed recently (Jiang et al., 2004). The ABQ method incorporates two improvements to define vertebral fractures: the method is a visual assessment tool which takes account of fracture of the vertebral endplate and has no minimum threshold for apparent reduction in vertebral height. Nevertheless, vertebral fracture detection still represents a challenge and remains problematic and suboptimal: over-diagnosis (confusion with other non-fracture deformities) and under-diagnosis remain a concern (Bouxsein, 2006).

Vertebral fractures occur when the forces applied to the vertebral body exceed its strength. Therefore, there are two main factors that should be considered when seeking to reduce fracture risk; the applied load (force direction and magnitude) and whole bone strength (Bouxsein, 2006). As mentioned previously, several factors may affect vertebral compressive strength: bone mass, bone morphology (shape, micro-architecture), and bone material properties (matrix mineralization, collagen characteristics, micro-damage) (Christiansen and Bouxsein, 2010). In terms of the load on the spine, several factors also are involved: body weight, tension in the spinal ligaments and the surrounding muscles, spinal curvature, intervertebral disc degeneration, and external loads (Christiansen and Bouxsein, 2010). Several studies indicate that the vertebral body takes most of compressive load on the spine, whilst the posterior elements take the interaction with

ligaments, muscles and facet joints. Generally, the upright posture can be assumed to be associated with axial compressive loading on the spine, whilst forward bending moment should be considered during erect standing due to anterior movement of the centre of gravity of the body as a whole.

Although aBMD by DXA is still the only clinical technique used to assess vertebral strength and fracture risk non-invasively, QCT has been in the spotlight in recent years since geometric and structural information is also considered to be an important factor for the determination of bone strength. Three dimensional volumetric QCT imaging can produce more accurate volumetric BMD (g/cm^3: vBMD) when compared with areal BMD (g/cm^2: aBMD) by DXA. QCT is also able to discriminate between trabecular and cortical bone. In common with the basic operating principle of DXA, QCT measurement is based on X-ray beam attenuation. CT images are obtained by two different processes: by gathering slice scan data made of voxels using a spiral scan mode and by reconstructing tomographic data using a mathematical process. Hounsfield units (HU), a linear parameter, are used to calibrate and standardise different types of CT scanners; air (-1000), fat (-200), water (0), muscle (30), and bone (300-3000). A bone mineral phantom is used to transform HUs to vBMD values. These approaches use validated correlations between either, bone density and bone strength, or between bone density with bone structure information and bone strength. In general, studies by DXA or QCT indicate modest correlations (R^2 =0.3-0.8) between aBMD assessed by DXA or vBMD by QCT and vertebral compressive strength, although they do not measure vertebral strength directly. Recently, QCT-based finite element analysis (FEA) has been adopted as an alternative non-invasive technique for assessing vertebral fracture risk. The advantage of FEA is that it can integrate all the information embedded in the scans such as bone shape, size, trabecular and cortical bone density distribution, as well as physiological loading conditions. Some studies suggest that QCT-based FEA has stronger correlation with vertebral compressive strength than aBMD by DXA or vBMD by QCT alone (Crawford et al., 2003a, Melton et al., 2007).

2.5 Finite element modelling of vertebrae: State-of-the-Art

A number of FEA studies of the spine have been published. These range from relatively simple individual vertebral body FE models, to realistic complex whole vertebrae column FE models. FEA models of the lumbar spine can be grouped according to the parts involved as shown in Figure 2.9: the vertebral body or the single vertebra, the FSU, three vertebrae, and the whole lumbar spine from vertebra L1 to vertebra L5 or from vertebra L1 to vertebra S1.

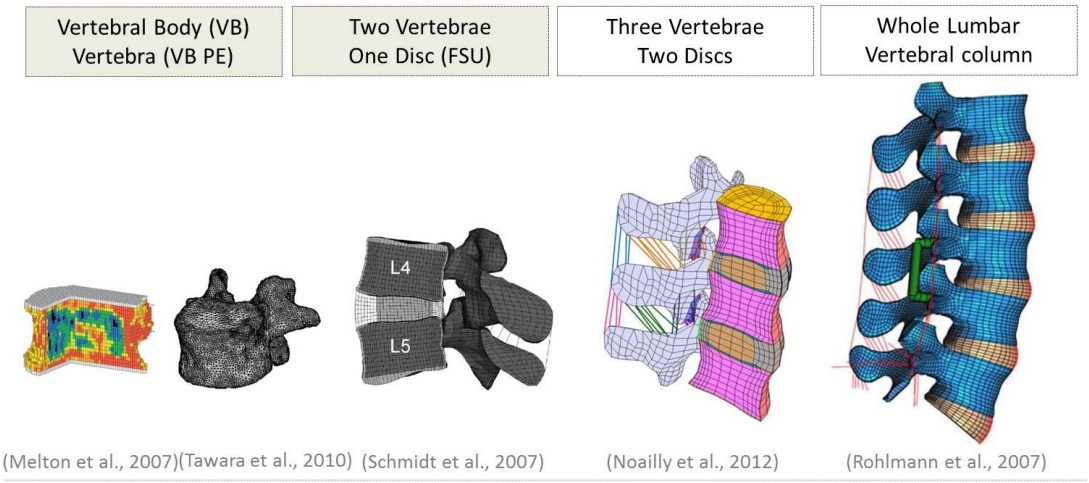

Figure 2.9: Different categories of finite element models applied in lumbar spine research (figures with permission from Melton et al., 2007; Tawara et al., 2010; Schmidt et al., 2007; Noailly et al., 2012; Rohlmann et la., 2007)

The main procedures used to develop FE models in spine research are similar, even though the research approach and the range of FE models are hugely depended on the specific aims of each study. The general process of three-dimensional finite element analysis of the spine can be described in terms of in three main steps: i) the generation of the geometry and mesh; ii) the assignment of material properties; and, iii) the application of boundary conditions. Each step is extremely crucial for an accurate finite element analysis. To generate the three dimensional geometry of a finite element model, one common method is to use medical images such as CT or MRI scans, whilst another is to use a generic FE model which has been developed after measuring several

dimensional parameters. However, not surprisingly, FE models based on medical images have been shown to give more accurate results when compared with experimental studies than those from generic FE models (Wilcox, 2007). Mesh generation is also a crucial step for obtaining an accurate FE result. Although several methods have been developed to build the mesh structure for a three-dimensional model, the most common approach is to generate a mesh model directly from the CT voxels. This uses pixel information obtained from CT data to generate cubic elements directly without the need to first create a solid model. However, a voxel mesh is not suitable to represent surface of the spinal structure due to the zigzag element shape. For this reason, other types of mesh model, such as tetrahedral and hexahedral mesh models, are often used to investigate surface strain and stress distribution after smoothing the surface. In terms of material properties, a wide range of different properties from a range of experimental studies has been suggested for use in vertebrae in spinal FE models. The most prevalent method employed in clinical research is to use the empirical relationships between CT number and bone density, and between density and Young's moduli. The loads and boundary conditions are then applied to the model to simulate a specific loading condition such as pure compression, bending or shear and finally, the FE model is solved using a FE solver.

Whilst several review papers are available, many of these are far too general for the purpose of this thesis (Villarraga and Ford, 2001, Fagan et al., 2002a, Ross, 2005, Jones and Wilcox, 2008). Fagan et al. (2002) categorised the finite element models by range within spine: whole spine models, vertebral body models, intervertebral disc and FSU models, lumbar and cervical spine models. They found that many researchers started with a simple individual model and then expanded it with the addition for more complex structure and components. Jones and Wilcox (2008) have also reviewed finite element modelling methods used for the spine, focusing on the verification, validation and sensitivity of the models. At the time of writing, only one review paper could be found that considered patient-specific finite element modelling of bones (Poelert et al., 2013). Although this reviewed the whole procedure in detail from the patient-specific point of view, only the femoral region was covered.

In this chapter, state-of-the-art finite element models have been reviewed which specifically focus on the FE model of the lumbar spine generated from medical images to

investigate vertebral strength and to predict fracture risk. Two specific groups of finite element models have been considered in particular: the vertebral body and vertebra model (at Macro level), and functional spinal unit model (FSU) - two vertebrae and the adjacent intervertebral disc as shown in Figure 2.9.

2.5.1 Vertebral body and vertebra FE model (Macro)

The majority of mechanical studies on vertebra consider the vertebral body without posterior elements. The rationale for this is that fracture usually occurs within the vertebral body. In keeping with this, many researchers have developed finite element models of the vertebral body without posterior elements and the adjacent intervertebral discs for studies of the spine (Homminga, 2001, Crawford et al., 2003a, Crawford et al., 2003b, Crawford RP, 2004, Keaveny et al., 2007, Melton et al., 2007, Buckley et al., 2007b, Chevalier et al., 2008, Chevalier et al., 2010, Chevalier Y, 2009, Dall'Ara et al., 2010, Maquer et al., 2013, Mirzaei et al., 2009, Zeinali et al., 2010, Liebschner et al., 2003, Imai et al., 2006, Imai et al., 2009). However, although small in comparison with the vertebral body, the posterior elements also share the load on the vertebra. Thus posterior elements should be considered when predicting realistic vertebral biomechanical characteristics *in vivo* (Imai et al., 2006). Very few FE models include the posterior elements within a vertebra FE model (Wijayathunga et al., 2008, Tawara et al., 2010). Wijayathunga et al. (2008) used the whole vertebral FE model to investigate the effect of cement augmentation on the vertebra, while Tawara et al. (2010) used an FE model to investigate the effects of treatment.

Voxel based FE models

The CT-based voxel method (direct conversion of the QCT voxel data from cadaveric vertebral body into a finite element model using 8-node brick elements), has commonly been used to create a finite element model from medical images. Using this method, material properties can be assigned using the empirical relationship between density and Young's modulus although there are wide ranges in empirical relationships. The detailed material properties and boundary conditions published in literature are summarised in Appendix A-1 and Appendix A-2.

Homminga et al. (2001) used a patient-specific finite element model from CT data for 49 lumbar vertebral bodies to investigate the load distribution and fracture-risk in healthy and degenerative IVD conditions. They considered an intervertebral disc model to generate a disc-vertebral body-disc unit. 1000 N load was applied with 2° forward flexion. They found that, in the case of a degenerated disc, the cortical shell carried more load than trabecular core and concluded that the load-sharing on the vertebra depends on the status of the disc (Homminga, 2001). Crawford et al. (2003a) developed a QCT-based voxel finite element model of a vertebral body without posterior elements to predict vertebral strength under compressive conditions. The results of the FEA were validated against experiment and demonstrated that the finite element model may give a more accurate strength prediction than BMD derived from QCT alone (Crawford et al., 2003a). Keaveny et al. (2007) used a QCT voxel-based FE model for investigating vertebral strength in a clinical trial. The results indicated teriparatide (TPTD) gives a greater improvement estimated vertebral strength than alendronate (ALN) although both have positive effects on vertebrae (Keaveny et al., 2007). Melton et al. (2007) applied QCT voxel-based FEM to study vertebral fracture-risk, comparing the results with other methods available such as BMD, geometric factors, microstructure, bone strength and risk factors. The analysis showed that the results of QCT-based FEA were well-correlated with aBMD, and concluded that QCT-based FEA could be regarded as a good predictor of fracture-risk (Melton et al., 2007). Buckley et al. (2007) directly compared vertebral strength under uniaxial compression with various predictive methods, namely: QCT-based BMD, QCT-based mechanics of the solid (MOS) model, QCT-based FEM, and mechanical testing. The results of MOS and FE models showed a strong correlation with those of mechanical testing, whilst BMD was the only method to give a poor correlation (Buckley et al., 2007b). Some studies using a vertebra FE model used the same approach to predict vertebral strength (Lewiecki, 2009, Mirzaei et al., 2009, Zeinali et al., 2010, Maquer et al., 2013).

Non-Voxel based FE models

Several studies generated the cortical shell explicitly using non-voxel mesh such as triangle shell elements or tetrahedral elements (Liebschner et al., 2003, Imai et al., 2006). Liebschner et al. (2003) developed a QCT-based FE model with a cortical shell modelled using 20-node brick elements in TrueGrid (XYZ Scientific Application Inc.,

Livermore, CA). The study found that incorporation of a 0.3 mm thick cortical shell with a Young's Modulus of 457 MPa improved the accuracy of the prediction of the biomechanical properties of the whole vertebra in the trabecular only FE model. Imai et al. (2006) proposed a nonlinear FE model to predict vertebral strength and the fracture site. This model was generated using MECHANICAL FINDER software (Mitsubishi Space Software Co., Tokyo, Japan). The trabecular bone and cortical shell portions of the model were constructed from 2 mm tetrahedral elements and 2 mm triangular plates, respectively. The FE model was validated against experiment in terms of fracture strength, fracture site, and the strain on the surface of the vertebrae. A Drucker-Prager equivalent stress criterion was used to find the yield point since, unlike metal, bone is not a ductile material. The fracture location was estimated at the location of the minimum principal strain.

Clinical Use

Of the many FE models of the vertebra described in the literature, only one QCT-based voxel FE model has been frequently used as a research tool in clinical osteoporosis studies (Keaveny et al., 2007, Mawatari et al., 2008, Melton et al., 2007, Lewiecki, 2009, Melton Iii et al., 2010, Chevalier et al., 2010, Graeff et al., 2009). Melton et al. (2007) showed that FE methods can be used to estimate vertebral fracture risk *in vivo*. Some studies have used the vertebral body FE model to investigate therapeutic effects on vertebral strength. Keaveny et al. (2007) found, by comparing vertebral strengths between baseline and follow up, that treatments (teripratide and alendronate) increased vertebral strength. Lewiecki et al. (2009) studied the effect of oral ibandronate on bone strength in 93 postmenopausal women and found that ibandronate recipients had increased vertebral strength at 12 months. Imai et al. (2009) assessed fracture risk and therapeutic effects using a L2 vertebral body FE model and were able to show that alendronate increased vertebral strength. This paper was also able to show that vertebral strength assessed using an FE model has higher discriminating power for vertebral fracture than the aBMD by DXA. Chevalier et al. (2010) applied a QCT-based nonlinear FE model to evaluate the effects of teriparatide after treatment with alendronate and risedronate.

2.5.2 Functional Spinal Unit FE model (FSU FE)

As mentioned previously, load transfer in the vertebral column can act in two ways: the majority of the load is transferred through intervertebral disc to the vertebral body, whilst the remainder is carried by the facet joints. Degeneration of the intervertebral disc, therefore, affects the loading conditions and the fracture patterns of the adjacent vertebrae (Pollintine et al., 2004a, Pollintine et al., 2004b, Adams and Dolan, 2005, Adams et al., 2006). For this reason, an FE model that incorporates an intervertebral disc may enhance the validity of the FE models as predictors of fracture. Previous FSU FE models are very different from point of view of a patient-specific approach. In general, in these CT-based models the geometry of the IVD is usually inferred from the locations of the end plates of adjacent vertebrae. Furthermore, due to the increased complexity of its overall structure, the FSU model commonly relies upon very simplified homogeneous material properties for the trabecular and cortical bone of the vertebra rather than using element-specific properties. However, they tend to use more complex model such as a poro-elastic material model for the IVD. In general, for the AF, isotropic material properties with layered cable elements aligned the fibre direction, or anisotropic material properties have been used, whereas the NP is represented with simple isotropic elastic properties or hyperelastic to incompressible fluid properties. Material properties that are shown in the literature for vertebral bone (cortical and trabecular bone), IVD (end plates, nucleus pulposus, annulus ground substance with annulus fibres) are summarised in Appendix A-3 and Appendix A-4.

The above-mentioned limitations can be overcome by complementing CT data with that from magnetic resonance imaging (MRI) scans. Data on the human disc obtained by MRI are directly correlated with both severity of the disc degeneration and water-/collagen-content, and intradiscal pressure (Pfirrmann et al., 2001, Pfirrmann et al., 2006, Johannessen et al., 2006, Nguyen et al., 2008). These, in turn, are related to the mechanical properties of the IVD and can be modelled in FE analyses.

FSU FE models including the IVD are explained in more detail in section which follows.

The first numerical model including an IVD was introduced by Belytschko (1974). This was an axisymmetric three-dimensional model of one quarter of the IVD and adjacent vertebrae and was developed to investigate the behaviour of the IVD under axial loading.

Isotropic, homogeneous material properties were assumed for the vertebrae, whilst the nucleus pulposus was modelled as an incompressible and in a hydrostatic state of stress, and the annulus fibrosus was composed of several lamellae with different homogeneous orthotropic material properties along the fibre directions (Belytschko et al., 1974).

The most well-known model of this type is the nonlinear viscoelastic FSU FE model suggested by (Shirazi-Adl et al., 1984). Many researchers have adopted this model to investigate the effects of a healthy IVD on the stress and strain distribution in the adjacent vertebrae (Wang et al., 1997, Polikeit et al., 2004, Goto et al., 2002). Polikeit et al. (2004) developed a ligamentous L2-L3 FSU FE model based on CT data sets using a spectrum of different material properties for the vertebra, such as isotropic, transversely isotropic, and composite, to investigate the effects of IVD degeneration and bone quality alteration associated with osteoporosis on load transfer on the vertebra. The NP was modelled as an incompressible material and the AF as a composite with several fibre layers. Seven tension-only ligaments were also considered. Goto et al. (2002) developed a three-dimensional L4-L5 lumbar FE model from CT data sets to investigate stress distribution on the endplates, facet joints, and IVD under flexion, extension and compression. The material properties used in the Goto's model were taken from papers published by Nachemson, Sato and Shirazi-Adl.

The FSU FE model can be used to investigate the effects of IVD degeneration on biomechanical behaviours such as the range of motion, stiffness, and intra-discal pressure of a lumbar FSU under physiological loading conditions. Rohlmann et al. (2006) suggested a nonlinear L3-L4 FSU FE model to investigate the influence of disc degeneration on the mechanical behaviour of the lumbar spine under conditions of flexion, extension, lateral bending and axial rotation. A transverse isotropic material property was used for vertebra and a hyperelastic property was chosen for the annulus ground substance with AF layers, whilst the NP was assumed to be an incompressible, fluid-filled cavity. Seven tension-only ligaments and curved facet joints were also included (Rohlmann et al., 2006). Schmidit et al. (2006) developed a nonlinear L4-L5 FSU FE model based on CT and MRI scans to determine the ideal material properties for the AF under flexion, extension, lateral bending, and axial rotation condition. The vertebrae were modelled with eight-node hexahedral solid elements. The AF was assumed to be ground substance with spring element of 8 collagen fibre layers (Schmidt et al., 2006).

The model developed was subsequently used to investigate IVD intra-discal pressure and effects of disc degeneration (Schmidt et al., 2009, Schmidt et al., 2007b, Schmidt et al., 2007c).

FSU FE models have also been used to study the effect of surgical intervention. Zhang et al. (2010) developed a L1-L2 FSU FE model to investigate the biomechanical effects of vertebral augmentation. (Zhang et al., 2010) and Totoribe et al. (1999) used a three-dimensional L4-L5 FSU FE model to investigate the effects of the posterolateral fusion on stability (Totoribe et al., 1999).

Some studies here proposed a FSU FE model using poroelasticity. Cheung et al. (2003) developed a poroelastic L4-L5 FSU FE model to investigate fluid flow and, stress distribution in and deformation of the IVD under static and dynamic loading conditions (Cheung et al., 2003). Natarajan used a poroelastic material for the IVD in a L3-L4 FSU FE model to study IVD failure under cyclic loading in order to mimic the normal, 24 hour, daily activities. The improved FE model included physiological parameters such as swelling pressure, and permeability (Natarajan et al., 2003, Natarajan et al., 2007).

To summarise all FE models described in this section, Table 2.4 categorises the FE models together with the image modalities used.

Table 2.4: FE models in literature

Model name	Components	References
QCT-based voxel VB FE model	vertebral body	Homminga et al., 2001 Crawford et al., 2003;2004 †Keaveny et al., 2007 †Melton et al., 2007;2010 Buckley et al., 2007 †Lewiecki et al., 2009 Mirzaei et al., 2009 Zeinali et al., 2010 †Chevalier et al., 2010 †Wang et al., 2011
HRQCT-based voxel VB FE model		†Graeff et al., 2009 †Gluer et al., 2013 Dall'Ara et al., 2010
HR pQCT-based voxel VB FE model		Chevalier et al., 2008;2009 Dall'Ara et al., 2012 Maquer et al., 2012
QCT-based VB FE model		Imai et al., 2006 †Imai et al., 2009 Liebshner et al, 2003
VB FE model (QCT)		Our model
QCT-based Vertebra FE model	vertebral body with post elements	†Tawara et al., 2010 Sakamoto et al.,
µCT-based Vertebra FE model		Wijayathunga et al., 2007
VB PE FE model (QCT)		Our model
FSU FE model (Direct measurement)	vertebra-disc-vertebra	Shirazi-Adl et al., 1984; 1986 Wang et al., 1997;2000
FSU FE model (QCT)		Totoribe et al., 1999 Goto et al., 2002 Cheung et al., 2004 Polikeit et al., 2003;2004 Natarajan et al., 2003; 2007 Rohlmann et al., 2006 Ahn et al., 2008 Ruberte et al., 2009 Zhang et al., 2010 Ezquerro et al., 2011
FSU FE model (QCT+MRI)		Schmidt et al., 2006;2007 El-Rich et al., 2009
FSU FE model (QCT+MRI)		Our model
DVD FE model (HR pQCT)	disc-vertebra-disc	Maquer et al., 2013
DVD FE model (QCT)		Our model
Multi-levels FE model	more than two vertebrae and discs	Cao et al., 2001 Noailly et al., 2003;2007 Renner et al., 2007

†FE model was used for clinical research

2.6 Subject-specific FE models of lumbar spine for clinical studies

In clinical investigations involving a large number of subjects the differences between individuals may affect the accuracy of the geometrical information and the material properties of the model. These factors are crucial to the accuracy of the results of FE analyses as illustrated in Figure 2.10.

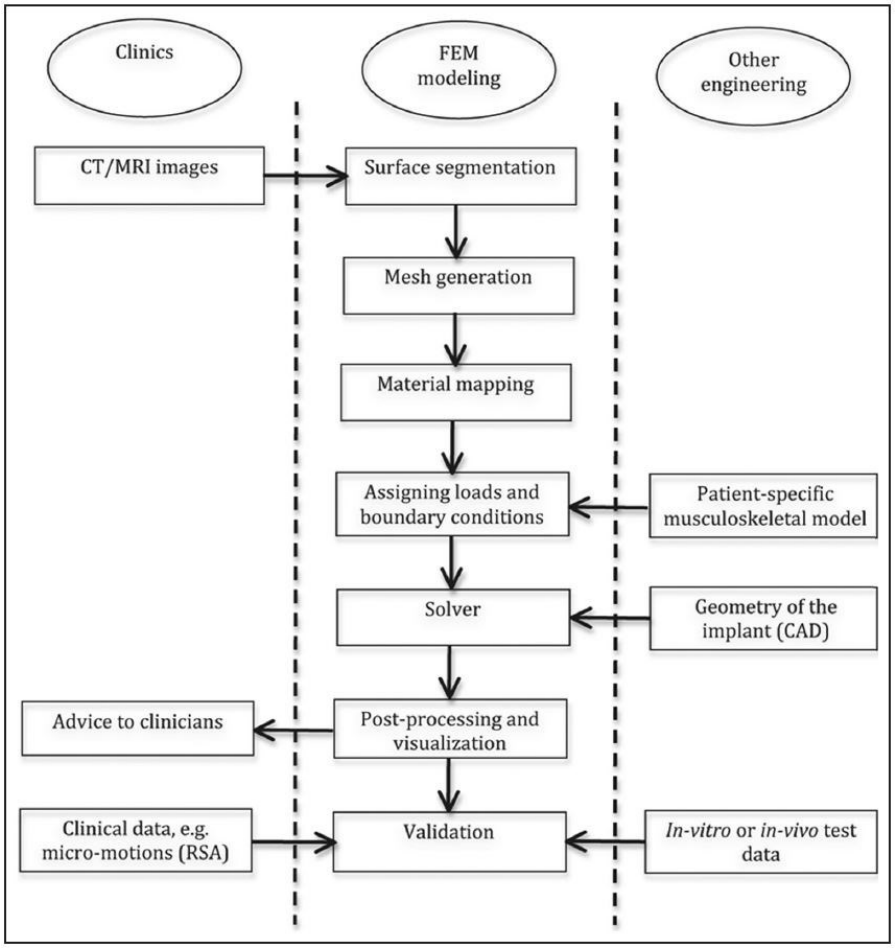

Figure 2.10: Schematic drawing of the steps involved in the construction, analysis, and validation of a typical patient-specific FE model of bones (Figure from (Poelert et al., 2013) with permission).

Furthermore, in routine clinical practice, QCT data is only available for the central skeleton such as spine and hip region. In this regard, according to the literature review (Chapter 2.4), the appropriate method to support a subject-specific finite element

model is a QCT-based voxel model of the vertebral body. The QCT based voxel method is robust and provides a fast way to generate a mesh and to assign material properties. The vertebral body FE model is well-validated and has been used in clinical trials. However, as mentioned previously, this model has limitations since the posterior elements of the vertebra and the adjacent intervertebral disc also play an important role in load transfer on the spine structures. For this reason, an FE model such as the FSU FE model (Chapter 2.5) that takes into account both the posterior elements and the IVD has been proposed, and used, to study the biomechanical characteristics of the lumbar spine. However, to the best of our knowledge a FSU FE model has not as yet been used in subject-specific way for clinical studies.

In this regard, we developed an FSU FE model, based on QCT and MRI scans, from sixteen cadaveric FSUs and validated this against vertebral strength measured on the bench. Furthermore, by selecting different regions of interest from the FSU FE model it was possible to diversify into different FE models i.e. a simple FE model of vertebral body and the vertebral body with posterior elements. These were then used for the comparison purposes in predicting vertebral strength using the same QCT and MRI data sets. From a cadaveric study carried out during the initial phases of this project, we proposed a new patient-specific FE model of a single vertebra with two adjacent intervertebral discs. This disc-vertebra-disc (DVD) FE model combines the two main approaches a QCT-based voxel model of the vertebral body and a FSU FE model in order to provide a model that is suitable for use in clinical studies. Hussein (2013) used an FE model of disc-vertebral body-disc unit to investigate the influence of the IVD on the mechanical properties and failure mechanisms of the vertebra (Hussein et al., 2013). Maquer (2013) used a DVD FE model to compare the effects of boundary conditions on vertebral strength (Maquer et al., 2013). Whilst the DVD FE model is clearly not a completely new concept, this type of model has not, as yet, been used for clinical applications.

At present, there is an obvious need for a simplified tool, accessed through a consistent full framework to generate FE models incorporating both the vertebra and IVD as well as further improving previous methods. The simple framework which standardises each step from geometry generation, to material property assignment, through to solving and checking results, can be updated as the model is developed further.

Chapter 3 will start to introduce the framework in detail. This was used throughout this thesis as the work moved towards a final patient-specific FE model which is applicable for clinical research.

CHAPTER 3 Development of a Framework for Image Processing and a Subject-specific Finite Element Model Generation

This chapter introduces the streamlined framework, 'SpineVox-Pro' that was specifically developed in the course of this project for the development of patient-specific finite element models of vertebra and the adjacent intervertebral disc from medical images. The framework provides a seamless and efficient workflow for image processing, voxel mesh generation and post-processing of the finite element models from QCT and MRI scans. SpineVox-Pro was implemented using MATLAB (Mathworks Inc., Natick, MA, USA) and ANSYS APDL (ANSYS Inc., Canonsburg, PA, USA) via a single MATLAB Graphical User Interface (GUI).

3.1 Introduction

Reflecting on the steps involved in the process of developing a patient-specific model, it is clear that a more integrated approach is needed. Medical images such as CT or MRI data are usually saved in a standard format, the Digital Imaging and Communication in Medicine (DICOM) format. DICOM was developed with the aim of providing a common standard to enable imaging equipment to communicate with other devices. There are many commercial and open-source programs for processing medical images (Mimics, Simpleware, Image J, AMIRA and VTK/ITK platform, for example), and for finite element mesh generation (for example, Hypermesh, Meshgrid, TetraGen and CUBIT). However, each of these software packages has its own data format. Additional steps are required for data format conversion, these can lead to loss of data quality. The process of

importing/exporting large datasets is also time-consuming. Furthermore, it is very difficult to ensure a high degree of consistency of FE model orientation, mesh density and quality, and boundary conditions that are required by clinical studies. Reliability and reproducibility are fundamental requirements for studies which involve the analysis of many patient scans to investigate group differences or changes from baseline.

Keyak et al. suggested an automated method of generating patient-specific three-dimensional finite element models of the proximal femur *in vivo*. The FE model was generated with a user-defined size of cubic element and assigned heterogeneous material properties from CT scans (Keyak et al., 1990). The technique has been well validated and used in studies of the hip for more than a decade. The same approach was used in studies of the vertebral body (Crawford et al., 2003a, Keaveny et al., 2007, Buckley et al., 2007b). The present work used a similar technique to develop a framework for generating FE model of the vertebra and adjacent intervertebral disc from CT and MRI scans.

SpineVox-Pro, a streamlined framework, provides full steps for image processing, voxel mesh generation and post-processing of the finite element models of the vertebra with adjacent intervertebral disc from QCT and MRI scans. SpineVox-Pro was implemented using MATLAB (Mathworks Inc., Natick, MA, USA) and ANSYS APDL (ANSYS Inc., Canonsburg, PA, USA) via a single MATLAB Graphical User Interface (GUI). In SpineVox-Pro, there are some additional options. These include functions which support the import/export the files with different types of formats (.stl, .png, .txt), and other functions which use commercial software such as Simpleware ScanIP (Simpleware, UK) to generate different types of mesh (e.g. a tetrahedral mesh). Figure 3.1 illustrates a schematic flow-chart for SpineVox-Pro and Figure 3.2 displays the main GUI, this is designed to be intuitive to the end user.

The “STEPS” column in Figure 3.1 lists the sequential tasks required to process spinal QCT scans, these are explained in detail later in this chapter. The “MATLAB MAIN GUI” lists the procedures in the GUI to perform the corresponding tasks. The third column lists the corresponding MATLAB functions developed. SpineVox-Pro includes about twenty main function scripts with approximately eighty nested function scripts. SpineVox-Pro supports a full process for image processing of the raw medical images and for finite element mesh generation and analysis through four main categories: 1)

patient data acquisition (vBMD calibration), 2) pre-processing (segmentation, interpolation, re-orientation, padding generation step), 3) simulation (voxel mesh generation and ANSYS APDL scripts generation), and 4) ANSYS post-processing. It should be pointed out that, except for image segmentation which requires a minimum amount of user interaction, all steps from the padding step onward are automatic without need for user interaction. This maximises consistency in FE analysis among different patient scans and precision of repeat analysis of same scans.

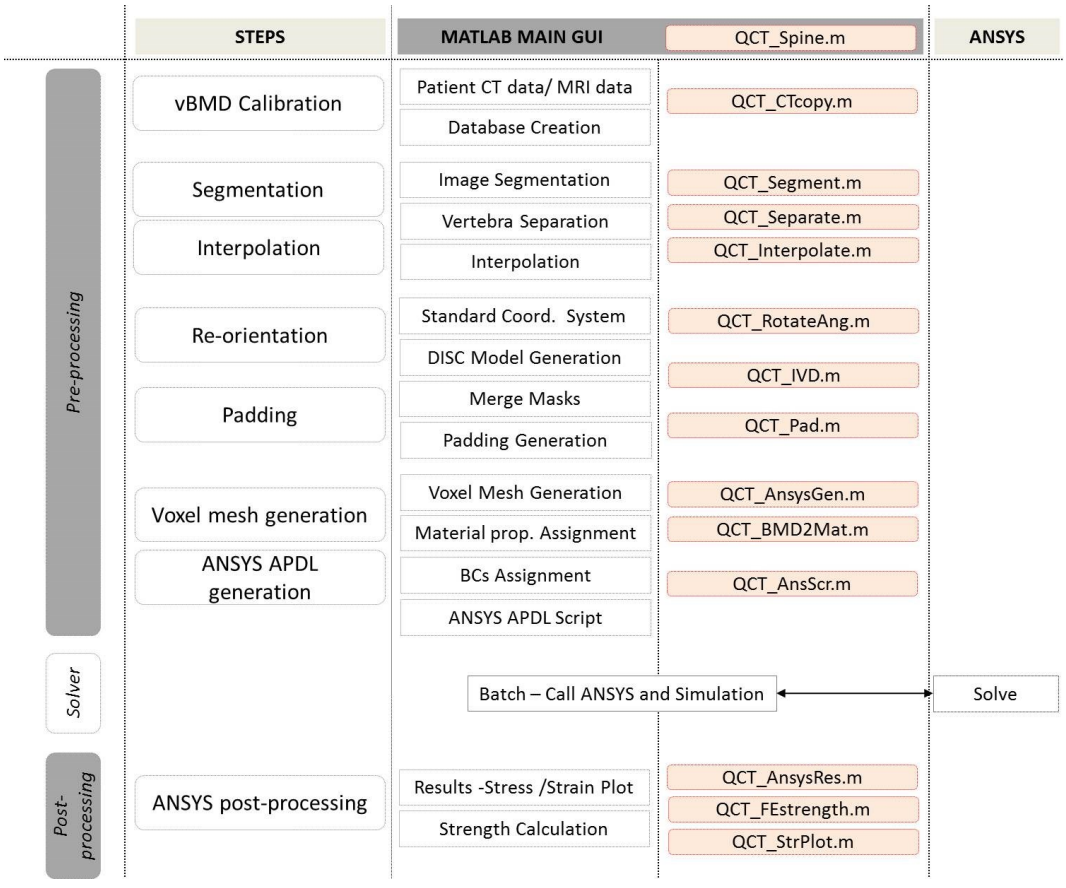

Figure 3.1: SpineVox-Pro V1.1, Schematic view of the framework

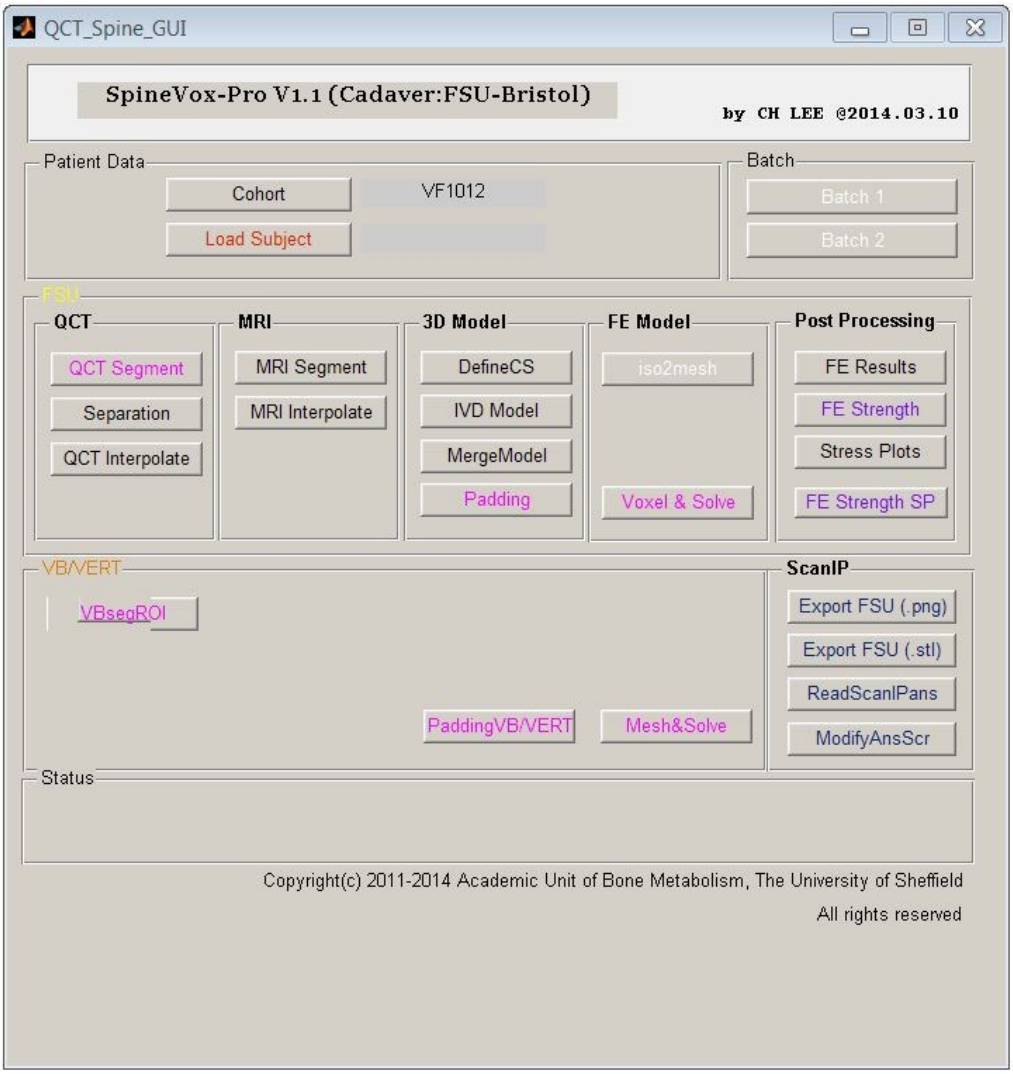

Figure 3.2: SpineVox-Pro V1.1, Main Graphical User Interface

3.2 Development of the SpineVox-Pro framework

3.2.1 Volumetric BMD (vBMD) Calibration

In the first step, the original CT and MRI data obtained in DICOM format (.dcm) are read and converted into MATLAB format (.mat) as shown in Figure 3.3. The basic structure of the DICOM file has two distinct parts: the header and data element set. The header has information about the patient, scanning device and data acquisition whilst the data set contains the image data. From the DICOM header, basic patient information such as the patient id and image acquisition information like slice thickness, pixel spacing, slice

location, and scanned pixel values are extracted and saved to a MATLAB structured form for each patient. In addition, each image included an image of a calibration phantom (see Figure 3.3).

In order to save data storage space, once the mean CT values for the five phantom tube circles on each CT slice are saved on the database, the external phantom part of the image is excluded from Region of Interest (ROI).

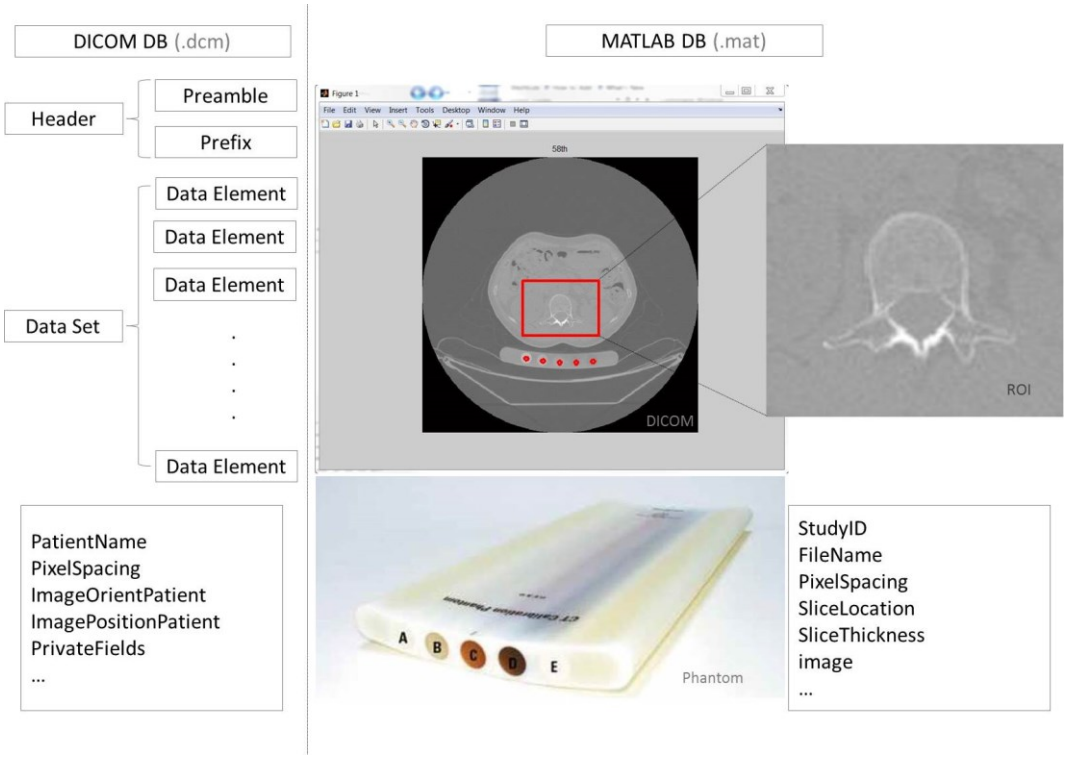

Figure 3.3: SpineVox-Pro V1.1, Calibration Phantom (Mindways Software Inc., Austin, TX, USA) on the axial CT image

The CT data in each slice are calibrated from Hounsfield units (HU) to hydroxyapatite (K_2HPO_4) equivalent density values using Mindways Model 3 CT calibration phantom (Mindways Software Inc., Austin, TX, USA) and associated techniques (Mindways, 2005). The phantom contains 5 different reference material rods embedded in a plastic base material. The rods contain known and varying amount of low and high atomic number materials, and their density information is expressed as water equivalent density and K_2HPO_4 equivalent density (Table 3.1).

Table 3.1: Typical composition of various solid reference materials

Typical composition of various solid reference materials		
Reference Rod	Eq. H_2O density (mg/cc)	Eq. K_2HPO_4 (mg/cc)
A	1012.2 ± 2.3	-51.8 ± 0.1
B	1057.0 ± 1.9	-53.4 ± 0.1
C	1103.6 ± 1.7	58.9 ± 0.1
D	1119.5 ± 1.8	157.0 ± 0.3
E	923.2 ± 2.1	375.8 ± 0.9

By using the known information for the reference material, unknown densities such as bone in the scanned QCT images can be estimated. The unknown material is characterised by estimating the density of K_2HPO_4 dissolved in water that would have the same attenuation properties as the unknown material under the conditions used to acquire the CT image data. The following equation was used first to characterise the response of the scanner to the changes in K_2HPO_4 in the reference material rods:

$$\mu_{ROI(phantom)} - \rho_{water} = \alpha_{ref} \cdot \rho_{K_2HPO_4} + \beta_{ref} \quad (3.1)$$

where,

$\mu_{ROI(phantom)} = HU$ of the Phantom Region Of Interest: circle

$\rho_{water} = H_2O$ Equivalent density of the reference material rods (mg/cc)

$\rho_{K_2HPO_4} = K_2HPO_4$ Equivalent density of the reference material rods (mg/cc)

$\alpha_{ref} =$ Imaging technique-specific parameter defining the response of the CT scanner to K_2HPO_4 (Slope of a linear regression exercise)

$\beta_{ref} =$ Imaging technique-specific parameter characteristic of the CT number scale (Intercept of a linear regression exercise)

The imaging technique-specific parameters: α_{ref} and β_{ref} are calculated in a least square manner using H_2O and K_2HPO_4 equivalent densities and the 5 mean CT numbers of the phantom ROIs. However, the slope (α_{ref}) and the intercept (β_{ref}) are not the values for CT calibration purposes since the above phantom is solid K_2HPO_4 (not an aqueous K_2HPO_4). The required slope α_{CT} and intercept β_{CT} for vBMD calibration are shown in Equations 3.2 and 3.3, respectively. The offset of - 0.2174 for α_{CT} comes

from physical consideration of the amount of water excluded when adding K_2HPO_4. When K_2HPO_4 is added to a volume of water, the overall volume of the solution increases. That is, K_2HPO_4 displaces some water. The offset of 0.2174 characterises the amount of water displaced by the addition of K_2HPO_4. The offset value of 999.6 for β_{CT} is the physical density of water at room temperature expressed in units of mg/cc.

$$\alpha_{CT} = \alpha_{ref} - 0.2174 \tag{3.2}$$

$$\beta_{CT} = \beta_{ref} + 999.6 \tag{3.3}$$

Finally, the following equation was used to convert every the CT values in the images into volumetric bone mineral density (vBMD).

$$\rho_{unknown} = \frac{\mu_{unknown} - \beta_{CT}}{\alpha_{CT}} \tag{3.4}$$

$where,$

$\mu_{unknown} = HU\ of\ the\ unknown\ materials\ in\ CT\ images$

The above procedure is executed by calling the sub-function QCT_CTcopy.m from the main GUI.

3.2.2 Segmentation and volume generation

A crucial step is to extract the geometric area, in a process called segmentation, from the CT or MRI data for generating finite element model. The segmentation functions of SpineVox-Pro shown in Figure 3.4 were developed in semi-automatic ways.

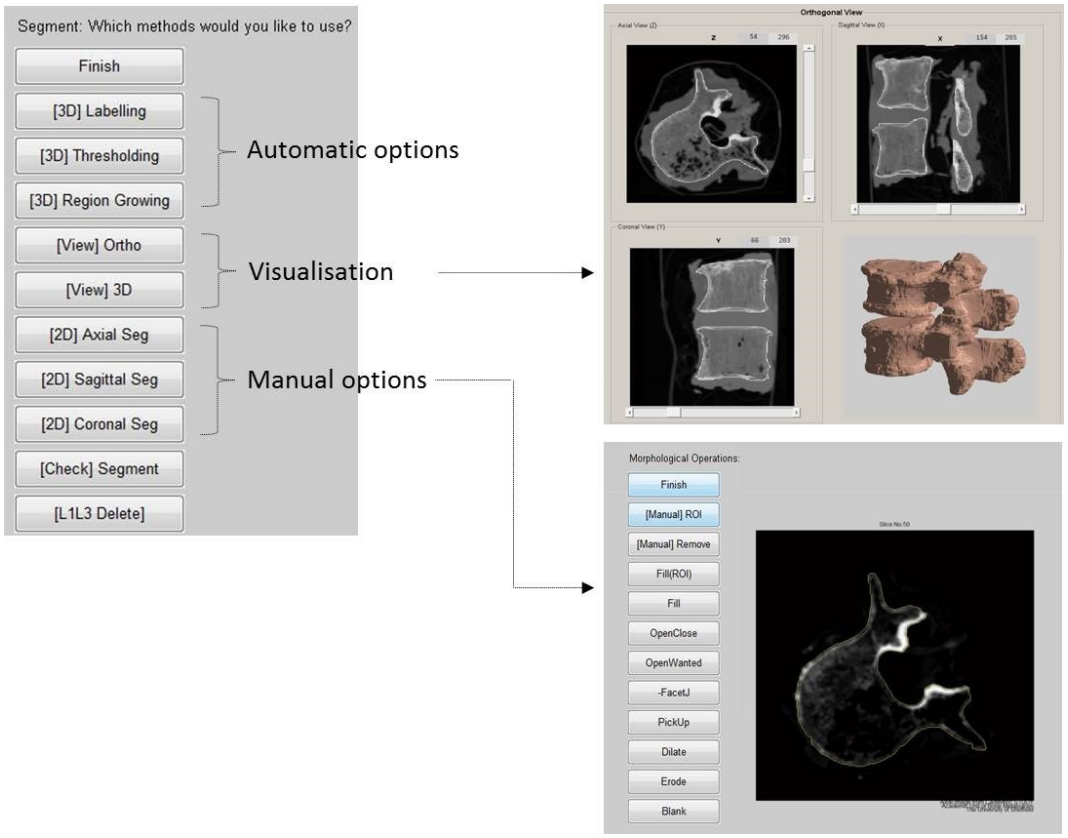

Figure 3.4: SpineVox-Pro V1.1, Automatic and manual segmentation functions with visualisation in SpineVox-Pro

Different options for the segmentation were developed using MATLAB built in functions in the image processing toolbox. The first three buttons of the segmentation options support automatic extraction of bone area: [3D] Labelling, [3D] Thresholding, and [3D] Region Growing. Segmentation is carried out with a combination of a simple thresholding method and automatic labelling of the binary coded values by the MATLAB function. The segmented area can be checked in a three-dimensional view as well as in two-dimensional views of axial, sagittal and frontal planes: [View] 3D, and [View] Ortho as displayed in Figure 3.4. For each image slice, a manual operation is supported to enable the segmented area to be modified on three different sectional views: [2D] Axial Seg, [2D] Sagittal Seg, and [2D] Coronal Seg. The ROI can be added and deleted by manually drawing a closed polygonal area on the axial images: [Manual] ROI, and [Manual] Remove. In addition, the ROI can be modified using morphological operations: open, close, dilate, erode and fill. A manual line option was also added to facilitate

separation of the small gap-like facet joint: - FacetJ. The required closed object can then be selected from amongst several closed segmented areas: PickUp.

MRI data can be segmented in a similar way to the CT image processing procedures to obtain the geometry of the intervertebral disc on axial, sagittal and frontal views. The above procedure is executed by calling the sub-function QCT_Segment.m and MRI_Segment.m from the main GUI.

The segmentation time depends on the CT slice number, the image resolution, and the quality of each image. The average manual segmentation time is approximately 20 minutes per vertebra for typical clinical research scans (0.9375x0.9375x0.625 mm^3; about 170 slices).

3.2.3 Interpolation and re-orientation

The segmented image datasets can be interpolated, if required, to achieve a desired isotropic voxel resolution and to align and merge vertebra and intervertebral disc (IVD) images in a standard orientation as illustrated in Figure 3.5.

The desired voxel resolution can be set by a user-input value and the images are interpolated using a linear method. The orientation angle can be tuned by translating a datum point and rotating a datum line. Once each segmented object are interpolated and aligned to the standard orientation, the segmented vertebrae mask is merged with the IVD mask by matching the centre point of each volume semi-automatic way.

Furthermore, artificial cement paddings with a desired thickness, width, and depth can be generated at the inferior and superior surfaces of the vertebra to mimic the experimental condition, if required (see Chapter 4). The parameters for the rescale and padding limit can be controlled by a user-input value. The above procedure is executed by calling the sub-function QCT_Separate.m/ QCT_Interpolate.m/ QCT_RotateAng.m/ QCT_IVD.m/ QCT_Pad.m from the main GUI.

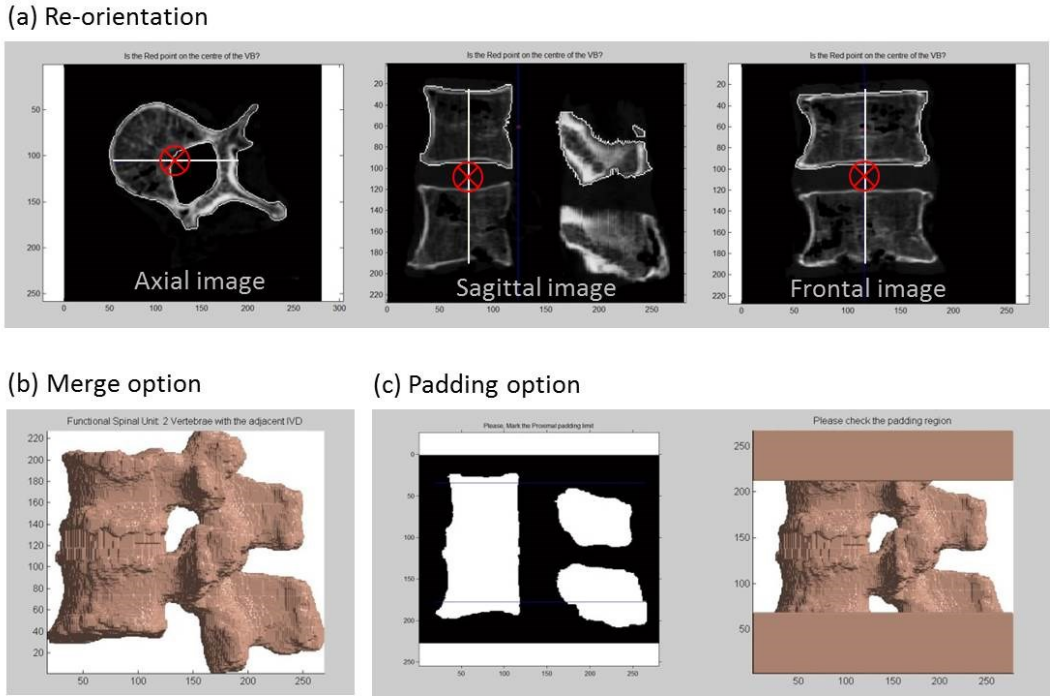

Figure 3.5: SpineVox-Pro V1.1, a) re-orientation; b) merge option; c) padding option of vertebral masks with intervertebral disc mask

3.2.4 Finite Element Voxel Mesh

There are two ways to generate the FE mesh model from the segmented object in SpineVox-Pro: direct voxel mesh generation, and an export/import option using commercial software such as Simpleware ScanIP and +CAD to generate different types of FE mesh model as shown in Figure 3.6. Use of different software packages in this way extends the flexibility of the FE models in terms of generating the mesh, but a few additional steps and several different file formats are required to follow this optional procedure.

The voxel-based meshing technique was adopted for the rest of this work. It is a robust automatic way to generate FE model from CT coordinate information and has been commonly used in hip FE models. A benefit of the automated voxel mesh generation is the application of the correlation between CT values and the elastic moduli. The method is especially useful in the generation of patient-specific finite element models. A MATLAB function QCT2NE.m was developed to convert the segmented scan images to a

finite element model directly. Each voxel is converted into an 8-node hexahedral element (Element type SOLID185 in ANSYS). The element size can be specified as an input variable of the function.

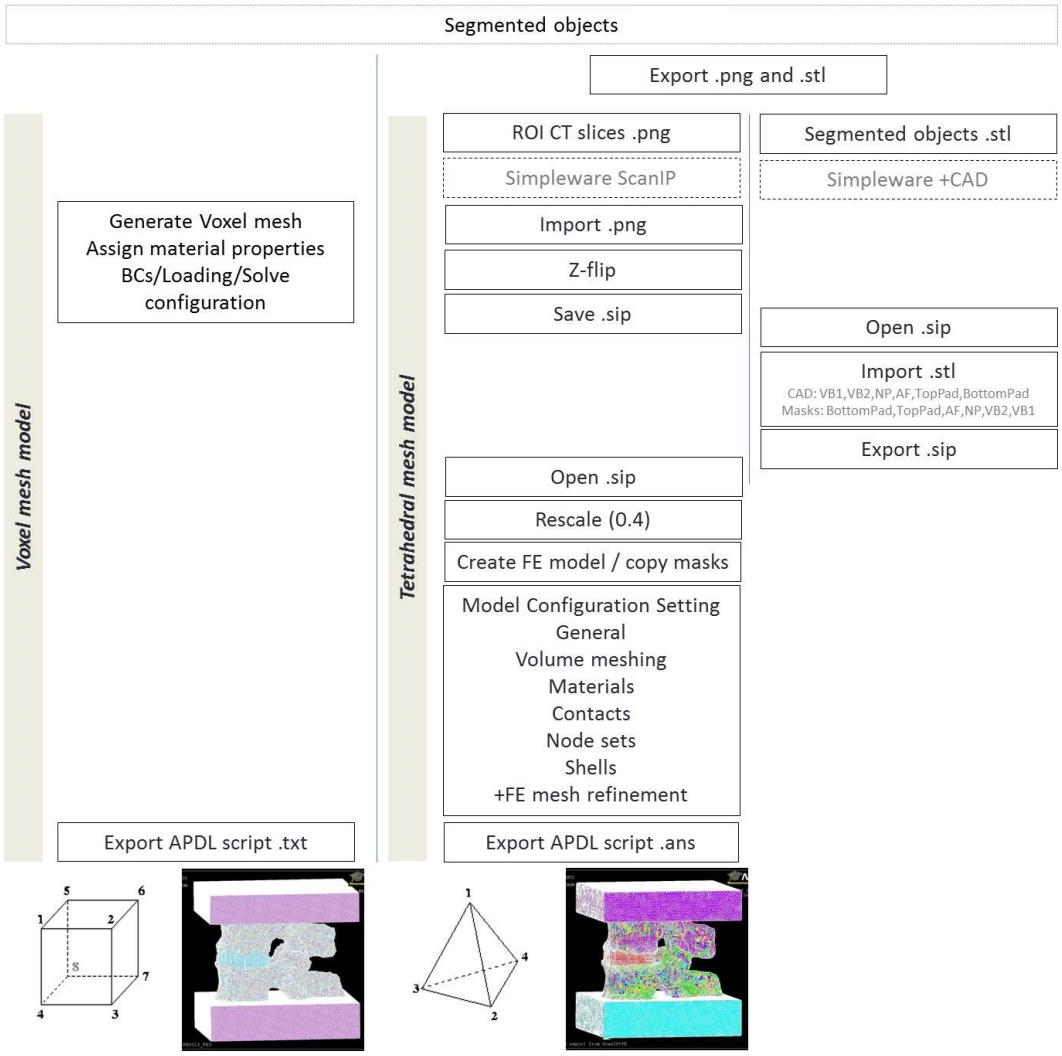

Figure 3.6: SpineVox-Pro V1.1, Voxel mesh and tetrahedral mesh generation

To assign material properties for vertebra, vBMDs of all voxels or elements are divided into one hundred equal intervals. Each voxel or element is categorised into one of these intervals and assigned a unique material number. The newly grouped BMD values are converted to an elastic modulus using one of empirical relationships such as $E\ (MPa) = -34.7 + 3230\rho_{QCT}(g/cm^3)$ (Kopperdahl et al., 2002).

Several different technical methods are supported to implement various types of material properties based on different empirical relationships between volumetric bone density and bone material properties. Figure 3.7 illustrates the procedure for assignment of material properties.

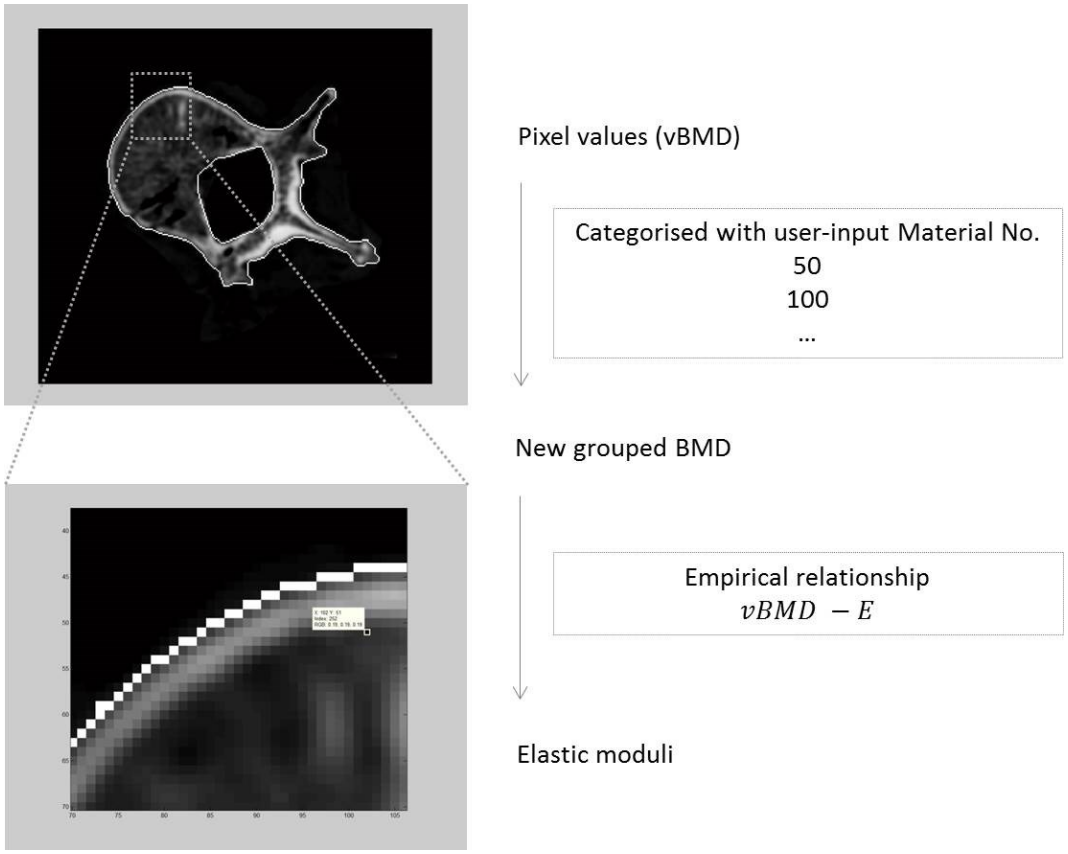

Figure 3.7: SpineVox-Pro V1.1, procedure for material properties assignment

In case of IVD material properties, two different types are available in SpineVox_Pro: a linear elastic material property for the nucleus pulposus (NP) and ground substance of the matrix of the annulus with 4 embedded fibre layers in the annulus fibrosus (AF); and a hyper elastic material property for both the NP and ground substance of the annulus with 4 fibre layers embedded in the AF. The embedded fibres were orientated in alternating layers, 30° and 150° from the horizontal axis (Wang et al., 1997, Schmidt et al., 2006, Strange et al., 2010).

Boundary conditions can be applied with displacement control or force control depending on the specific problem: pure compression, bending, or if considering a physical experimental rig. The above procedure is executed by calling the sub-function QCT_AnsysGen.m/ QCT_BMD2MAT.m from the main GUI.

3.2.5 ANSYS APDL scripts (.batch)

The pre-processing script of ANSYS APDL can be generated and saved in a file by SpineVox-Pro. This script includes all the information required by ANSYS to solve a specific FE problem: i.e. node coordinate information, element connectivity, material properties, boundary conditions and solution options as shown in Figure 3.8.

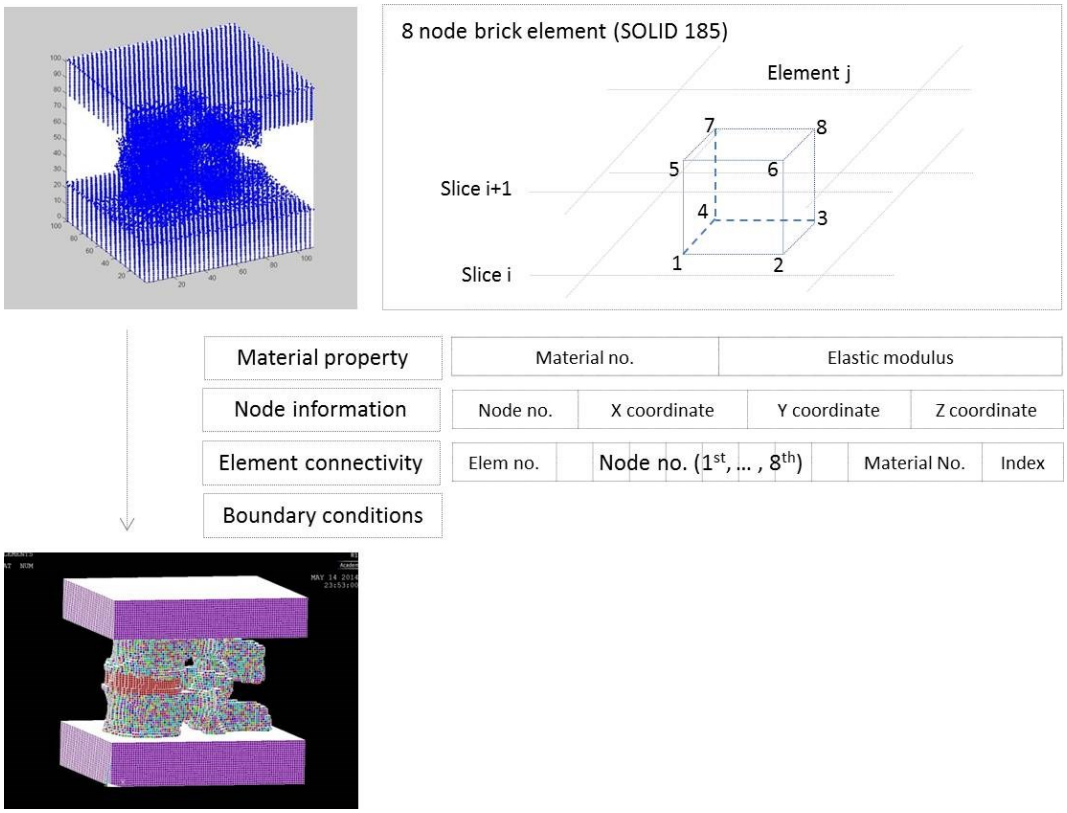

Figure 3.8: SpineVox-Pro V1.1, Generation of the voxel mesh. An ANSYS APDL script includes the material properties and boundary conditions

The script also instructs ANSYS to save the analysis results to files for post-processing by SpineVox-Pro. The finite element analysis can be performed on any computer with ANSYS installed. SpineVox_Pro also supports the 'batch' mode which can run ANSYS without opening the program directly through import/export data triggered by ANSYS APDL scripts. The average simulation, with the large deformation option, typically takes 30 minutes per vertebra FE model (with about 380,000 elements) with ANSYS 14.5 using a parallel option through the INSIGNEO node on Iceberg (Linux based High Performance Computing Cluster, University of Sheffield). The above procedure is executed by calling the sub-function QCT_AnsysScr.m from the main GUI.

3.2.6 ANSYS Results processing

Simulation results such as reaction forces, principal stress and strain values, von Mises equivalent stress and strain values are saved automatically as text files. SpineVox_Pro reads the results and uses the results to calculate fracture strength and to visualise the results in images. Two different types of vertebral strength definition are used in SpineVox_Pro according the analysis options: linear and nonlinear analysis.

For linear analyses, stress or strain ratio is computed for each element using specific yield criteria, i.e., von Mises stress or strain yield criteria.

$$stress\ (strain) ratio = \frac{equivalent\ stress\ (strain)}{element\ yield\ strength} \tag{3.5}$$

In theory, fracture is initiated from the element that has the stress (strain) ratio bigger than 1. The equivalent stress (strain) is based on different yield criteria (see Chapter 4.6). However, failure of one element or a few elements are usually scattered in the vertebra of the FE model, which is sensitive to noise and does not mean a failure of the whole bone. In this regard, a specific volume is used to define the fracture location using a bunch of elements adjacent to each other where the stress ratios are high. For instance, fracture strength based on von Mises stress is defined as: the load that caused minimum von Mises stress exceeding a yield stress, or stress/strain ratio greater than 1, in contiguous elements that occupied at least a volume of 7.5^3 = 422 mm^3, i.e.

approximately 1.5 % of the vertebral body. The larger the volume, the lower the estimated strength.

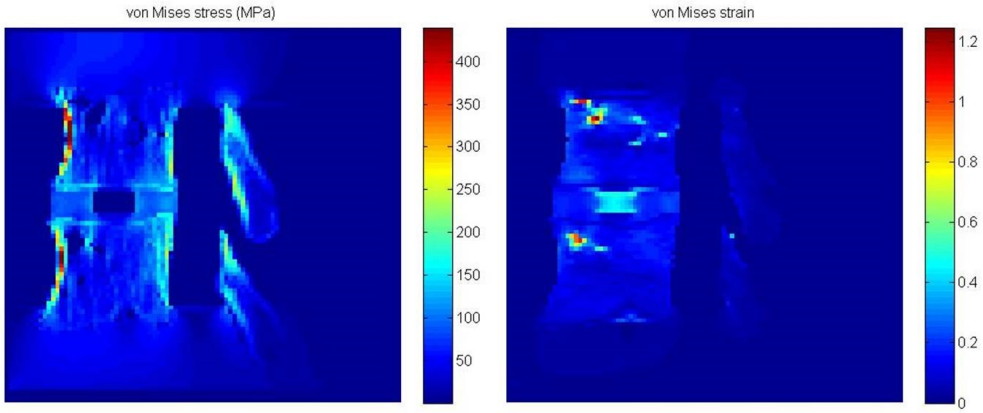

(a) Von Mises stress and strain plots

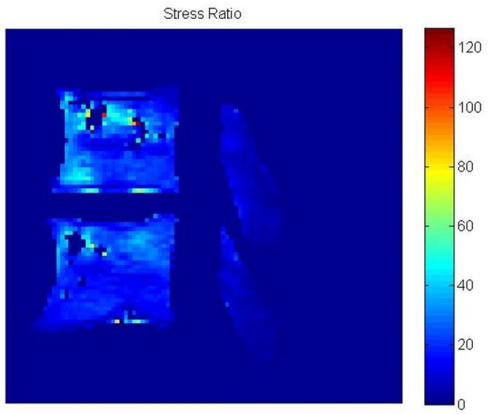

(b) Stress ratio plot

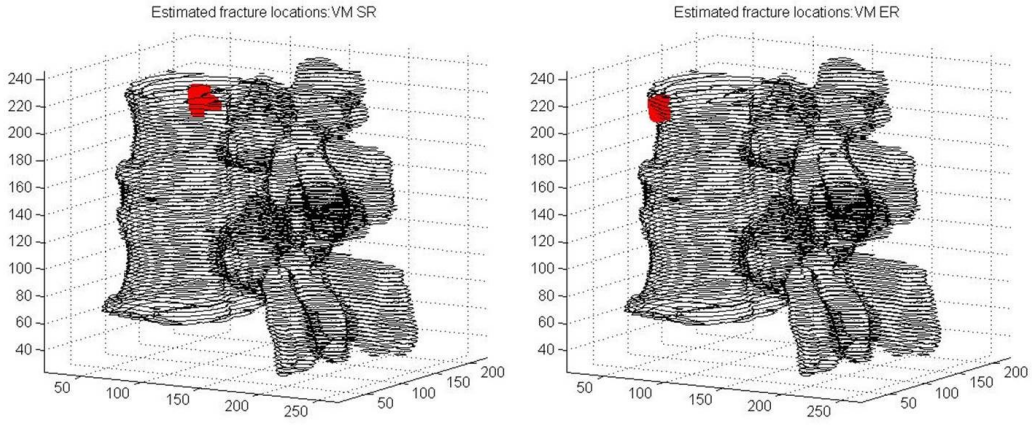

(c) Estimated fracture locations based on: von Mises stress (VM SR) and strain (VM ER) yield criteria

Figure 3.9: SpineVox-Pro V1.1, Post-processing: (a) stress and strain plots, (b) stress ratio plots, (c) estimated fracture locations

Figure 3.9 shows the stress and strain plots, stress ratio plot, and estimated fracture locations in the SpineVox-Pro (MATLAB environment). The predicted fracture locations can be displayed with different yield criteria such as von Mises stress/strain, and Drucker-Prager criteria.

For nonlinear analyses which take into account of the post yield behaviour of the bone, fracture strength is defined on the load-displacement curve: intersection point between 0.2 % offset line from the linear portion of the load-displacement curve and the original load-displacement curve. The 0.2 % offset method is commonly used, if there is no clear yield point. The points plotted in the load-displacement curve represent the results at each step of the non-linear FEA, in which the load was added incrementally. To obtain the load-displacement curve from the result datasets, 6th-order polynomial curve fitting was used. The 0.2% offset line was drawn using the gradient of the initial linear portion of the curve and the displacement value corresponding to 0.2% strain. The final intersection point between the load-displacement curve and the offset line was defined as the yield point.

The load-displacement curve can be displayed automatically with 0.2 % offset line to define the fracture strength in SpineVox_Pro as shown in Figure 3.10.

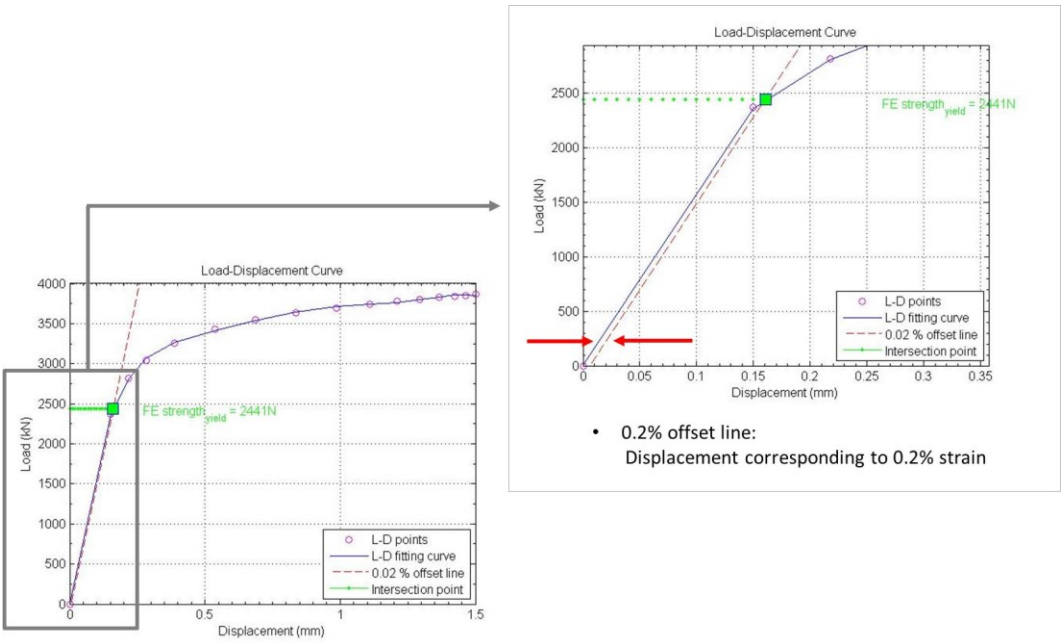

Figure 3.10: A load-displacement curve with 0.2% offset line

The above procedure is executed by calling the sub-function QCT_AnsysRes.m/ QCT_FEstrength.m/ QCT_StrPlot.m from the main GUI.

3.3 Results

SpineVox-Pro supports a full process for image processing of raw medical images and for finite element mesh generation and analysis via patient data acquisition, image processing, voxel mesh generation and ANSYS script generation, and ANSYS post-processing in the single MATLAB GUI. All the steps are automatic without need for user interaction except for the image segmentation which requires minimal user interaction. This maximises both consistency in FE analysis between different patient scans and the precision of repeat analysis of the same scans.

As the segmentation methods are not fully automated, this may be one source of error which may affect the subsequent finite element analysis. For this reason, we conducted a segmentation repeatability test in SpineVox-Pro using clinical research scans. Thirty scans from the Health Outcomes and Reduced Incidence with Zolendronic Acid Once Yearly_Pivotal Fracture Trial (HORIZON_PFT) study and duplicated sets were segmented by the author.

These segmented data were used to assess precision (repeatability). The parameters used for this comparison were; the total volume of the segmented object, the sum of the segmented area, the volumetric BMD, and the sum of areal BMD. The precision was calculated using International Society for Clinical Densitometry (ISCD) advanced precision calculating tool and expressed as a Coefficient of Variation (CV) as shown in Table 3.2.

Table 3.2: Precision- CV (%)

	Total Volume	Sum of ROI area	vBMD	Sum of aBMD
Author	4.1	3.9	1.7	3.1

Whilst there was no clear reference value for CV the coefficient of variation was considered to be a little high (Total volume 4.1%; Sum of ROI area 3.9%; vBMD 1.7%; Sum of aBMD 3.1%). One of main reasons for the large difference of CV is a different image quality in the sample scans. Furthermore, the resolution of HORIZON clinical trial scans is relatively low, and in particular, the slice thickness is much bigger than that used in the most recent clinical research scans (0.9766 x 0.9766 x 2.5 mm^3 HORIZON; 0.9375 x 0.9375 x 0.625 mm^3 for the FORSTEO *in vivo* discussed in Chapter 7; 0.3867 x 0.3867 x 0.3867 mm^3 for the Bristol cadaveric study presented in Chapter 4). Better resolution would improve the CV results. In addition, it should be noted that intra-user reliability studies are recommended and a more robust segmentation method is required.

3.4 Conclusion

A full framework for generating a subject-specific FE model from QCT/ MRI scans was developed and implemented in MATLAB via single GUI called SpineVox-Pro.

Whilst the individual algorithms used are not new, SpineVox-Pro is a novel framework. Although, some user-interaction is required for image segmentation, all the steps are pursued in an automatic way. This maximises consistency in FE analysis across different patient scans and also the precision of repeat analyses on same scans and ultimately this will be used in patient-specific fracture risk estimation.

Since its initial development, SpineVox-Pro was continuously updated during the following studies:

1) For cadaver studies: development of subject-specific FE models of the functional spinal unit (FSU) and validation of the FSU FE model as discussed in Chapter 4, comparison of vertebral strengths from different spinal FE models (vertebral body, vertebra, FSU) as described in Chapter 5.
2) For clinical studies: fracture discrimination and drug treatment studies using clinical research scans as shown in Chapters 6 and 7.

CHAPTER 4 Development and Validation of a Subject-specific Finite Element Model of the Functional Spinal Unit

This chapter proposes a subject-specific Functional Spinal Unit (FSU) FE model to determine vertebral fracture strength under more physiological conditions. A subject-specific FSU FE model based on QCT and MRI data sets was developed in SpineVox-Pro and the FSU FE model was validated with the experiment.

4.1 Introduction

Finite element analysis of QCT scans integrates information about *in vivo* loading conditions with the data on bone geometry and density distribution embedded in the scans. This allows stress and strain to be calculated non-invasively to determine bone strength. Many researchers have developed continuum finite element models of the vertebral body without posterior elements to assess vertebral strength under pure compressive loading and these models are well validated (Melton et al., 2007, Silva Matthew J., 1998, Homminga, 2001, Crawford et al., 2003a, Crawford et al., 2003b, Crawford RP, 2004, Keaveny et al., 2007, Buckley et al., 2007b, Liebschner et al., 2003, Kopperdahl et al., 2000, Imai et al., 2006, Imai et al., 2009, Lewiecki, 2009, Chevalier et al., 2010, Zeinali et al., 2008, Chevalier et al., 2008, Chevalier Y, 2009, Zeinali et al., 2010). Although many vertebral FE models have been described in the literature, only one-QCT-based voxel FE model has been well used as a research tool in clinical osteoporosis studies (Keaveny et al., 2007, Melton et al., 2007). This FE model is used to investigate

vertebral strength under pure compressive loading which is generally representative of the standing posture.

As the primary loading of the human vertebral body is asymmetrical, an anterior wedge fracture is the most frequent type of osteoporotic fracture (Eastell et al., 1991, Wasnich RD, 1996, Jackson S.A., 2000). For this reason, the forward bending needs to be considered with greater loads on the anterior part of the vertebrae. Load on the vertebrae is not transferred directly through vertebral body but via the intervertebral disc and facet joints. Whilst the exact mechanism of load transfer to the vertebrae is not, as yet, completely understood, degeneration of the IVD, is known to affect the loading conditions and fracture patterns in adjacent vertebrae (Pollintine et al., 2004a, Adams and Dolan, 2005, Pollintine et al., 2004b). The boundary conditions under forward bending for load transfer through the IVD and facet joint cannot be represented on an FE model of the vertebral body alone. For this reason, a functional spinal unit (FSU) or spinal motion segment (SMS) model has been proposed. The FSU consists of two adjacent vertebrae with the intervertebral disc and all adjoining ligaments and is the smallest physiological motion unit of the spine that can represent biomechanical characteristics close to those of the entire spine. The FSU model has been investigated under compression and flexion loading conditions (Wang et al., 1997, Natarajan et al., 2003, Cheung et al., 2003, Polikeit et al., 2004, Rohlmann et al., 2006, Shirazi-Adl et al., 1984, Goto et al., 2002). Previous studies using generic FSU FE models generally focus on influence of intervertebral disc degeneration on biomechanical behaviours such as the range of motion, and the intervertebral disc pressure. As yet, there has been no investigation of vertebral strength using a subject-specific FSU FE model.

The aim of this chapter is to propose a subject-specific FSU FE model to determine vertebral fracture strength under more physiological conditions such those experienced in forward bending. The objectives were to; first, develop a subject-specific FE model of the FSU based on QCT and MRI data sets in SpineVox-Pro (developed and described as in Chapter 3), and validate the FSU FE model against experimental data.

4.2 Methods

4.2.1 Specimen preparation

Eight thoracolumbar spines (T11-L5) were obtained from cadavers (Female = 5, Male = 3; 74 - 97 years old) that had been donated for medical research.

The *in vitro* experiment was approved by the South West REC 5 (Frenchay) (REC Ref No. 10/H0107/27) at the Centre for Comparative and Clinical Anatomy, University of Bristol.

Table 4.1 summarises the FSU level, BMD, age, sex, and disc degeneration status information of sixteen FSUs. Two FSUs were dissected from each cadaveric spine. Prior to mechanical testing, the frozen specimens were sealed in plastic bags and transported to the University of Sheffield in a dry ice box for scanning as shown in Figure 4.1. The specimens were stored at -20 C° and defrosted at +4 C° prior to scanning.

Figure 4.1: One of dissected functional spinal units in sealed bag

Table 4.1: Basic information of specimen; data from University of Bristol

FSU no.	Spine Index	FSU Level	BMD (mg/cm^2)		Age	Sex	Disc Degeneration (Adams: scale 1-4)
			Top	Bottom			
0001	2710v	T12-L1	16.88	19.67	90	M	4
0003	2710k	L2-L3	11.20	16.30	90	M	4
0005	6211k	L2-L3	7.88	7.37	84	M	2
0007	6211v	L4-L5	13.95	-	84	M	2
0009	6811k	L1-L2	3.19	5.84	98	F	2
0011	6811v	T11-T12	2.31	2.65	98	F	2
0013	7011k	L1-L2	15.00	20.22	74	F	3
0015	7011v	L3-L4	19.11	40.62	74	F	4
0017	7509k	L1-L2	31.30	30.82	84	M	3
0019	7509v	T11-T12	13.29	17.93	84	M	4
0021	8911v	L3-L4	16.80	13.37	89	F	3
0023	8911k	T11-T12	3.07	4.30	89	F	3
0025	9311v	L1-L2	6.38	11.21	88	F	2
0027	9311k	L3-L4	11.64	28.89	88	F	4
0029	10211k	L3-L4	6.11	8.94	97	F	3
0031	10211v	L1-L2	7.44	6.73	97	F	3
Mean			11.60	15.66	88		
SD			7.47	10.97	7.43		
SE			1.87	2.83	1.86		

* Specimens were labelled for k (kyphoplasty) and v (vertebroplasty)

The specimens were scanned using a clinical QCT machine (LightSpeed VCT, GE Medical Systems, 120kV, 60 mAs/slice, 0.3867 x 0.3867 x 0.3867 mm^3) at the Northern General Hospital, Sheffield by a CT team member. A solid calibration phantom (Mindways Software Inc., San Francisco, CA) was used to calibrate Hounsfield unit (HU) values to bone mineral density. Furthermore, the samples were scanned with MRI (MAGNETOM Avanto, SIEMENS AG, Germany) by a MRI team member at the Northern General Hospital, Sheffield. Several series of scan sets were obtained in axial and sagittal views using different settings of echo time (TE), repetition time (TR), and T1 weighted or T2 weighted images. After examining the data, one specific condition was chosen to obtain the geometry of the IVD. This was as follows: TE=20, TR=2000, T1 SE Axial, 0.85938 x 0.85938 x 3 mm^3.

Both QCT data sets and MRI data sets were used to develop the FSU finite element model in this research.

4.2.2 Bone Mineral Density

Before testing, the bone mineral content (BMC) and bone mineral density (BMD) of each vertebral body was measured using dual energy X-ray absorptiometry (PIXImus densitometer, Lunar Corp., Madison, WI, USA).

4.2.3 *In vitro* Experiment

The *in vitro* experiments were performed by Dr. P Landham, Prof. M Adams and Dr. T Dolan at the Centre for Comparative and Clinical Anatomy, University of Bristol. As a part of Dr. Landham's Degree of MD, they conducted an *in vitro* experimental study with the aim of determining whether kyphoplasty has any advantages over vertebroplasty in terms of its ability to restore vertebral shape and biomechanical function after severe vertebral wedge fracture.

The experiments consisted of two stages: the generation of a vertebral wedge fracture, and kyphoplasty or vertebroplasty. The results from the initial fracture part of the experimental study provided the validation data used in this thesis.

The experimental tests using a computer-controlled hydraulic material testing machine (Dartec-Zwick-Roell, Leominster, UK) were performed at the Spine Biomechanics Laboratory, University of Bristol and are described in detail by Luo et al (Luo et al., 2010). The test setup is shown in Figure 4.2 and the procedures are described briefly here.

The metal specimen holders were attached to baseplates and loaded via low-friction rollers attached to the upper base plate; the angle of the upper plate could be varied to allow complex loading to be applied to the FSU. Each FSU was positioned in flexion in order to simulate a stooped posture.

The FSU was then compressed at a rate of 3mm/s for 1.25 s while a graph of compressive load versus displacement was plotted in real time as shown in Figure 4.3.

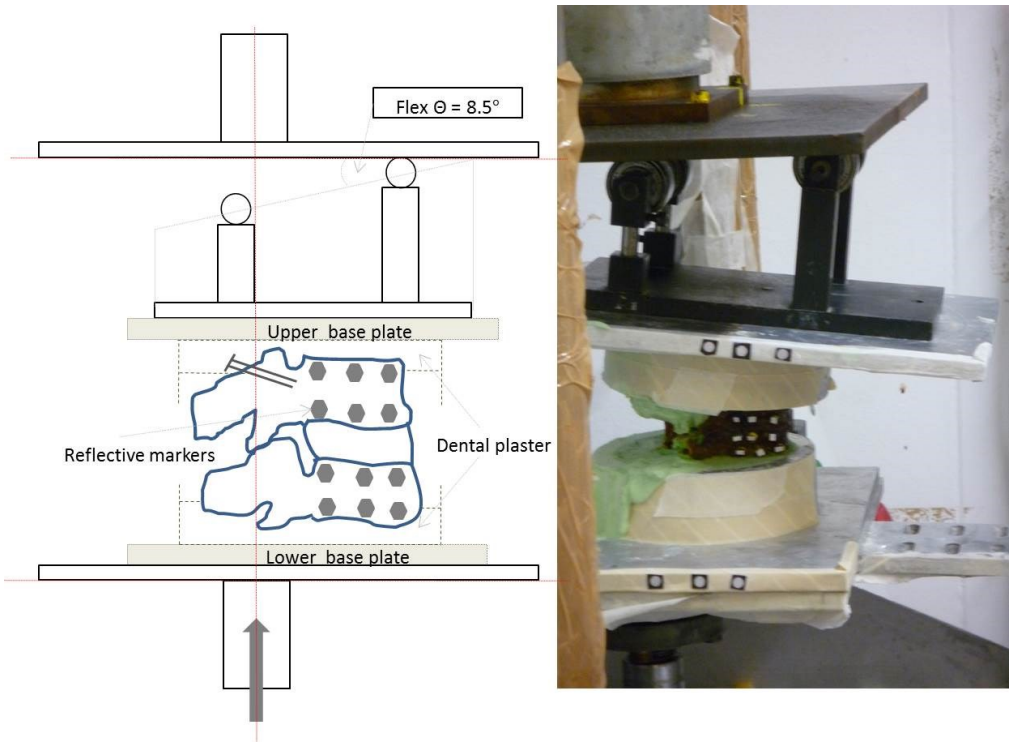

Figure 4.2: Schematic view and photograph of the experimental test and experimental apparatus

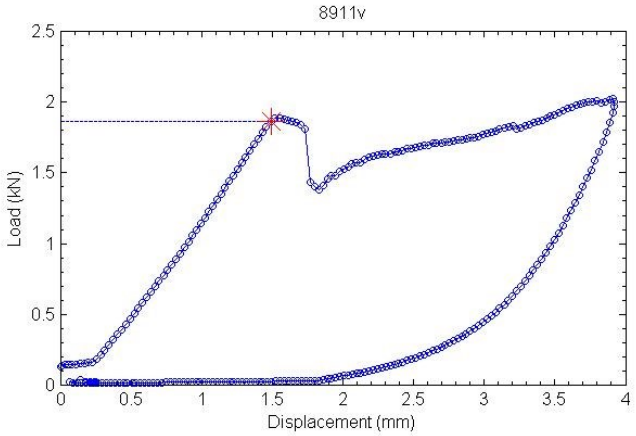

Figure 4.3: Load-displacement curve from the experimental test (Full load-displacement datasets can be found in Appendix B)

Fracture was detected from a reduction in gradient (stiffness) on the load-displacement curve. The compressive force applied at this point was recorded as the yield strength as shown in Table 4.2. The full load-displacement datasets can be found in Appendix B. This loading technique usually creates an endplate fracture, often accompanied by fracture of the anterior cortex, of a single vertebra within the FSU (Luo et al., 2010). The fracture location was identified by taking a lateral radiograph, and was subsequently confirmed by dissection.

Table 4.2: Results of mechanical testing carried out at the University of Bristol

FSU no.	Spine Index	FSU Level	Fracture Level Top/Bottom	Fracture Load (kN)
0001	2710v	T12-L1	T	1.104
0003	2710k	L2-L3	T	1.600
0005	6211k	L2-L3	B	1.180
0007	6211v	L4-L5	B	1.685
0009	6811k	L1-L2	T	1.663
0011	6811v	T11-T12	T	1.708
0013	7011k	L1-L2	T	3.090
0015	7011v	L3-L4	T	4.412
0017	7509k	L1-L2	B	3.399
0019	7509v	T11-T12	B	2.906
0021	8911v	L3-L4	B	1.861
0023	8911k	T11-T12	T	1.194
0025	9311v	L1-L2	T	1.930
0027	9311k	L3-L4	B	2.215
0029	10211k	L3-L4	B	Test failure
0031	10211v	L1-L2	T	1.319
Mean				2.086
SD				0.924
SE				0.231

* Specimens were labelled for k (kyphoplasty) and v (vertebroplasty)

4.2.4 Development of FSU FE model in SpineVox-Pro

SpineVox-Pro was used to generate a subject-specific finite element model of the FSU. The program was developed in MATLAB (Mathworks Inc., Natick, MA, USA) and used

ANSYS APDL (ANSYS Inc., Canonsburg, PA, USA) and explained in the previous chapter 3. A brief description of the full procedure is presented below. The workflow used is illustrated in Figure 4.4.

CT and MRI scan data in DICOM format (.dcm) were converted into MATLAB format (.mat). The CT data were converted from Hounsfield Units to density values after calibration using hydroxyapatite phantom (Mindways Software Inc., Austin, TX, USA), K_2HPO_4 equivalent densities. The converted CT/MRI images were used to extract the vertebra and intervertebral disc area.

In SpineVox-Pro, the initial segmentation of the vertebra was carried out with thresholding and the label function automatically. Manual segmentation options were used to modify the segmented area on each slice after the automatic segmentation areas were checked in both three-dimensional and two-dimensional views. Manual drawing and morphological operations like open, close, dilate, erode and fill are available in 2D. The MRI data was also segmented in a similar way in order to obtain the geometrical information for the IVD.

The vertebral component was separated into two independent vertebrae after segmentation. The image objects of the two vertebrae and the IVD were interpolated to achieve the desired resolution of 1.2 x 1.2 x 1.2 mm^3. These were then aligned and merged to form a FSU, and then rotated if necessary to a standard orientation in order to apply the correct boundary conditions. In addition, artificial cement paddings, 15 mm thickness, were generated at the inferior surface of the inferior vertebra and at the superior surface of the superior vertebra to mimic the experiment condition. The size and position of the cement padding can be controlled by thickness, width, and depth with the centre point. The re-oriented and merged FSU was directly converted to a finite element model with each voxel being converted into an 8-node hexahedral element (Element type SOLID185 in ANSYS).

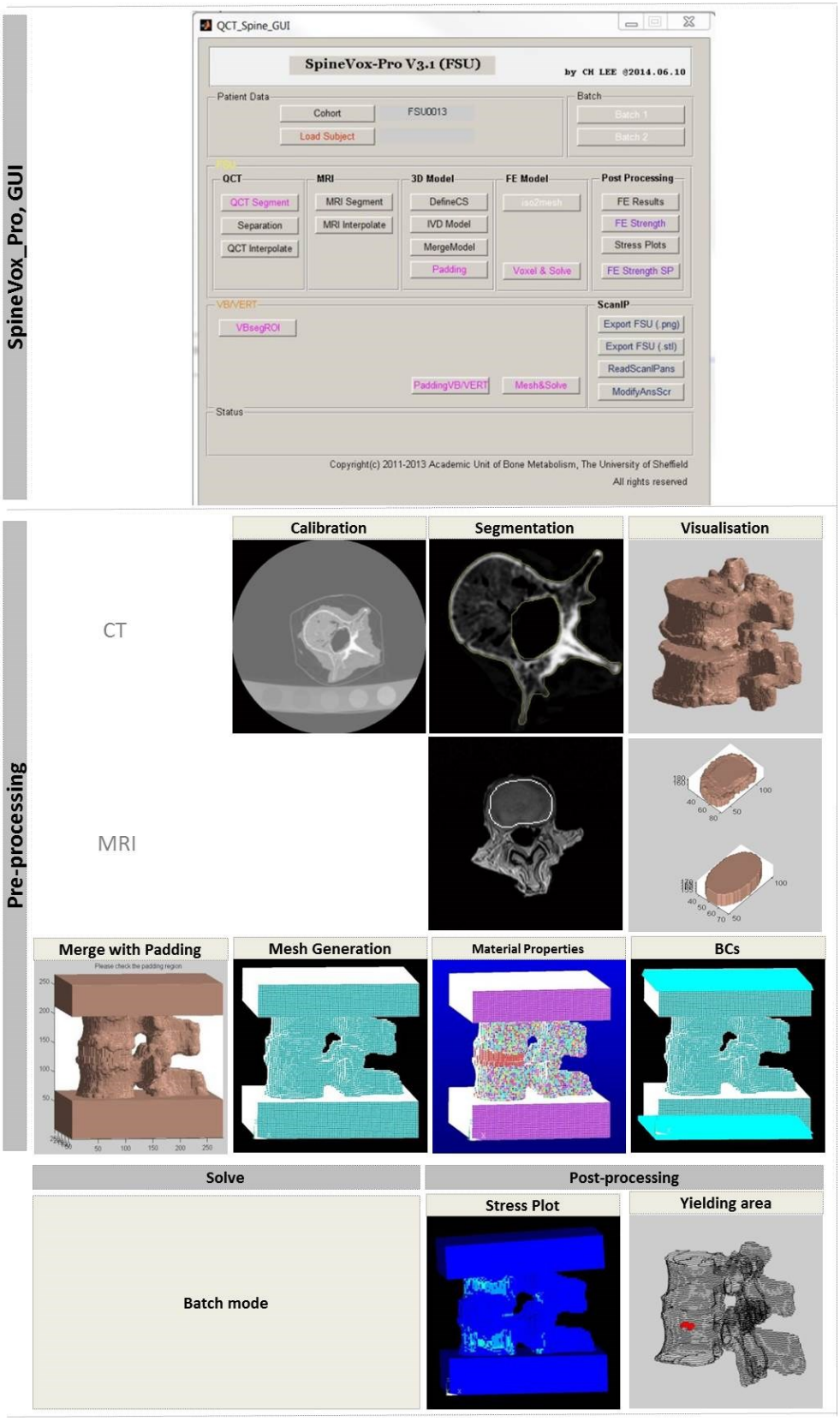

Figure 4. 4: SpineVox-Pro, the workflow for the creation of a subject-specific finite element model of functional spinal unit

Table 4.3 summarises the material properties that were used for the vertebrae and IVD in this research. Transversely isotropic linear-elastic material properties were considered for the vertebra. The vertebra, including the vertebral body and posterior elements, was modelled as transversely isotropic material, that is, material properties in the longitudinal direction are different from in the transverse direction. The properties in the transverse plane are direction-independent. Cortical and trabecular bones were not modelled separately, since the resolution of the clinical QCT scans in this study could not distinguish the cortical shell. To assign longitudinal material properties for the vertebra, empirical relationships between volumetric bone density (ρ_{QCT}, g/cm^3) and bone material properties were used to determine the longitudinal elastic modulus (E_z, MPa) and compressive yield stress limit (σ_{yc}, MPa) (Kopperdahl et al., 2002). The original volumetric BMD values were divided into 100 intervals to limit the number of materials in the FE model. The remaining material properties in the transverse plane were defined by assuming fixed ratios of the elastic constants with respect to the longitudinal elastic modulus. The Poisson's ratios, $\nu_{xy} = 0.381$ and $\nu_{xz} = \nu_{yz} = 0.104$ were assigned. The ν_{xy} expresses the strain in the y-direction divided by the strain in the x-direction in response to a load in the x-direction (Ulrich et al., 1999). Values for the tensile yield stress limit σ_{yt} (Keaveny et al., 1994), ultimate stress limit σ_{uc} (Crawford et al., 2003a, Morgan and Keaveny, 2001), yield strain limit ε_y (Kopperdahl et al., 2002), and ultimate strain limit ε_u (Morgan et al., 2003) of the vertebra were assigned from the literature. In the case of the IVD data, it is difficult to obtain information for mechanical subject-specific properties except qualitative information from water content. For this reason, simple homogeneous linear-elastic properties were assigned to the nucleus pulposus and annulus fibrosus, taken from the literature (Denozière and Ku, 2006).

The mechanical properties of the dental cement used for the artificial padding were obtained from the manufacturer's manual ($E = 2000\,MPa, \nu = 0.3$; Ultrahard Die Stone ISO-Type IV, Kerr).

Table 4.3: Assigned material properties of the FSU model; vertebra, IVD, and padding

Part	Properties	References
Vertebra	$E_z\ (MPa) = -34.7 + 3230\rho_{QCT}\ (g/cm^3)$	Kopperdahl et al. 2002
	$E_x\ (MPa) = E_y = 0.333E_z$	
	${\nu_{xy}}^1 = 0.381$	
	${\nu_{xz}}^1 = {\nu_{yz}}^1 = 0.104$	Ulrich et al. 1999
	$G_{xz}\ (MPa) = G_{yz} = 0.157E_z$	
	$G_{xy}\ (MPa) = \frac{E_x}{2(1+\nu_{xy})} = 0.121E_z$	
	$\sigma_{yc}\ (MPa) = -0.75 + 24.9\rho_{QCT}\ (g/cm^3)$	Kopperdahl et al. 2002
	$\sigma_{yt}\ (MPa) = \sigma_{yc} * 0.79$	Keaveny et al. 1994
	$\sigma_{uc}\ (MPa) = 1.2 *\ \sigma_y$	Crawford 2003; Morgan and Keaveny 2001
	$\varepsilon_y = 0.0078$	Kopperdahl et al. 2002
	$\varepsilon_u = 0.145$	Morgan et al. 2003
Padding	$E = 2000\ MPa$	Lewis 1997
	$\nu = 0.3$	
IVD	$E_{NP} = 8\ MPa$	Denoziere and Ku 2006
	$\nu_{NP} = 0.499$	
	$E_{AF} = 500\ MPa$	Denoziere and Ku 2006
	$\nu_{AF} = 0.3$	

4.2.5 Boundary conditions

A simple, pure compression and a forward bending condition can both be simulated using SpineVox-Pro. A forward-bending loading condition (theta ° = 8.5°) was simulated to represent the mechanical test as shown in Figure 4.5. Two sets of boundary conditions for the forward bending condition were investigated. The first were those associated with a simplified rig, and the second with generating the experimental rig explicitly in detail as described in Appendix C. The simplified rig condition was used in this chapter.

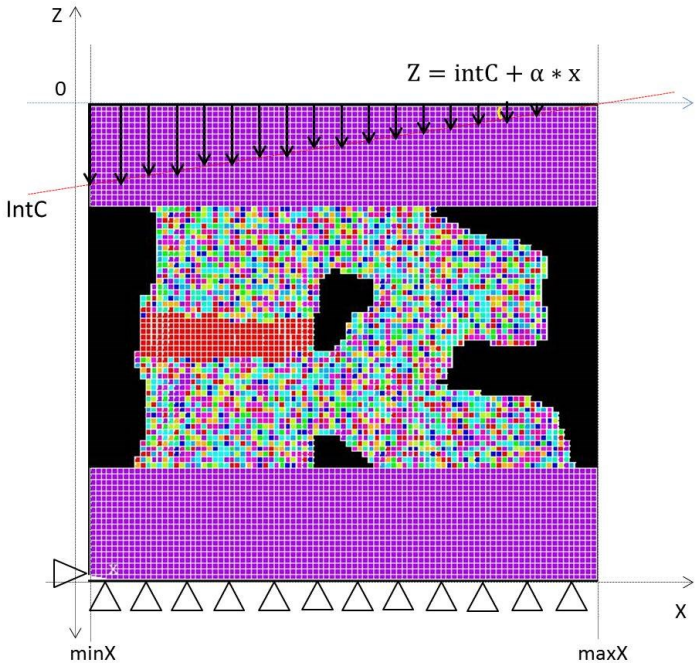

Figure 4.5: Simplified rig for forward bending condition; ramped displacement applied (Purple: Upper and lower padding parts; Red: IVD part; Mixed colours: vertebral bone material number based on assigned Young's modulus)

The inferior surface of the lower padding was constrained for all degrees of freedom, and tilted displacement boundary conditions were applied at the superior surface of the upper padding. FE models were solved using a commercial software package, ANSYS (ANSYS Inc., Canonsburg, PA, USA) in the batch mode of SpineVox-Pro. Whilst both, linear and nonlinear options could be selected, for the work carried out in this chapter, only the linear option was used.

4.2.6 Vertebral strength using different yield criteria

In FE studies of bone fracture in the literature, isotropic yield criteria such as von Mises and Drucker-Prager theories are commonly used to investigate the yield limits of the femur (Keyak and Rossi, 2000, Bessho et al., 2007, Yosibash Zohar, 2010). Keyak and Rossi (2000) investigated the failure load of the hip under stance-, and fall-, loading conditions using nine-different failure theories: Distortion energy, Hoffman, strain-based

Hoffman, maximum normal stress and strain, maximum shear strain and stress, Coulomb-Mohr, and modified Mohr failure theory. They found that the distortion energy and maximum shear stress had a strong correlation with the experimental results for both loading conditions (Keyak and Rossi, 2000). Yosibash (2010) investigated predicted hip strength with isotropic and orthotropic material properties and four different yield criteria: von Mises, Drucker-Prager, and maximum principal stress and strain (Yosibash Zohar, 2010). Unfortunately, since only one experimental femur was used, the work does not provide sufficient evidence for the conclusion to be used here.

In order to establish the best suitable yield criterion for vertebral strength in the FSU FE model, estimates of yield strength from finite element models of FSU under forward-bending condition with linear analysis were compared using six different isotropic yield criteria as follows:

1) von Mises stress (VM SR): the load that caused the minimum von Mises stress exceeding a yield stress in contiguous elements that occupied at least a volume of 422 mm^3
2) von Mises strain (VM ER): the load that caused the minimum von Mises strain exceeding a constant yield strain of 0.78% in contiguous elements that occupied at least a volume of 422 mm^3
3) Drucker-Prager stress (DP SR): the load that caused minimum Drucker-Prager stress exceeding a yield stress in contiguous elements that occupied at least a volume of 422 mm^3
4) Maximum principal stress (MX SR): the load that caused minimum of maximum principal stresses exceeding a yield stress in contiguous elements that occupied at least a volume of 422 mm^3
5) Maximum principal strain (MX ER): the load that caused the minimum of maximum principal strains exceeding a constant yield strain of 0.78% in contiguous elements that occupied at least a volume of 422 mm^3
6) Maximum shear stress (CM SR): the load that caused the minimum of maximum shear stresses exceeding a yield stress in contiguous elements that occupied at least a volume of 422 mm^3

In the post-processing step of SpineVox-Pro, vertebral strength can be calculated with the above yield criteria. The equivalent stress for yield criteria which were used in this study are summarised in Appendix D.

The final results were visualised in SpineVox-Pro with the calculated strength based on the above yield criteria, the stress and strain plot, and the estimated fracture locations. Figure 4.6 and 4.7 shows one example of the predicted fracture locations.

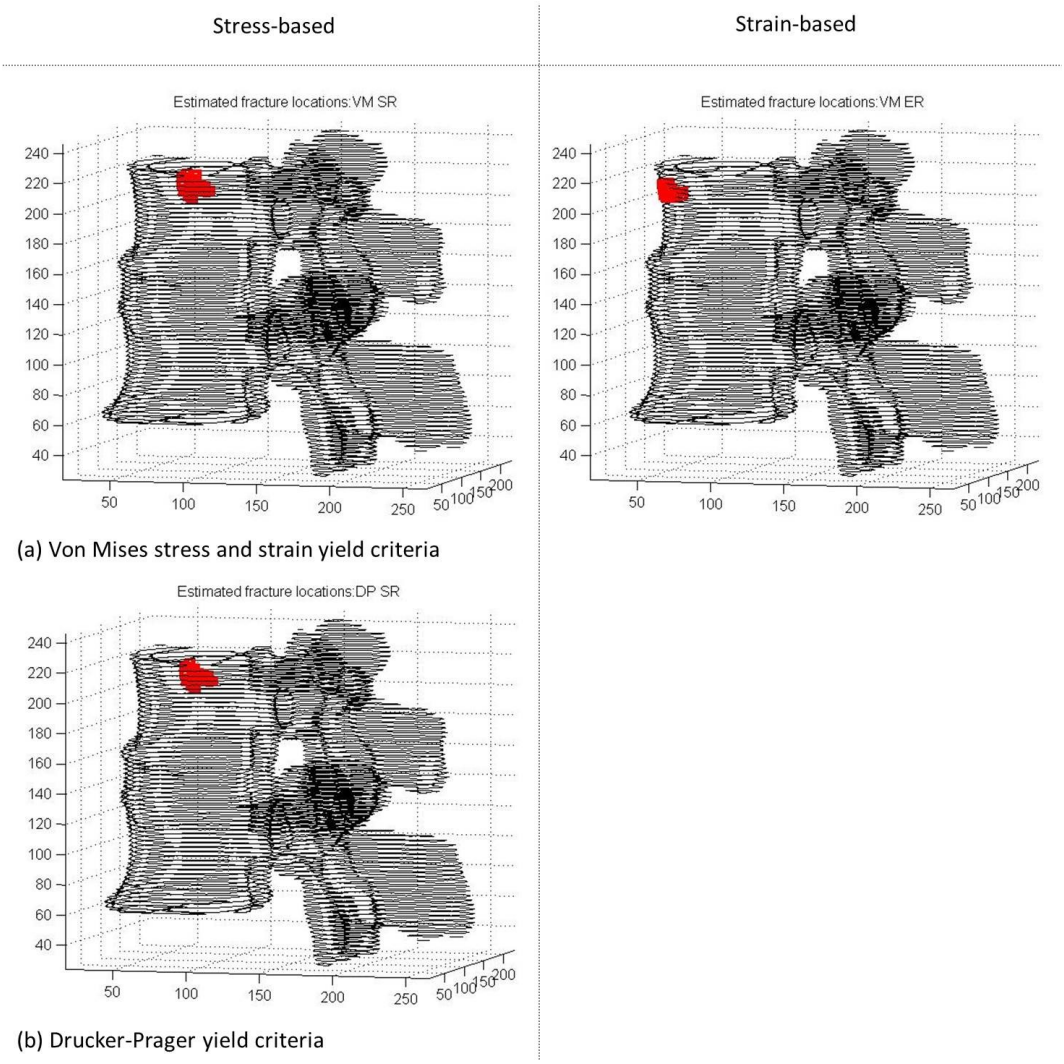

Figure 4.6: SpineVox-Pro, estimated fracture locations using six different yield criteria: a) von Mises stress and strain; b) Drucker-Prager yield criteria

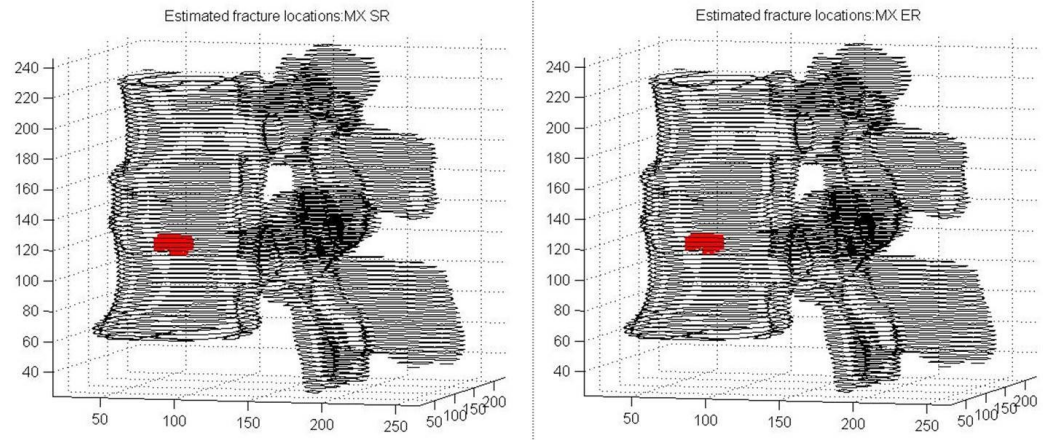

(c) Maximum principal stress and strain yield criteria

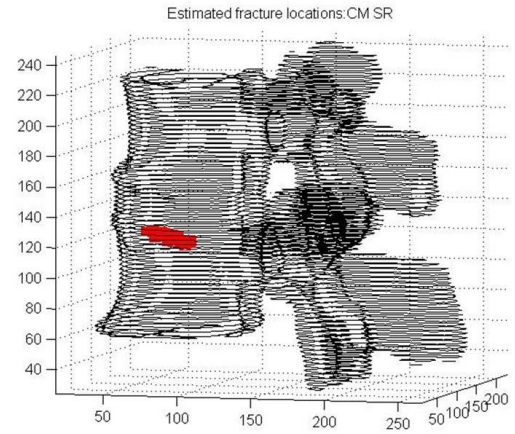

(d) Coulomb-Mohr yield criteria

Figure 4.7: SpineVox-Pro, estimated fracture locations using six different yield criteria: c) Maximum principal stress and strain; d) Coulomb-Mohr yield criteria

4.3 Results

Linear regression analysis was performed for both the FE- and experiment-derived vertebral strength. Two specimens (No.0009, 0011) were excluded from the analysis due to poor image quality and one specimen (No. 0029) was discarded due to failure of the experimental test. A typical FE simulation took approximately 20 minutes of CPU time on 3.6 GHz Intel core i5 CPU with 8GB RAM (about 380,000 elements).

Simple isotropic material properties were considered in order to maintain the consistency of the models, because the strength was defined by von Mises isotropic yielding theory.

A positive correlation was found between strength measured by experiment and the strength predicted by the FSU FE model for all failure criteria ($p < 0.001$) as shown in Table 4.4.

Table 4.4: Linear regression analysis between Experiment- and FE-derived strength (six-different yield criteria)

Yield Criteria		Isotropic mat.		Transversely isotropic mat.	
		*Y=Slope*x+Intercept*	R^2	*Y=Slope*x+Intercept*	R^2
Von Mises Stress	VM SR	$1.08 * x + 477.06$	0.86	$1.25 * x + 453.16$	0.87
Von Mises Strain=0.78%	VM ER	$0.86 * x + 163.13$	0.86	$1.09 * x + 125.11$	0.80
Drucker-Prager Stress	DP SR	$0.94 * x + 587.31$	0.86	$1.11 * x + 535.35$	0.85
Max. Normal Stress	MX SR	$0.16 * x + 900.68$	0.71	$0.21 * x + 134.67$	0.88
Max. Normal Strain=0.78%	MX ER	$0.16 * x + 531.63$	0.74	$0.46 * x + 240.59$	0.78
Coulomb-Mohr Stress	CM SR	$0.11 * x + 790.67$	0.57	$0.06 * x + 984.87$	0.54

Vertebral strength based on von Mises stress ($R^2 = 0.86$ VM SR Iso; $R^2 = 0.87$ VM SR Trans) and strain ($R^2 = 0.86$ VM ER Iso; $R^2 = 0.80$ VM ER Trans) yield criteria showed the strongest correlation with the experimentally determined yield strength of the FSU. In addition, the Drucker-Prager stress criterion also showed strong correlation with experimental results ($R^2 = 0.86$ DP SR Iso; $R^2 = 0.85$ DP SR Trans).

According to the results of this study for the FSU FE model, the strength based on von Mises yield criteria showed better correlation with the experimental strength ($R^2 = 0.80$ - 0.87) when compared to the areal BMD ($R^2 = 0.54$) by DXA as shown in Figure 4.8.

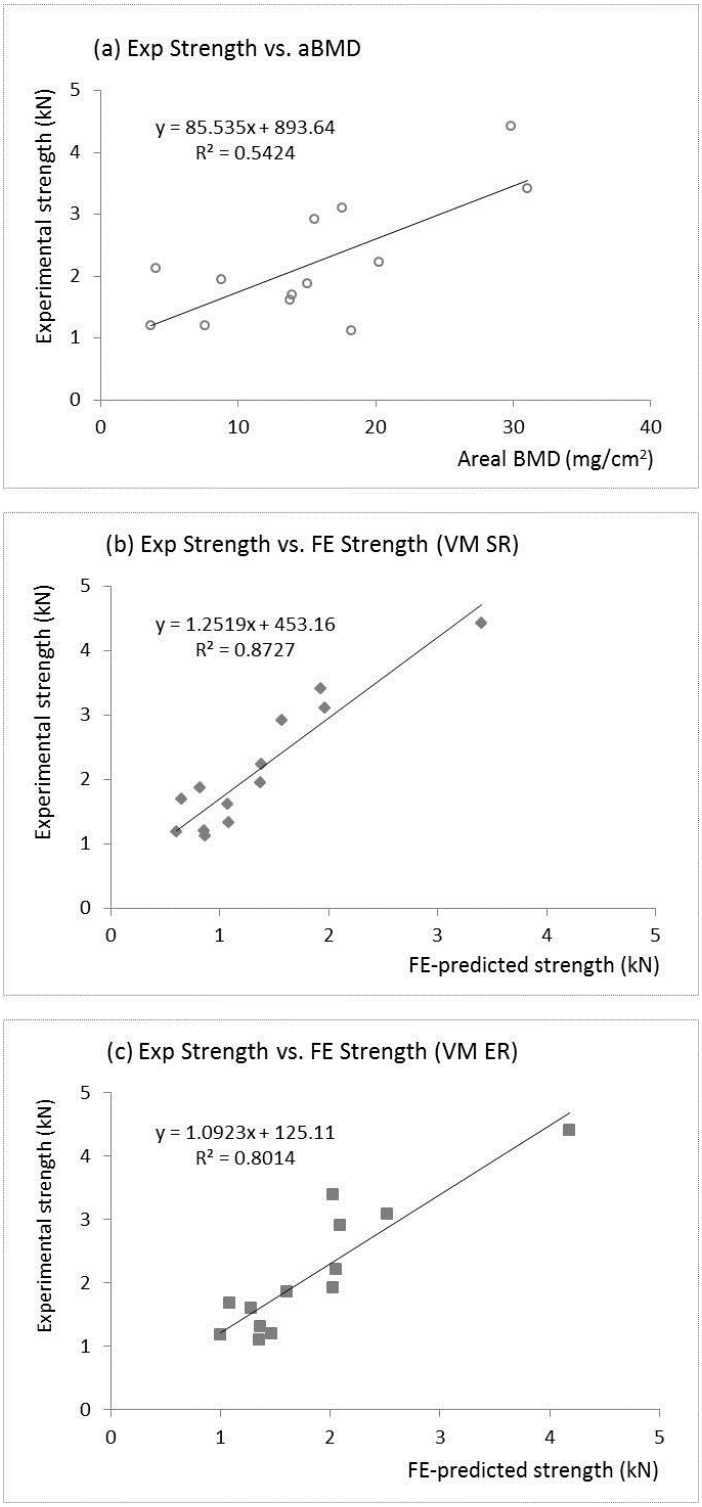

Figure 4.8: Linear regressions ($p < 0.001$) of the experimental vertebral strength as a function of (a) areal bone mineral density by DXA (b) FSU FE derived strength based on von Mises stress (c) FSU FE derived strength based on von Mises strain

There is one extreme outlier (FSU0015) it weigh the correlation power between the FE analysis and the experiment. If the value was omitted from the result, the correlation coefficient is a bit lower than the original results (0.87 -> 0.81 VM SR; 0.80 -> 0.68 VM ER). In this regard, Spearman's rank was calculated to verify the results. Both FE strengths based on VM SR and VM ER have strong correlation (ρ=0.83 and 0.84) whereas the aBMD has modest correlation (ρ=0.67) with the experimental strength.

Furthermore, the predicted fracture location in the FSU model was compared with that seen in experiment as shown in Table 4.5. According to the results, the predicted fracture location varied depending on the yield criterion used to define the vertebral fracture. Among them, the VM ER and MX SR yield criteria show the best matching performance with the experimental results, even though there is no statistical significance according to Cohen's Kappa values as shown in Table 4.5.

Table 4.5: Fracture incidence in the FE models and in the experimental tests (T: top level on FSU, B: bottom level on FSU)

FSU no.	Spine Index	FSU Level	Fx Level Top/Bottom	VM SR	VM ER	DP SR	MX SR	MX ER	CM SR
0001	2710v	T12-L1	T	B	B	T	T	B	B
0003	2710k	L2-L3	T	B	T	B	B	T	B
0005	6211k	L2-L3	B	T	B	B	B	T	B
0007	6211v	L4-L5	B	B	B	T	B	B	B
0013	7011k	L1-L2	T	T	T	B	T	T	B
0015	7011v	L3-L4	T	B	T	B	T	B	B
0017	7509k	L1-L2	B	T	T	B	T	T	T
0019	7509v	T11-T12	B	B	B	B	B	B	B
0021	8911v	L3-L4	B	B	B	B	B	B	B
0023	8911k	T11-T12	T	T	T	B	B	B	B
0025	9311v	L1-L2	T	B	B	B	T	B	B
0027	9311k	L3-L4	B	T	T	T	T	T	B
0031	10211v	L1-L2	T	T	T	T	T	T	T
	Matching		13	6	**9**	6	**9**	6	6
Cohen's Kappa value				-0.14	**0.38**	-0.04	**0.38**	-0.14	-0.02

* Specimens were labelled for k (kyphoplasty) and v (vertebroplasty)

4.4 Discussion

The primary aim of the study was to develop a subject-specific FSU FE model based on QCT and MRI scans and to validate the outputs of this FSU FE model against experimental test. This study shows that the outputs of the FSU FE models developed show a positive correlation with the experimental data in terms of vertebral strength (VM SR and VM ER R^2 = 0.80 - 0.87). As, earlier mentioned, the correlation coefficient is a bit lower than the original results (0.87 -> 0.81 VM SR; 0.80 -> 0.68 VM ER), if the one extreme outlier (FSU0015) was omitted from the result. The revised correlation is still higher than that between aBMD by DXA and the experimental strength (R^2 = 0.54).

The correlation coefficients obtained are similar to those published by other researchers as summarised in Table 4.6.

Table 4.6: Correlation coefficients between FE derived strength and experimental strength in the literature

Authors	Correlation	R^2	N
Liebschner et al. 2003	Pearson	0.79	19
Crawford et al. 2003	Pearson	0.86	13
Buckely et al. 2007	Pearson	0.80	77
Chevalier et al. 2008	Pearson	0.77	12
Zeinali et al. 2010	Pearson	0.83	9
Da'llara et al. 2012	Pearson	0.78	37
Pahr et al. 2012	Pearson	0.77	37

With the exception of Crawford et al. (2003), who used linear analysis, all of the studies shown in Table 4.6 used a vertebral body alone FE model to estimate vertebral strength under compressive loading, with the nonlinear option, and defined vertebral strength based on the load-displacement curve. In contrast, the current work uses the linear option and defines vertebral strength as a yield point in a specified volume of elements. The fracture strength predicted by an FE models varies with different fracture/yield definitions. The Von Mises criterion has been used to estimate fracture strength in a hip

FE model (Keyak et al., 1998, Lotz et al., 1991a, Lotz et al., 1991b). This criterion assumes that ultimate bone strength is equal under tension and compression whereas, in reality the tensile strength of bone is lower than its compressive strength. There are a few hip FE studies that have been carried out using the Drucker-Prager stress. These take account of the differences in ultimate strength under tension and compression (Bessho et al., 2007, Koivumaki et al., 2012) and show a fairly good correlation with the results from experiment (R^2 = 0.87, 0.89).

As yet, there is no comparative study of different yield criteria for vertebral FE models. In the results presented in this chapter, Fisher's r-to-z transformation indicates that there is little difference in R^2 values between the von Mises criteria and the Drucker-Prager criteria. Vertebral strength determined from DP SR is slightly higher than that from VM SR. This difference may come from the hydrostatic stress term that is presented in Drucker-Prager criterion. An element has to be subjected to a larger external load for its DP SR to be large in order to fit the yield criterion. Thus, by introducing the DP SR as the yield criterion, a larger external load is needed in order to bring about the yielding of an element. In addition, the DP criteria are affected by the ratio of the yield in the tension and the yield in compression. In the present study, this was assumed to be 0.8 (Keaveny et al., 1994, Morgan and Keaveny, 2001). However, the literature also shows that this ratio varies with different anatomical sites and loading conditions (Keaveny et al., 1994, Kopperdahl and Keaveny, 1998, Morgan and Keaveny, 2001, Bayraktar et al., 2004).

Furthermore, we identified the fracture site in the FE model by our fracture estimation definition. The experiment normally generated a wedge type fracture as commonly seen clinically. The process of fracture in our model was also thought to be fairly close to the results of the experiment. A few studies have compared the fracture site predicted by hip FE models with that obtained experimentally and have shown agreement between them: 13 out of 18 with linear analysis (Keyak et al., 2001), and 15 out of 18 with nonlinear analysis (Bessho et al., 2007). Fracture strength based on VM ER has shown to give a better estimation (10 out of 13) although, in our study, predicted fracture location also varied with yield criterion. However, it should be noted that detailed fracture site information could not be obtained from normal X-ray images since part of the top and bottom vertebrae had to be potted within the PMMA in order to perform the

experiment. In the absence of this information, it was only possible to determine which of the two vertebrae in the FSU was fractured. This judgement was made from the reduction in vertebral height, with the vertebra with the greatest height reduction being assumed to be the first to fracture (the one of the two vertebrae). To validate the FSU FE model in terms of predicting the exact fracture location, a slightly different experimental test is recommended. This could be carried out on a specimen with two IVDs and adjacent vertebra (similar to the DVD FE model; described in Chapters 6 and 7) or three vertebrae with two adjacent IVDs (i.e. the multi-segment FE model briefly reviewed in Chapter 2).

A wide range of material properties have been used for the vertebra and intervertebral disc of FE models reported in the literature and as described in Chapter 2 the material properties are important factors which effect to the FE results. The FSU FE model described above used one of the empirical relationships, a linear relationship between the elastic modulus and the QCT equivalent density, and between the yield stress and the QCT equivalent density published by Kopperdahl (Kopperdahl et al., 2002) to assign the material properties for the vertebrae. This gave good agreement between the FE predicted strength and the experimental strength. Although the direct QCT density-mechanical property regressions by Kopperdahl et al. can improve the fidelity of the FE models, some limitations should be noted for using this relationship. Cylindrical trabecular specimens (ρ = 0.09 – 0.38 g/cm3) were used for the regressions, whereas the FSU FE model used whole vertebra. Furthermore, the use of vertebra beyond the density range of the specimens may introduce some errors, since trabecular architecture may vary with density as well as anatomical sites.

Some studies suggest that a power-law relationship gives better correlation between yield stress and density for the vertebra (Mosekilde et al., 1987, Kopperdahl and Keaveny, 1998, Ebbesen et al., 1999).

Kopperdahl et al. (2002) showed regression results using both linear and power-law relationship as shown in Table 4.7. According to their results, the simple linear relationship gives an equally strong correlation to that shown by the power-law. In terms of the distribution of residuals, the linear relationship is preferable.

Table 4.7: The empirical relationships between the QCT equivalent density and the elastic modulus (Kopperdahl et al. 2002)

	$\rho_{QCT} - E$	$\rho_{QCT} - \sigma_{yc}$
Linear Law	$E_z = -34.7 + 3230 * \rho_{QCT}$	$\sigma_{yc} = -0.75 + 24.9 * \rho_{QCT}$
Power Law	$E_z = 2980 * {\rho_{QCT}}^{1.05}$	$\sigma_{yc} = 37.4 * {\rho_{QCT}}^{1.39}$

Material properties for the vertebrae using a power law relationship were also assigned in the current work for comparison purposes, and in agreement with the findings of Kopperdahl et al. (2002) there was no significant difference between the two fits. Also the coefficients of determination from the linear regression between the FE strength and the experimental strength were similar (linear law R^2=0.8727, 0.8014; power law R^2= 0.8577, 0.8258) as shown in Table 4.8 and Figure 4.9.

Table 4.8: FE-derived strength: based on the linear relationship and the power law

FSU no.	Linear regression		Power law		Experiment
	FE strength (N) (VM_SR)	FE strength (N) (VM_ER)	FE strength (N) (VM_SR)	FE strength (N) (VM_ER)	Strength (N)
0001	862	1358	952	1428	1104
0003	1073	1281	1180	1619	1600
0005	607	998	774	1215	1180
0007	654	1081	846	1286	1685
0013	1967	2523	1888	2393	3090
0015	3399	4176	3370	3834	4412
0017	1930	2022	1887	1977	3399
0019	1570	2095	1541	2166	2906
0021	817	1604	873	1579	1861
0023	857	1469	839	1456	1194
0025	1374	2026	1236	1886	1930
0027	1387	2051	1327	1976	2215
0031	1079	1366	1172	1364	1319
Mean	1352	1850	1376	1860	2146
SD	759	834	707	694	1018
SE	211	231	196	192	282

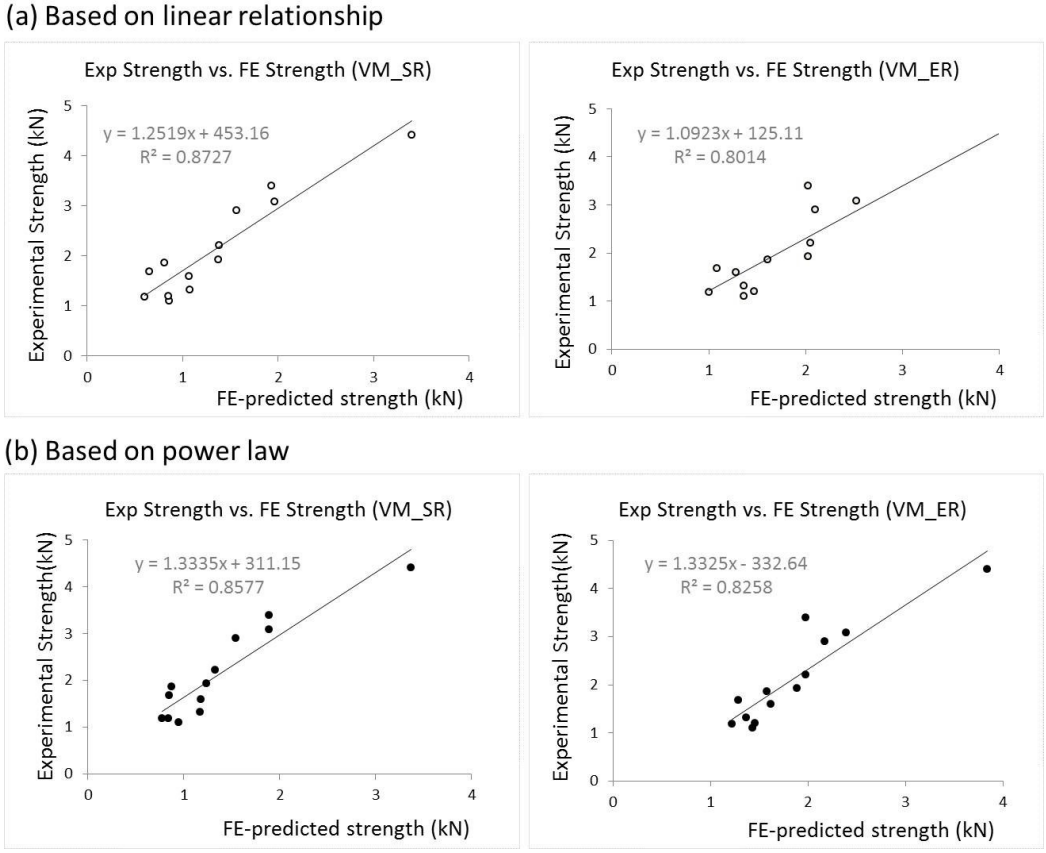

Figure 4.9: FE-derived strength: a) from Linear Regression ($p < 0.001$); b) Power Law

In addition, according to the result from Spearman's rank, all the FE strengths have strong correlation with the experimental strengths ($\rho = 0.83$ - 0.88). For this reason, in all the studies in this thesis which follow, the linear relationships for vertebral material properties were used in all FE models.

The material properties of the IVD of the FSU model described above were assumed to be linear-elastic. In the healthy IVD, the nucleus pulposus (NP) has often been modelled as a non-linear incompressible solid governed by Mooney-Rivlin law or as a fluid (Strange et al., 2010). However, the degenerated IVD loses its fluid-like region (Wognum et al., 2006) and the NP becomes more like a solid (Iatridis et al., 1996), hence, because the cadaveric specimens used had degenerated discs, the NP tissue was assumed to have homogeneous isotropic mechanical properties. The compressive modulus of the NP was assumed to be of the order of 8 MPa (Johannessen and Elliott, 2005). For the annulus fibrosus (AF), although this has a layered composite structure, its compressive

mechanical properties are not highly anisotropic, suggesting that they are not strongly influenced by collagen fibre direction (Berlemann et al., 1998, Urban and Roberts, 2003). In this way, we conducted simple parametric study to find out the effects of the material properties using five different combinations of material properties for the NP and the AF (Fagan et al., 2002b) as shown in Table 4.9.

Table 4.9: Assigned material properties for NP and AF (five different combinations for the parametric study)

DISC MAT.	Nucleus pulposus (NP)		Annulus fibrosus (AF)	
	Young's Modulus	Poisson's R	Young's Modulus	Poisson's R
1	$E_{NP} = 1\ MPa$	$\nu_{NP} = 0.499$	$E_{AF} = 500\ MPa$	$\nu_{AF} = 0.3$
2	$E_{NP} = 1\ MPa$	$\nu_{NP} = 0.499$	$E_{AF} = 250\ MPa$	$\nu_{AF} = 0.3$
3	$E_{NP} = 8\ MPa$	$\nu_{NP} = 0.499$	$E_{AF} = 500\ MPa$	$\nu_{AF} = 0.3$
4	$E_{NP} = 8\ MPa$	$\nu_{NP} = 0.3$	$E_{AF} = 500\ MPa$	$\nu_{AF} = 0.3$
5	$E_{NP} = 8\ MPa$	$\nu_{NP} = 0.3$	$E_{AF} = 250\ MPa$	$\nu_{AF} = 0.3$

According to the parametric studies on the IVD material properties, the FE strength values are insensitive to the five different disc moduli and Poisson's ratios as shown in Table 4.10.

Table 4.10: Linear regression from five different combinations

DISC	VM_SR		VM_ER	
MAT.	Y	R^2	Y	R^2
1	$Y = 1.2522 * X + 434.39$	$R^2 = 0.8687$	$Y = 1.0583 * X + 129.56$	$R^2 = 0.7853$
2	$Y = 1.2885 * X + 402.7$	$R^2 = 0.8643$	$Y = 1.0433 * X + 165.86$	$R^2 = 0.7833$
3	$Y = 1.2487 * X + 424.84$	$R^2 = 0.8620$	$Y = 1.0582 * X + 113.70$	$R^2 = 0.7912$
4	$Y = 1.2519 * X + 453.16$	$R^2 = 0.8727$	$Y = 1.0923 * X + 125.11$	$R^2 = 0.8014$
5	$Y = 1.2726 * X + 437.54$	$R^2 = 0.8699$	$Y = 1.0747 * X + 161.91$	$R^2 = 0.7993$

Isotropic elastic material properties might not be enough to represent the physiological characteristics of disc degeneration on the IVD of the FSU under the loading conditions

which generate severe wedge fractures in the vertebra. Whilst disc degeneration was present in the specimens, in order for the model to have wider application, a more realistic material model such as biphasic material model which represents water with solid fibres might be required for the IVD.

Several limitations of this study should be noted. Firstly, only linear analysis with linear elastic properties was carried out for the vertebrae and IVD (NP and AF), because a large forward bending condition (theta ° = 8.5°) was applied to the FE models in order to mimic the experimental status as closely as possible. The large angle of bending used led to higher peak values of stress and strain values especially in the anterior region. Therefore, this large angle makes the element fail easily, and to overcome the problem requires a more accurate material law which can describe the behaviour in the post yield region than is used here. In several *in vivo* studies relatively small angles such as 1 - 2 degrees of flexion, based on *in vivo* statistics for the spine, were used (Adams and Dolan, 1991, Homminga, 2001, Melton et al., 2007). In addition, although the IVD properties vary from one subject to another, only constant values were assigned to every FE models. It also did not account for viscoelastic properties and the fibres in AF. In fact the initial stiffness of experimental curve should be related to the IVD stiffness. Secondly, the endplates were not separated in the FE model as the QCT and MRI resolution is not high enough to distinguish the endplate area. Thirdly, the number of specimen is small which limits the study power. Finally, the average age of the specimen donors is old, which limits the conclusion to this age range.

In summary, the results of this study indicate that the linear FSU FE models are validated well against the experiment, namely, the strength derived from the FSU FE model could estimate the vertebral strength of the FSU specimen under forward bending. The validated FSU FE models could be used to improve the vertebral strength estimates in future clinical studies for fracture risk assessment and treatment effect monitoring.

CHAPTER 5 Comparison of Vertebral Strengths derived from FE models of the Vertebral Body, the Vertebral Body with Posterior Elements, and Functional Spinal Unit

Findings from the validated FSU FE model in Chapter 4 are extended through comparison studies with different types of FE models in terms of vertebral strength. Two additional types of subject-specific FE models were developed based on the specimens used in Chapter 4. These were a vertebral body (VB) model, and a model of the vertebral body with posterior elements (VB PE).

5.1 Introduction

A FSU FE model which takes account of the posterior elements and intervertebral disc was developed and validated, under the forward bending condition, with the results from the *in vitro* experiment as described in Chapter 4. Previous findings were extended through comparison studies of vertebral strength using an additional two different FE models: vertebral body (VB) FE model and vertebral body with posterior elements (VB PE) FE model.

One of these models, the VB FE model, has previously been used to investigate vertebral body strength under pure compressive loading, a test condition which is generally representative of the standing posture. The hypothesis was made that artificially removing the posterior elements in the model disrupts the continuity of the cortex and trabecular network and this may weaken the vertebral body causing strength to be

under-estimated (Wasnich RD, 1996, Jackson S.A., 2000). In addition, osteoporotic vertebral fractures often occur during forward bending activities. This concentrates loading on the anterior vertebral body, and it is this type of loading rather than pure compression that causes the anterior wedge fractures commonly observed in life. FE models that simulate loading in flexed postures may result in different strength estimates to those that simulate pure axial compression.

Furthermore, load on the vertebrae is not transferred directly through vertebral body but via an intervertebral disc and facet joints. Although the exact load transfer mechanism on the vertebrae is not yet clearly understood, degeneration of the IVD affects the loading conditions and fracture patterns of the adjacent vertebrae (Pollintine et al., 2004a, Adams and Dolan, 2005, Pollintine et al., 2004b). In this regards, the VB FE model and the VB PE FE model may give different strength patterns from those of the FSU FE model.

The specific aim of this Chapter is to compare vertebral strengths derived from three different types of FE models (Vertebral body (VB), vertebral body with posterior elements (VB PE), and FSU FE model (FSU)) based on experimental data obtained from the same specimens described in Chapter 4 measured experimentally under forward bending conditions.

5.2 Methods

The specimens, specimen preparation technique, bone mineral density, and *in vitro* experiments and experimental data obtained has already been described in Chapter 4 (Chapter 4: 4.2.1 to 4.2.3).

5.2.1 Subject-specific Finite Element Modelling

Using the same CT and MRI data the FSU FE model was deployed to give three different types of subject-specific finite element model as shown in Figure 5.1.

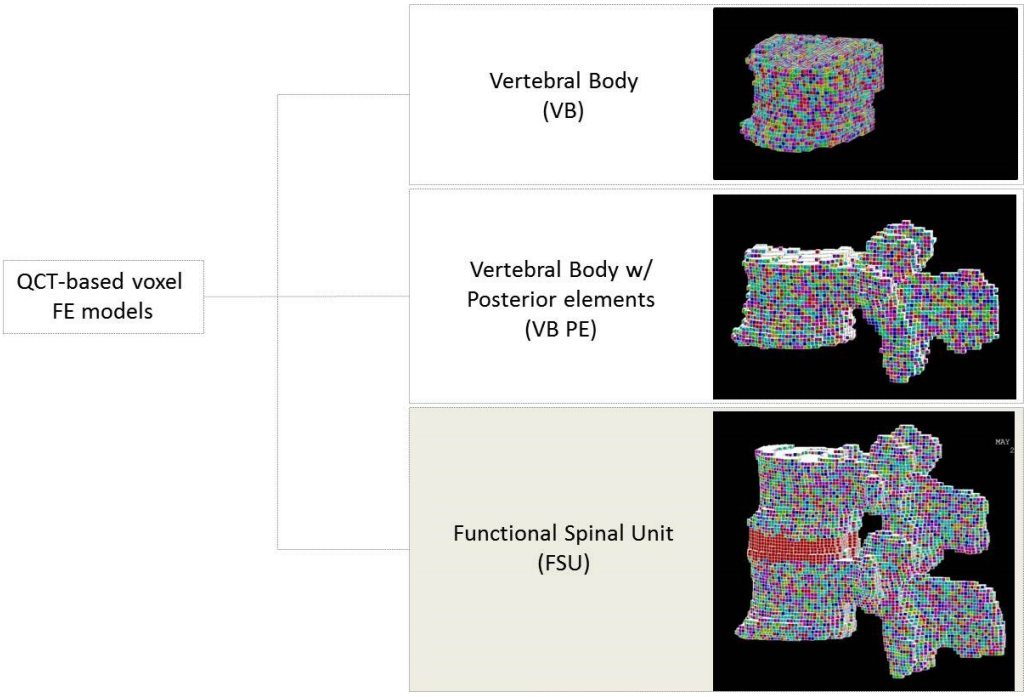

Figure 5.1: Subject-specific FE models; vertebral body, vertebral body with posterior elements, and functional spinal unit (Multiple-coloured part: vertebra with assigned material properties; red-coloured part: intervertebral disc with assigned material properties)

SpineVox-Pro was used to generate all FE models as before:

1) Vertebral body FE model (VB) – soft tissues and posterior elements were removed at the origin of the pedicles during the segmentation step in SpineVox-Pro.

2) Vertebra with posterior elements FE model (VB PE) – soft tissues were removed during the segmentation step in SpineVox-Pro.

3) The functional spinal unit FE model (FSU) which was developed and validated in Chapter 4 (4.2.4).

As mentioned earlier, to mimic the experiment condition, for the FSU model artificial cement paddings were generated at the inferior surface of the inferior vertebra and at the superior surface of the superior vertebra. To match the boundary conditions, the artificial cement paddings were considered for the VB and VB PE models at the inferior and superior surfaces of the vertebra. All the FE models were generated with each voxel being converted into an 8-node hexahedral element (Element type SOLID185 in ANSYS).

Material properties for the vertebra and the artificial paddings were the same as those used for the FSU FE model in Chapter 4.

5.2.2 Boundary conditions

For the VB FE model and the VB PE FE model, simple pure compression and a forward bending condition were both simulated in SpineVox-Pro. The bottom surface of the lower padding was constrained in all degrees of freedom. One of two possible boundary conditions, a tilted displacement or a three millimetre distributed displacement boundary condition was applied on the top surface of the upper padding for the forward-bending loading condition (theta ° = 8.5°) and pure compression, respectively. All FE models were then solved using a commercial software package, ANSYS (ANSYS Inc., Canonsburg, PA, USA) in the batch mode of SpineVox-Pro using the linear option.

5.2.3 Vertebral strength

Vertebral strength was defined using von Mises criteria. This was defined in two different ways for all FE models:

i. the load that caused minimum von Mises strain exceeding a yield strain of 0.78% (VM ER) in contiguous elements that occupied at least a volume of 422mm³
ii. the load that caused minimum von Mises stress exceeding a yield stress (VM SR) in contiguous elements that occupied at least a volume of 422mm³

The contiguous region was identified as the site with greatest likelihood of initial failure.

Since each FSU consisted of two vertebrae, two different ways were used to choose the fractured vertebra to compare with the FSU results:

SET 1) the vertebra which has a smaller FE strength

SET 2) the fractured vertebra of the FSU in the *in vitro* experiment

5.3 Results

Linear regression was performed between FE- and experiment-derived vertebral strength. Two specimens (No.0009, 0011) were excluded due to poor image quality and one specimen (No. 0029) was discarded due to failure of the experimental test. The FE-derived vertebral mean ± SD strengths from the three different types of FE models are presented in Table 5.1 (SET 1) and Table 5.2 (SET2). According to the results from the same strength definition of the FSU FE model, the FE strength under pure compression could be estimated most closely to the strength from the in vitro test on FSU specimens (2146N): VB 2026N, VB PE 2150N in set 1, and VB 2185N, VB PE 2300N in set 2.

*Table 5.1: FE- and Experiment- derived vertebral mean strength (N) based on **SET 1** criteria*

Pure	VB (N)	VB PE (N)		
VM SR p	1255 ± 723	1424 ± 787		
VM ER p	2026 ± 969	2150 ± 914		
Forward	VB (N)	VB PE (N)	FSU (N)	In vitro (N)
VM SR f	1019 ± 535	1030 ± 493	1352 ± 759	2146 ± 1018
VM ER f	1525 ± 604	1361 ± 580	1850 ± 834	

* SET 1) the vertebra which has a smaller FE strength

* VB: vertebral body; VB PE: vertebral body with posterior elements; FSU: functional spinal unit

*Table 5.2: FE- and Experiment- derived vertebral mean strength (N) based on **SET 2** criteria*

Pure	VB (N)	VB PE (N)		
VM SR p	1363 ± 761	1501 ± 785		
VM ER p	2185 ± 899	2300 ± 912		
Forward	VB (N)	VB PE (N)	FSU (N)	In vitro (N)
VM SR f	1071 ± 550	1076 ± 502	1352 ± 759	2146 ± 1018
VM ER f	1653 ± 606	1499 ± 597	1850 ± 834	

* SET 2) the fractured vertebra of the FSU in the in vitro experiment

* VB: vertebral body; VB PE: vertebral body with posterior elements; FSU: functional spinal unit

5.3.1 Vertebral strength of VB model: Pure compressive loading vs. forward bending

The strength measured experimentally showed a positive correlation with the strength based on von Mises stress obtained for the VB FE model both in pure compressive loading and forward bending (SET 1: R^2 = 0.83 VM SR p, R^2 = 0.79 VM SR f; SET 2: R^2 = 0.87 VM SR p, R^2 = 0.78 VM SR f) as did the strength based on von Mises strain for the VB FE model (SET 1: R^2 = 0.84 VM SR p, R^2 = 0.75 VM SR f; SET 2: R^2 = 0.79 VM SR p, R^2 = 0.66 VM SR f) as shown in Figures 5.2 and 5.3.

According to the Fisher's r-to-z transformation, there is no significant difference statistically between the correlation coefficient from the pure compressive loading and that from forward bending VM SR (SET 1: z = 0.31 p = 0.38; SET 2: z = 0.68 p = 0.25) and VM ER (SET 1: z = 0.55 p = 0.29; SET 2: z = 0.59 p = 0.28), even though the correlation coefficient from the pure compression condition is slightly higher than that from the forward bending.

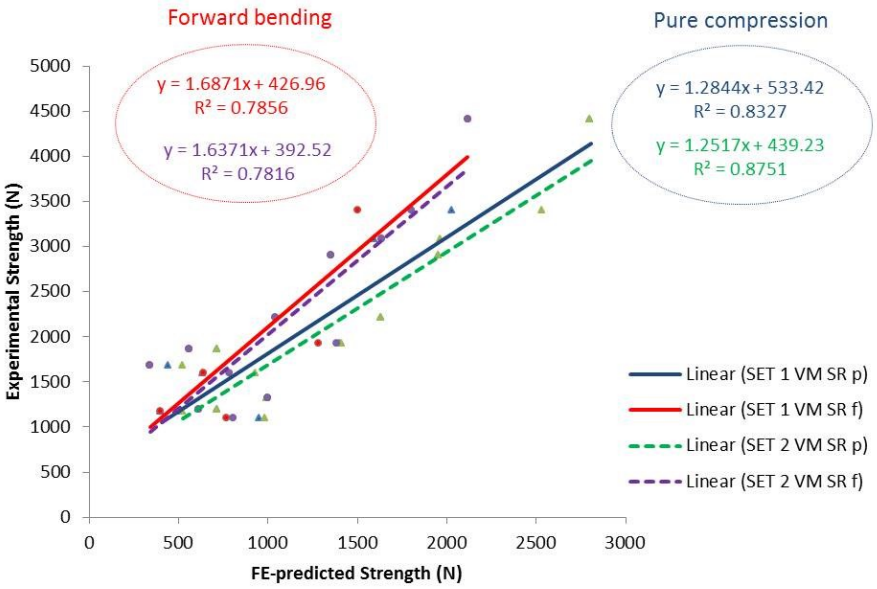

*Figure 5.2: Linear regression between Experiment- and FE-derived strength from the vertebral body FE model derived from: von Mises Stress in pure compression (VM SR p); from von Mises stress in forward bending (VM SR f). * Note: SET 1) the vertebra which has a smaller FE strength, and SET 2) the fractured vertebra of the FSU in the in vitro experiment*

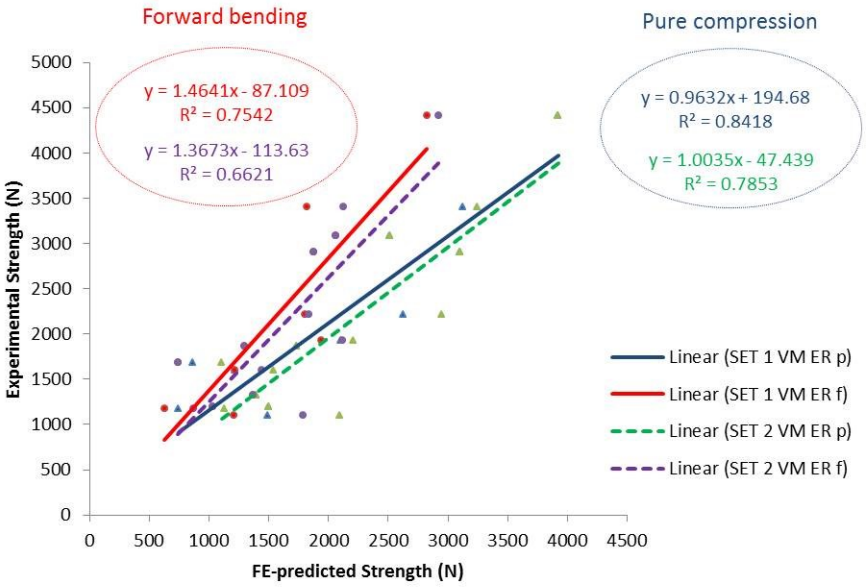

*Figure 5.3: Linear regression between Experiment- and FE-derived strength (FE model of vertebral body alone derived from: von Mises Strain in pure compression (VM ER p); von Mises strain in forward bending (VM ER f). * Note: SET 1) the vertebra which has a smaller FE strength, and SET 2) the fractured vertebra of the FSU in the in vitro experiment*

Figures 5.4 and 5.5 show the assigned elastic moduli, the von Mises stress and strain distribution of one example (VB 13 top and bottom vertebral body) under pure compression and forward bending, respectively. As expected, the anterior cortex shows the highest stress values under forward bending. On the other hand, in pure compression, the stress is distributed more evenly on the vertebra body compared with the results of the forward bending analysis, even though the peak value is still on the anterior cortex region. The strain peak value and the distribution is quite similar from both loading except the top vertebra under forward bending which shows slightly higher strain on relatively large area than the others.

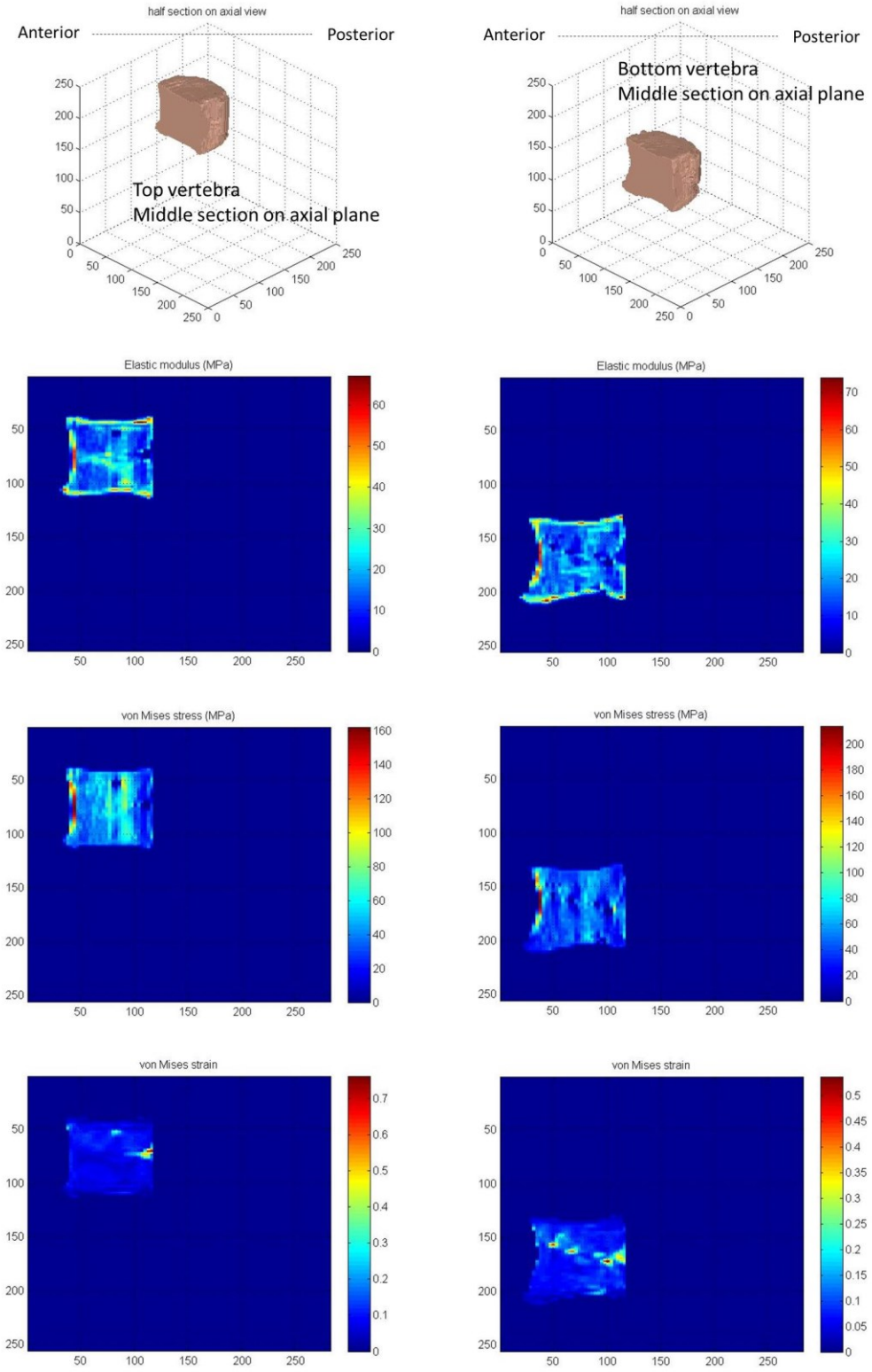

Figure 5.4: Elastic modulus, von Mises stress and strain plots of VB 13 under pure compression: (left) top vertebral body, (right) bottom vertebral body

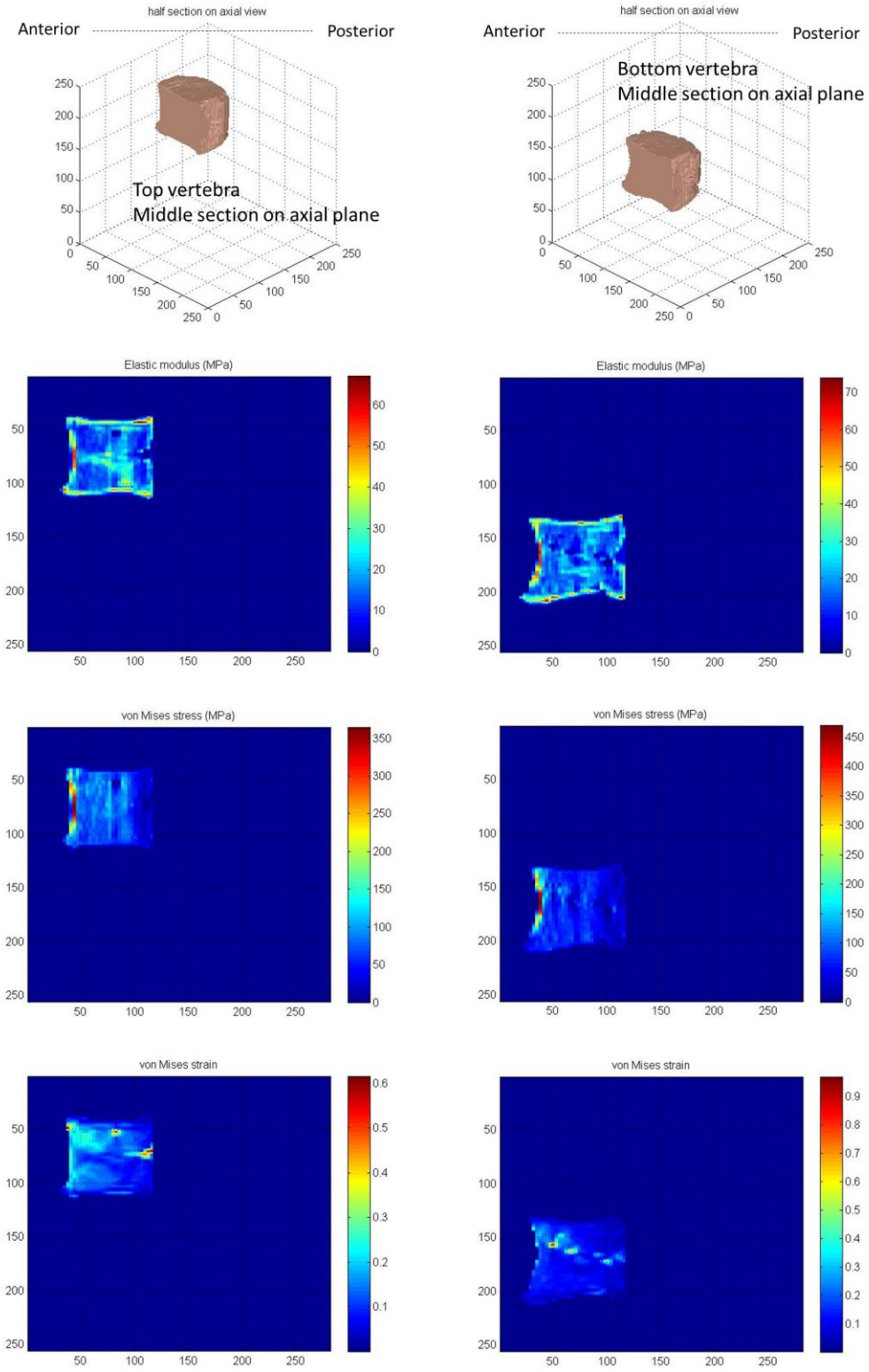

Figure 5.5: Elastic modulus, von Mises stress and strain plots of VB 13 under forward bending: (left) top vertebral body, (right) bottom vertebral body

5.3.2 Vertebral strength of VB PE model: Pure compressive loading vs. forward bending

The strength obtained from experiment was positively correlated with the strength based on von Mises stress of the VB PE FE model in pure compressive loading and forward bending (SET 1: R^2 = 0.83 VM SR p, R^2 = 0.75 VM SR f; SET 2: R^2 = 0.85 VM SR p, R^2 = 0.78 VM SR f) and also with the strength based on von Mises strain of the VB PE FE model (SET 1: R^2 = 0.85 VM SR p, R^2 = 0.68 VM SR f; SET 2: R^2 = 0.76 VM SR p, R^2 = 0.59 VM SR f) as shown in Figures 5.6 and 5.7.

According to the Fisher's r-to-z transformation, once again like the results from the VB FE model, there is no significance of the difference statistically between the correlation coefficient from the pure compressive loading and forward bending VM SR (SET 1: z = 0.49 p = 0.31; SET 2: z = 0.45 p = 0.33) and VM ER (SET 1: z = 0.99 p = 0.16; SET 2: z = 0.70 p = 0.24), even though the correlation coefficient from the pure compression condition is slightly higher than that from the forward bending..

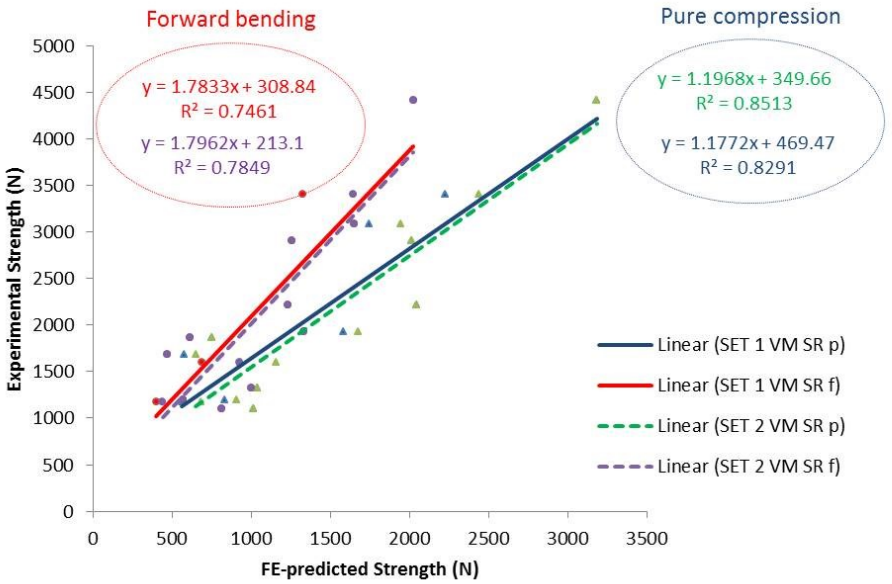

*Figure 5.6: Linear regression between Experiment- and FE-derived strength from the vertebra with posterior elements FE model derived from: von Mises Stress in pure compression (VM SR p); von Mises stress in forward bending (VM SR f). * Note: SET 1) the vertebra which has a smaller FE strength, and SET 2) the fractured vertebra of the FSU in the in vitro experiment*

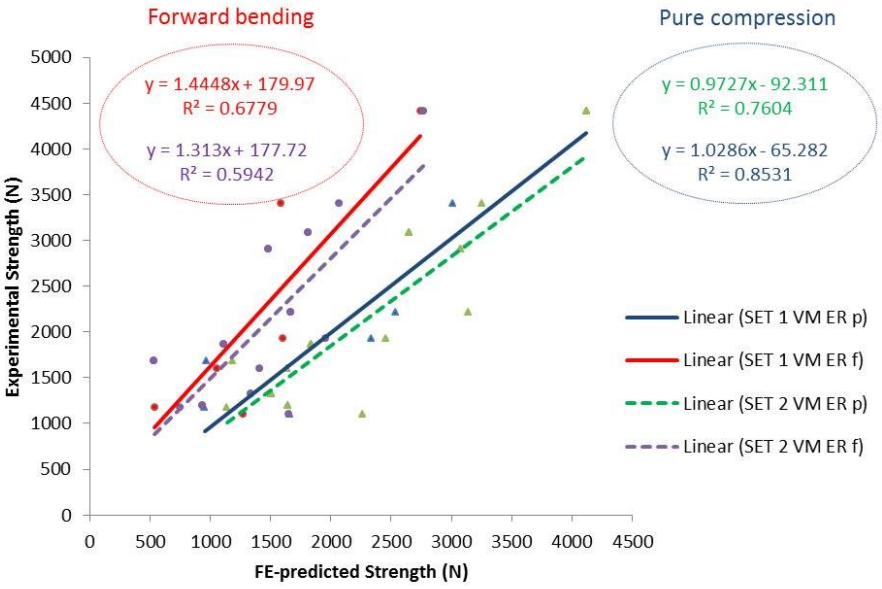

*Figure 5.7: Linear regression between Experiment- and FE-derived strength from the vertebra with posterior elements FE model derived from: von Mises Strain in pure compression (VM ER p); von Mises strain in forward bending (VM ER f). *Note: SET 1) the vertebra which has a smaller FE strength, and SET 2) the fractured vertebra of the FSU in the in vitro experiment*

Figures 5.8 and 5.9 show the assigned elastic moduli, the von Mises stress and strain distributions of one example (VB PE 13 top and bottom vertebra) under pure compression and forward bending, respectively. As before (Figures 5.4 and 5.5), the anterior cortex shows the highest stress values under forward bending and once again, in pure compression, the stress is distributed more evenly on the vertebra body compared with the results of the forward bending analysis, even though the peak value is still on the anterior cortex region. The strain peak value from the pure compression is near the posterior cortex, while the strain peak value from the forward bending is slightly on the front of the vertebra.

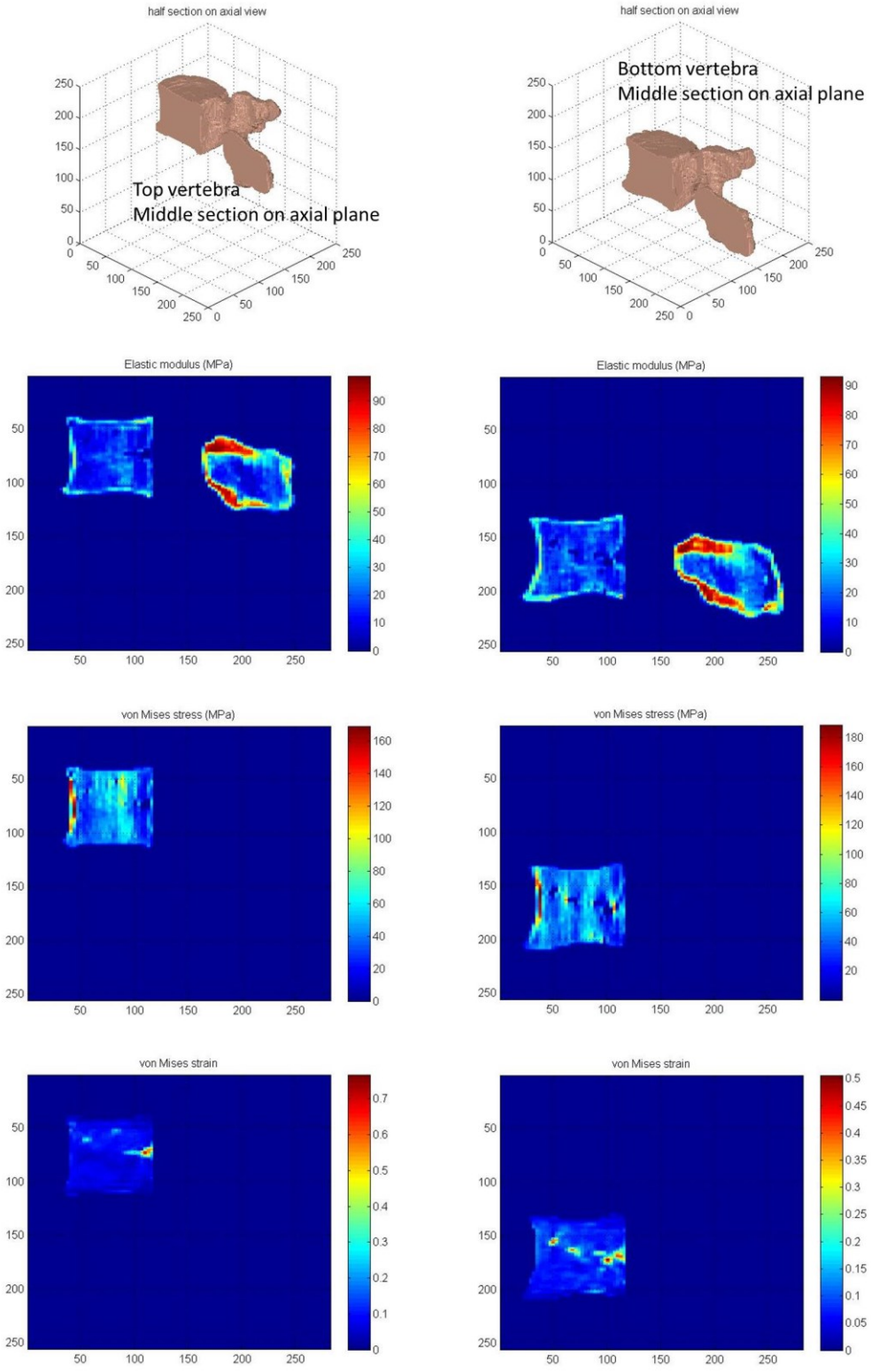

Figure 5.8: Elastic modulus, von Mises stress and strain plots of Vertebra 13 under pure compression: (left) top vertebra, (right) bottom vertebra

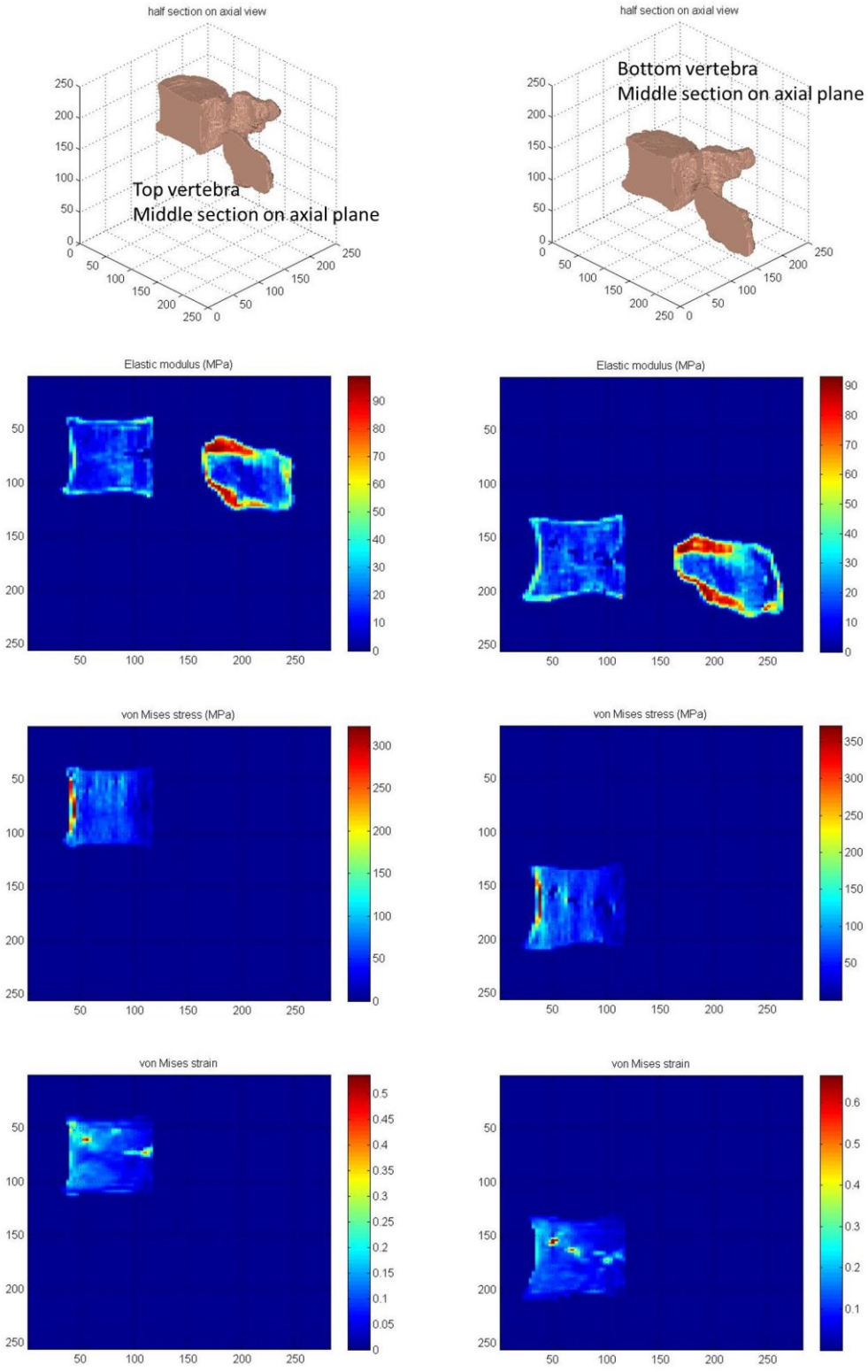

Figure 5.9: Elastic modulus, von Mises stress and strain plots of Vertebra 13 under forward bending: (left) top vertebra, (right) bottom vertebra

5.3.3 Comparison of vertebral strength between VB, VB PE, and FSU models under forward bending

The correlation coefficients for the VB and VB PE FE model were compared with the results (as described in Chapter 4) from the validated FSU model under forwarding bending only. As mentioned previously, under the forward bending condition, the strength measured by experiment showed a positive correlation with that based on von Mises stress for all FE models investigated (R^2 = 0.79 VB, R^2 = 0.75 VB PE, R^2 = 0.87 FSU). A similar relationship was found for von Mises strain (R^2 = 0.75 VB, R^2 = 0.68 VB PE, R^2 = 0.80 FSU) as shown in Figures 5.10 and 5.11. The strength from FSU FE model has higher correlation value based on both yield criteria although the Fisher r-to-z transformation reported no significant difference statistically between correlation coefficient.

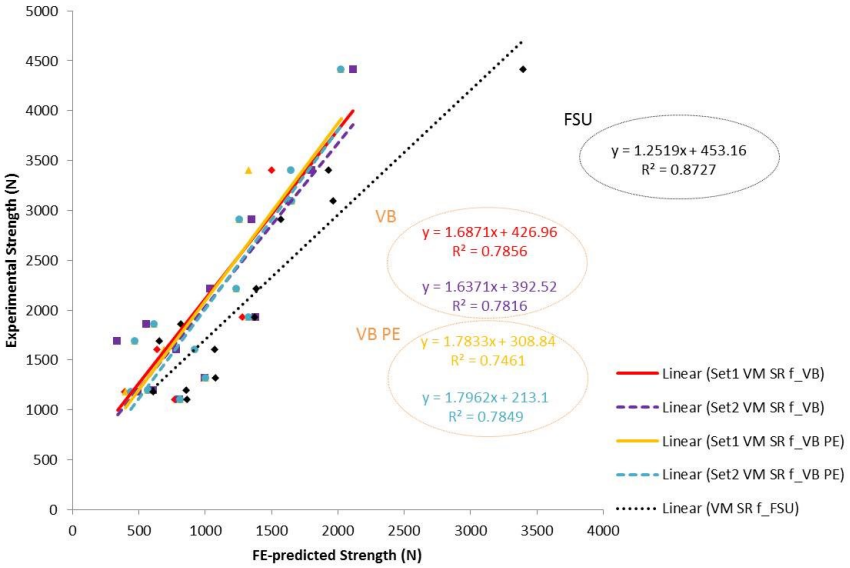

*Figure 5.10: Linear regression between Experiment- and FE-derived strength from FE model of FSU derived from: von Mises Stress in forward bending (VM SR f_FSU); the vertebral body FE model derived from von Mises Stress in forward bending (VM SR f_VB); the vertebra with posterior elements FE model derived from von Mises Stress in forward bending (VM SR f_VB PE). * Note: SET 1) the vertebra which has a smaller FE strength, and SET 2) the fractured vertebra of the FSU in the in vitro experiment*

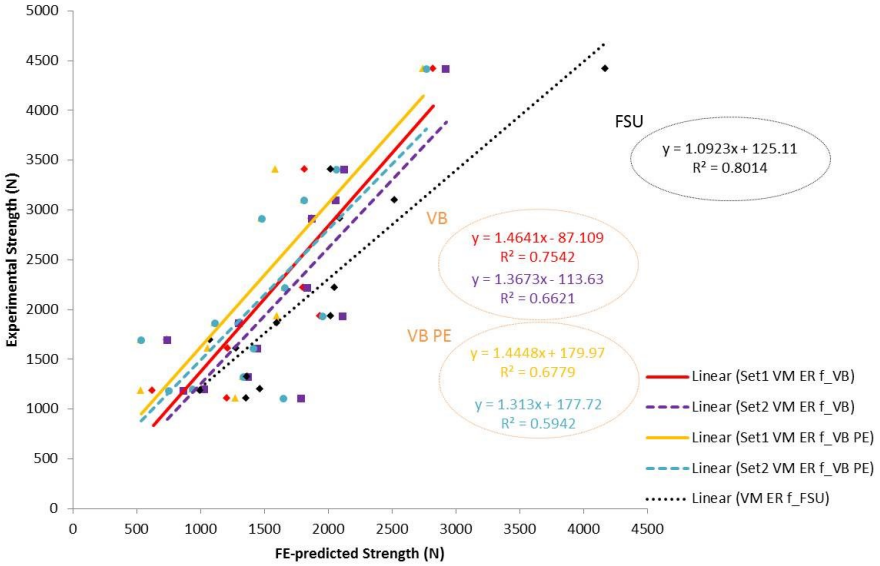

*Figure 5.11: Linear regression between Experiment- and FE-derived strength from FE model of FSU derived from: von Mises Strain in forward bending (VM ER f_FSU); the vertebral body FE model derived from von Mises Strain in forward bending (VM ER f_VB); the vertebra with posterior elements FE model derived from von Mises Strain in forward bending (VM ER f_VB PE). * Note: SET 1) the vertebra which has a smaller FE strength, and SET 2) the fractured vertebra of the FSU in the in vitro experiment*

Figures 5.12 show the assigned elastic moduli, the von Mises stress and strain plots of one example (FSU 13) under forward bending. The peak stress can be seen in anterior cortex region on both top and bottom vertebrae. This result is similar with the previous results from VB and VB PE under forward bending. On the other hand, the peak strain value is near the posterior cortex region, even though the anterior cortex region on the vertebrae has relatively higher strain distribution.

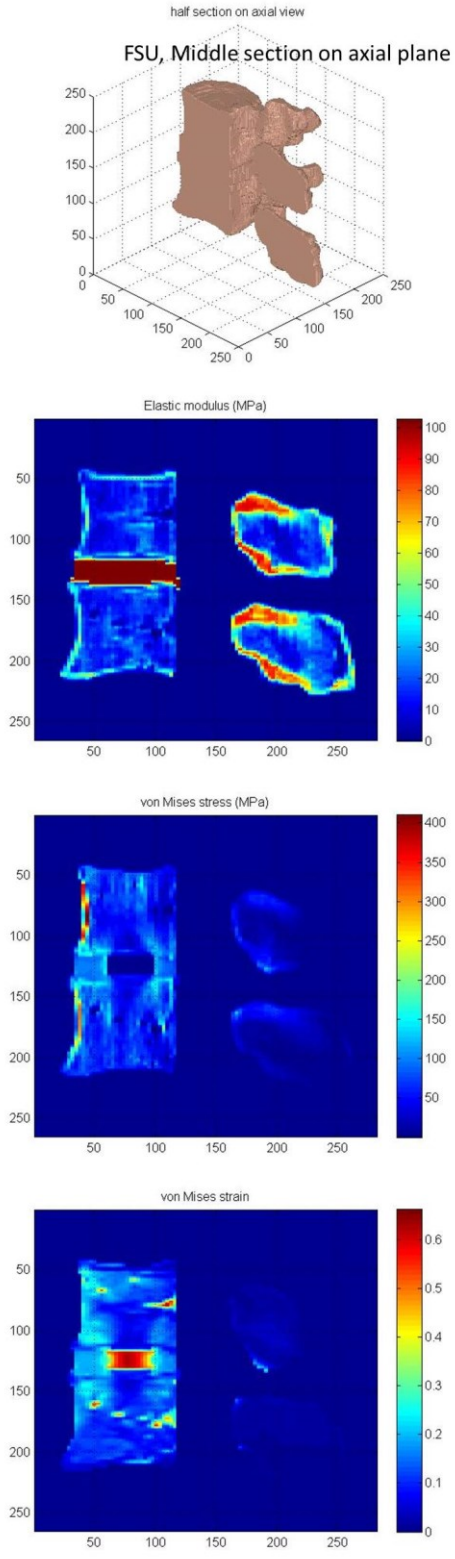

Figure 5.12: Elastic modulus, von Mises stress and strain plots of FSU 13 under forward bending

5.3.4 Comparison of estimated fracture locations between VB, VB PE, and FSU models under pure compression and forward bending

The predicted fracture locations found in the FE models were compared with that seen in the experimental results as shown in Table 5.3.

Table 5.3: Estimated fracture level (T: top level of FSU, B: bottom level of FSU)

FSUs experiment			VB FE model				VB PE FE model				FSU FE	
no.	Level	Fx Level	VM SR f	VM ER f	VM SR p	VM ER p	VM SR f	VM ER f	VM SR p	VM ER p	VM SR f	VM ER f
0001	T12-L1	T	B	B	B	B	T	B	T	B	B	B
0003	L2-L3	T	B	B	B	B	B	B	B	T	B	T
0005	L2-L3	B	T	T	T	T	T	T	T	T	T	B
0007	L4-L5	B	B	B	T	T	B	B	T	T	B	B
0013	L1-L2	T	T	T	B	T	T	T	B	T	T	T
0015	L3-L4	T	T	B	T	T	T	B	T	T	B	T
0017	L1-L2	B	T	T	T	T	T	T	T	T	T	T
0019	T11-T12	B	B	B	B	B	B	B	B	B	B	B
0021	L3-L4	B	B	B	B	B	B	B	B	B	B	B
0023	T11-T12	T	T	T	B	T	T	T	B	T	T	T
0025	L1-L2	T	B	B	B	B	T	B	B	B	B	B
0027	L3-L4	B	B	T	B	T	B	B	B	T	T	T
0031	L1-L2	T	T	T	T	T	T	T	T	T	T	T
Matching		13	8	6	5	6	**10**	7	6	7	5	9
Cohen's Kappa Value			0.24	-0.07	-0.21	-0.10	0.53	0.09	-0.07	0.05	-0.14	0.38

According to the results, the predicted fracture locations varied depending on the type of FE model and the yield criterion which used to define the vertebral fracture. To comparison purpose, FSU 0013 results are chosen to visualize. Figures 5.13 to 5.21 illustrate the predicted fracture locations based on von Mises stress and strain yield criteria of three different FE models.

Among them, the vertebra with posterior elements (VB PE) FE model based on von Mises stress showed the best agreement with experiments (10 out of 13 cases), even though there was no statistical significance according to the Cohen's Kappa values as shown in Table 5.3.

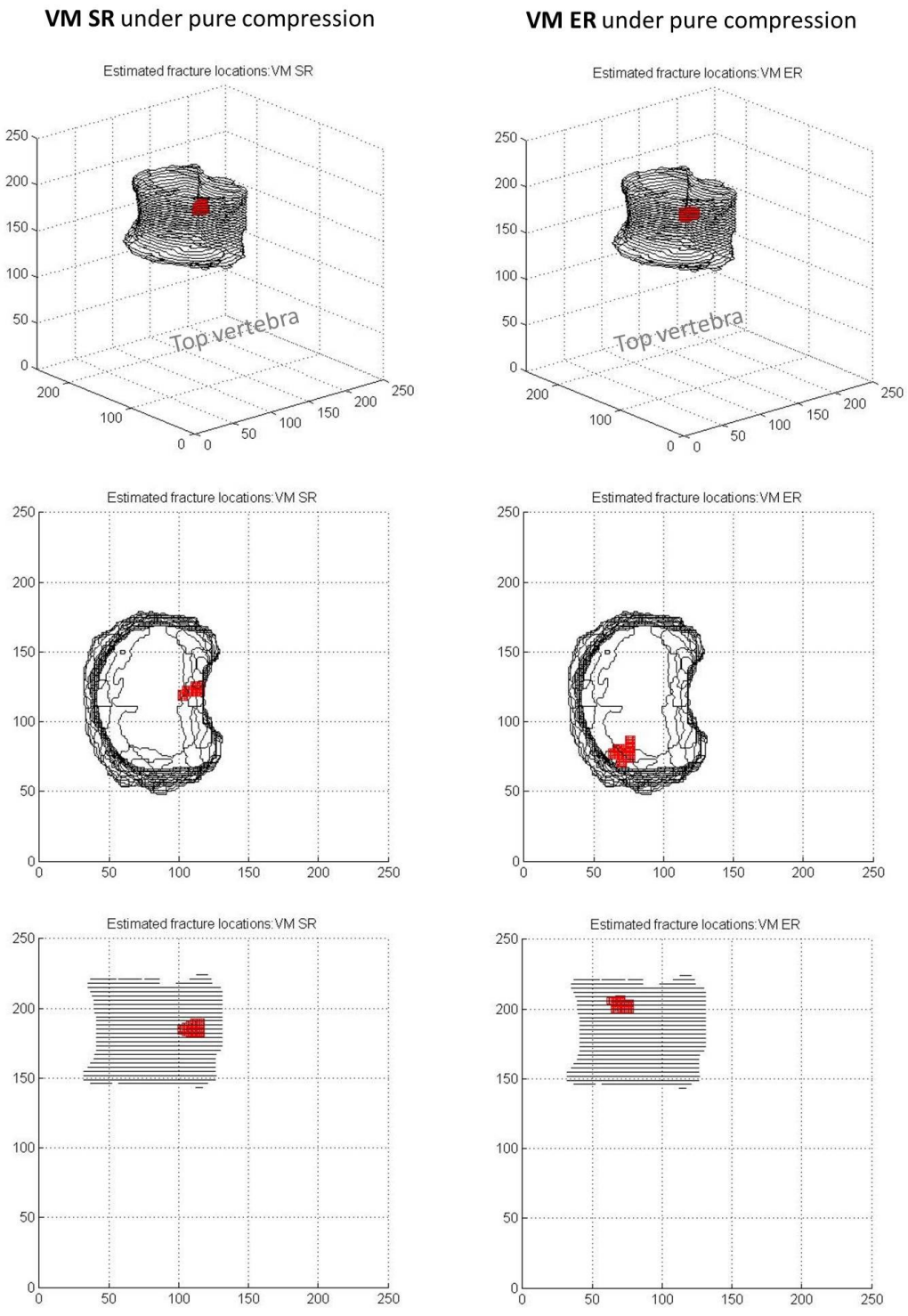

Figure 5.13: Estimated fracture locations on VB 13 (top vertebral body) based on von Mises stress and von Mises strain yield criteria under pure compression

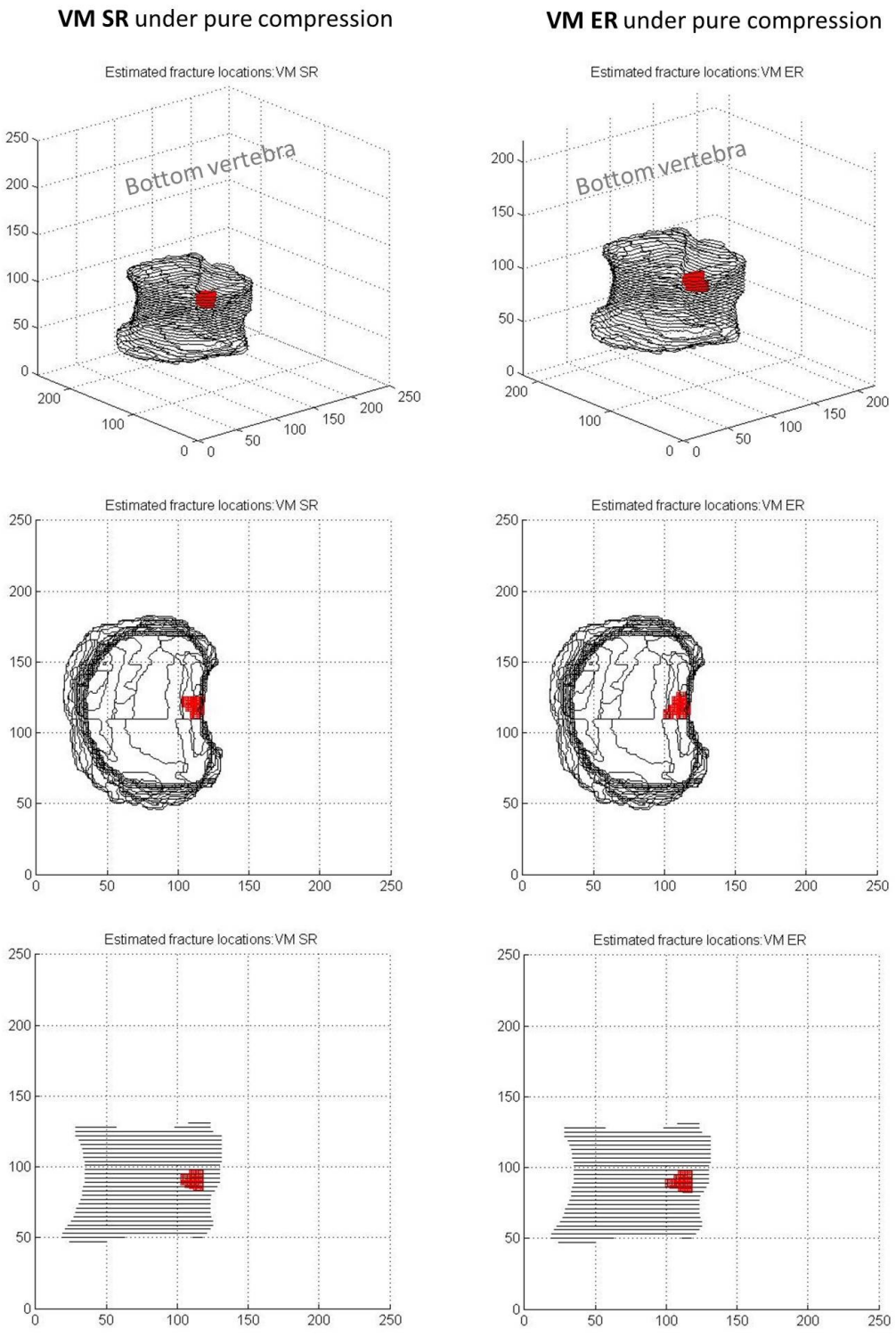

Figure 5.14: Estimated fracture locations on VB 13 (bottom vertebral body) based on von Mises stress and von Mises strain yield criteria under pure compression

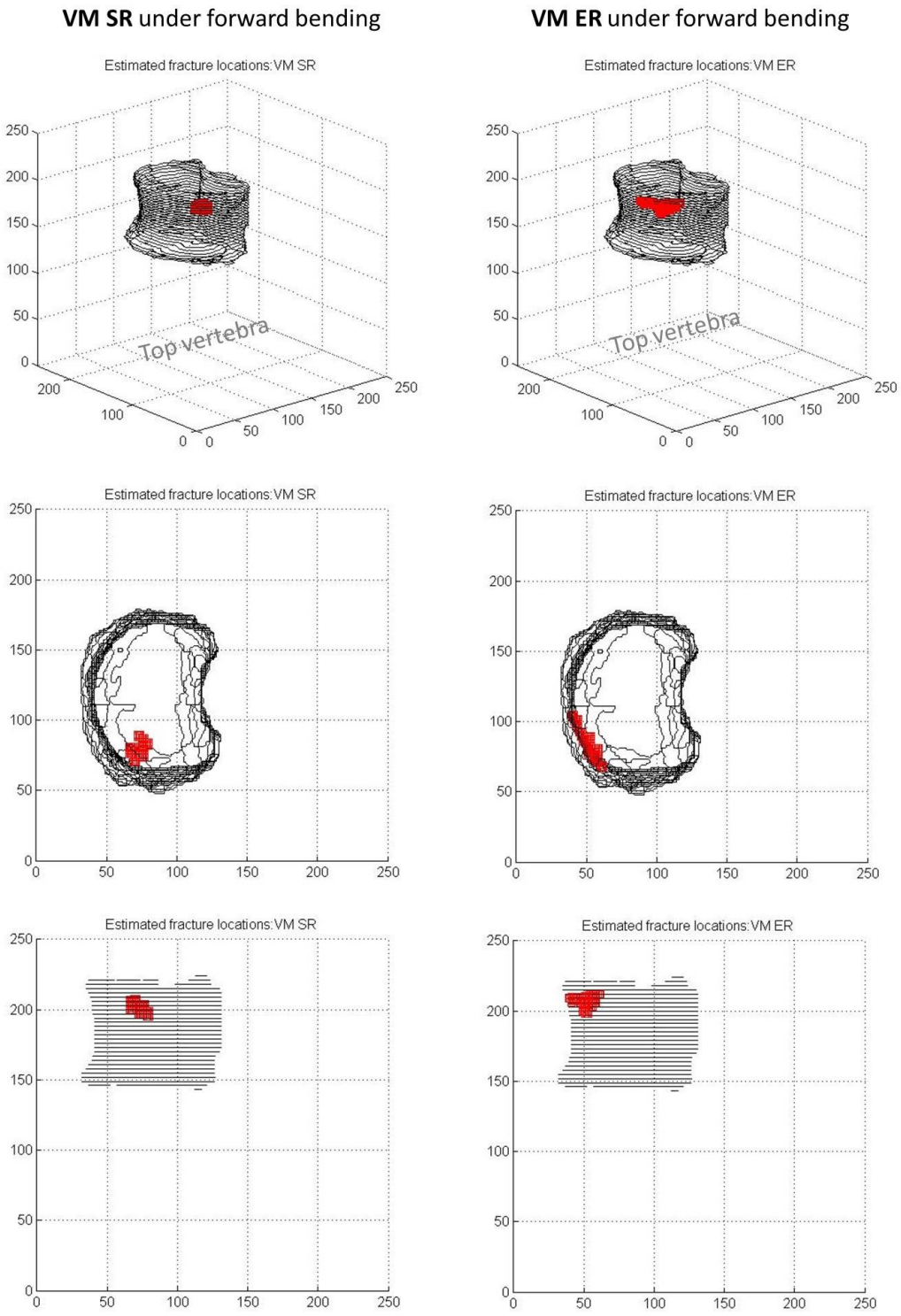

Figure 5.15: Estimated fracture locations on VB 13 (top vertebral body) based on von Mises stress and von Mises strain yield criteria under forward bending

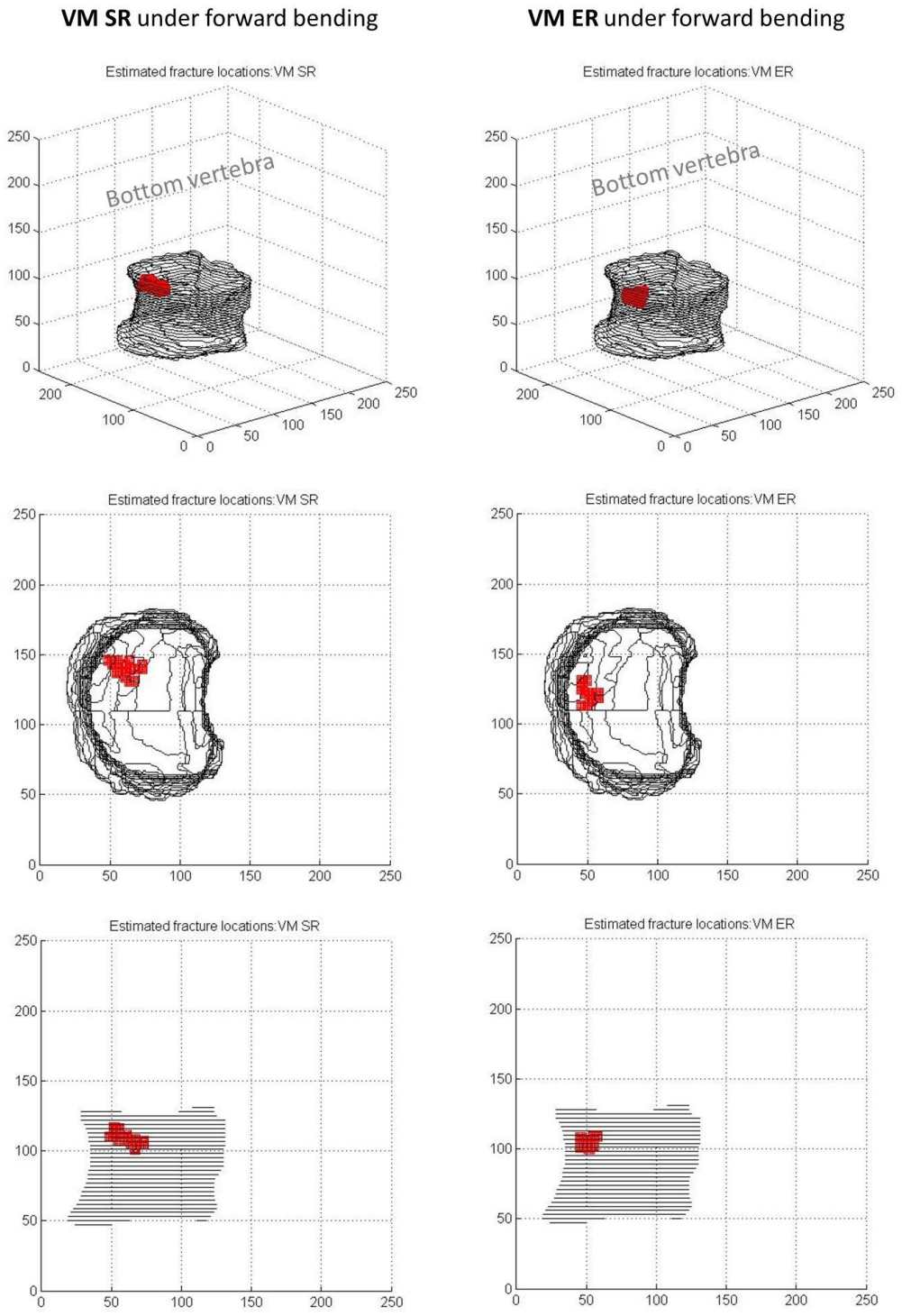

Figure 5.16: Estimated fracture locations on VB 13 (bottom vertebral body) based on von Mises stress and von Mises strain yield criteria under forward bending

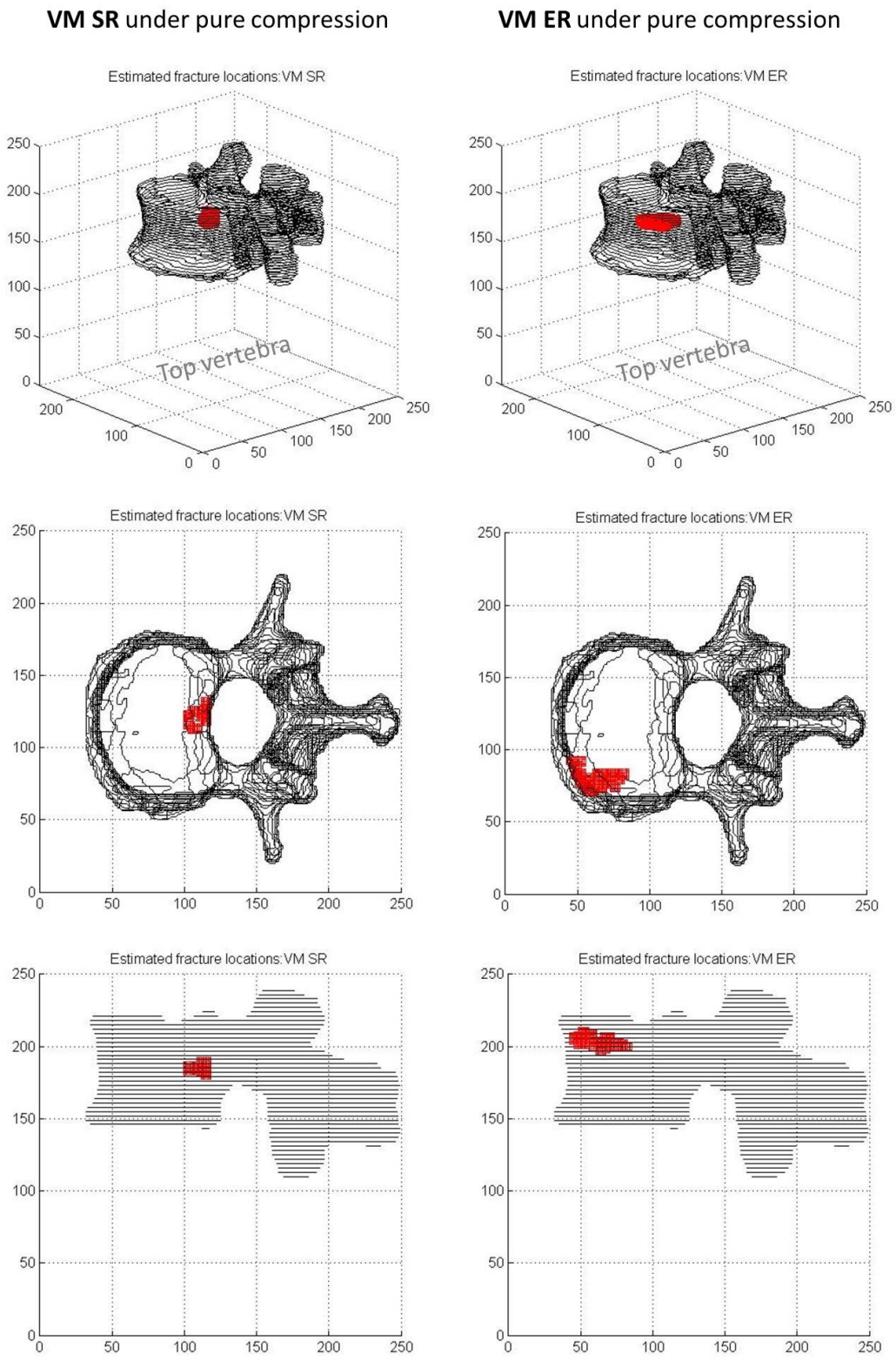

Figure 5.17: Estimated fracture locations on Vertebra 13 (top vertebra) based on von Mises stress and von Mises strain yield criteria under pure compression

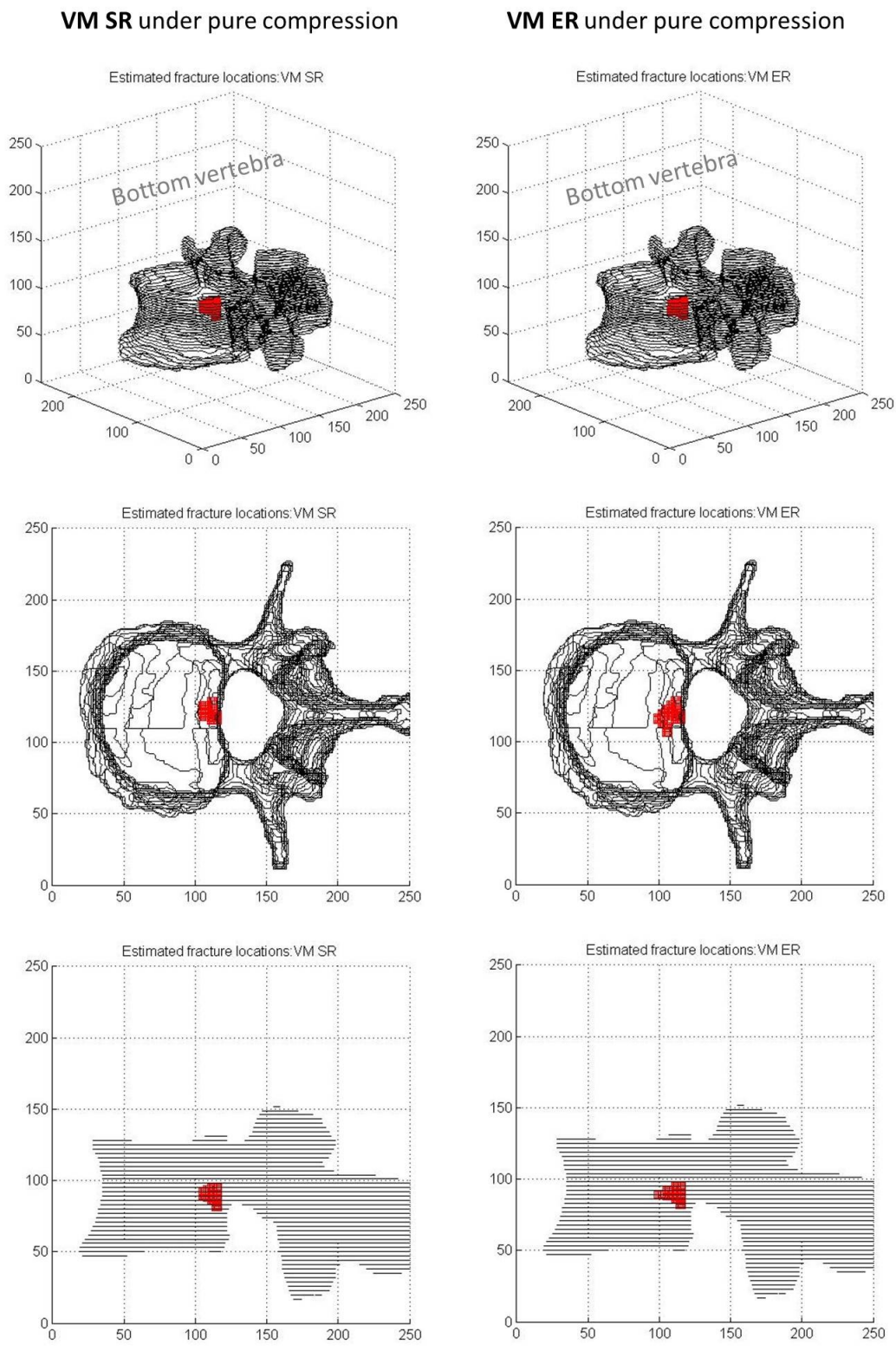

Figure 5.18: Estimated fracture locations on Vertebra 13 (bottom vertebra) based on von Mises stress and von Mises strain yield criteria under pure compression

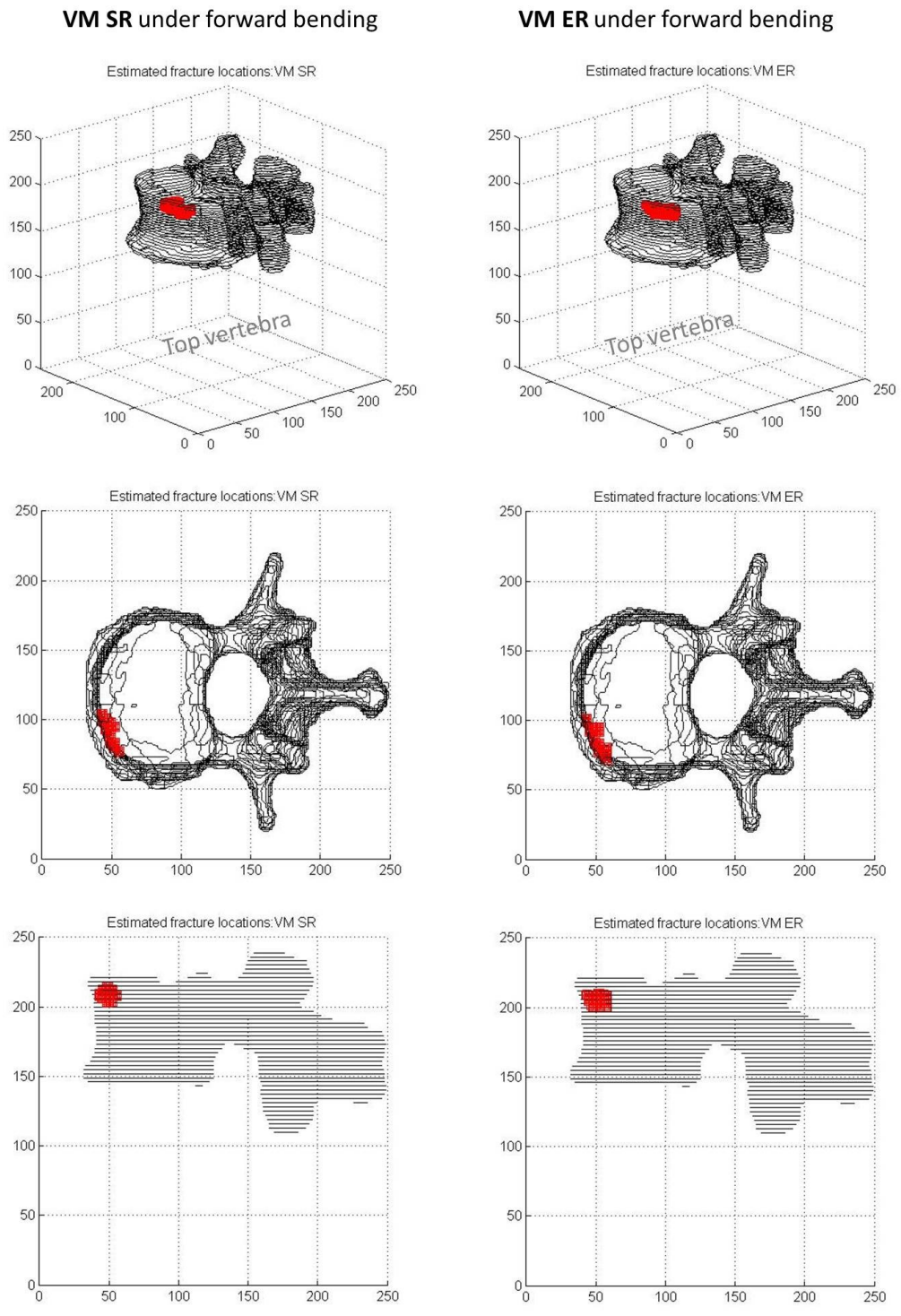

Figure 5.19: Estimated fracture locations on Vertebra 13 (top vertebra) based on von Mises stress and von Mises strain yield criteria under forward bending

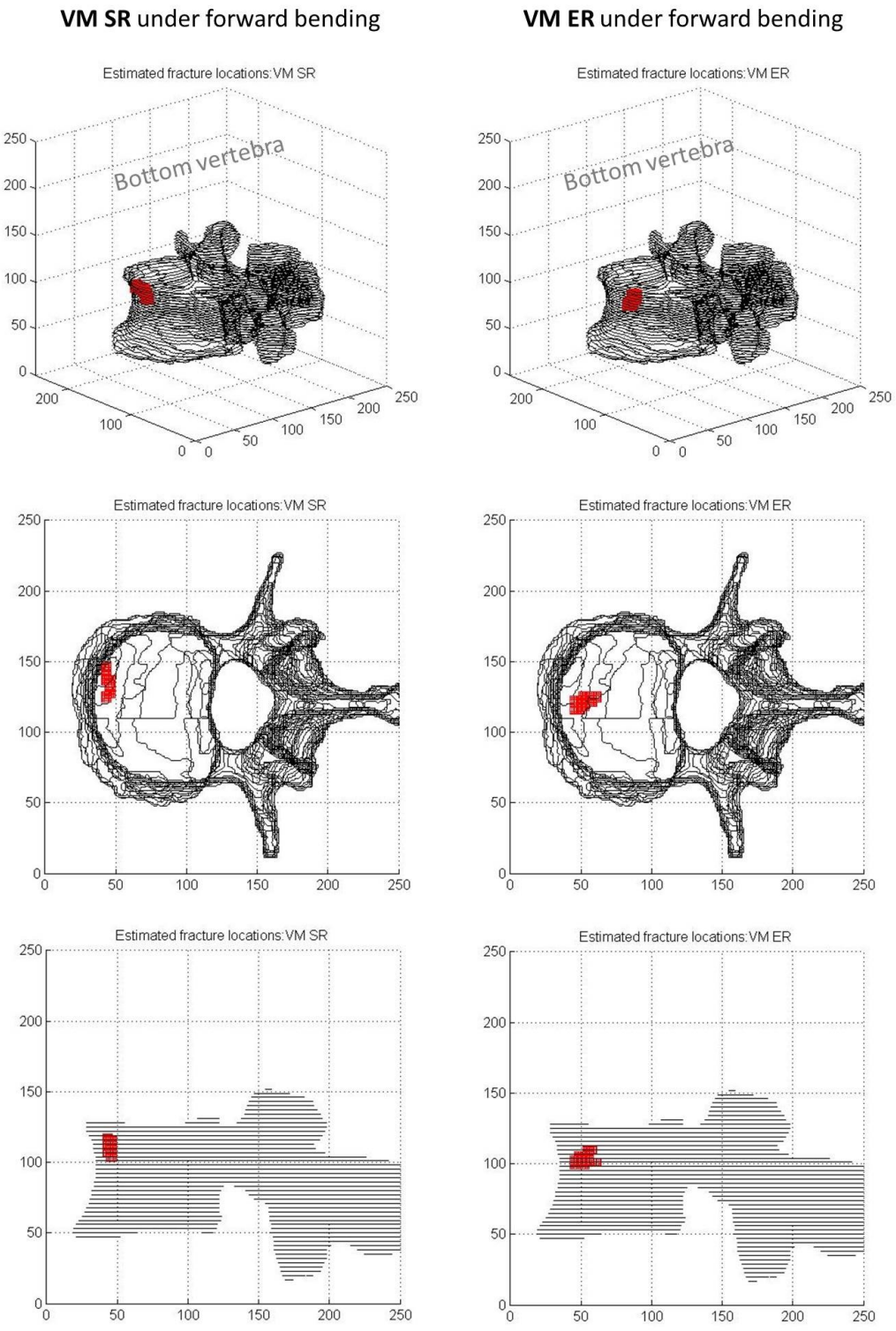

Figure 5.20: Estimated fracture locations on Vertebra 13 (bottom vertebra) based on von Mises stress and von Mises strain yield criteria under forward bending

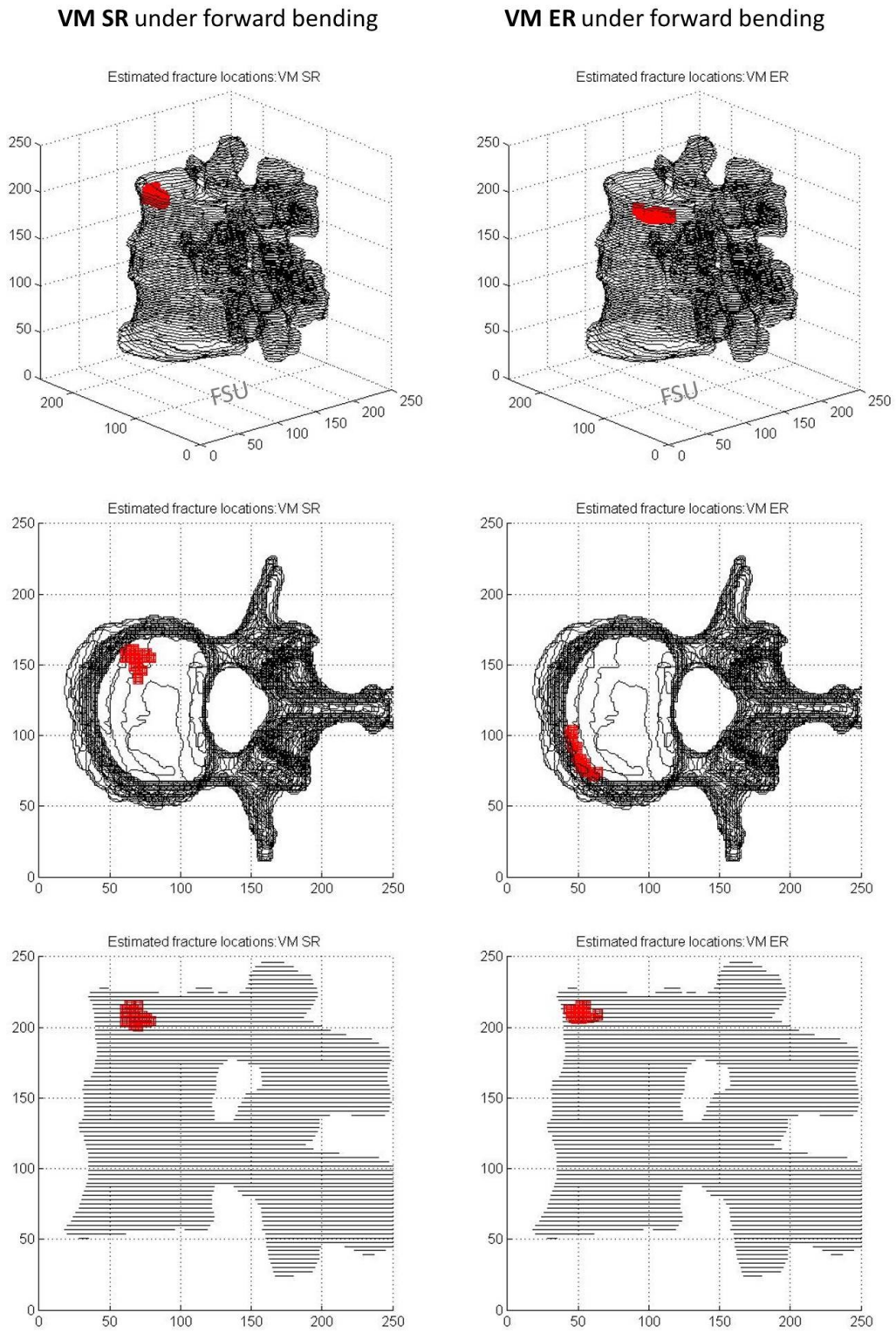

Figure 5.21: Estimated fracture locations on FSU 13 based on von Mises stress and von Mises strain yield criteria under forward bending

5.4 Discussion

This study was based on the premise that vertebral strength obtained from a FE model of the vertebral body alone under pure compressive loading could not represent the strength of an individual vertebra during different loading conditions. The hypothesis of this study in this chapter is that different FE models may influence the result of the FE analysis. FE models of the vertebrae simulating loading in flexed postures may result in different strength estimates to those that simulate pure compression. Furthermore, by artificially removing the posterior elements and IVD the model fails to represent the load transfer through the IVD and facet joint. This study has shown that all FE models investigated, as well as the FSU FE model, give results that are positively correlated with the experimental data (R^2= 0.68 - 0.87 in forward bending; R^2= 0.83 – 0.85 in pure compression). The correlation coefficients were similar for VB and VB PE models whereas the FSU model gave a slightly higher correlation. In other words, there is no significant difference statistically in terms of predicting vertebral strength between three different types of FE models under forward bending: VM SR (z = 0.59 p = 0.28 FSU vs. VB; z = 0.81 p = 0.21 FSU vs. VB PE) and VM ER (z = 0.28 p = 0.39 FSU vs. VB; z = 0.6 p = 0.27 FSU vs. VB PE). The FE models being compared first followed by their z and p-values. This provides a justification for the current use of the VB model instead of VB PE or FSU for estimating vertebral strength. Furthermore, as earlier mentioned in Chapter 4, the correlation was compared by the Spearman's rank to omit the effect of the extreme outlier (FSU0015). The results from FSU FE model showed the highest value, even though all FE strengths had strong correlation (ρ=0.83 - 0.84 FSU; ρ=0.78 - 0.82 VB; and ρ=0.76 - 0.79).

However, it is important to remember that the mean FE strength were different: the mean FE strength (1850 N) from the FSU FE model could estimate most closely to the strength (2146N) from the in vitro test on FSU specimens: VB 1525N, VB PE 1361N in set 1, and VB 1653N, VB PE 1499N in set 2. Furthermore, the stress and strain distributions on the vertebral body differ from the type of FE models: VB, VB PE, and FSU. Our results show that the predicted locations generally towards the anterior part of vertebra in the forward bending condition, while those towards the posterior part of vertebra in the

pure compression for all the FE models. However, the predicted fracture locations were varied with the FE model types as well as the yield criteria. Especially, the predicted fracture locations on the VB FE models were quite different from each other. Among these three types of FE models, the VB PE FE model show the better prediction on the fracture locations compared with the experimental results (10 out 13), even though there was no statistical significance.

From the results from the VB FE model, the FE strengths under the pure compression was a bit higher than those under the forward bending based on both von Mises stress and strain yield criteria: (VM SR pure 1255 - 1363N; VM SR forward 1019 - 1071N), and (VM ER pure 2185 – 2026N; VM ER forward 1525 – 1653N). However all of the FE strengths were positively correlated with the experimental strengths, namely, there is no significance difference statistically between the correlation coefficients. There are few validated FE studies using the isolated vertebral body FE model in the literature which investigate vertebral strength under anterior bending (Buckley et al., 2007a, Dall'Ara et al., 2010, Dall'Ara et al., 2012). Buckley et al. (2007a) investigated vertebral strength of the isolated vertebral body under anterior bending and showed a rather poor correlation (R^2 = 0.34 - 0.40) between the FE-derived strength from VB FE model and the experimental strength. In contrast, Dall'Ara et al. (2010, 2012) were able to find a better correlation (R^2 = 0.79). However, it must be noted that the above studies predicted vertebral strength based on the vertebral body alone FE model under anterior bending and, in particular, it is important to emphasise that Dall'Ara et al. used a vertebral body FE model without endplates.

There is one *in vivo* study that has investigated vertebral strength from the vertebral body FE model under a number of different loading conditions, namely: forward bending, uniaxial compression, and in the erect standing posture (Matsumoto et al., 2009). This work shows a significant correlation between FE-derived strength under uniaxial compression and the strength under forward bending (R^2 = 0.83, $p < 0.0001$). The mean fracture load under forward bending was reported to be significantly lower than the mean fracture load under uniaxial compression (2693N vs. 3062N, p = 0.00017).

As earlier mentioned, the studies reported in this chapter show similar results to the findings above: there is a significant correlation between vertebral strength based on the VB FE model under forward bending and that in pure compression (R^2 =0.91 VM SR;

R^2 = 0.87 VM ER). Also the mean vertebral strength under forward bending is smaller than that in pure compression (1019N vs.1255N VM SR; 1525N vs. 2025N VM ER).

Some limitations of this study should be noted. First, all the FE models used consider only the specific forward bending condition (Θ = 8.5°) which was used in the *in vitro* experiment. To investigate the physiological loading associated with daily life, a gentler flexion condition would be recommended for a study more representative of the *in vivo* situation (Homminga, 2001, Melton et al., 2007). Second, there was no consideration of the FSU FE model under pure compression due to lack of compatibility using a voxel mesh for the contact analysis near the area of the facet joints. At surfaces of the voxel mesh model, the zigzagged boundary interrupts the analysis of sliding at the mesh interfaces. The effect of the voxel mesh is crucial at the facet joints area where stresses are not proportional to load because the engaged contact area changes as load is increased. Due to this strong geometric nonlinearity, more accurate representation of the contacting surfaces than voxel mesh is required. Last, the results for all the FE models were compared with experimental data obtained by generating a wedge fracture in a single vertebral body within a FSU rather than loading a single vertebra alone. The results might be improved, if there will be the fracture validation study on the single vertebra instead of FSU. Finally, as earlier mentioned in Chapter 4, there is one outlier (FSU 0015), the bigger estimated FE strength might affect the results of the linear regression for all the comparisons.

In conclusion, the results of this study indicate that the mean FE strength (1850 N) from the FSU FE model under the forward bending condition could estimate most closely to the mean strength (2146N) from the in vitro test on FSU specimens, even though all FE strengths are positively correlated with the experimental data. The predicted fracture locations differ from the type of FE models as well as the yield criteria. Among them the VB PE FE model show the better prediction on the fracture locations compared with the experimental results (10 out 13). Furthermore, there is a tendency that the FE strengths under the pure compression are higher than those from the forward bending condition.

The strength derived from the simple vertebral body FE model under the pure compression can still be used to estimate the vertebral compressive strength without posterior elements or the functional spinal unit with large population of patients for the clinical studies. The reason is that one of main burdens for generating vertebral FE

model based on CT is the segmentation process. The removal of posterior elements from the ROI makes the process of the segmentation much easier. However, our results might address the limitations of the current approach in that, the FE model should incorporate the posterior elements and IVD as well as the loading conditions.

CHAPTER 6 Vertebral Fracture Discrimination in Postmenopausal Women using a Patient-Specific Finite Element Model of the Disc-Vertebra-Disc Unit

This chapter introduces a new patient-specific FE model of the Disc-Vertebra-Disc unit (DVD) that incorporates the vertebra and adjacent intervertebral discs. The DVD FE model was adapted, for clinical research, from the FSU FE model described in Chapters 4 and 5. The underpinning premise in the design of this model was that vertebral strength and load distribution, via the vertebral endplates, is dependent on the properties of the IVD. A case-control study was conducted to investigate the sensitivity and specificity of the DVD FE model by comparison between the predicted strengths for patients with fractures and patients without fractures in order to investigate the discrimination power of the FE model.

6.1 Introduction

Fractures that result from osteoporosis are a major cause of pain, disability and death. There are over 200,000 fractures each year in the UK with an estimated cost to the NHS of £1.7 billion. As both clinical and sub-clinical vertebral fractures are associated with increased mortality and morbidity (Poole and Compston, 2006, Kado et al., 1999). It is essential that patients with osteoporosis and secondary fractures are investigated and treated effectively. Areal Bone Mineral Density (BMD) assessed by dual-energy X-ray absorptiometry (DXA), is found to be low in vertebral fracture patients. However, BMD only explains 51-71 % of vertebral strength (Bjarnason et al., 1996, Wegrzyn et al., 2010) with about half of fragility fractures occurring in patients with BMD above the

osteoporosis threshold (Roux et al., 2010, Siris et al., 2004). This is because bone strength is influenced by not only BMD, but also other factors including bone shape, bone size and bone structure. In recent years, patient-specific finite element (FE) models of the vertebral body based on quantitative computed tomography (QCT) have been used to estimate vertebral strength and assess fracture risk. Finite element analysis (FEA) integrates all of the available data (obtained from both measurement and imaging techniques), on bone density, bone geometry, microarchitecture and the material properties of bone with assessments of external forces and loading using patient-specific *in vivo* loads. These factors are used to calculate the stress and strain in the bone, from which bone strength can then be determined. Finite element analysis therefore provides an opportunity to assess bone strength accurately, and non-invasively. The majority of previous patient-specific FE models described in the literature do not include the IVD and, furthermore, an isolated vertebral body is used. However, vertebral strength and load distribution on the vertebra via endplates depends on the condition of the IVD. For this reason, a new patient-specific FE model of the Disc-Vertebra-Disc unit (DVD), based on CT was developed. This incorporates the vertebra and adjacent intervertebral discs. To investigate the power of discrimination power of this it was necessary to conduct a case-controlled study to investigate the sensitivity and specificity of the CT-based FEM by comparing the predicted strengths between patients with fractures and patients without fractures (Bessho et al., 2009).

The purpose of the work described in this chapter was to investigate whether vertebral strength derived from the DVD FE models could discriminate between women with and without vertebral fracture using data from an existing case-control study QCT scans.

6.2 Materials and methods

6.2.1 Study Population

The original clinical study for the data which used in this chapter was designed to investigate into the relationship between serum oestradiol and other hormones, and the risk of osteoporotic vertebral fracture using novel imaging technology and measurement of biochemical markers. The clinical study was approved by the South Yorkshire

Research Ethics Committee (REC Ref No. 11/H1310/2). The study was carried out by the principal investigator Dr. Miguel Debono, a clinical research fellow at the University of Sheffield,

This cross sectional case-control study included 81 postmenopausal women (age 59-82) in 3 groups: a case group (n=18) with osteopenia/osteoporosis (total hip or vertebral BMD T-score < -1) and prevalent vertebral fracture, an age- and BMD-matched control group (n=29), and an age-matched non-osteopenia/osteoporosis control group (n=34). The two control groups were combined to form a single control group for statistical analysis. Several scans for spine could not be obtained (2 in case group, 6 in control group). Basic information for the study population is summarised in Table 6.1.

Table 6.1: Basic information for the study population

	Case group (N= 16/18)	Control group (N= 57/63)
Age (years)	71 ± 6.04	70 ± 5.92
Weight (kg)	65.52 ± 8.92	74.94 ± 17.39
Height (cm)	158.51 ± 5.01	160.07 ± 14.06
DXA		
Hip BMC	28.45 ± 4.52	31.49 ± 5.25
Hip aBMD (g/cm^2)	0.79 ± 0.11	0.89 ± 0.12
Lumbar spine BMC	41.27 ± 8.97	53.60 ± 13.26
Lumbar spine aBMD (g/cm^2)	0.80 ± 0.10	0.95 ± 0.15
QCT		
vBMD at L2 (mg HA/cm^3)	79.77 ± 22.28	108.60 ± 26.43

* Values represent the mean ±SD.

6.2.2 Bone Mineral Density (BMD)

BMD was acquired for the lumbar spine in both the posterior-anterior and lateral projections and for right hip in the posterior-anterior (PA) projection using a Hologic Discovery A densitometer (Hologic Inc., Bedford, MA, USA). Mean areal BMD (g/cm^2) was calculated for vertebrae L1 to L4 and for the total hip region. As spinal BMD cannot be measured reliably in fractured vertebrae, for analysis of BMD, the study participants were required to have a minimum of two un-fractured lumbar vertebrae; participants

with fractures of all lumbar vertebrae were excluded from the study. For this reason a lumbar spine BMD scan was acquired first to ensure that the participant was eligible for the study. If the right hip had been fractured or replaced, the left hip was imaged.

6.2.3 Vertebral fracture assessment (VFA)

DXA-based VFA of the thoracolumbar spine was conducted using the Hologic Discovery A device (Hologic Inc., Bedford, MA, USA). This produces high definition images of vertebrae T4 to L4 in both the PA and lateral projections. Spinal radiography remains the standard for diagnosis of vertebral fracture, but VFA confers much lower doses of ionising radiation. Vertebral fracture assessment (VFA) is a useful tool for identifying existing and new vertebral fractures (Ferrar et al., 2008). The images were read by technicians trained using an algorithm-based qualitative method for the identification of vertebral fractures. Images that exhibited definite or possible evidence of vertebral fracture were reviewed by a clinician. Any fractures identified were confirmed by conventional radiography. This ruled out the possibility of abnormal appearance due to causes other than osteoporotic fracture.

6.2.4 Quantitative Computed Tomography (QCT)

The right hip and lumbar spine were scanned with a clinical QCT machine (LightSpeed VCT, GE Medical Systems, 120kV, 60 mAs/slice, 0.9375 x 0.9375 x 0.625 mm voxel size), in the Diagnostic Imaging Department, Northern General Hospital, Sheffield. The left hip was measured if the patient had a fractured or a prosthetic in the right hip. Scans were acquired using a study-specific operating procedure. Quantitative computed tomography enables the acquisition of 64 slices, 0.625mm thick from which the assessment of geometric and compartmental properties of bone can be made. These measurements were used to assess volumetric cortical and trabecular BMD and strength of the vertebra and proximal femur. A solid calibration phantom (Mindways, Mindways, San Francisco, CA) was used to calibrate Hounsfield unit (HU) values with bone mineral density.

6.2.5 Subject-specific Finite Element Model of Disc-Vertebra-Disc Unit in SpineVox-Pro

A new patient-specific FE model of the Disc-Vertebra-Disc unit (DVD) was developed incorporating the vertebra and adjacent two intervertebral discs. In general, QCT scans of the lumbar 1 to lumbar 3 (L1-L3) in clinical research do not include the lumbar 1 and lumbar 3 completely, so only the lumbar 2 and its adjacent IVDs can be generated fully into FE models. Therefore, for using clinical research scans, the DVD FE model is proposed in this Chapter. The FE model still takes account of the effects IVDs on loading transfer to the vertebra. The model was generated from the L2 vertebral component of L1 to L3 QCT scans. Once again, SpineVox-Pro was used to generate patient-specific models using the procedure illustrated in Figure 6.1.

The procedure used to generate the DVE FE model is almost the same as that for the FSU FE model (Chapter 4.2.4), except in this case two IVD are included in the FE model. The procedure is described here briefly. The CT data were calibrated from Hounsfield units to hydroxyapatite equivalent density using the phantom. The converted CT images were segmented semi-automatically to extract the vertebra and intervertebral disc (IVD). The IVD masks were generated from the information of the gap from the frontal and sagittal plane of QCT images. The NP was assumed to be an elliptic cylinder occupying 45% of the IVD volume. It was assumed to be placed on the centre of the IVD, even though the position of the NP within the disc varies regionally. The extracted images were interpolated to achieve the desired resolution of 1.2 x 1.2 x 1.2 mm^3 and rotated if necessary to a standard orientation. The images were directly converted to a finite element model with each voxel being converted into an 8-node hexahedral element (Element type SOLID185 in ANSYS).

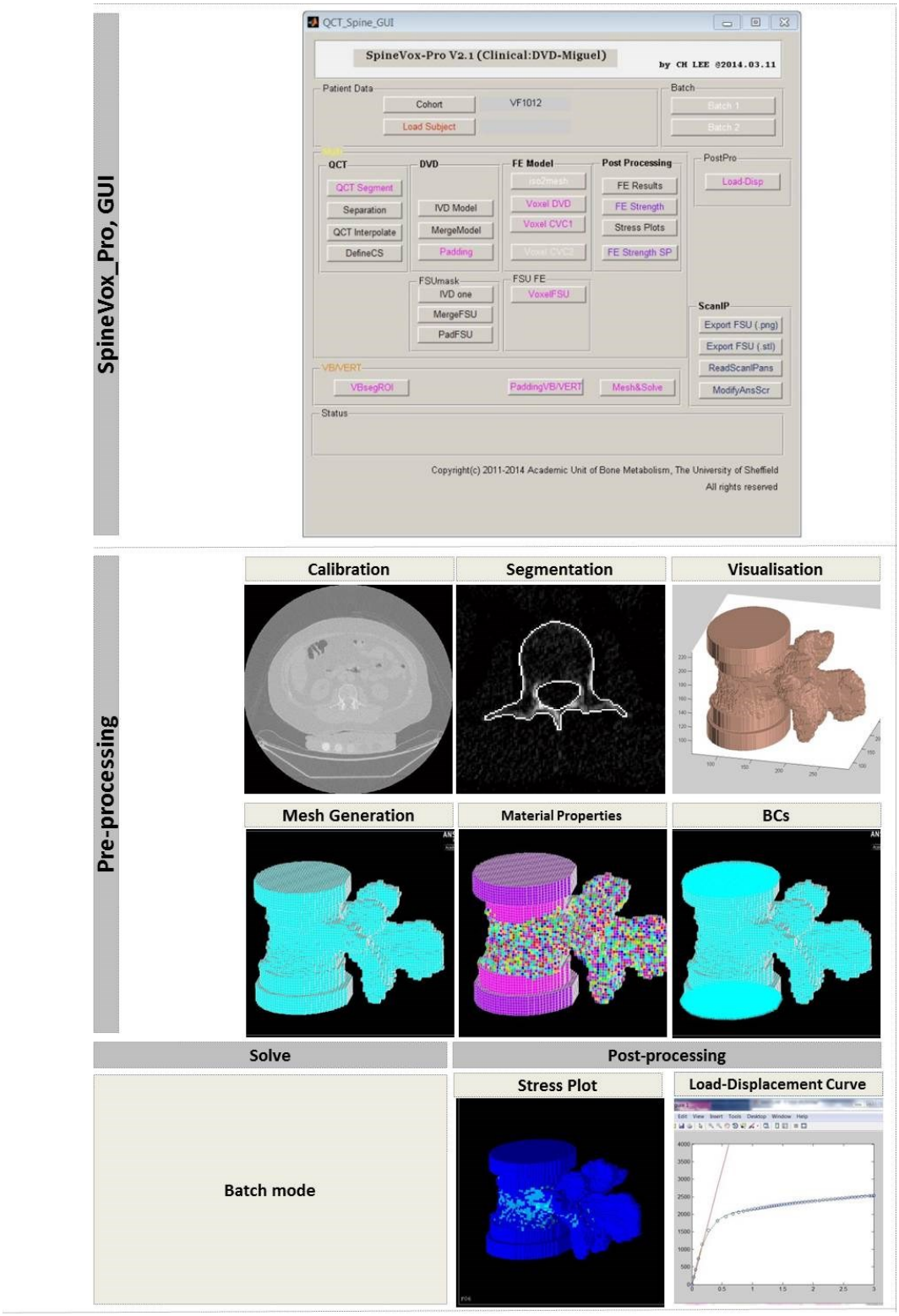

Figure 6.1: SpineVox-Pro, procedure to generate the DVD FE model

Isotropic, elastic-perfectly plastic material properties were considered for the vertebra. To assign material properties for the vertebra, empirical relationships between volumetric bone density and bone material properties were used to determine the elastic modulus E and compressive yield stress limit σ_{yc} for the vertebra as before. The original volumetric BMD values were divided into 100 intervals to limit the number of materials in the FE model. The ultimate stress limit σ_{uc} and yield strain limit ε_y and ultimate strain limit ε_u of the vertebra were assigned according to the literature (Morgan and Keaveny, 2001, Kopperdahl et al., 2002, Crawford et al., 2003a, Morgan et al., 2003).

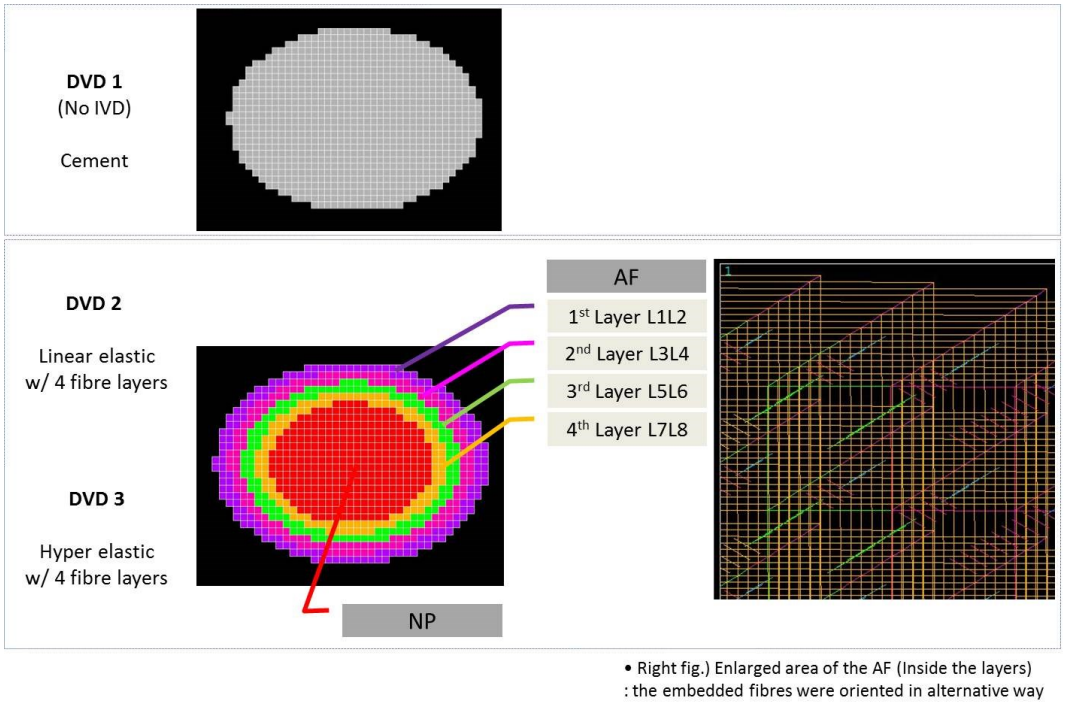

Figure 6.2: Three different types of material properties are assigned for the IVD area of the subject-specific finite element model of DVD unit: DVD 1) simple linear elastic cement for both the nucleus pulposus (NP) and annulus fibrosus (AF); DVD 2) a linear elastic material property for the NP and ground substance of the matrix of the annulus with 4 embedded fibre layers in the AF; DVD 3) a hyper elastic material property for both the NP and ground substance of the annulus with 4 fibre layers embedded in the AF. The embedded fibres were orientated in alternating layers, 30° and 150° from the horizontal axis.

For comparison purposes, three different types of material properties were assigned to the IVD area as shown in Figure 6.2, which resulted in 3 different DVD FE models labelled as: DVD 1, DVD 2, DVD 3. The first material chosen was one that is often used in research into vertebral strength this was used previously in the vertebral body FE model without the IVD. The DVD 1 used simple linear elastic cement for both the nucleus pulposus (NP) and annulus fibrosus (AF). For second and third IVD material models, two representative material properties for the FSU FE models in the spinal research were chosen: DVD 2) a linear elastic material property for the NP and ground substance of the matrix of the annulus with 4 embedded fibre layers in the AF; DVD 3) a hyper elastic material property for both the NP and ground substance of the annulus with 4 fibre layers embedded in the AF (Wang et al., 1997, Schmidt et al., 2006, Strange et al., 2010). The embedded fibres were orientated in alternating layers, 30° and 150° from the horizontal axis.

The mechanical properties of the dental cement used for the padding were obtained from the manufacturer's manual ($E = 2000\ MPa, \nu = 0.3$; Ultrahard Die Stone ISO-Type IV, Kerr) as discussed in the previous study described in Chapter 4. The material properties of vertebra and IVD used are summarised in Tables 6.2 and 6.3.

Table 6.2: Material properties (Vertebra)

Component	Material properties	
Vertebra	$E\ (MPa) = -34.7 + 3230\rho_{QCT}\ (g/cm^3)$	
	$\nu = 0.381$	
	$\sigma_{yc}\ (MPa) = -0.75 + 24.9\rho_{QCT}\ (g/cm^3)$	
	$\sigma_{uc}\ (MPa) = 1.2 * \sigma_y\ (MPa)$	
	$\varepsilon_y = 0.0078$	
	$\varepsilon_u = 0.145$	
Padding	$E = 2000\ MPa$	$\nu = 0.3$

Table 6.3: Material properties (IVD)

	Part		Material properties	
DVD 1	Cement	Elastic	$E = 3000\ MPa$	v = 0.3
DVD 2	Nucleus pulposus[1]	Elastic	$E = 2\ MPa$	v = 0.499
	Annulus ground substance[1]	Elastic	$E = 8\ MPa$	v = 0.4
	Annulus fibrosus[2]	Elastic	$E_{L1L2} = 500\ MPa$ $E_{L3L4} = 485\ MPa$ $E_{L5L6} = 420\ MPa$ $E_{L7L8} = 360\ MPa$	v = 0.3
DVD 3	Nucleus pulposus[3]	Hyperelastic Mooney-Rivlin	$C_1 = 0.12$ $C_2 = 0.03$ $D_1 = 0.0667$	
	Annulus ground substance[3]	Hyperelastic Mooney-Rivlin	$C_1 = 0.56$ $C_2 = 0.14$ $D_1 = 0.143$	
	Annulus Fibrosus[2] (REINF265)	Elastic	$E_{L1L2} = 500\ MPa$ $E_{L3L4} = 485\ MPa$ $E_{L5L6} = 420\ MPa$ $E_{L7L8} = 360\ MPa$	v = 0.3

* 1/ Wang et al., 1997, 2/ Strange et al., 2010, 3/ Schmidt et al., 2006

* L1 to L8: represents the number of fibre layer embedded in the AF

For the hyperelastic model (DVD 3), the fluid-like behaviour of the annulus ground substance and NP was simulated using an in incompressible, hyper-elastic, two parameter Mooney-Rivlin (C_1, C_2) formulated with the following strain energy function W:

$$W = C_1(I_1 - 3) + C_2(I_2 - 3) + \frac{1}{d}(J - 1)^2 \quad (6.1)$$

Where,

C_1, C_2 : Material constants characterizing the deviatoric deformation of the material

I_1, I_2 : First/second invariants of the deviatoric strain tensor

$d = 2/K$: Material incompressibility parameter

$J = V/V_0$: Local volume ratio

K : Initial bulk modulus of the material

A simple pure compression condition was simulated with the inferior surface of the lower padding constrained in all degrees of freedom. Three millimetre distributed displacement boundary conditions were applied on the superior surface of the upper padding. The FE models were then solved using ANSYS (ANSYS Inc., Canonsburg, PA, USA) in batch mode of the SpineVox-Pro. Nonlinear analysis was performed using the Newton-Rahpson method with a postyield modulus of 0.05 MPa (Bayraktar et al., 2004, Reilly and Burstein, 1975). A 0.2% offset method in the load-displacement curve was chosen to define vertebral strength.

6.2.6 Statistical Analysis

Statistical analysis was carried out using STATA11 (StataCorp LP., TX, USA). The 2 control groups were combined to form a single control group for statistical analysis. Group means and standard deviations were calculated for the case and control groups. Differences in the estimated strength from the total study population were also expressed in absolute values scaled to the SD of the total study population. The odds ratio (OR) for vertebral fracture for 1 SD decrease in covariates was derived from logistic regression, and the area under the curve (AUC) was obtained from analysis of receiver operating characteristics.

6.3 Results

Compared to the controls, the fracture cases had significantly ($p < 0.0001$) lower vertebral BMD (0.79 ± 0.11 v. 0.89 ± 0.12 g/cm^2), volumetric BMD (0.08 ± 0.02 v. 0.11 ± 0.03 g/cm^3) and FE-strength (1405.06 ± 90 v. 2155.74 ± 88 N for DVD 1, 1231.25 ± 79 v. 1801.26 ± 62 N for DVD 2, 1206.19 ± 78 v. 1694.37 ± 54 N for DVD 3).

Table 6.4 summarises the FE strength results together with the basic information for the study population.

Table 6.4: FE strength results of the case group and control group

	Case Group (N= 16)	Control Group (N= 57)	SD score (Case)	SD score (Control)
Age (years)	71 ± 6.04	70 ± 5.92	0.12	-0.03
Weight (kg)	†65.52 ± 8.92	†74.94 ± 17.39	-0.45	0.13
Height (cm)	158.51 ± 5.01	160.07 ± 14.06	-0.10	0.03
DXA				
Hip BMC	28.45 ± 4.52	31.49 ± 5.25	-0.45	0.13
Hip aBMD (g/cm^2)	0.79 ± 0.11	0.89 ± 0.12	-0.59	0.17
Lumbar spine BMC	41.27 ± 8.97	53.60 ± 13.26	-0.72	0.20
Lumbar spine aBMD (g/cm^2)	0.80 ± 0.10	0.95 ± 0.15	-0.77	0.22
QCT				
vBMD at L2 (mg HA/cm^3)	79.77 ± 22.28	108.60 ± 26.43	-0.80	0.22
FE-strength DVD 1	1405.06±360.76	2155.74±665.05	-0.86	0.24
FE-strength DVD 2	1231.25±314.46	1801.26±468.15	-0.89	0.25
FE-strength DVD 3	1206.19±311.53	1694.37±408.17	-0.87	0.24

* Values represent the mean ±SD.

†p = 0.003

Logistic regression analysis showed that FE-strength was significantly ($P < 0.0001$) associated with vertebral fracture, and the odds ratios (ORs) for vertebral fracture (95% CI) being 12.2 (3.0-49.2) for DVD 1, 8.35 (2.6-26.8) for DVD 2, 6.9 (2.4-20.3) for DVD 3, as was BMD 3.7 (1.6-8.5) and volumetric BMD 4.8 (1.9-12.4) as shown in Table 6.5. After adjustment for BMD, the ORs of FE-strength were still significant ($P < 0.05$): 11.4 (2.4-53.9) for DVD 1, 6.7 (2.0-23.3) for DVD 2 and 5.3 (1.6-17.0) for DVD 3.

Table 6.5: Odds ratio per SD decreases in variables

Variables	Odds ratio 95% CI	P value
Total spine aBMD	3.72 (1.62-8.53)	0.002
L2 vBMD	4.85 (1.89-12.45)	0.001
FE-strength DVD 1	12.22 (3.03-49.24)	0.000
FE-strength DVD 2	8.35 (2.60-26.84)	0.000
FE-strength DVD 3	6.94 (2.37-20.34)	0.000

The AUC (95% CI) for FE-strength was 0.86 (0.77-0.96) for DVD 1, 0.87 (0.78-0.95) for DVD 2, 0.85 (0.76-0.95) for DVD 3, higher but not significantly higher than that for BMD (0.79).

In a model where we added FE strength to BMD, AUC increased to 0.89 (0.80-0.97) for DVD 1, 0.89 (0.81-0.96) for DVD 2, and 0.87 (0.78-0.96) for DVD 3 as shown in Figure 6.3. The AUCs for DVD 1 and DVD 2 were significantly ($p<0.05$) larger than that for BMD alone.

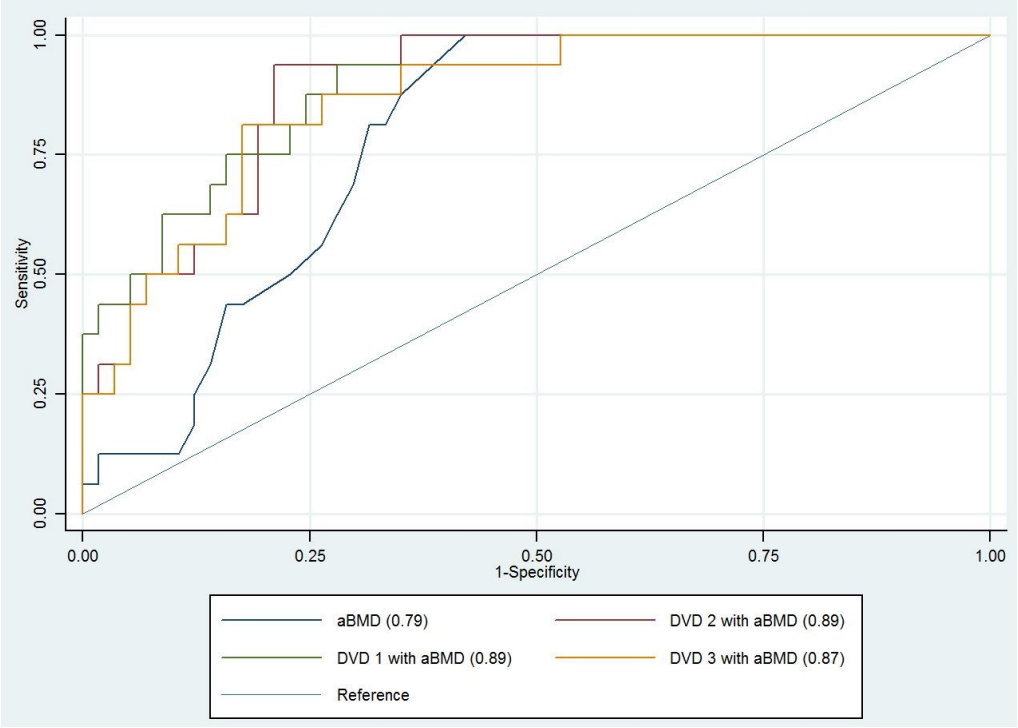

Figure 6.3: AUC curve

6.4 Discussion

The aim of the study described in this chapter was to investigate whether vertebral strength derived from the DVD FE model can discriminate between women with and without vertebral fracture. FE strength from the developed DVD FE model was able to discriminate between women with and without vertebral fracture according to the ORs (3.72 for aBMD; 12.22 for DVD 1; 8.35 for DVD 2; 6.94 for DVD 3).

Some studies of the discrimination power of aBMD by DXA and vBMD by QCT have been published. Volumetric BMD by QCT generally has been found to have superior discriminatory power to DXA. Yu et al. (1995) reported that QCT trabecular BMD offered the best discrimination power between post-menopausal women with and without fractures according to the area under the ROC (0.81 for QCT; 0.72 for L-DXA; 0.65 for PA-DXA), although low BMD by QCT and DXA is strongly associated with the prevalence of vertebral fracture (Yu et al., 1995). Gugliemlmi et al. (1999) also showed that QCT has stronger power according to odds ratios by age-adjusted logistic regression analysis (2.9 for QCT; 1.5 for DXA) and some other groups support this conclusion (Guglielmi et al., 1999, Duboeuf et al., 1995, Grampp et al., 1997). However, one study using DXA and QCT showed that the discrimination power of QCT is not significantly different to that of DXA (Lang et al., 2002).

In addition, several studies have also been reported that investigate the power of fracture discrimination by the QCT-based FE models. QCT-based FE derived bone strength showed a better ability to discriminate between women with and without vertebral fractures than BMD by DXA according to AUC (0.8 for FE strength; 0.73 for aBMD by DXA; 0.79 vBMD by QCT) (Melton et al., 2007). Wang et al. (2012) investigated the discrimination power of QCT-based FE derived strength in men and reported that FE strength predicted by QCT-based FE models has better power than BMD with age-adjusted hazard ratios (7.2 for FE strength; 3.2 for aBMD by DXA) (Wang et al., 2012). Imai et al. (2008) also showed that the predicted vertebral strength at L2 in the nonfracture group was greater than that in the fracture group (2489 ± 580 vs. 1764 ± 588 $p < 0.0001$) (Imai et al., 2008). The work described here gave similar results to these studies.

The majority of patient-specific FE models do not include an IVD and isolated vertebral bodies are also used in mechanical testing due to the ease of both the loading control and the calculation of vertebral stiffness. However, vertebral strength and the distribution of load on the vertebra via endplates depend on the condition of the IVD: i.e. whether the IVD is healthy or degenerated with changes in geometry and material properties. In this study, the patient-specific geometry of IVD was represented using information on the gap between vertebrae on the L1 to L3 QCT scan. For comparison of the stress and strain distribution in the vertebral body, three different types of material models for the IVD area were assigned for each patient. DVD 1 represents vertebra without the IVD, DVD 2 and DVD 3 represent vertebra with IVD. The first material (DVD 1) chosen was one that is often used in research into vertebral strength. This was used previously in the vertebral body FE model without the IVD. Therefore, simple linear elastic material property was considered for both the nucleus pulposus (NP) and annulus fibrosus (AF). For second and third material models, two representative material properties for the FSU FE models in the spinal research were chosen: a linear elastic material property for the NP and ground substance of the matrix of the annulus with 4 embedded fibre layers in the AF (DVD 2); a hyper elastic material property for both the NP and ground substance of the annulus with 4 fibre layers embedded in the AF (DVD 3). The embedded fibres were orientated in alternating layers, 30° and 150° from the horizontal axis. Higher stiffness and vertebral FE strength was found in DVD 1 compared to DVD 2 and DVD 3. Figure 6.4 show the FE strength values from one patient data (VF 3001) on each load-displacement curve (4070 N for DVD 1; 3335 N for DVD 2; 2972 N for DVD 3). The proportion of forces transferred to the endplate and deeper into the inner trabecular network may be lower than in a more realistic DVD representation, which gives a higher overall vertebral FE strength as shown in Figure 6.5.

These results support previous research which found that the embedded cement disc model has a higher yield strength than the that of the DVDs models (Maquer et al., 2013). Hussein et al. (2013) also showed similar results in *ex vivo* mechanical testing of rabbit thoracic vertebral bodies using digital volume correlation (Hussein et al., 2013). The technique quantified deformations throughout the vertebral body using the recorded micro CT scans at each loading step. Specimens that included an IVD showed lower stiffness and lower ultimate force and higher ultimate displacement under mechanical tests than the isolated vertebral body.

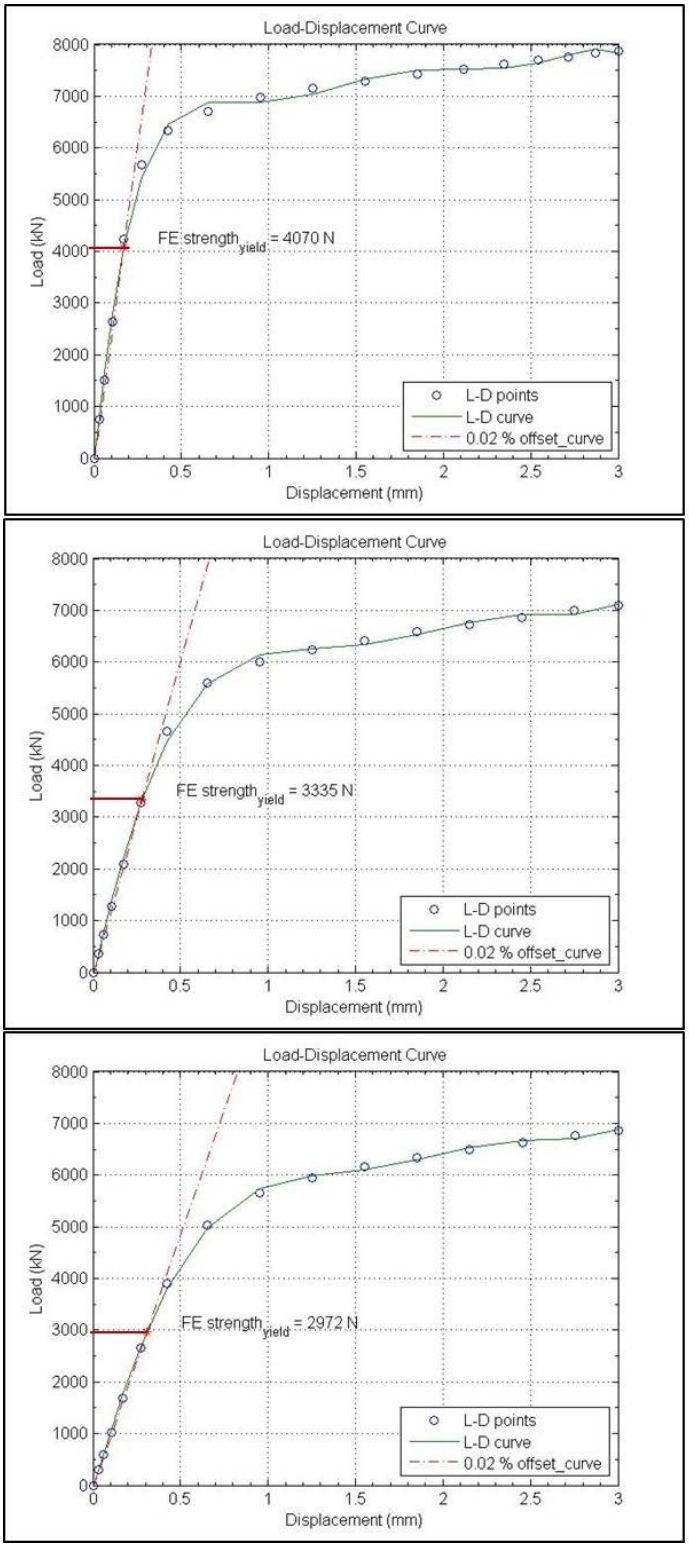

Figure 6.4: FE strengths from one patient data (VF 3001) on each Load-displacement curve: DVD 1, DVD 2 and DVD 3 FE models

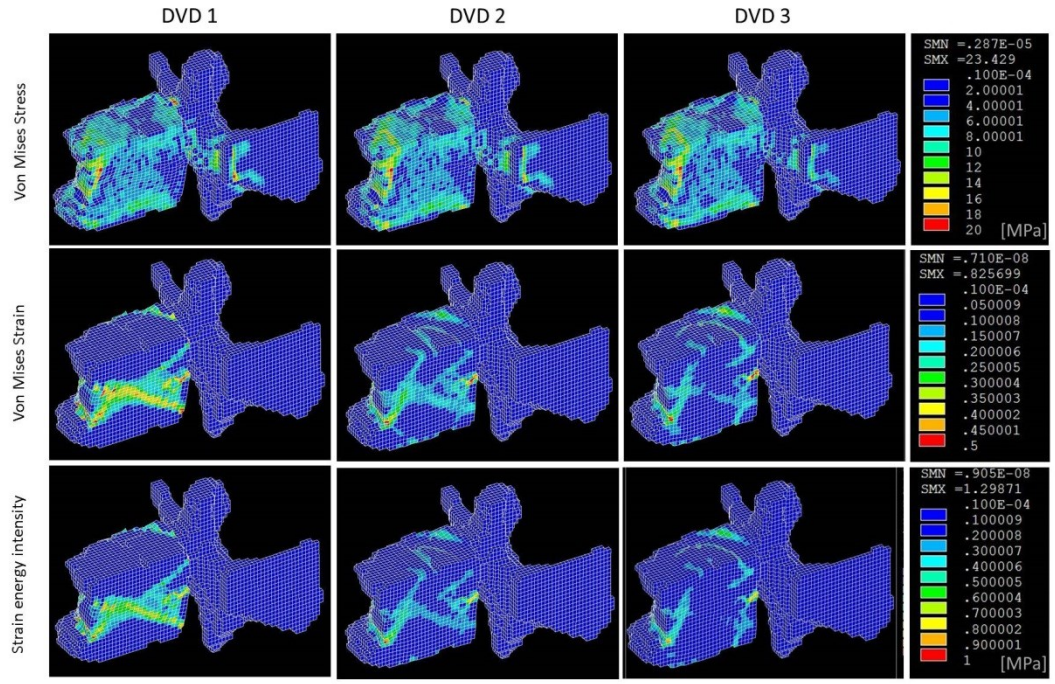

Figure 6.5: Stress and strain plots from one patient data (VF 3001)

Buckley et al. (2006) suggested that it might not be necessary to generate an IVD explicitly in order to predict vertebral compressive strength since the load distribution on the endplate had low impact on strength estimation (Buckley et al., 2006). However, this study indicated that the stress distribution on the endplates can affect predicted strength. It is important to note that the FE models were simulated with generic boundary conditions, so this was not a study that was representative of *in vivo* loading conditions nor was an experimental. For these reasons, direct interpretation of the results and comparison with the current work might not be appropriate.

Again, some limitations of the current work should be noted. Even though the FE model used was generated based on patient-specific geometry, it was not able to reflect the difference in IVD material properties related to the specific IVD health status of each patient. Further images, for example MRI scans, are required to obtain patient-specific information for IVD, as only QCT scans were available in clinical studies. In addition, this study is limited to a small number of scans and a cross-sectional case-control design. A further longitudinal study with many more scans is required if the discriminative power

of the model is to be determined. Furthermore, fracture-case patients had fractures at different levels of the spine which were not necessarily coincided with the FE modelled L2. These differences might affect the discrimination power.

Despite these limitations, the main outcome is that it clearly shows that a patient-specific DVD FE model was able to discriminate between women with and without vertebral fracture independent of aBMD by DXA by means of the predicted vertebral strength. Furthermore, this study indicates the importance of considering an IVD within the vertebral FE model in terms of predicting the vertebral strength and stress/strain distribution. The DVD FE model represents a patient-specific FE model that would provide a feasible method for clinical research application.

CHAPTER 7 Impact of Teriparatide Treatment on Vertebral Strength in Postmenopausal Women using a Patient-Specific Finite Element Model of the Disc-Vertebra-Disc Unit

This chapter presents a second clinical application of the patient-specific DVD FE model to investigate the effect of a two year period of teriparatide (TPTD) treatment on vertebral strength in postmenopausal women.

7.1 Introduction

The majority of treatments for osteoporosis act by the inhibition of bone resorption (anti-resorptive treatments). However, treatments which simulate bone formation (anabolic treatments) such as Parathyroid hormone (PTH 1-34: Teriparatide, Forsteo; PTH 1-84: intact PTH, Preotact) have been developed recently. These treatments have been shown to result in a decrease in fracture risk: vertebral fracture risk was reduced by 65 - 69% depending on dose (Neer et al., 2001, Greenspan et al., 2007). Teriparatide (PTH 1-34) is the only licensed anabolic therapy for osteoporosis in postmenopausal women in the UK. Several studies using bone turnover markers have shown that PTH increases bone formation that precedes bone resorption (Black et al., 2003, Chen et al., 2005, Eastell et al., 2006, Bauer et al., 2006). Treatment effects are investigated using bone densitometric parameters: aBMD by DXA, vBMD by QCT. PTH increases spine BMD but not femoral neck BMD. In women with postmenopausal osteoporosis treated with teriparatide a mean increase in spine BMD of 6% at 6 months and 13% at 24 months was observed (Obermayer-Pietsch et al., 2008). However, the increase in aBMD by DXA is not

sufficient to explain the reduction in fracture risk observed in response to the therapy. The increase of aBMD by DXA with TPTD treatment for the lumbar spine explains 30-41% of the vertebral fracture risk reduction and the remaining portion is associated with non-BMD parameters (Chen et al., 2006). Imaging parameters determined with high-resolution CT (HRCT) are used for monitoring the treatment effect on bone. One PTH study by HRCT reported an increase in trabecular bone volumetric BMD of 13% at 6 months and showed that high resolution CT of the spine allowed the measurement of parameters of bone microstructure that increased by 16% at 6 months (Graeff et al., 2007).

Recently, studies have used the vertebral strength derived from a QCT-based vertebral body FE model to investigate the therapeutic effects on vertebral strength (Keaveny et al., 2007, Lewiecki, 2009, Imai et al., 2009, Graeff et al., 2009, Chevalier et al., 2010) and used the QCT femoral FE model to determine the effect on the femoral strength (Keaveny et al., 2008, Keaveny et al., 2011). This research showed that the FE estimated strength has a larger treatment effect relative to the baseline on bone than densitometric variables.

The aim of this chapter is to use the patient-specific Disc-Vertebra-Disc unit (DVD) FE model to investigate the effect of teriparatide (TPTD) treatment on vertebral strength in postmenopausal women. The development and application of DVD FE model for clinical study has already been described in the previous chapter (The study of vertebral fracture discrimination in postmenopausal women).

7.2 Materials and methods

7.2.1 Study Population

In this open-label, single centre study, postmenopausal women with osteoporosis (n=20, BMD T score < -2.5 at spine or hip) were treated with teriparatide (FORSTEO, 20 micro grams daily) for 104 weeks. The original clinical study was carried out by Dr. Richard Eastell, Professor of Bone metabolism, University of Sheffield. The clinical study was approved by the North West 2 Research Ethics Committee (REC Ref No. 10/H1005/59).

The treatment under study (Forsteo) is licensed in the UK for the treatment of osteoporosis. In addition to the study drug, all subjects received a vitamin D3 load of 100,000 IU at the start of the study and six-monthly thereafter. All subjects also received 600mg of elemental calcium and 400 IU of vitamin D per day throughout the study. Table 7.1 details the treatments.

The purpose of the original study was to develop a strategy for evaluating the effectiveness of teriparatide using biochemical markers of bone turnover and changes in BMD. At the time of writing this study is still on going and 4 patients will have their last visit by the end of January, 2015.

Table 7.1: Treatment for patients

IMP	Dose Form and Strength	Manufacturer, Name
Teriparatide	20 mcg subcutaneous injection once daily	Eli Lilly and Company, Basingstoke, Hamps, Forsteo
Non-IMP		
Cholecalciferol (Dekristol or equivalent)	5 x 20,000 IU capsules at screening and six-monthly thereafter (see below for full details of dosing).	Jenapharm Gmbh, Germany, Dekristol
Calcium/Vitamin D (Adcal D3,or equivalent)	Single chewable tablet containing 600mg calcium and 400IU Vitamin D3 once a day	Prostraken Ltd, Galashiels, UK, Adcal D3

*Timeline: Visit02: Baseline 1 (-28 ± 6days); Visit08: Week 26 (175 ± 7days); Visit10: Week 52 (364 ± 7days); Visit14: Week 104 or end of study visit (728 ± 7days)

7.2.2 Bone Mineral Density (DXA)

DXA was used to measure bone mineral density of the lumbar spine (L1 - L4) and total hip. Vertebral fracture assessment of the thoraco-lumbar spine was performed at the screening visit in those subjects with BMD T score of ≤-2.5 at the spine and/or hip and also at week 104 in those completing the study. If a participant withdraws early from the

study they were asked to return for an end of study visit which include the DXA measurements that would have been obtained at week 104 if they had completed the study.

7.2.3 Quantitative Computed Tomography (QCT)

Bone mineral density at the spine and hip were measured by DXA (Discovery, Hologic Inc.) and QCT (LightSpeed, GE Medical Systems) at baseline (weeks -1), 26, 52, and 104 weeks. The QCT scanning parameters were 120kV, 60mAs/slice, 0.9375 x 0.9375 x 0.625 mm voxel size. The characteristics of the participants in the biomechanical analysis by CT and DXA at each visit are as shown in Table 7.2.

Table 7.2: Characteristics of participants in the biomechanical analysis CT and DXA at each visit

		Baseline -28 ± 6days	Week 26 175 ± 7days	Week 52 364 ± 7days	Week 104 728 ± 7days
Age (years)	Years	64.40±15.35			
Weight	Kg	63.82±8.43	63.45±8.22	63.18±8.70	64.25±11.14
Height	cm	161.13±4.52	161.08±4.64	161.20±4.78	161.70±3.32
DXA					
Hip aBMD	g/cm^2	0.76±0.08	0.76±0.08	0.77±0.08	0.79±0.10
spine aBMD(L1-L4)	g/cm^2	0.73±0.04	0.77±0.05	0.79±0.04	0.82±0.05
QCT					
vBMD (L1-L3)	mg/cm^3	86.13±16.99	95.77±19.74	103.91±20.04	99.82±21.84
vBMD at L2	mg/cm^3	87.02±19.32	97.55±22.23	105.08±20.21	103.48±20.82

* Values represent mean SD.

A solid calibration phantom (Mindways, San Francisco, CA) was used to calibrate Hounsfield unit (HU) values to bone mineral density as before. L1 to L3 were used to generate DVD FE models of the L2 vertebra.

7.2.4 Subject-specific Finite Element Model of Disc-Vertebra-Disc Unit in Spine Vox-Pro

The patient-specific FE model of the Disc-Vertebra-Disc unit (DVD), previously developed and described in Chapter 6, was used. The L2 part from L1 to L3 patient QCT scans were used to generate the DVD FE model. SpineVox-Pro was used to generate the FE models. The procedure used to generate the DVD FE model is identical to that described in Chapter 6.2.5 and illustrated in Figure 6.1: calibration, segmentation, visualisation, mesh generation, material properties assignment, boundary condition assignment, and fracture load definition.

Of the 3 different types of material properties for the IVD area which were used in Chapter 6, only two types of material properties which actually took account into the IVD on the DVD FE models were considered in this chapter. These were: DVD 2 and DVD 3.

7.2.5 Statistical Analysis

Statistical analysis was carried out using STATA11 (StataCorp LP., TX, USA) as before. Group means and standard deviations were calculated for all visits and percentage changes from baseline were found on a group basis. Changes in the estimated strength from baseline were also expressed in absolute values scaled to the SD of the baseline visit. This method allows the comparison of differently scaled variables. Significance of the changes from baseline was assessed by a one sample, two-sided t-test.

7.3 Results

Table 7.3 summarises the mean absolute baseline values for densitometric data and mean percentage change from baseline at each visit throughout the FORSTEO study. In addition, the difference from baseline at each visit was also shown in standard deviation units using the mean and SD of the baseline. Some data could not be obtained for different reasons: image data corruption (F18 at baseline, F05 at 6 months, F14 at 12 months), patient withdraw (F09 at 6 months, F02 at 12 months, F01 and F13 at 24

months), and scheduled at the analysis point (F05, F14-F16) as shown in Tables 7.4 and 7.5.

According to the densitometric results the treatment had positive effects on vertebral density. The values of areal BMD by DXA and vBMD by QCT for the spine showed increases from the baseline at each visit. However, whilst the vBMD by QCT increased until 12 months, it was found to have a slight decrease at 24 months.

Table 7.3: Absolute baseline values of densitometric data and mean percentage change from baseline at each visit of the FORSTEO study

			Percent change (%)			SD score		
		Baseline	Week 26	Week 52	Week 104	Week 26	Week 52	Week 104
DXA								
Hip aBMD	g/cm^2	0.76±0.08	-0.37	-0.06	1.55	-0.08	-0.04	0.12
L1-L4 aBMD	g/cm^2	0.73±0.04	5.21	7.59	10.87	1.10	1.59	2.28
QCT								
L1-L3 vBMD	mg/cm^3	86.13±16.99	11.94	22.73	21.91	0.59	1.11	1.04
vBMD at L2	mg/cm^3	87.02±19.32	13.01	22.31	22.42	0.30	0.94	0.89

Tables 7.4 and 7.5 present the results of the DVD FE model with materials DVD2 and DVD 3, respectively. The treatments also had a positive effect on vertebral strength from the both DVD FE models. The result shows that the vertebral strength increased from baseline at 6, 12, 24 months. Strength increased rapidly until 12 months of treatment, increasing by 30 % (DVD 2) and 27 % (DVD 3) at 12 months and then stabilising as shown Figure 7.1.

Although the strength values obtained with the two IVD material models were slightly different, the overall predicted differences with respect to the treatment were not significant.

Table 7.4: FE-derived strength_DVD2

	Baseline1 -28 ± 6days	Week 26 175 ± 7days	Week 52 364 ± 7days	Week 104 728 ± 7days
F01	1001	977	1221	Withdrawn
F02	1339	1305	Withdrawn	Withdrawn
F03	1066	1536	1805	1681
F04	1255	2253	2107	2211
F05	1503	Invalid scan	1758	Scheduled
F06	1094	930	1307	1095
F07	1645	1445	2081	1546
F08	1108	1279	1380	1280
F09	1145	Withdrawn	Withdrawn	Withdrawn
F10	1375	1794	1935	2169
F11	1902	2147	2473	2441
F12	1362	1526	1560	1651
F13	1076	1594	1902	Withdrawn
F14	1801	2072	Invalid scan	Scheduled
F15	1426	1807	2029	Scheduled
F16	1190	1703	1804	Scheduled
F17	1892	1913	1828	1843
F18	Invalid scan	1307	1499	1476
F19	1285	1703	1722	2192
F20	1396	1614	1609	1933
Mean	1361.11 ± 279.01	1605.83 ± 367.36	1765.88 ± 319.71	1793.17 ± 411.41
SE	64.01	86.59	77.54	118.77
PC (%)	0.00	20.27	34.28	32.48
SD Score	-	1.03	1.73	1.69
Count	19	18	17	12

* Values represent the mean ±SD.

Table 7.5: FE-derived strength_DVD3

	Baseline1 -28 ± 6days	Week 26 175 ± 7days	Week 52 364 ± 7days	Week 104 728 ± 7days
F01	981	946	1175	Withdrawn
F02	1183	1287	Withdrawn	Withdrawn
F03	1084	1507	1753	1667
F04	1257	2171	2002	2114
F05	1421	Invalid scan	1665	Scheduled
F06	1012	933	1290	1070
F07	1566	1401	1862	1530
F08	1099	1273	1350	1263
F09	1088	Withdrawn	Withdrawn	Withdrawn
F10	1334	1415	1830	1974
F11	1769	1953	2271	2049
F12	1360	1525	1568	1618
F13	1079	1568	1804	Withdrawn
F14	1684	1992	Invalid scan	Scheduled
F15	1340	1657	1742	Scheduled
F16	1422	1570	1741	Scheduled
F17	1806	1775	1730	1730
F18	Invalid scan	1289	1441	1431
F19	1166	1583	1575	2034
F20	1391	1590	1561	1892
Mean	1318.00±250.69	1540.06±326.67	1668.24±267.87	1697.67±332.27
SE	57.51	77.00	64.97	95.92
PC (%)	0.00	18.27	29.42	29.94
SD score	-	0.91	1.45	1.49
Count	19	18	17	12

* Values represent the mean ±SD.

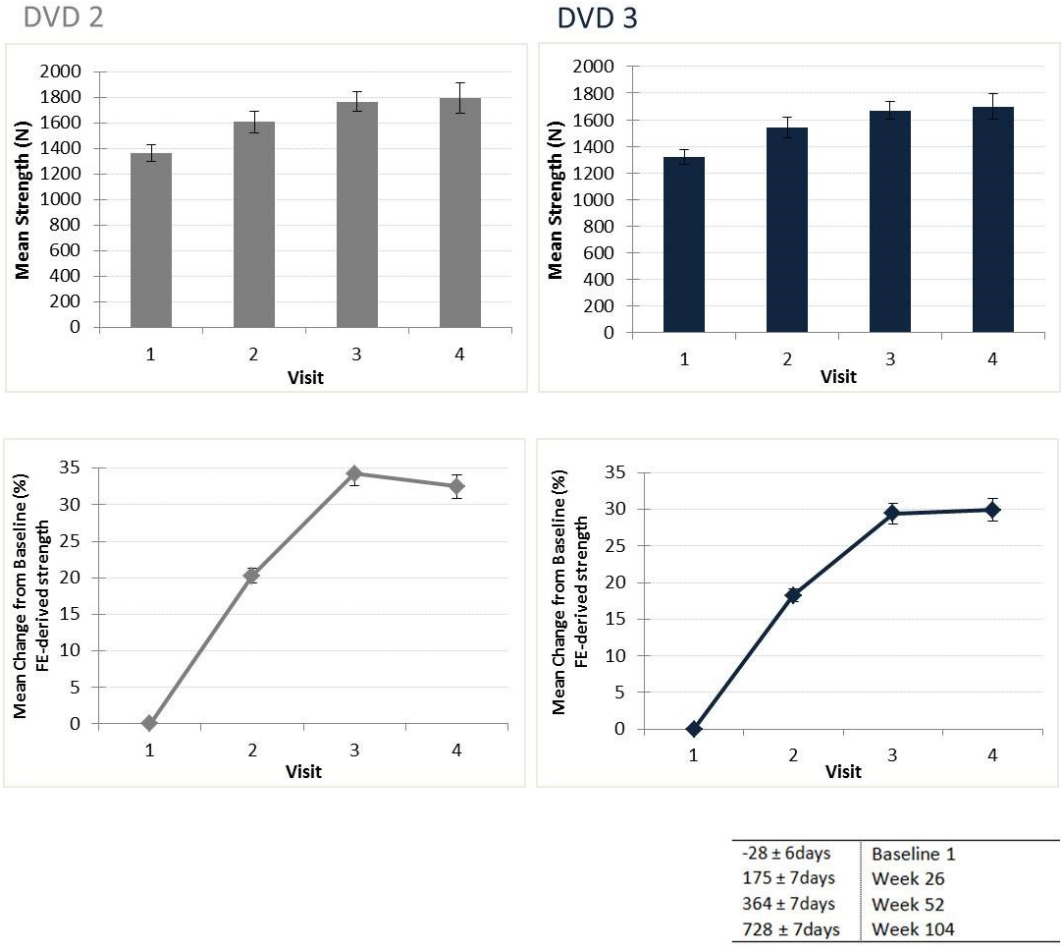

Figure 7.1: Mean FE strength and mean percentage change from baseline at each visit (DVD 2 and DVD 3)

Figure 7.2 shows the individual percentage changes of the FE strength from baseline at each visit in model with DVD 3 material. Most of the patients show positive treatment effect except the F07 and F17 at the final visit, although the treatment effect is varied with the patient at each visit (there were some negative values at week 26). Two patients showed gradual increasing of the FE strength during the treatment period (F10 and F12).

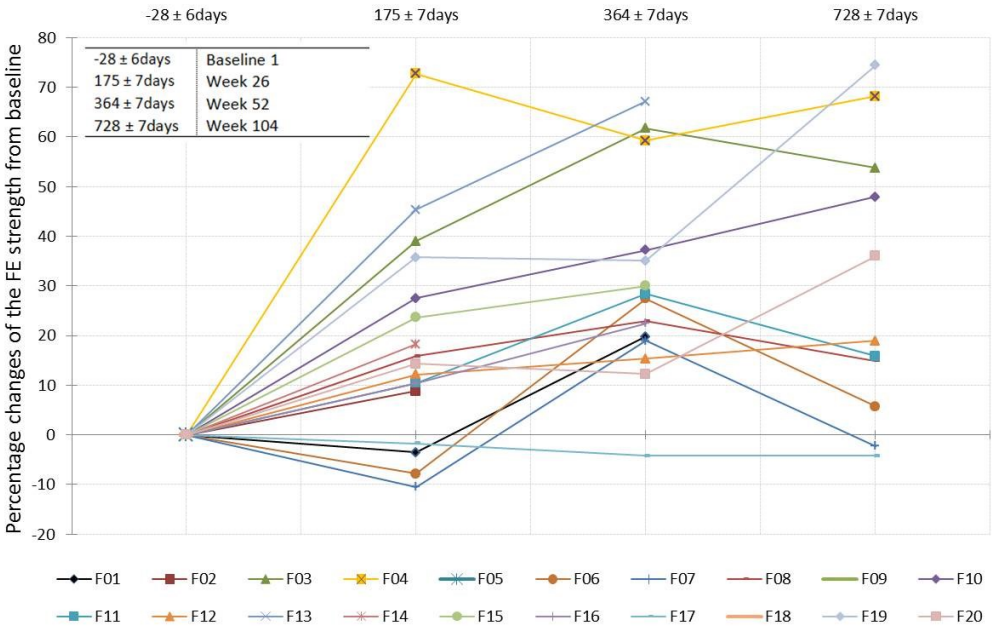

Figure 7.2: Individual percentage changes of the FE strength from baseline at each visit

Figures 7.3 and 7.4 illustrated a load-displacement curve and strain energy intensity plot of the F12 DVD FE model using DVD 3 material properties at each visit.

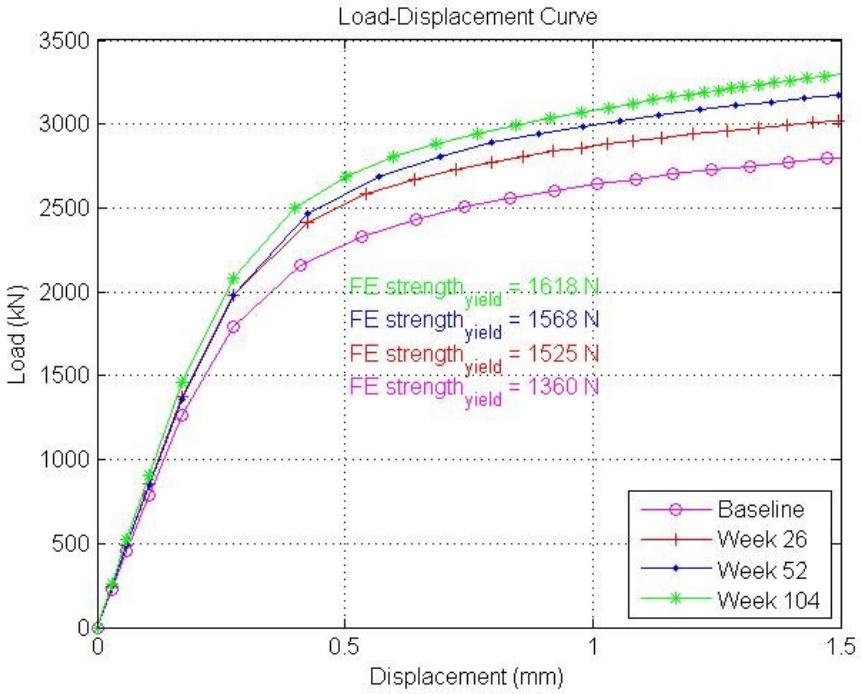

Figure 7.3: Typical load-displacement at all four visits for one patient (F12: DVD 3)

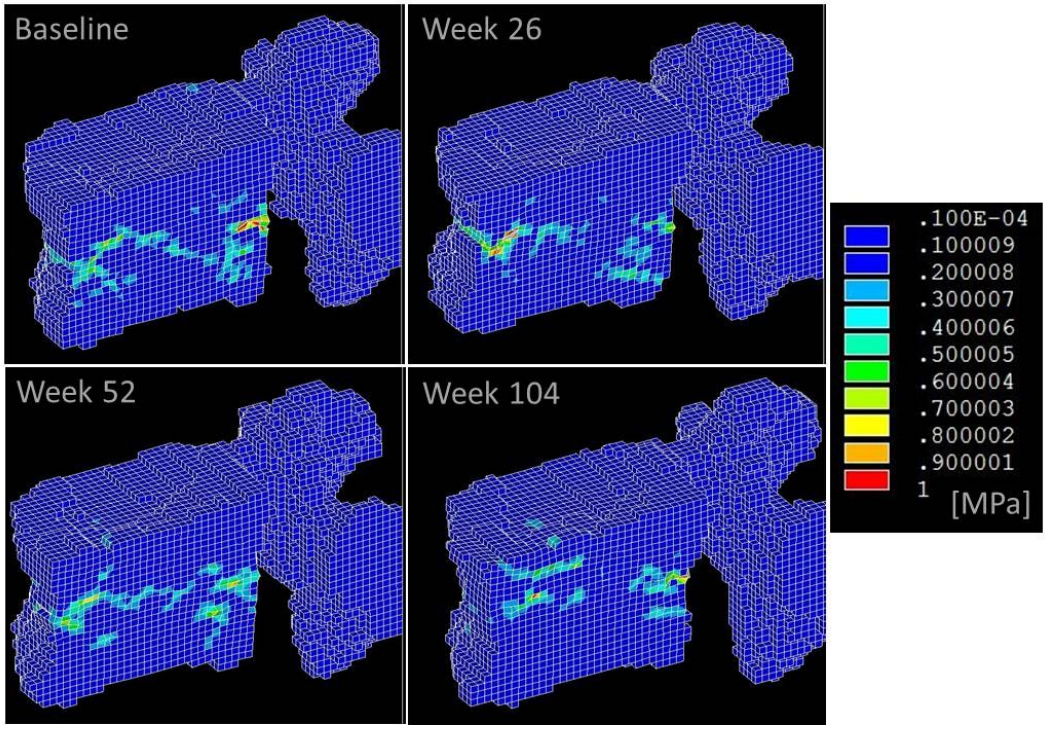

Figure 7.4: Typical strain energy intensity plot at all four visits for one patient (F12: DVD 3)

7.4 Discussion

The aim of this study was to investigate the effect of teriparatide treatment on vertebral strength in postmenopausal women after 6, 12 and 24 months using DVD FE models. The study indicates that the treatment increased not only the densitometric variables but also the vertebral strength as predicted by DVD FE model. At the 2 year follow up study, the increases at the end of visit were 10% for DXA spine aBMD, 14% for QCT vBMD (L1-L3), and 16% for QCT vBMD (L2). FE predicted strength went up by approximately 30% for DVD 3 as shown in Figure 7.5.

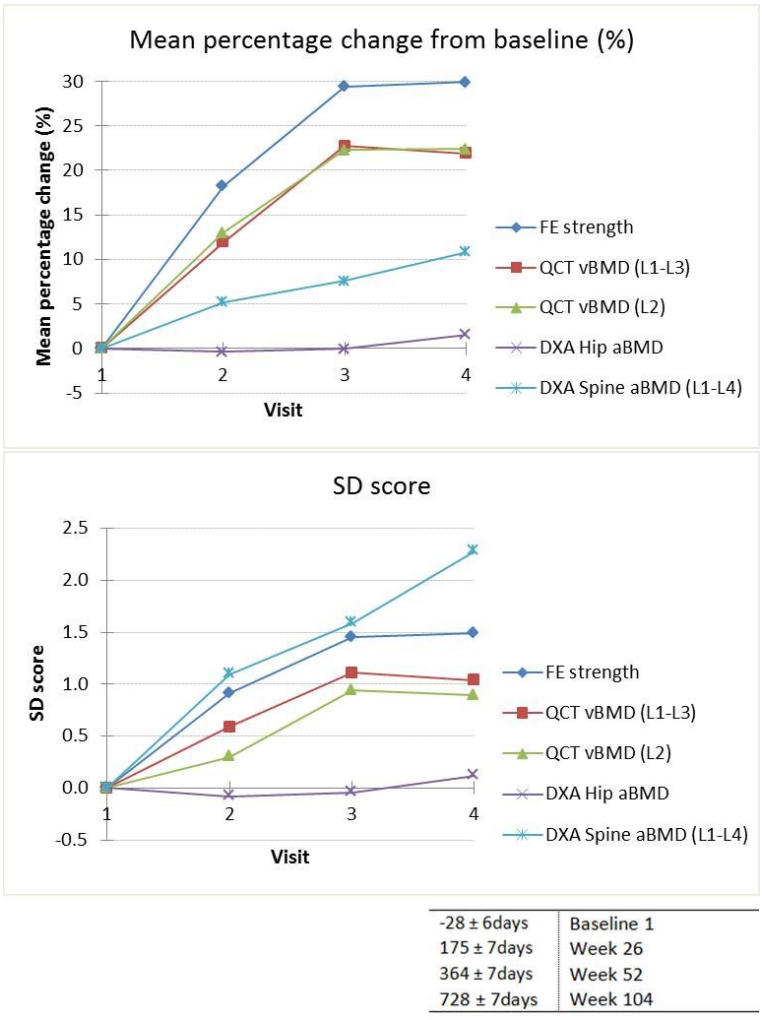

Figure 7.5: Mean percentage change from baseline and SD score: FE strength, QCT vBMD (L1-L3), QCT vBMD (L2), DXA hip aBMD, DXA spine aBMD (L1-L4)

The top graph in Figure 7.5 indicated that the FE strength has a larger treatment effect relative to the baseline value than densitometric variables. However, it does not mean the FE strength is the most sensitive indicator. According to the SD score in Figure 7.5 (bottom), this study shows that the aBMD (L1-L4) is the most sensitive on the TPTD treatment among the densitometric variables and the FE strength.

These results show good agreement with studies carried out by other groups in recent years (Keaveny et al., 2007, Graeff et al., 2009). Keaveny et al. (2007) compared effects of treatment with TPTD and Alendronate (ALN) using L3 vertebral body FE models in a clinical trial. The study indicated that the median percentage change of FE-predicted strength increase for TPTD was greater than for ALN, 21.1%, and 3.7% at 18 months. Graeff et al. (2009) also investigated the effect of teriparatide treatment on vertebral body strength, but in this study a T12 High Resolution CT scan was used to generate vertebral body FE models. The FE predicted strength increased by 28% at 24 months. These two studies did not consider the IVD in the FE model.

The unique feature of the current study is that proposed DVD FE model takes account of the effect of IVD on the vertebra.

A recent study used a vertebral body FE model to investigate combination treatment effects, namely: ALN + TPTD and Risedronate + TPTD (Chevalier et al., 2010). Other studies have used QCT-based FE model of femur to investigate the effect of treatment on femoral strength (Keaveny et al., 2008, Keaveny et al., 2011). All these FE studies support the efficacy of QCT based FE models in the clinical studies of treatments efficacy. Whilst no prospective clinical studies have yet been carried out using a FE model based on QCT together with treatment for predicting vertebral fracture, some clinical case-control studies that have used QCT based FE models have shown better fracture discrimination power for the spine (Melton et al., 2007, Wang et al., 2012). The previous chapter, Chapter 6, showed that the DVD FE model also had better discrimination power for vertebral fracture.

Some limitations should be noted here. First, only compressive strength was considered even though the DVD FE model considered the IVD on the vertebra. The other loading condition such as bending through IVD may affect the vertebral strength. Graeff et al. (2009) showed the FE predicted strength in compression and bending were nearly

identical changes with treatments although their model did not take into account the IVD. Second, the present study is not able to show whether the DVD FE model is a better predictor in treatment effect than other densitometric variables. The study only showed the vertebral strength based on the DVD FE model has a sensitive indicator of effect of treatment on the vertebra. Thirdly, the DVD FE model does not represent the state of the art, for example, the IVD FE model is not patient-specific and does not model the endplates separate, whereas the vertebral FE model uses only linear elastic material properties.

In conclusion, the FE predicted strength has a larger treatment effect relative to the baseline value than densitometric variables. This supports the use of vertebral strength based on the DVD FE model as an additional tool for monitoring TPTD treatment effects on the vertebra in clinical trials.

CHAPTER 8 Conclusions

8.1 Original contributions

This study proposes the use of a patient-specific DVD FE model to investigate vertebral strength in clinical osteoporosis studies non-invasively. The final DVD FE model was developed through developing the full framework (SpineVox-Pro), generation and validation of the FSU FE model, comparison of the vertebral strength from the different types of FE model (VB, VB PE, and FSU FE model), and development of the DVD FE model and its clinical application.

The most important outcomes of this work are as follows:

1. **Standardisation**: SpineVox_Pro standardises the full framework for various vertebral FE model based on medical images.
2. **Validation** of FSU FE model: the FSU FE models were well validated against experimental data on sixteen cadaveric FSU units.
3. **Novelty**: the DVD FE models incorporated the state of the art FE modelling of the IVD and were evaluated successfully in clinical research studies (case-control study for vertebral fractures and clinical trials for two years TPTD treatment)

8.2 Discussion and limitations

To summarise the studies in this thesis, the strengths and limitations based on each chapter are highlighted below. In addition, future work is addressed based on these limitations and further applications.

Chapter 3 SpineVox-Pro: Development of a framework for image processing and a subject-specific finite element model generation

The SpineVox-pro provides a new framework to support a streamlined full workflow of generating a subject-specific FE model of vertebra(e) based on medical images. The framework has been implemented in MATLAB via single GUI. Whilst the individual algorithms used are not new, SpineVox-Pro has some novel characteristics. All steps in SpineVox-Pro workflow are operational in an automatic way without the need for user interaction except for refinement of the image segmentation. Automation maximises both consistency in the FE analysis among different patient scans and precision of repeat analysis of same scans. Consistency and precision are key considerations if the software is eventually to be used in the target application: for patient-specific fracture risk estimation. Using the framework in SpineVox-Pro, several different types of FE models were developed for estimating vertebral fracture strength. These were: the vertebral body alone, the single vertebra, the FSU, and the DVD FE models. From these, one model, the FSU FE model was validated against experiment in terms of predicting vertebral fracture load. In addition, a further development of the FSU model, the DVD FE model was applied for estimating the vertebral fracture load in a clinical study. The SpineVox_Pro framework is available for researchers in the Department for further development and for use.

Whilst, the utility of SpineVox_Pro was demonstrated it does have some minor limitations and there are some aspects which can still be improved.

Limitations:

- Whilst SpineVox-Pro is designed to produce a mesh automatically from a clinical image datasets, the segmentation step requires a small amount of user-interaction. Manual processing tools are provided for this purpose. This is an aspect which may introduce unwanted variability in the models.

- Only voxel-mesh type is embedded in the MATLAB script of SpineVox_Pro: other types of mesh models can be implemented through an import/export step via other software, if required, but this increases process time.
- SpineVox-pro is not suitable for the surface or contact analyses as the framework does not support a surface smoothing step
- Finally, additional software is required for solving the FE models

Chapter 4 Development and validation of a subject-specific finite element model of the functional spinal unit

The subject-specific FSU FE model based on the QCT and MRI scans can be used to estimate the vertebral strength under forward bending following validation of the strength derived from the FSU FE model against experimental tests. Vertebral strength predicted by the FSU model based on von Mises stress/strain and Drucker-Prager stress showed strong correlation with experimental results among different six-yield criteria. The validated FSU FE model shows an excellent potential in terms of its use in future clinical studies to improve vertebral strength estimates for fracture risk assessment and monitoring the effects of treatment.

Limitations:

- Only linear analyses with linear elastic properties were carried out for vertebrae and IVD (NP and AF), because for consistency with the experiments a large forward bending condition was considered. This large angle makes the element fail easily, thus the model requires a more accurate assumption of the material law. This was beyond the scope of the current work. In general, the FSU FE model which takes account into the facet joints and ligaments requires nonlinear analysis as these components were generated with contact elements and cable elements, respectively. To avoid the need for complex analysis, in this validation study the facet joints and ligaments are ignored in the FSU FE model, but were not removed from the cadaveric FSUs during the experimental tests.
- A good representation of the geometry of the patient-specific anatomy of IVD could be extracted from the corresponding MRI scans. Nevertheless, the signal information could not be used to obtain the important material properties of IVD in subject-specific way.

- There is an obvious need for further experimental study to validate the estimated fracture location properly

Chapter 5 Comparison of vertebral strengths derived from FE models of the vertebral body, vertebral body with posterior elements, and the FSU

This study was based on the premise that vertebral strength obtained from a FE model of the vertebral body alone under pure compressive loading could not represent the strength of an individual vertebra during different loading conditions. Our hypothesis was that different FE models may influence the result of the FE analysis. FE models of the vertebrae that simulate loading under flexed postures may result in different strength estimates to those that simulate pure compression. Furthermore, the artificial removal of posterior elements and IVD in the model prevents load transfer through the IVD and facet joint to be represented.

In terms of vertebral strength, that the mean FE strength (1850 N) from the FSU FE model under the forward bending condition could estimate most closely to the mean strength (2146N) from the in vitro test on FSU specimens. Although, all FE strengths are positively correlated with the experimental data and there is no significant difference statistically, several findings are should be addressed; the FE strengths under the pure compression are higher than those from the forward bending condition. The predicted fracture locations differ from the type of FE models as well as the yield criteria. Among them the VB PE FE model show the better prediction on the fracture locations compared with the experimental results (10 out 13).

One of main burdens for generating vertebral FE model based on CT is the segmentation process. The removal of posterior elements from the ROI makes the process of the segmentation much easier. In this regards, the strength derived from the simple vertebral body FE model under the pure compression can still be used to estimate the vertebral compressive strength without posterior elements or the functional spinal unit with large population of patients for the clinical studies. However, our results might address the limitations of the current approach in that, the FE model should incorporate the posterior elements and IVD as well as the loading conditions.

Limitations:

- There was no consideration of the FSU FE model under pure compression due to lack of compatibility when using a voxel mesh for the contact analysis near the facet joints area under bending or torsion loading conditions.
- In the absence of experimental validation data for the VB and VB PE FE model, the results from all the FE models were compared with experimental data obtained by generating a wedge fracture in a single vertebral body of a FSU rather than in a single vertebra alone.

Chapter 6 Clinical application: vertebral fracture discrimination in postmenopausal women using a patient-specific finite element model of the disc-vertebra-disc unit

A patient-specific FE model of the Disc-Vertebra-Disc unit (DVD) was proposed for use in clinical research studies. The study highlighted the importance of considering the influence of the IVD on the vertebra FE model in the prediction of vertebral strength and stress/strain distribution and clearly showed that vertebral strength derived from DVD FE model based on QCT images from *in vivo* clinical studies was able to discriminate between women with and without vertebral fracture independent of aBMD by DXA.

Limitations:

- The model is unable to reflect the IVD health status for each patient. Although this model is based on patient-specific geometry, routine clinical QCT scans are unable to provide data required for the development of patient-specific IVD material properties.
- There is a large variation in the vertebral level which contains fracture (T4 – L4) in the fracture group. These differences might affect the discrimination power of the FE model.

Chapter 7 Clinical application: impact of teriparatide on vertebral strength in postmenopausal women using a patient-specific finite element model of the disc-vertebra-disc unit

The study indicated that FE-predicted strength from the DVD FE model showed the highest response in mean percentage change from the baseline than that of the densitometric variables at the 2 year follow up study. The prediction of vertebral strength based on the DVD FE model could be an additional tool for monitoring TPTD treatment effect on the vertebra in clinical trials with the conventional densitometric variables.

Limitations:

- Only pure compressive loading condition was simulated. Other loading conditions such as forward bending and torsion through IVD may affect vertebral strength.
- The DVD FE model requires further validation study against experimental tests under different loading conditions: pure compression, forward bending, and torsion.
- Further longitudinal *in vivo* studies with many more scans are required to evaluate the FEA using the DVD FE model for fracture risk assessment and treatment monitoring.

8.3 Future work

The uses of FE models in bone research are increasing with the concept of using a patient-specific FE model to provide a surrogate marker of bone fragility. For clinical research such as assessment of fracture risk and evaluation of treatment effects, the FE models still need refinement and further studies may be needed to refine our patient-specific DVD FE model in SpineVox-Pro.

- In this thesis, the image processing procedure required user interaction. Accurate semiautomatic (Kaminsky et al., 2004) and fully automatic segmentation methods (Kim and Kim, 2009) for three-dimensional lumbar spine structure would improve the current FE model.
- Material properties for the vertebra in all the FE models of this thesis are based on the linear empirical relationship between elastic modulus - density proposed by Kopperdahl et al. (2002) for the elastic region. In addition, simply elastic

perfectly plastic material law is considered for the post-yield region as illustrated in Figure 8.1 (E - elastic region; D - damage region; P - plastic region) (Fyhrie and Schaffler, 1994, Keaveny et al., 1999). The simplified assumption for the material law was not able to describe post-yield characteristics such as fracture modes and damage accumulation in detail.

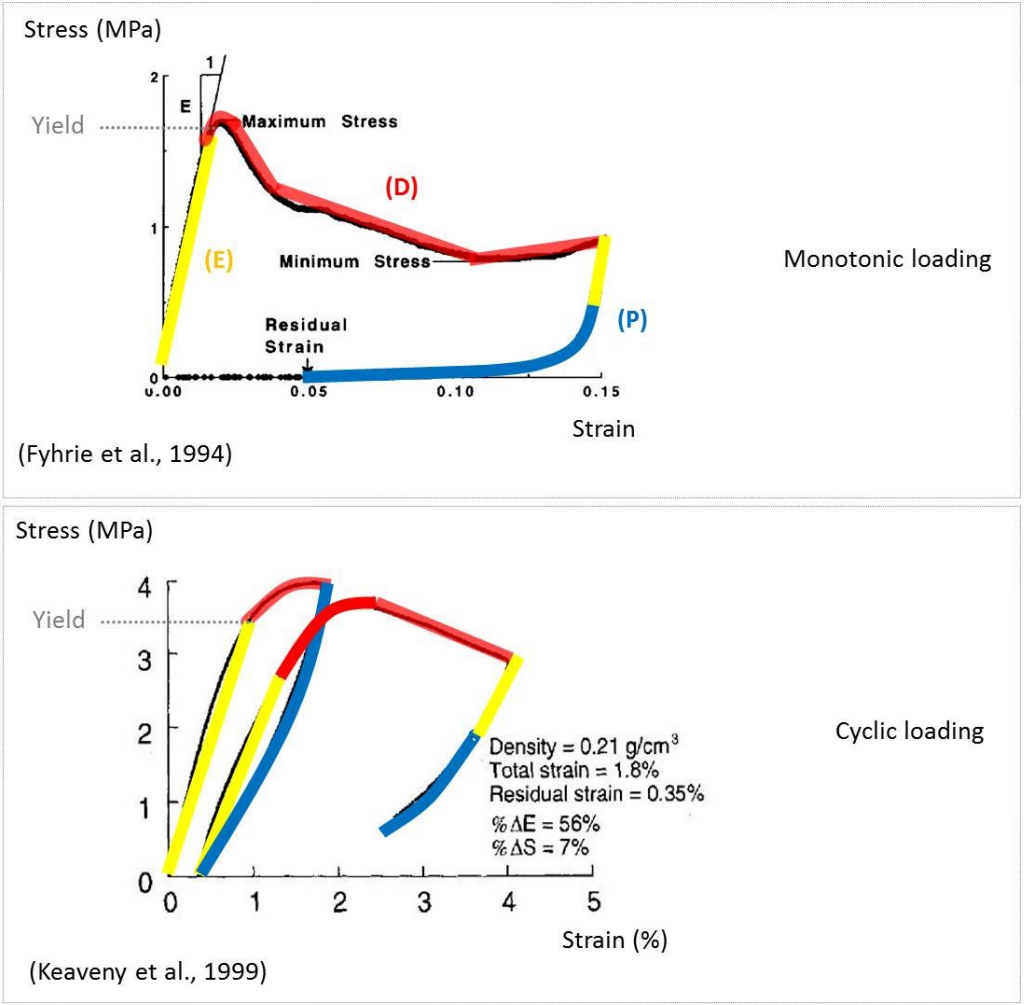

Figure 8.1: A typical load-displacement curve from compression testing of vertebra: (top) monotonic loading; (bottom) cyclic loading (figures from Fyhrie et al. 1994 and Keaveny et al. 1999 with permission)

There is a constitutive model, proposed by (Garcia et al., 2009), which includes the damage parameters based on the Zysset and Curnier theoretical model. The

material model is based on trabecular anisotropy expressed by the fabric tensor as well as a generalised anisotropic form of Hooke's law (Zysset and Curnier, 1995, Zysset and Curnier, 1996). This material law could be adopted in further research. In addition, the use of high resolution scans such as HR-pQCT or micro-CT have the potential to improve the trabecular characteristics in the FE model with, for example, the incorporation of the anisotropy of the trabecular network.

- Larger clinical studies are required in order to evaluate the DVD FE model for fracture risk assessment and treatment monitoring for use with both men and women, for example Parathyroid Hormone and Alendronate for Osteoporosis (PaTH), Health Outcomes and Reduced Incidence with Zoledronic Acid Once Yearly- Pivotal Fracture Trial (HORIZON-PFT), or Osteoporotic Fractures in Men (MrOS) studies (UC, 2014).

Appendix A-1

Material Properties of Vertebral body and Vertebra FE model in Literature

Author	Specimen Type	Material model	Trabecular	Material model	Cortical	References
Homminga et al. 2001	49 Cadaveric Vertebral body + artificial disc	Elastic[1]	$\mathrm{E} = 0.366 \cdot \mathrm{E_t} \cdot {\rho_{app}}^{1.7}$ $\mathrm{E_t} = 14$ GPa $\nu = 0.3$	Elastic[1,2,3]	$\mathrm{E} = 0.366 \cdot \mathrm{E_t} \cdot {\rho_{app}}^{1.7}$ $\mathrm{E_t} = 14$ GPa $\nu = 0.3$	1 Homminga et al. 1998 2 Mosekilde 1993 3 Mosekilde 1998
Crawford 2003a, 2004	17 Cadaveric Vertebral body (T11-L4)	Elastic[1] Transverse isotropy[2,3]	$E_z = -34.7 + 3230\rho_{QCT}$ $E_x = E_y = 0.333E_z$ ${\nu_{xy}}^1 = 0.381$ ${\nu_{xz}}^1 = {\nu_{yz}}^1 = 0.104$ $G_{xz} = G_{yz} = 0.157E_z$ $G_{xy} = \frac{E_x}{2(1+\nu_{xy})} = 0.121E_z$	Elastic[1]	Same as Trabecular bone Voxel dimensions > typical cortical shell[4] (0.35mm)	1 Kopperdahl et al. 2002 2 Moskilde et al. 1987 3 Ulrich et al. 1999 4 Silva et al. 1994
Keaveny et al. 2007	**Clinical Trials:** Vertebral body L3 at baseline, 6, and 8 months	Elastic[1] Transverse isotropy[2,3] Side-artifact[5,6]	$E_z = -34.7 + 3230\rho_{QCT}$ $E_x = E_y = 0.333E_z$ ${\nu_{xy}}^1 = 0.381$ ${\nu_{xz}}^1 = {\nu_{yz}}^1 = 0.104$ $G_{xz} = G_{yz} = 0.157E_z$ $G_{xy} = \frac{E_x}{2(1+\nu_{xy})} = 0.121E_z$ $\sigma_u = \left(1.2 * \sigma_y\right) * 1.28$	Elastic[1]	Same as Trabecular bone Voxel dimensions > typical cortical shell[4] (0.35mm)	1 Kopperdahl et al. 2002 2 Moskilde et al. 1987 3 Ulrich et al. 1999 4 Silva et al. 1994 5 Crawford et al. 2003 6 Homminga et al. 2001
Melton et al. 2007	**Clinical Trials:** 74 Vertebral body L3		Same as above		Same as above	
Lewiecki et al. 2009	**Clinical Trials:** 86 Vertebral body		Same as above		Same as above	
Buckley et al. 2007	44 Cadaveric		Same as above		Same as above	

	Vertebral body (T1-L5)					
Liebschner et al. 2003	23 Cadaveric Vertebral body (T12-L3) With explicit Cortical shell	Elastic[1] Anistropy[2]	$E_z = -81.9 + 3850\rho_{QCT}$ $E_x = 0.42E_z$ $E_y = 0.287E_z$ ${\nu_{xy}}^1 = 0.226$ ${\nu_{xz}}^1 = 0.399$ ${\nu_{yz}}^1 = 0.381$ $G_{xz} = 0.131E_z$ $G_{yz} = 0.183E_z$ $G_{xy} = 0.153E_z$	Elastic-isotropic	Cortical shell th=0.35mm $\nu = 0.3$	1 Kopperdahl et al. 2002 2 Ulrich et al. 1999
Imai et al. 2006	12 Cadaveric Vertebral body (T11-L1)	Bilinear elastoplastic	Ref. 1 $\mathrm{Hardening_c} = 0.05$		Cortical shell th=0.4mm $\mathrm{E_c} = 10$ GPa $\nu = 0.4$	1 Keyak et al. 1998
Imai et al. 2009	**Clinical Trials:** 37 Vertebral body L2		Same as above		Same as above	
Mirzaei et al. 2009	13 Cadaveric Vertebral body	Elastic[1] Transverse isotropy[2] Ref[3,4]	$E_z = -34.7 + 3230\rho_{QCT}$ $E_z = 2980 * {\rho_{QCT}}^{1.05}$ $E_x = E_y = 0.333E_z$ ${\nu_{xy}}^1 = 0.381$ ${\nu_{xz}}^1 = {\nu_{yz}}^1 = 0.104$ $G_{xz} = G_{yz} = 0.157E_z$ $G_{xy} = \frac{E_x}{2(1+\nu_{xy})} = 0.121E_z$ $\sigma_{ys} = -0.75 + 24.9 * \rho_{QCT}$ $\sigma_{ys} = 37.4 * {\rho_{QCT}}^{1.39}$ $\sigma_{ult} = 1.2 * \sigma_{ys}$	Same	1 Kopperdahl et al. 2002 2 Ulrich et al. 1999 3 Crawford et al. 2003 4 Morgan et al. 2001 5 Kopperdahl et al. 1998 6 Morgan et al. 2003

		Ref[5,6] Linearly elastic-perfectly plastic	$\varepsilon_y = \frac{\sigma_{ys}}{E}$ $\varepsilon_{ult} = 0.0145$		
Zeinali et al. 2010	9 Cadaveric Vertebral body	Linearly elastic-perfectly plastic Linearly elastic-linearly plastic	Same as above	Same as above	

Appendix A-2

Boundary Conditions of Vertebral body and Vertebra FE model in Literature

Author	Mesh Type	Loading Type	Boundary Conditions	Analysis Type	Fracture	References
Homminga et al. 2001	Voxel-based FEM	Flexion 2°	$1000\ N$ (2*normal standing)[1,2]		$Strain > 5000\ \mu strain$[3]	1 Nachemson 1981 2 Schultz et al. 1982 3 Kopperdahl and Keaveny 1998
Crawford 2003a	Voxel-based FEM	Compression 0.15 mm/s	*Superior surface: uniform vertical displacement with lateral constraints *inferior surface: constrained all DOF	Linear analysis (ABAQUS)	$F_{FE} = 0.0068 \cdot K_{FE} \cdot H$	
Keaveny et al. 2007	Voxel-based FEM $1 \times 1 \times 1.5mm^3$	Compression	Uniform compressive displacement	Nonlinear analysis[1]	$\varepsilon_{comp} * 0.002 = \frac{\delta}{H}$	1 Crawford et al. 2004

		Bending 1°				
Melton et al. 2007	Voxel-based FEM		Uniform compressive displacement	Nonlinear analysis[1]	$\varepsilon_{comp} * 0.002 = \frac{\delta}{H}$	1 Crawford et al. 2004
Lewiecki et al. 2009	Voxel-based FEM		Same as above		Same as above	
Buckley et al. 2007	Voxel-based FEM		Uniform inferior axial displacement	Nonlinear-Large deformation analysis	$\varepsilon_{comp} * 0.003 = \frac{\delta}{H}$	
Liebschner et al. 2003	20-noded brick (TrueGrid)		Uniform compressive displacement			
Imai et al. 2006, 2009	(MECHANICAL FINDER)		Uniaxial compressive load	Nonlinear analysis by the Newton-Raphson method Drucker-Prager equivalent stress criterion	$\varepsilon_{min} < -10000\ \mu strain$	
Chevalier et al. 2010	Voxel-based FEM Hexahedral FE		Axial compression displacement	Nonlinear		
Maquer et al. 2013						
Mirzaei et al. 2009	Voxel-based FEM	Compression		Nonlinear	$F_{FE} = 0.0068 \cdot K_{FE} \cdot H$	
Zeinali et al. 2010	Voxel-based FEM	Compression		Nonlinear	$F_{FE} = 0.0068 \cdot K_{FE} \cdot H$	
Wijayathunga et al. 2008	Hexa and Tetrahedral (ScanIP)	Compression		Nonlinear	1 mm offset line	
Tawara et al. 2010	Tetrahedral (MECHANICAL FINDER)	Compression	$1000\ N$	Linear		

Appendix A-3

Material properties of bone in FSU FE model

Author	Model type	Material Model	Trabecular	Material Model	Cortical	Material Model	Endplates	Ref.
(Wang et al., 1997)	FSU	Elastic[1]	$E = 100\ MPa$ $\nu = 0.2$	Elastic[1]	$E = 12000\ MPa$ $\nu = 0.3$	Elastic[1]	$E = 24\ MPa$ $\nu = 0.4$	1(Shirazi-Adl et al., 1986)
Strange et al. 2010	FSU					Elastic	$E1 = 325\ MPa$ $E2 = 375\ MPa$ $E3 = 450\ MPa$ $E4 = 500\ MPa$ $\nu = 0.3$	
Kuo							$E1 = 360\ MPa$ $E2 = 550\ MPa$ $\nu = 0.3$	
(Cheung et al., 2003)		Poroelastic with fluid	$E = 100\ MPa$ $\nu = 0.2$ $k_0 = 1.0E-13$ $e_0 = 0.40$	Elastic	$E = 12000\ MPa$ $\nu = 0.3$	Poroelastic with fluid	$E = 25\ MPa$ $\nu = 0.1$ $k_0 = 7.0E-15$ $e_0 = 4.00$	
(Schmidt et al., 2006, Schmidt et al., 2007b, Schmidt et al., 2007a, Schmidt et al., 2009)		Elastic[1]	$E_{xx} = 140\ MPa$ $E_{yy} = 140\ MPa$ $E_{zz} = 200\ MPa$ $G_{xy} = 48.3\ MPa$ $G_{xy} = 48.3\ MPa$ $G_{xy} = 48.3\ MPa$ $\nu_{xy} = 0.45$ $\nu_{xy} = 0.315$ $\nu_{xy} = 0.315$	Elastic[1]	$E_{xx} = 11300\ MPa$ $E_{yy} = 11300\ MPa$ $E_{zz} = 22000\ MPa$ $G_{xy} = 3800\ MPa$ $G_{xy} = 5400\ MPa$ $G_{xy} = 5400\ MPa$ $\nu_{xy} = 0.484$ $\nu_{xy} = 0.203$ $\nu_{xy} = 0.203$	Elastic[1,2]	$E_{bony} = 12000\ MPa$ $\nu = 0.3$ $E_{cartil} = 23.8\ MPa$ $\nu = 0.4$	1(Lu et al., 1996) 2(Edwards et al., 2001)
(Ahn et al., 2008)			$E = 100\ MPa$ $\nu = 0.2$		$E = 12000\ MPa$ $\nu = 0.3$		$E = 25\ MPa$ $\nu = 0.25$	
(El-Rich et al., 2009)		Elasto-plastic[1]	$E = 291\ MPa$ $\nu = 0.25$	Elasto-plastic[1]	$E = 14000\ MPa$ $\nu = 0.3$			1(Kopperdahl and Keaveny, 1998)
(Polikeit et al., 2003, Polikeit et al., 2004)		Elastic[1]	$E_{osteo} = 34\ MPa$ $\nu = 0.2$	Elastic[1]	$E_{osteo} = 8040\ MPa$ $\nu = 0.3$	Elastic[1]	$E_{osteo} = 670\ MPa$ $\nu = 0.4$	
(Zhang et al., 2010)		Elastic[1]	$E_{osteo} = 34\ MPa$	Elastic[1]	$E_{osteo} = 8040\ MPa$	Elastic[1]	$E_{osteo} = 670\ MPa$	1(Polikeit et al., 2003)

		$\nu = 0.2$		$\nu = 0.3$		$\nu = 0.4$	
(Goto et al., 2002)	Elastic[1]	$E = 100\ MPa$ $\nu = 0.2$	Elastic[1]	$E = 12000\ MPa$ $\nu = 0.3$	Elastic[1]	$E = 23.8\ MPa$ $\nu = 0.4$	1(Shirazi-Adl et al., 1986)
(Li and Wang, 2006)				$E = 200\ MPa$ $\nu = 0.3$			
(Homminga, 2001)	Elastic[1]	$E = 0.366 \cdot E_t \cdot \rho^{1.7}$ $E_t = 14\ GPa$ $\nu = 0.3$	Elastic[1]	$E = 0.366 \cdot E_t \cdot \rho^{1.7}$ $E_t = 14\ GPa$ $\nu = 0.3$	Elastic[1]	$E = 0.366 \cdot E_t \cdot \rho^{1.7}$ $E_t = 14\ GPa$ $\nu = 0.3$	1(Homminga et al., 1998)
(Ruberté et al., 2009)	Elastic[1]	$E = 100\ MPa$ $\nu = 0.2$	Elastic[2]	$E = 12000\ MPa$ $\nu = 0.3$	Elastic[3]	$E = 24\ MPa$ $\nu = 0.4$	1(Goulet et al., 1994) 2(Cassidy et al., 1989) 3(Shirazi-Adl et al., 1986)
(Totoribe et al., 1999)	Elastic[1,2]	$E = 100\ MPa$ $\nu = 0.2$	Elastic[1,2]	$E = 12000\ MPa$ $\nu = 0.3$	Elastic[3]	$E = 23.8\ MPa$ $\nu = 0.4$	1(Shirazi-Adl et al., 1984) 2(Shirazi-Adl et al., 1986) 3(Belytschko et al., 1974)

Appendix A-4

Material properties of IVD in FSU FE model

Author	Model type	Material Model	Annulus Ground	Material Model	Nucleus Pulposus	Material Model	Annulus Fibres	Ref.
(Wang et al., 1997)		Viscoelastic (Prony)	$E = 8\ MPa$ $\nu = 0.45$ $g_i\ k_i\ \tau_i$: attached	Viscoelastic (Prony)	$E = 2\ MPa$ $\nu = 0.49$ $g_i\ k_i\ \tau_i$: attached	Viscoelastic (Zener model)[1]	Nonlinear spring and dashpot	1(Haut and Little, 1972)
Strange et al. 2010	FSU	Hyperelastic Mooney-Rivlin	$C1 = 0.56$ $C2 = 0.14$ $D1 = 0.143$	Hyperelastic Mooney-Rivlin	$C1 = 0.12$ $C2 = 0.03$ $D1 = 0.0667$	Elastic	$E1 = 325\ MPa$ $E2 = 375\ MPa$ $E3 = 450\ MPa$ $E4 = 500\ MPa$ $\nu = 0.3$	
Kuo			$E = 4.2\ MPa$ $\nu = 0.45$		$E = 1\ MPa$ $\nu = 0.4999$		$E1 = 360\ MPa$ $E2 = 550\ MPa$ $\nu = 0.3$	
(Cheung et al., 2003)	1 L4-L5 FSU	Poroelastic	$E = 4.2\ MPa$	Poroelastic	$E = 1\ MPa$	Elastic	$E = 500\ MPa$	

	CT	with fluid	$\nu = 0.1$ $k_0 = 3.0E-16$ $e_0 = 2.33$	with fluid	$\nu = 0.1$ $k_0 = 3.0E-16$ $e_0 = 4.00$		$\nu = 0.3$	
(Schmidt et al., 2006)	1 L4-L5 FSU CT & MRI	Hyperelastic Mooney-Rivlin[1]	$C1 = 0.56$ $C2 = 0.14$ $(\approx E = 4.2\ MPa)$ $\nu = 0.45$	Hyperelastic Mooney-Rivlin[2]	$C1 = 0.12$ $C2 = 0.09$ $\nu = 0.4999$	Stress-strain curve[3]		1(Goel et al., 1995) 2(Smit et al., 1997) 3(Shirazi-Adl et al., 1986)
(Schmidt et al., 2007b, Schmidt et al., 2007a)	1 L4-L5 FSU CT & MRI	Hyperelastic Mooney-Rivlin[1]	$C1 = 0.18$ $C2 = 0.045$ $\nu = 0.45$	Hyperelastic Mooney-Rivlin[2]	$C1 = 0.12$ $C2 = 0.03$ $\nu = 0.4999$	Stress-strain curve[3]		1(Schmidt et al., 2006) 2(Smit et al., 1997) 3(Shirazi-Adl et al., 1986)
(Schmidt et al., 2007c, Schmidt et al., 2009)	1 L4-L5 FSU CT & MRI	Hyperelastic Mooney-Rivlin[1,2] No degeneration effect[4,5]	$C1 = 0.18$ $C2 = 0.045$	Hyperelastic Mooney-Rivlin[1,2]	$E_{grade0} = 0.9\ MPa$ $C1 = 0.12$ $C2 = 0.03$ $E_{grade1} = 1.07\ MPa$ $C1 = 0.14$ $C2 = 0.035$ $E_{grade2} = 1.25\ MPa$ $C1 = 0.17$ $C2 = 0.041$ $E_{grade3} = 1.41\ MPa$ $C1 = 0.19$ $C2 = 0.045$	Stress-strain curve[3]		1(Wilke et al., 2006) 2(Rohlmann et al., 2006) 3(Shirazi-Adl et al., 1986) 4(Ebara et al., 1996) 5(Holzapfel et al., 2005)
(Ahn et al., 2008)	1 L3-L4 FSU CT		$E = 4.2\ MPa$ $\nu = 0.45$		$E = 1\ MPa$ $\nu = 0.4999$		$E1/2 = 550\ MPa$ $E3/4 = 495\ MPa$ $E5/6 = 413\ MPa$ $E7/8 = 358\ MPa$	
(El-Rich et al., 2009)	1 L2-L3 FSU CT	Hyperelastic Mooney-Rivlin[1]	$C1 = 0.18$ $C2 = 0.045$ $\nu = 0.45$	Hyperelastic Mooney-Rivlin[1]	$C1 = 0.12$ $C2 = 0.03$ $\nu = 0.495$	Nonlinear elastic curve[2]		1(Schmidt et al., 2007b) 2(Shirazi-Adl et al., 1986)
(Polikeit et al., 2003)	1 L2-L3 FSU CT		$E = 4.2\ MPa$ $\nu = 0.45$		$E = 0.2\ MPa$ $\nu = 0.4999$		$Eout = 550\ MPa$ $E2 = 495\ MPa$ $E3 = 440\ MPa$ $E4 = 420\ MPa$ $E5 = 385\ MPa$ $Einner = 360\ MPa$ $\nu = 0.3$	
(Zhang et al., 2010)	1 L1-L2 FSU	Elastic[1]	$E = 4.2\ MPa$	Hyperelastic	$C1 = 0.12$		$E = 455\ MPa$	1(Polikeit et al., 2003)

	CT		$\nu = 0.45$	Mooney-Rivlin[2,3]	$C2 = 0.047$ $\nu = 0.4999$		$\nu = 0.3$	2(Baroud et al., 2003) 3(Noailly et al., 2005)
(Goto et al., 2002)	1 L4-L5 FSU CT		$E = 4.2\ MPa$ $\nu = 0.45$	Intradiscal pressure[1,2]	$E_{Flexion} = 1.32\ MPa$ $E_{Upright} = 0.54\ MPa$ $E_{Extension} = 0.59\ MPa$	Nonlinear		1(Nachemson, 1966) 2(Sato et al., 1999)
(Li and Wang, 2006)					$E = 4\ MPa$ $\nu = 0.4999$			
(Homminga, 2001)	49 D-VB-D CT			Elastic[1]	$E_{health} = 100\ MPa$ $E_{degen} = 1MPa$ $\nu = 0.49$	Elastic[2,3,4]	$E = 10\ MPa$ $\nu = 0.45$	1(Furlong and Palazotto, 1983) 2(Kurowski and Kubo, 1986) 3(Lane et al., 1998) 4(Spilker et al., 1986)
(Ruberté et al., 2009)	1 L4-L5 FSU	Hyperelastic Mooney-Rivlin	$C1 = 0.2$ $C2 = 0.05$ $C1 = 0.4$ $C2 = 0.1$ $C1 = 0.9$ $C2 = 0.23$	Elastic[1,2,3]	$E_{health} = 1\ MPa$ $\nu = 0.49$ $E_{degen1} = 1.26\ MPa$ $\nu = 0.45$ $E_{degen2} = 1.66\ MPa$ $\nu = 0.4$			1(Umehara et al., 1996) 2 latris 1997 3 (Elliott and Setton, 2001)
(Totoribe et al., 1999)	1 L4-L5 FSU	Elastic[1,2,3]	$E = 4.2\ MPa$ $\nu = 0.45$	Elastic[4]	$E = 1\ MPa$ $\nu = 0.4999$	Nonlinear Elastic[1,2,5]		1(Shirazi-Adl et al., 1984) 2(Shirazi-Adl et al., 1986) 3(Wu and Yao, 1976) 4(Goel et al., 1995) 5(Sanjeevi et al., 1982)

'-': Information is not applicable.

APPENDIX

Hyperelastic behaviour

An incompressible, hyper-elastic, two parameter Mooney-Rivlin (C1,C2) formulation with the following strain energy function W:

$$W = C_1(I_1 - 3) + C_2(I_2 - 3) + \frac{1}{d}(J - 1)^2 \quad \text{(A.1)}$$

Where,

C_1, C_2 material constants characterizing the deviatoric deformation of the material

I_1, I_2 first/second invariants of the deviatoric strain tensor

$d = 2/K$ material incompressibility parameter

$J = V/V_0$ local volume ratio

K initial bulk modulus of the material

Viscoelastic behaviour

The equation of stiffness for the Prony series can be described as:

$$G_R(t) = \frac{G(t)}{G_0} = 1 - \sum_{i=1}^{n} g_i(1 - e^{-t/\tau_i}) \quad \text{(A.2)}$$

Where,

$G_R(t)$ normalised relaxation modulus

g_i weighing factor ranged from 0 to 1

τ_i relaxation time constant

G_0 instantaneous stiffness at t=0

Appendix B

In vitro load-displacement curves were drawn by the author, University of Sheffield (based on the experiment data from the University of Bristol)

*Note: red star (fracture load were defined from experiment, University of Bristol), green star (FE strength based on von Mises strain yield criteria), DDD (disc degeneration scale by prof. Adams, University of Bristol)

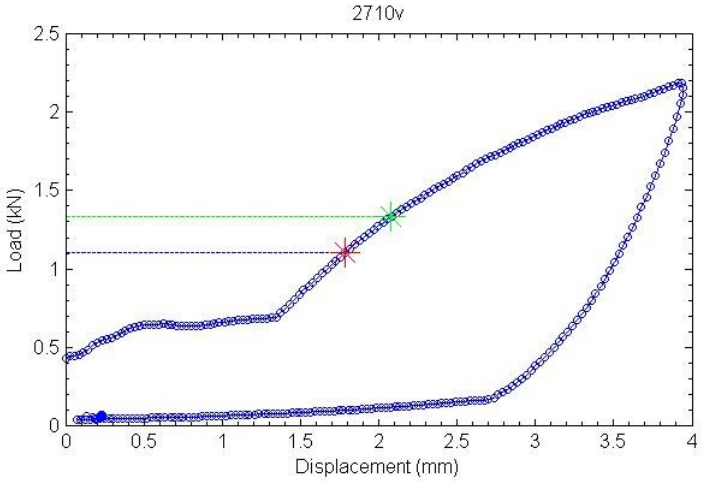

Figure B.1: Specimen 2710v (Fracture load: 1.104 kN; FE strength: 1.335 kN; DDD: grade 4)

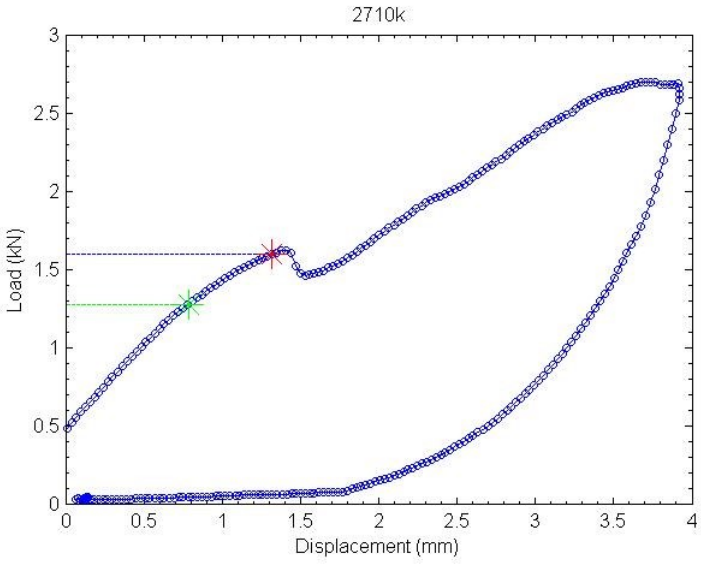

Figure B.2: Specimen 2710k (Fracture load: 1.600 kN; FE strength: 1.281 kN; DDD: grade 4)

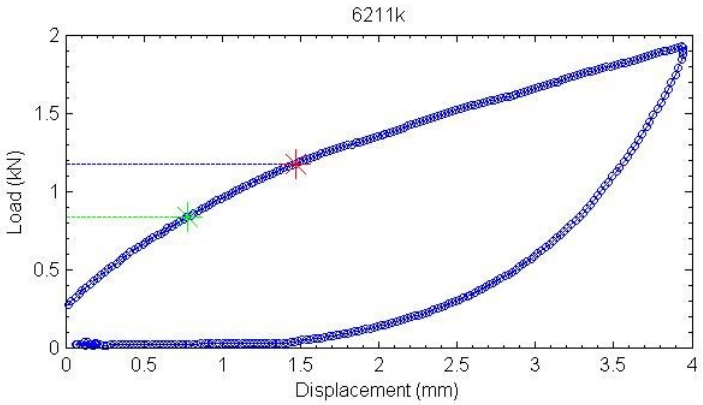

Figure B.3: Specimen 6211k (Fracture load: 1.180 kN; FE strength: 0.836 kN; DDD: grade 2)

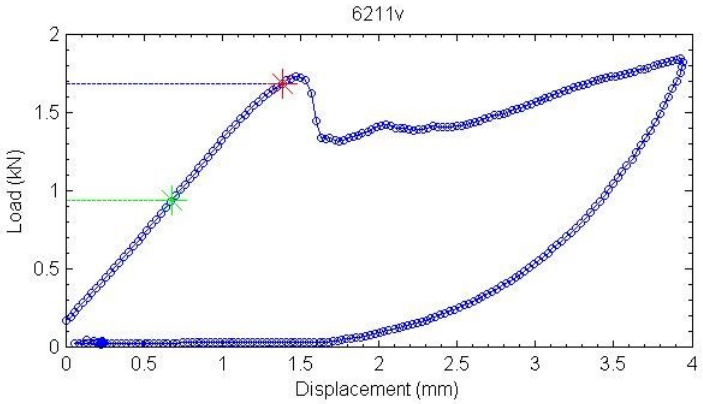

Figure B.4: Specimen 6211v (Fracture load: 1.685 kN; FE strength: 0.936 kN; DDD: grade 2)

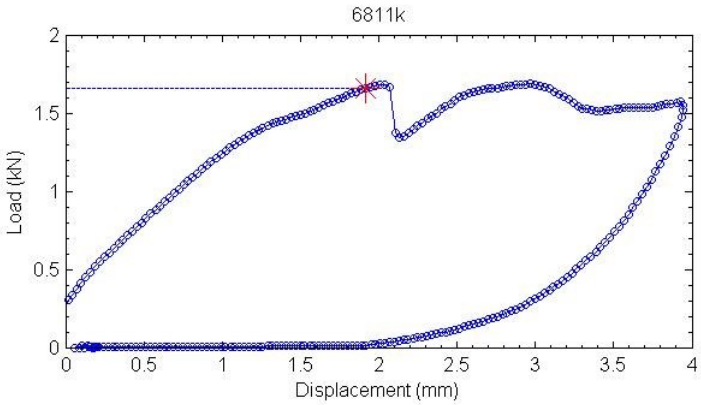

Figure B.5: Specimen 6811k (Fracture load: 1.663 kN; FE strength: NA; DDD: grade 2)

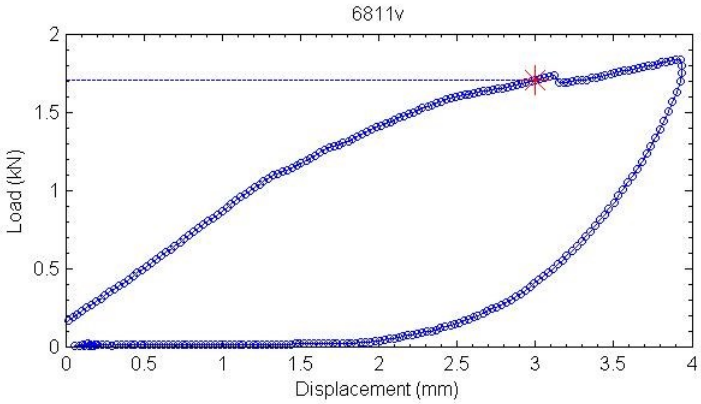

Figure B.6: Specimen 6811v (Fracture load: 1.708 kN; FE strength: NA; DDD: grade 2)

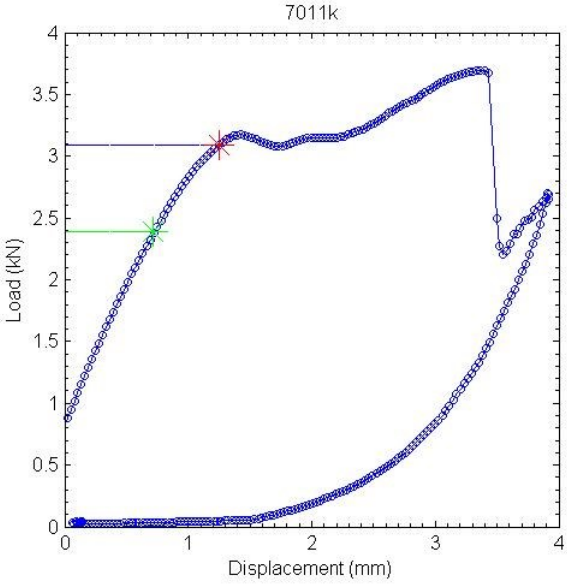

Figure B.7: Specimen 7011k (Fracture load: 3.090 kN; FE strength: 2.388 kN; DDD: grade 3)

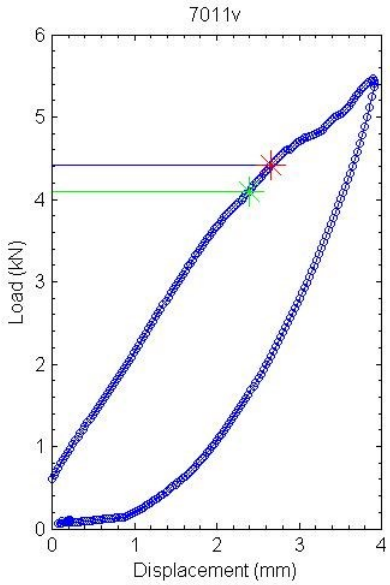

Figure B.8: Specimen 7011v (Fracture load: 4.412 kN; FE strength: 4.093 kN; DDD: grade 4)

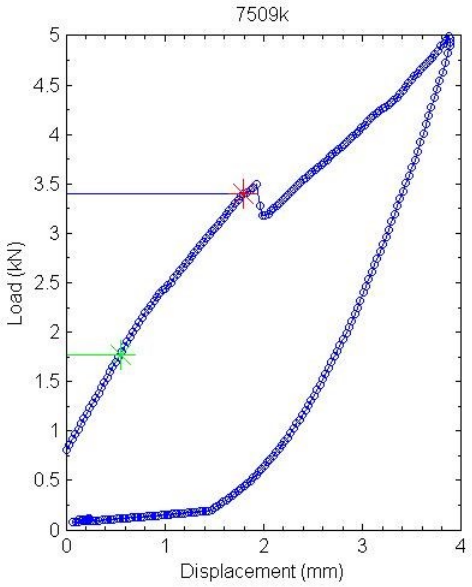

Figure B.9: Specimen 7509k (Fracture load: 3.399 kN; FE strength: 1.775 kN; DDD: grade 3)

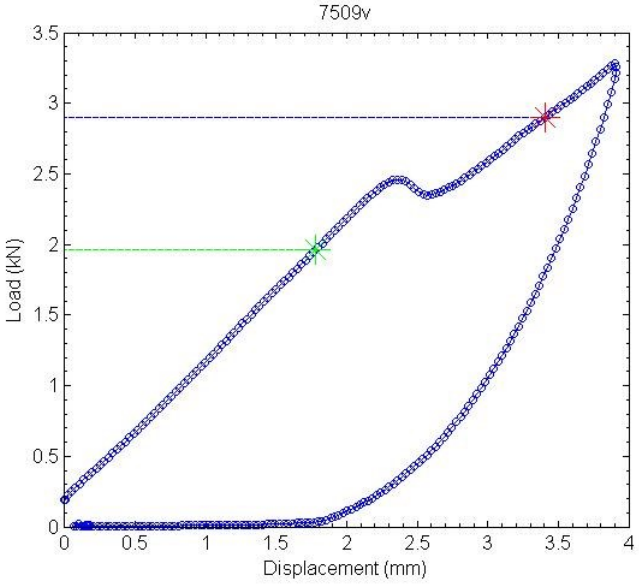

Figure B.10: Specimen 7509v (Fracture load: 2.906 kN; FE strength: 1.962 kN; DDD: grade 4)

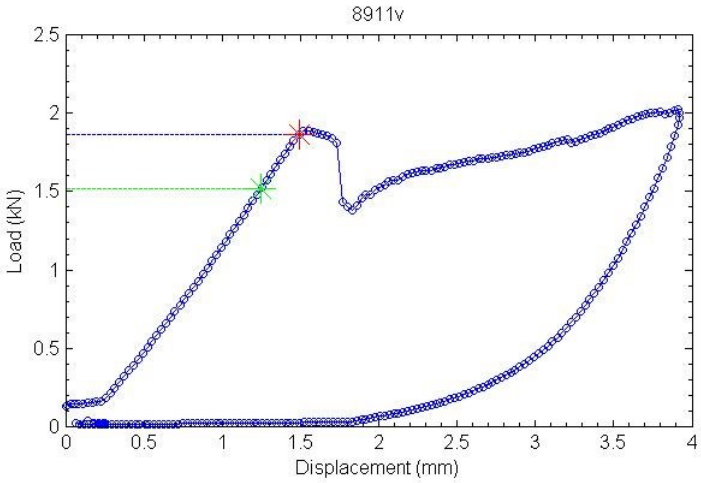

Figure B.11: Specimen 8911v (Fracture load: 1.861 kN; FE strength: 1.515 kN; DDD: grade 3)

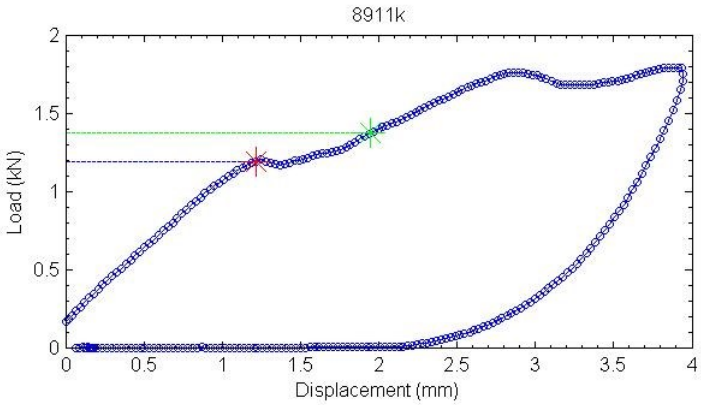

Figure B.12: Specimen 8911k (Fracture load: 1.194 kN; FE strength: 1.378 kN; DDD: grade 3)

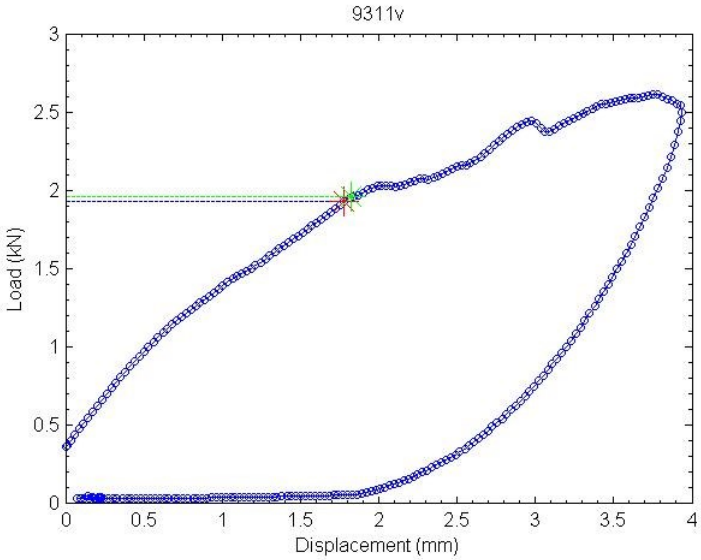

Figure B.13: Specimen 9311v (Fracture load: 1.930 kN; FE strength: 1.958 kN; DDD: grade 2)

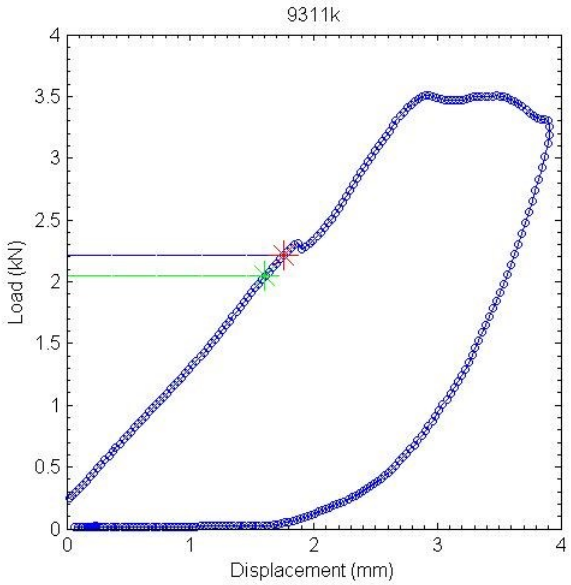

Figure B.14: Specimen 9311k (Fracture load: 2.215 kN; FE strength: 2.051 kN; DDD: grade 4)

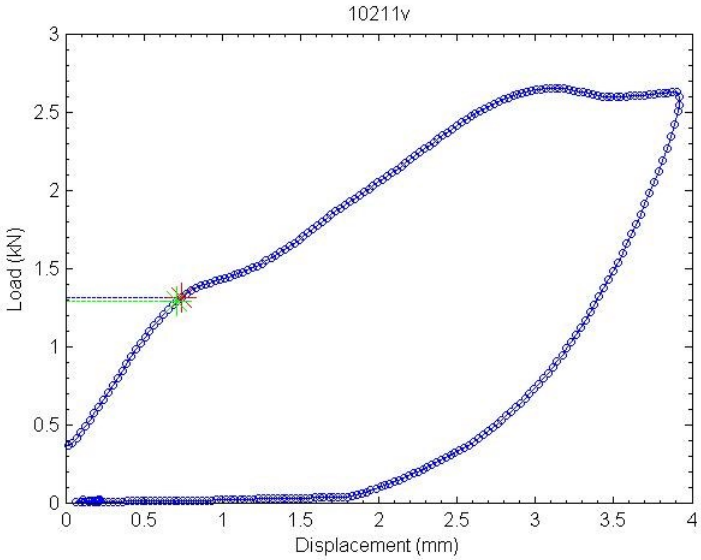

Figure B.15: Specimen 10211v (Fracture load: 1.319 kN; FE strength: 1.291 kN; DDD: grade 3)

Appendix C

Yield criteria

Each yield function could be described in principal stress term $(\sigma_1, \sigma_2, \sigma_3)$ and yield stress/strain term(Y).

Von Mises: Distortion energy (VM SR and VM ER)

Yield function can be defined as follow:

$$f = \sigma_e - Y \tag{D.1}$$

Where,

Equivalent stress σ_e

$$= \left[\frac{1}{2}(\sigma_1 - \sigma_2)^2 + \frac{1}{2}(\sigma_2 - \sigma_3)^2 + \frac{1}{2}(\sigma_3 - \sigma_1)^2\right]^{\frac{1}{2}}$$

$$= \left[\frac{1}{2}((\sigma_x - \sigma_y)^2 + (\sigma_y - \sigma_z)^2 + (\sigma_z - \sigma_x)^2) + 3({\tau_{xy}}^2 + {\tau_{yz}}^2 + {\tau_{xz}}^2)\right]^{\frac{1}{2}}$$

and, equivalent strain ε_e

$$= \frac{1}{(1+\nu)\sqrt{2}}\left[(\varepsilon_x - \varepsilon_y)^2 + (\varepsilon_y - \varepsilon_z)^2 + (\varepsilon_z - \varepsilon_x)^2 + \frac{3}{2}({\gamma_{xy}}^2 + {\gamma_{yz}}^2 + {\gamma_{xz}}^2)\right]^{\frac{1}{2}}$$

Drucker-prager criterion (DP SR)

Yield function can be defined as follow:

$$f = \sigma_e + \alpha * \sigma_m - Y \tag{D.2}$$

where,

σ_e = equivalent stress,

$$\sigma_m = I_1 = \frac{1}{3}(\sigma_1 + \sigma_2 + \sigma_3)$$

The Drucker-Prager yield criterion was presented by Drucker and Prager (1952) as an approximation to the Mohr-Coulomb law and a modification of the von Mises yield criterion (Owen and Hinton, 1980). Drucker-Prager yield criterion is described by the following equations, i.e. the influence of a hydrostatic stress component on yielding was introduced by inclusion of an additional term in the von Mises expression;

α is a parameter that reflects the dilative potential of the material and it is related to the proportions of the volumetric and deviatoric strains. The alpha value which we found only in the bone research was chosen as 0.07 as yosibash et al (Yosibash Zohar, 2010). However, the alpha value is based on a correlation with yielding in concrete and should be calibrated to bone tissue specimens.

Maximum Principal stress and strain (MX SR and MX ER)

Yield function can be defined as follow:

$$f = \max(|\sigma_1|, |\sigma_2|, |\sigma_3|) - Y \tag{D.3}$$

Maximum Shear stress (CM SR)

Yield function can be defined as follow:

$$f = \max\left(\left|\frac{\sigma_1 - \sigma_2}{2}\right|, \left|\frac{\sigma_2 - \sigma_3}{2}\right|, \left|\frac{\sigma_3 - \sigma_1}{2}\right|\right) - \frac{Y}{2} \tag{D.4}$$

References

ADAMS, M., BOGDUK, N., BURTON, K. & DOLAN, P. 2002. *The Biomechanics of Back Pain*, Churchill Livingstone.

ADAMS, M. & HUTTON, W. 1980. The effect of posture on the role of the apophysial joints in resisting intervertebral compressive forces. *Journal of Bone & Joint Surgery, British Volume,* 62-B**,** 358-362.

ADAMS, M., POLLINTINE, P., TOBIAS, J. H., WAKLEY, G. K. & DOLAN, P. 2006. Intervertebral Dics Degeneration Can Predispose to Anterior Vertebral Fractures in the Thoracolumbar Spine. *Journal of Bone and Mineral Research,* 21**,** 1409-1416.

ADAMS, M. A. & DOLAN, P. 1991. A technique for quantifying the bending moment acting on the lumbar spine in vivo. *Journal of Biomechanics,* 24**,** 117-126.

ADAMS, M. A. & DOLAN, P. 2005. Spine biomechanics. *Journal of Biomechanics,* 38**,** 1972-1983.

ADAMS, M. A. & ROUGHLEY, P. J. 2006. What is Intervertebral Disc Degeneration, and What Causes It? *Spine,* 31**,** 2151-2161.

AHN, Y.-H., CHEN, W.-M., LEE, K.-Y., PARK, K.-W. & LEE, S.-J. 2008. Comparison of the load-sharing characteristics between pedicle-based dynamic and rigid rod devices. *Biomedical Materials,* 3**,** 044101.

BAROUD, G., NEMES, J., HEINI, P. & STEFFEN, T. 2003. Load shift of the intervertebral disc after a vertebroplasty: a finite-element study. *European Spine Journal,* 12**,** 421-426.

BAUER, D., GARNERO, P., BILEZIKIAN, J., GREENSPAN, S., ENSRUD, K., ROSEN, C., PALERMO, L. & BLACK, D. 2006. Short-Term Changes in Bone Turnover Markers and Bone Mineral Density Response to Parathyroid Hormone in Postmenopausal Women with Osteoporosis. *The Journal of Clinical Endocrinology & Metabolism,* 91**,** 1370-1375.

BAYRAKTAR, H. H., F., M. E., NIEBUR, G. L., MORRIS, G. E., WONG, E. K. & KEAVENY, T. M. 2004. Comparison of the elastic and yield properties of human femoral trabecular and cortical bone tissue. *Journal of Biomechanics,* 37**,** 27-35.

BELYTSCHKO, T., KULAK, R. F. & SCHULTZ, A. B. 1974. Finite Element Stress Analysis of an Intervertebral Disc. *Journal of Biomechanics,* 7**,** 277-285.

BERLEMANN, U., GRIES, N. C. & MOORE, R. J. 1998. The relationship between height, shape and histological changes in early degeneration of the lower lumbar discs. *European spine journal : official publication of the European Spine Society, the European Spinal Deformity Society, and the European Section of the Cervical Spine Research Society,* 7**,** 212-217.

BESSHO, M., OHNISHI, I., MATSUMOTO, J., MATSUMOTO, T., IMAI, K. & NAKAMURA, K. 2007. Prediction of strength and strain of the proximal femur by a CT-based finite element method. *Journal of Biomechanics,* 40**,** 1745-1753.

BESSHO, M., OHNISHI, I., MATSUMOTO, T., OHASHI, S., MATSUYAMA, J., TOBITA, K., KANEKO, M. & NAKAMURA, K. 2009. Prediction of proximal femur strength using a CT-based nonlinear finite element method: Differences in predicted fracture load and site with changing load and boundary conditions. *Bone,* 45**,** 226-231.

BJARNASON, K., HASSAGER, C., SVENDSEN, O. L., STANG, H. & CHRISTIANSEN, C. 1996. Anteroposterior and lateral spinal DXA for the assessment of vertebral body strength: Comparison with hip and forearm measurement. *Osteoporosis International,* 6**,** 37-42.

BLACK, D. M., ARDEN, N. K., PALERMO, L., PEARSON, J. & CUMMINGS, S. R. 1999. Prevalent Vertebral Deformities Predict Hip Fractures and New Vertebral Deformities but Not Wrist Fractures. *Journal of Bone and Mineral Research,* 14**,** 821-828.

BLACK, D. M., CUMMINGS, S. R., KARPF, D. B., CAULEY, J. A., THOMPSON, D. E., NEVITT, M. C., BAUER, D. C., GENANT, H. K., HASKELL, W. L., MARCUS, R., OTT, S. M., TORNER, J. C., QUANDT, S. A., REISS, T. F. & ENSRUD, K. E. 1996. Randomised trial of effect of alendronate on risk of fracture in women with existing vertebral fractures. *The Lancet,* 348**,** 1535-1541.

BLACK, D. M., DELMAS, P. D., EASTELL, R., REID, I. R., BOONEN, S., CAULEY, J. A., COSMAN, F., LAKATOS, P., LEUNG, P. C., MAN, Z., MAUTALEN, C., MESENBRINK, P., HU, H., CAMINIS, J., TONG, K., ROSARIO-JANSEN, T., KRASNOW, J., HUE, T. F., SELLMEYER, D., ERIKSEN, E. F. & CUMMINGS, S. R. 2007. Once-Yearly Zoledronic Acid for Treatment of Postmenopausal Osteoporosis. *New England Journal of Medicine,* 356**,** 1809-1822.

BLACK, D. M., GREENSPAN, S. L., ENSRUD, K. E., PALERMO, L., MCGOWAN, J. A., LANG, T. F., GARNERO, P., BOUXSEIN, M. L., BILEZIKIAN, J. P. & ROSEN, C. J. 2003. The Effects of Parathyroid Hormone and Alendronate Alone or in Combination in Postmenopausal Osteoporosis. *New England Journal of Medicine,* 349**,** 1207-1215.

BLAKE, G. M., NAEEM, M. & BOUTROS, M. 2006. Comparison of effective dose to children and adults from dual X-ray absorptiometry examinations. *Bone,* 38**,** 935-942.

BOUXSEIN, M. L. 2005. Determinants of skeletal fragility. *Best Practice & Research Clinical Rheumatology,* 19**,** 897-911.

BOUXSEIN, M. L. 2006. Biomechanics of Osteoporotic Fractures. *Bone and Mineral Metabolism,* 4**,** 143-154.

BOYDE, A. 2002. Morphologic detail of aging bone in human vertebrae. *Endocrine,* 17**,** 5-14.

BUCKLEY, J. M., CHENG, L., LOO, K., SLYFIELD, C. & XU, Z. 2007a. Quantitative computed tomography-based predictions of vertebral strength in anterior bending. *SPINE,* 32**,** 1019-1027.

BUCKLEY, J. M., LEANG, D. C. & KEAVENY, T. M. 2006. Sensitivity of Vertebral Compressive Strength to Endplate Loading Distribution. *Journal of Biomechanical Engineering,* 128**,** 641-646.

BUCKLEY, J. M., LOO, K. & MOTHERWAY, J. 2007b. Comparison of quantitative computed tomography-based measures in predicting vertebral compressive strength. *Bone,* 40**,** 767-774.

CASSIDY, J. J., HILTNER, A. & BAER, E. 1989. Hierarchical structure of the intervertebral disc. *Connective tissue research,* 23**,** 75-88.

CHEN, P., MILLER, P. D., DELMAS, P. D., MISURSKI, D. A. & KREGE, J. H. 2006. Change in Lumbar Spine BMD and Vertebral Fracture Risk Reduction in Teriparatide-Treated Postmenopausal Women With Osteoporosis. *Journal of Bone and Mineral Research,* 21**,** 1785-1790.

CHEN, P., SATTERWHITE, J. H., LICATA, A. A., LEWIECKI, E. M., SIPOS, A. A., MISURSKI, D. M. & WAGMAN, R. B. 2005. Early Changes in Biochemical Markers of Bone

Formation Predict BMD Response to Teriparatide in Postmenopausal Women With Osteoporosis. *Journal of Bone and Mineral Research,* 20**,** 962-970.

CHESNUT, C. H., SKAG, A., CHRISTIANSEN, C., RECKER, R., STAKKESTAD, J. A., HOISETH, A., FELSENBERG, D., HUSS, H., GILBRIDE, J., SCHIMMER, R. C., DELMAS, P. D., FOR THE ORAL IBANDRONATE OSTEOPOROSIS VERTEBRAL FRACTURE TRIAL IN NORTH, A. & EUROPE 2004. Effects of Oral Ibandronate Administered Daily or Intermittently on Fracture Risk in Postmenopausal Osteoporosis. *Journal of Bone and Mineral Research,* 19**,** 1241-1249.

CHEUNG, J. T.-M., ZHANG, M. & CHOW, D. H.-K. 2003. Biomechanical responses of the intervertebral joints to static and vibrational loading: a finite element study. *Clinical Biomechanics,* 18**,** 790-799.

CHEVALIER, Y., CHARLEBOIS, M., PAHR, D., VARGA, P., HEINI, P., SCHNEIDER, E. & ZYSSET, P. 2008. A patient-specific finite element methodology to predict damage accumulation in vertebral bodies under axial compression, sagittal flexion and combined loads. *Computer Methods in Biomechanics and Biomedical Engineering,* 11**,** 477-487.

CHEVALIER Y, P. D., ZYSSET PK. 2009. The role of cortical shell and trabecular fabric in finite element analysis of the human vertebral body. *Journal of Biomechanical Engineering,* 131.

CHEVALIER, Y., QUEK, E., BORAH, B., GROSS, G., STEWART, J., LANG, T. & ZYSSET, P. 2010. Biomechanical effects of teriparatide in women with osteoporosis treated previously with alendronate and risedronate: Results from quantitative computed tomography-based finite element analysis of the vertebral body. *Bone,* 46**,** 41-48.

CHRISTIANSEN, B. & BOUXSEIN, M. 2010. Biomechanics of Vertebral Fractures and the Vertebral Fracture Cascade. *Current Osteoporosis Reports,* 8**,** 198-204.

CONSENSUSDEVELOPMENTCONFERENCE 1993. Diagnosis, prophylaxis, and treatment of osteoporosis. *American Journal of Medicine.*

COOPER, C., ATKINSON, E. J., JACOBSEN, S. J., O'FALLON, W. M. & MELTON, L. J. 1993. Population-Based Study of Survival after Osteoporotic Fractures. *American Journal of Epidemiology,* 137**,** 1001-1005.

CRANNEY, A., GUYATT, G., GRIFFITH, L., WELLS, G., TUGWELL, P. & ROSEN, C. 2002. IX: Summary of Meta-Analyses of Therapies for Postmenopausal Osteoporosis. *Endocrine Reviews,* 23**,** 570-578.

CRAWFORD, R. P., CANN, C. E. & KEAVENY, T. M. 2003a. Finite element models predict in vitro vertebral body compressive strength better than quantitative computed tomography. *Bone,* 33**,** 744–750.

CRAWFORD, R. P., KEAVENY, T. M. & ROSENBERG, W. S. 2003b. Quantitative Computed Tomography-Based Finite Element Models of the Human Lumbar Vertebral Body: Effect of Element Size on Stiffness, Damage, and Fracture Strength Predictions. *Journal of Biomechanical Engineering,* 125**,** 434-438.

CRAWFORD RP, K. T. 2004. Relationship between axial and bending behaviors of the human thoracolumbar vertebra. *Spine,* 29**,** 2248-55.

CUMMINGS, S. R., BATES, D. & BLACK, D. M. 2002. Clinical use of bone densitometry: Scientific review. *JAMA,* 288**,** 1889-1897.

DALL'ARA, E., PAHR, D., VARGA, P., KAINBERGER, F. & ZYSSET, P. 2012. QCT-based finite element models predict human vertebral strength in vitro significantly better than simulated DEXA. *Osteoporosis International***,** 563-572.

DALL'ARA, E., SCHMIDT, R., PAHR, D., VARGA, P., CHEVALIER, Y., PATSCH, J., KAINBERGER, F. & ZYSSET, P. 2010. A nonlinear finite element model validation study based on

a novel experimental technique for inducing anterior wedge-shape fractures in human vertebral bodies in vitro. *Journal of Biomechanics,* 43**,** 2374-2380.

DELMAS, P. D., RECKER, R. R., CHESNUT, C. H., III, SKAG, A., STAKKESTAD, J. A., EMKEY, R., GILBRIDE, J., SCHIMMER, R. C. & CHRISTIANSEN, C. 2004. Daily and intermittent oral ibandronate normalize bone turnover and provide significant reduction in vertebral fracture risk: results from the BONE study. *Osteoporosis International,* 15**,** 792-798.

DENOZIÈRE, G. & KU, D. N. 2006. Biomechanical comparison between fusion of two vertebrae and implantation of an artificial intervertebral disc. *Journal of Biomechanics,* 39**,** 766-775.

DONNELLY, E. 2011. Methods for Assessing Bone Quality: A Review. *Clinical Orthopaedics and Related Research®,* 469**,** 2128-2138.

DUBOEUF, F., JERGAS, M., SCHOTT, A. M., WU, C. Y., GLÜER, C. C. & GENANT, H. K. 1995. A comparison of bone densitometry measurements of the central skeleton in post-menopausal women with and without vertebral fracture. *The British Journal of Radiology,* 68**,** 747-753.

EASTELL, R., CEDEL, S. L., WAHNER, H. W., RIGGS, B. L. & MELTON, L. J. 1991. Classification of vertebral fractures. *Journal of Bone and Mineral Research,* 6**,** 207-215.

EASTELL, R., KREGE, J. H., CHEN, P., GLASS, E. V. & REGINSTER, J.-Y. 2006. Development of an algorithm for using PINP to monitor treatment of patients with teriparatide. *Current Medical Research and Opinion,* 22**,** 61-66.

EBARA, S., IATRIDIS, J. C., SETTON, L. A., FOSTER, R. J., MOW, V. C. & WEIDENBAUM, M. 1996. Tensile Properties of Nondegenerate Human Lumbar Anulus Fibrosus. *Spine,* 21**,** 452-461.

EBBESEN, E. N., THOMSEN, J. S., BECK-NIELSEN, H., NEPPER-RASMUSSEN, H. J. & MOSEKILDE, L. 1999. Lumbar vertebral body compressive strength evaluated by dual-energy X-ray absorptiometry, quantitative computed tomography, and ashing. *Bone,* 25**,** 713-724.

EDWARDS, W., ZHENG, Y., FERRARA, L. & YUAN, H. 2001. Structural features and thickness of the vertebral cortex in the thoracolumbar spine. *Spine,* 26**,** 218-25.

EL-RICH, M., ARNOUX, P.-J., WAGNAC, E., BRUNET, C. & AUBIN, C.-E. 2009. Finite element investigation of the loading rate effect on the spinal load-sharing changes under impact conditions. *Journal of Biomechanics,* 42**,** 1252-1262.

ELLIOTT, D. M. & SETTON, L. A. 2001. Anisotropic and inhomogeneous tensile behavior of the human anulus fibrosus: Experimental measurement and material model predictions. *Journal of Biomechanical Engineering,* 123**,** 256-263.

ETTINGER, B., BLACK, D. M., MITLAK, B. H. & ET AL. 1999. Reduction of vertebral fracture risk in postmenopausal women with osteoporosis treated with raloxifene: Results from a 3-year randomized clinical trial. *JAMA,* 282**,** 637-645.

FAGAN, M. J., JULIAN, S. & MOHSEN, A. M. 2002a. Finite element analysis in spine research. *Proc Instn Mech Engrs: J Engineering in Medicine,* 216.

FAGAN, M. J., JULIAN, S., SIDDALL, D. J. & MOHSEN, A. M. 2002b. Patient-specific spine models. Part1: finite element analysis of the lumbar intervertebral disc-a material sensitivity study. *Proc Instn Mech Engrs: J Engineering in Medicine,* 299-314.

FERRAR, L., JIANG, G., SCHOUSBOE, J. T., DEBOLD, C. R. & EASTELL, R. 2008. Algorithm-based qualitative and semiquantitative identification of prevalent vertebral fracture: agreement between different readers, imaging modalities, and diagnostic approaches. *J Bone Miner Res,* 23**,** 417-24.

FIELDS, A. J., LEE, G. L., LIU, X. S., JEKIR, M. G., GUO, X. E. & KEAVENY, T. M. 2011. Influence of vertical trabeculae on the compressive strength of the human vertebra. *Journal of Bone and Mineral Research,* 26**,** 263-269.

FROST, H. M. 1987. Bone "mass" and the "mechanostat": A proposal. *The Anatomical Record,* 219**,** 1-9.

FURLONG, D. R. & PALAZOTTO, A. N. 1983. A finite element analysis of the influence of surgical herniation on the viscoelastic properties of the intervertebral disc. *Journal of Biomechanics,* 16**,** 785-795.

FYHRIE, D. P. & SCHAFFLER, M. B. 1994. Failure mechanisms in human vertebral cancellous bone. *Bone,* 15**,** 105-109.

GARCIA, D., ZYSSET, P., CHARLEBOIS, M. & CURNIER, A. 2009. A three-dimensional elastic plastic damage constitutive law for bone tissue. *Biomechanics and Modeling in Mechanobiology,* 8**,** 149-165.

GEHLBAH, S. H., BIGELOW, C., HEIMISDOTTIR, M., MAY, S., WALKER, M. & KIRKWOOD, J. R. 2000. Recognition of Vertebral Fracture in a Clinical Setting. *Osteoporosis International,* 11**,** 577-582.

GOEL, V., RAMIREZ, S., KONG, W. & GILBERTSON, L. 1995. Cancellous bone Young's modulus variation within the vertebral body of a ligamentous lumbar spine-application of bone adaptive remodeling concepts. *J Biomech Eng,* 117**,** 266 - 271.

GOTO, K., TAJIMA, N., CHOSA, E., TOTORIBE, K., KUROKI, H., ARIZUMI, Y. & ARAI, T. 2002. Mechanical analysis of the lumbar vertebrae in a three-dimensional finite element method model in which intradiscal pressure in the nucleus pulposus was used to establish the model. *Journal of Orthopaedic Science,* 7**,** 243-246.

GOULET, R. W., GOLDSTEIN, S. A., CIARELLI, M. J., KUHN, J. L., BROWN, M. B. & FELDKAMP, L. A. 1994. The relationship between the structural and orthogonal compressive properties of trabecular bone. *Journal of Biomechanics,* 27**,** 375-377,379-389.

GRAEFF, C., CHEVALIER, Y., CHARLEBOIS, M., VARGA, P., PAHR, D., NICKELSEN, T. N., MORLOCK, M. M., GLÜER, C. C. & ZYSSET, P. K. 2009. Improvements in Vertebral Body Strength Under Teriparatide Treatment Assessed In Vivo by Finite Element Analysis: Results From the EUROFORS Study. *Journal of Bone and Mineral Research,* 24**,** 1672-1680.

GRAEFF, C., TIMM, W., NICKELSEN, T. N., FARRERONS, J., MARÍN, F., BARKER, C. & GLÜER, C. C. 2007. Monitoring Teriparatide-Associated Changes in Vertebral Microstructure by High-Resolution CT In Vivo: Results From the EUROFORS Study. *Journal of Bone and Mineral Research,* 22**,** 1426-1433.

GRAMPP, S., GENANT, H. K., MATHUR, A., LANG, P., JERGAS, M., TAKADA, M., GLÜER, C.-C., LU, Y. & CHAVEZ, M. 1997. Comparisons of Noninvasive Bone Mineral Measurements in Assessing Age-Related Loss, Fracture Discrimination, and Diagnostic Classification. *Journal of Bone and Mineral Research,* 12**,** 697-711.

GREENSPAN, S. L., BONE, H. G., ETTINGER, M. P., HANLEY, D. A., LINDSAY, R., ZANCHETTA, J. R., BLOSCH, C. M., MATHISEN, A. L., MORRIS, S. A. & MARRIOTT, T. B. 2007. Effect of Recombinant Human Parathyroid Hormone (1-84) on Vertebral Fracture and Bone Mineral Density in Postmenopausal Women with OsteoporosisA Randomized Trial. *Annals of Internal Medicine,* 146**,** 326-339.

GUERIN, H. A. L. & ELLIOTT, D. M. 2006. Structure and Properties of Soft Tissues in the Spine. *In:* KURTZ, S. M. & EDIDIN, A. A. (eds.) *Spine Technology Handbook.* Elsevier.

GUGLIELMI, G., CAMMISA, M., DE SERIO, A., SCILLITANI, A., CHIODINI, I., CARNEVALE, V. & FUSILLI, S. 1999. Phalangeal US velocity discriminates between normal and vertebrally fractured subjects. *European Radiology,* 9**,** 1632-1637.

GUO, X. E. & KIM, C. H. 2002. Mechanical consequence of trabecular bone loss and its treatment: a three-dimensional model simulation. *Bone,* 30**,** 404-411.

HARRIS, S. T., WATTS, N. B., GENANT, H. K. & ET AL. 1999. Effects of risedronate treatment on vertebral and nonvertebral fractures in women with postmenopausal osteoporosis: A randomized controlled trial. *JAMA,* 282**,** 1344-1352.

HAUT, R. C. & LITTLE, R. W. 1972. A constitutive equation for collagen fibers. *Journal of Biomechanics,* 5**,** 423-430.

HERNANDEZ, C. J. & KEAVENY, T. M. 2006. A biomechanical perspective on bone quality. *Bone,* 39**,** 1173-1181.

HOLZAPFEL, G. A., SCHULZE-BAUER, C. A. J., FEIGL, G. & REGITNIG, P. 2005. Single lamellar mechanics of the human lumbar anulus fibrosus. *Biomechanics and Modeling in Mechanobiology,* 3**,** 125-140.

HOMMINGA, J., WEINANS, H., VAN RIETBERGEN, B., RUEGSEGGER, P. & HUISKES, R. 1998. Trabecular bone from osteoporotic patients is stiffer than expected. *Journal of Biomechanics,* 31**,** 153.

HOMMINGA, J. M., *†; WEINANS, HARRIE PHD,†; GOWIN, WOLFGANG PHD,‡; FELSENBERG, DIETER PHD,‡ AND; HUISKES, RIK PHD*§ 2001. Osteoporosis Changes the Amount of Vertebral Trabecular Bone at Risk of Fracture but Not the Vertebral Load Distribution. *Spine,* 26**,** 1555-1560.

HUSSEIN, A., MASON, Z. D. & MORGAN, E. F. 2013. Presence of Intervertebral Discs Alters Observed Stiffness and Failure Mechanisms in the Vertebra. *Journal of biomechanics,* 46**,** 1683-1688.

IATRIDIS, J., WEIDENBAUM, M., SETTON, L. A. & MOW, V. C. 1996. Is the nucleus pulposus a solid or a fluid?-Mechanical behaviors of the nucleus pulposus of the human intervertebral disc. *Spine,* 21**,** 1174-84.

IATRIDIS, J. C., SETTON, L. A., FOSTER, R. J., RAWLINS, B. A., WEIDENBAUM, M. & MOW, V. C. 1998. Degeneration affects the anisotropic and nonlinear behaviors of human anulus fibrosus in compression. *Journal of Biomechanics,* 31**,** 535-544.

IATRIDIS, J. C., SETTON, L. A., WEIDENBAUM, M. & MOW, V. C. 1997. Alterations in the mechanical behavior of the human lumbar nucleus pulposus with degeneration and aging. *Journal of Orthopaedic Research,* 15**,** 318-322.

IMAI, K., OHNISHI, I., BESSHO, M. & NAKAMURA, K. 2006. Nonlinear Finite Element Model Predicts Vertebral Bone Strength and Fracture Site. *Spine,* 31**,** 1789-1794 10.1097/01.brs.0000225993.57349.df.

IMAI, K., OHNISHI, I., MATSUMOTO, T., YAMAMOTO, S. & NAKAMURA, K. 2009. Assessment of vertebral fracture risk and therapeutic effects of alendronate in postmenopausal women using a quantitative computed tomography-based nonlinear finite element method. *Osteoporosis International,* 20**,** 801-810.

IMAI, K., OHNISHI, I., YAMAMOTO, S. & NAKAMURA, K. 2008. In Vivo Assessment of Lumbar Vertebral Strength in Elderly Women Using Computed Tomography-Based Nonlinear Finite Element Model. *Spine,* 33**,** 27-32 10.1097/BRS.0b013e31815e3993.

JACKSON S.A., T. A., ROBERTSON L., CAMOS STUDY GROUP 2000. Vertebral Fracture Definition from Population-Based Data: Preliminary Results from the Canadian Multicenter Osteoporosis Study (CaMos). *Osteoporosis International,* 11**,** 680.

JIANG, G., EASTELL, R., BARRINGTON, N. A. & FERRAR, L. 2004. Comparison of methods for the visual identification of prevalent vertebral fracture in osteoporosis. *Osteoporosis International,* 15**,** 887-896.

JOHANNESSEN, W., AUERBACH, J., WHEATON, A., KURJI, A., BORTHAKUR, A., REDDY, R. & ELLIOTT, D. M. 2006. Assessment of human disc degeneration and proteoglycan content using T1rho-weighted magnetic resonance imaging. *Spine,* 31**,** 1253-7.

JOHANNESSEN, W. & ELLIOTT, D. M. 2005. Effects of Degeneration on the Biphasic Material Properties of Human Nucleus Pulposus in Confined Compression. *Spine,* 30**,** E724-E729.

JONES, A. C. & WILCOX, R. K. 2008. Finite element analysis of the spine: Towards a framework of verification, validation and sensitivity analysis. *Medical Engineering & Physics,* 30**,** 1287-1304.

KADO, D. M., BROWNER, W. S., PALERMO, L. & ET AL. 1999. Vertebral fractures and mortality in older women: A prospective study. *Archives of Internal Medicine,* 159**,** 1215-1220.

KAMINSKY, J., KLINGE, P., RODT, T., BOKEMEYER, M., LUEDEMANN, W. & SAMII, M. 2004. Specially adapted interactive tools for an improved 3D-segmentation of the spine. *Computerized Medical Imaging and Graphics,* 28**,** 119-127.

KANIS, J. A., BURLET, N., COOPER, C., DELMAS, P. D., REGINSTER, J. Y., BORGSTROM, F. & RIZZOLI, R. 2008. European guidance for the diagnosis and management of osteoporosis in postmenopausal women. *Osteoporosis International,* 19**,** 399-428.

KANIS, J. A. & GLÜER, C. C. 2000. An update on the diagnosis and assessment of osteoporosis with densitometry. Committee of Scientific Advisors, International Osteoporosis Foundation. *Osteoporosis international : a journal established as result of cooperation between the European Foundation for Osteoporosis and the National Osteoporosis Foundation of the USA,* 11**,** 192-202.

KEAVENY, T. M. & BUCKLEY, J. M. 2006. Biomechanics of Vertebral Bone. *In:* KURTZ, S. M. & EDIDIN, A. A. (eds.) *Spine Technology Handbook.*

KEAVENY, T. M., DONLEY, D. W., HOFFMANN, P. F., MITLAK, B. H., GLASS, E. V. & SAN MARTIN, J. A. 2007. Effects of Teriparatide and Alendronate on Vertebral Strength as Assessed by Finite Element Modeling of QCT Scans in Women With Osteoporosis. *Journal of Bone and Mineral Research,* 22**,** 149-157.

KEAVENY, T. M., HOFFMANN, P. F., SINGH, M., PALERMO, L., BILEZIKIAN, J. P., GREENSPAN, S. L. & BLACK, D. M. 2008. Femoral Bone Strength and Its Relation to Cortical and Trabecular Changes After Treatment With PTH, Alendronate, and Their Combination as Assessed by Finite Element Analysis of Quantitative CT Scans. *Journal of Bone and Mineral Research,* 23**,** 1974-1982.

KEAVENY, T. M., MCCLUNG, M. R., WAN, X., KOPPERDAHL, D. L., MITLAK, B. H. & KROHN, K. 2011. Femoral strength in osteoporotic women treated with teriparatide or alendronate. *Bone,* 50**,** 165-170.

KEAVENY, T. M., MORGAN, E. F., NIEBUR, G. L. & YEH, O. C. 2001. Biomechanics of trabecular bone. *Annu. Rev. Biomed. Eng.,* 3**,** 307-33.

KEAVENY, T. M., WACHTEL, E. F., FORD, C. M. & HAYES, W. C. 1994. Differences between the tensile and compressive strengths of bovine tibial trabecular bone depend on modulus. *Journal of Biomechanics,* 27**,** 1137-1146.

KEAVENY, T. M., WACHTEL, E. F. & KOPPERDAHL, D. L. 1999. Mechanical behavior of human trabecular bone after overloading. *Journal of Orthopaedic Research,* 17**,** 346-353.

KEYAK, J. H., MEAGHER, J. M., SKINNER, H. B. & MOTE JR, C. D. 1990. Automated three-dimensional finite element modelling of bone: a new method. *Journal of Biomedical Engineering,* 12**,** 389-397.

KEYAK, J. H. & ROSSI, S. A. 2000. Prediction of femoral fracture load using finite element models: an examination of stress- and strain-based failure theories. *Journal of Biomechanics,* 33**,** 209-214.

KEYAK, J. H., ROSSI, S. A., JONES, K. A., LES, C. M. & SKINNER, H. B. 2001. Prediction of fracture location in the proximal femur using finite element models. *Medical Engineering & Physics,* 23**,** 657-664.

KEYAK, J. H., ROSSI, S. A., JONES, K. A. & SKINNER, H. B. 1998. Prediction of femoral fracture load using automated finite element modeling. *Journal of Biomechanics,* 31**,** 125-133.

KIM, Y. & KIM, D. 2009. A fully automatic vertebra segmentation method using 3D deformable fences. *Computerized Medical Imaging and Graphics,* 33**,** 343-352.

KOIVUMAKI, J. E. M., THEVENOT, J., PULKKINEN, P., KUHN, V. & LINK, T. M. 2012. Ct-based finite element models can be used to estimate experimentally measured failure loads in the proximal femur. *Bone,* 50**,** 824-829.

KOPPERDAHL, D. L. & KEAVENY, T. M. 1998. Yield strain behavior of trabecular bone. *Journal of Biomechanics,* 31**,** 601-608.

KOPPERDAHL, D. L., MORGAN, E. F. & KEAVENY, T. M. 2002. Quantitative computed tomography estimates of the mechanical properties of human vertebral trabecular bone. *Journal of Orthopaedic Research,* 20**,** 801-805.

KOPPERDAHL, D. L., PEARLMAN, J. L. & KEAVENY, T. M. 2000. Biomechanical consequences of an isolated overload on the human vertebral body. *Journal of Orthopaedic Research,* 18**,** 685-690.

KUROWSKI, P. & KUBO, A. 1986. The relationship of degeneration of the intervertebral disc to mechanical loading conditions on lumbar vertebrae. *Spine,* 11.

LANE, N. E., THOMPSON, J. M., HAUPT, D., KIMMEL, D. B., MODIN, G. & KINNEY, J. H. 1998. Acute Changes in Trabecular Bone Connectivity and Osteoclast Activity in the Ovariectomized Rat In Vivo. *Journal of Bone and Mineral Research,* 13**,** 229-236.

LANG, T. F., GUGLIELMI, G., VAN KUIJK, C., DE SERIO, A., CAMMISA, M. & GENANT, H. K. 2002. Measurement of bone mineral density at the spine and proximal femur by volumetric quantitative computed tomography and dual-energy x-ray absorptiometry in elderly women with and without vertebral fractures. *Bone,* 30**,** 247-250.

LEWIECKI, E. M. K., TONY M.; KOPPERDAHL, DAVID L.; GENANT, HARRY K.; ENGELKE, KLAUS; FUERST, THOMAS; KIVITZ, ALAN; DAVIES, RICHARD Y.; FITZPATRICK, LORRAINE A. 2009. Once-Monthly Oral Ibandronate Improves Biomechanical Determinants of Bone Strength in Women with Postmenopausal Osteoporosis. *The Journal of Clinical Endocrinology & Metabolism,* 94**,** 171-180.

LEWIS, M., BLAKE, G. M. & FOGELMAN, I. 1994. Patient dose in dual x-ray absorptiometry. *Osteoporosis International,* 4**,** 11-5.

LI, H. & WANG, Z. 2006. Intervertebral disc biomechanical analysis using the finite element modeling based on medical images. *Computerized Medical Imaging and Graphics,* 30**,** 363-370.

LIEBSCHNER, M. A. K., KOPPERDAHL, D. L., ROSENBERG, W. S. & KEAVENY, T. M. 2003. Finite Element Modeling of the Human Thoracolumbar Spine. *Spine,* 28**,** 559-565.

LINDSAY, R., SILVERMAN, S. L., COOPER, C. & ET AL. 2001. RIsk of new vertebral fracture in the year following a fracture. *JAMA,* 285**,** 320-323.

LORENZ, M., PATWARDHAN, A. & VANDERBY, R. J. 1983. Load-Bearing Characteristics of Lumbar Facets in Normal and Surgically Altered Spinal Segments. *Spine,* 8**,** 122-130.

LOTZ, J. C., CHEAL, E. J. & HAYES, W. C. 1991a. Fracture prediction for the proximal femur using finite element models: Part1-Linear analysis. *Journal of Biomechanical Engineering,* 113**,** 353-360.

LOTZ, J. C., CHEAL, E. J. & HAYES, W. C. 1991b. Fracture prediction for the proximal femur using finite element models: Part2-Nonlinear analysis. *Journal of Biomechanical Engineering,* 113**,** 361-365.

LU, Y., HUTTON, W. & CHARPURAY, V. 1996. Do bending, twisting, and diurnal fluid changes in the disc affect the propensity to prolapse? A viscoelastic finite element model. *Spine,* 21**,** 2570-9.

LUO, J., BERTRAM, W., SANGAR, D., ADAMS, M. A., ANNESLEY-WILLIAMS, D. J. & DOLAN, P. 2010. Is kyphoplasty better than vertebroplasty in restoring normal mechanical function to an injured spine? *Bone,* 46**,** 1050-1057.

MAQUER, G., SCHWIEDRZIK, J. & ZYSSET, P. 2013. Embedding of human vertebral bodies leads to higher ultimate load and altered damage localisation under axial compression. *Computer Methods in Biomechanics and Biomedical Engineering***,** 1-12.

MARSHALL, D., JOHNELL, O. & WEDEL, H. 1996. Meta-analysis of how well measures of bone mineral density predict occurrence of osteoporotic fractures. *BMJ (Clinical research ed.),* 312**,** 1254-1259.

MATSUMOTO, T., OHNISHI, I., BESSHO, M., IMAI, K., OHASHI, S. & NAKAMURA, K. 2009. Prediction of vertebral strength under loading conditions occuring in activities of daily living using a computed tomography-based nonlinear finite element method. *SPINE,* 34**,** 1464-1469.

MAWATARI, T., MIURA, H., HAMAI, S., SHUTO, T., NAKASHIMA, Y., OKAZAKI, K., KINUKAWA, N., SAKAI, S., HOFFMANN, P. F., IWAMOTO, Y. & KEAVENY, T. M. 2008. Vertebral strength changes in rheumatoid arthritis patients treated with alendronate, as assessed by finite element analysis of clinical computed tomography scans: A prospective randomized clinical trial. *Arthritis & Rheumatism,* 58**,** 3340-3349.

MELTON III, L. J., ATKINSON, E. J., COOPER, C., O'FALLON, W. M. & RIGGS, B. L. 1999. Vertebral Fractures Predict Subsequent Fractures. *Osteoporosis International,* 10**,** 214-221.

MELTON III, L. J., RIGGS, B. L., KEAVENY, T. M., ACHENBACH, S. J., KOPPERDAHL, D., CAMP, J. J., ROULEAU, P. A., AMIN, S., ATKINSON, E. J., ROBB, R. A., THERNEAU, T. M. & KHOSLA, S. 2010. Relation of vertebral deformities to bone density, structure, and strength. *Journal of Bone and Mineral Research,* 25**,** 1922-1930.

MELTON, L. J., KAN, S. H., FRYE, M. A., WAHNER, H. W., O'FALLON, M. & RIGGS, B. L. 1989. Epidemiology of Vertebral Fractures in Women. *American Journal of Epidemiology,* 129**,** 1000-1011.

MELTON, L. J., LANE, A. W., COOPER, C., EASTELL, R., O'FALLON, M. & RIGGS, B. L. 1993. Prevalence and Incidence of Vertebral Deformities. *Osteoporosis International,* 3**,** 113-119.

MELTON, L. J., RIGGS, B. L., KEAVENY, T. M., ACHENBACH, S. J., HOFFMANN, P. F., CAMP, J. J., ROULEAU, P. A., BOUXSEIN, M. L., AMIN, S., ATKINSON, E. J., ROBB, R. A. & KHOSLA, S. 2007. Structural Determinants of Vertebral Fracture Risk. *Journal of Bone and Mineral Research,* 22**,** 1885-1892.

MINDWAYS, S. 2005. QCT PRO TM Bone Mineral Densitometry Software Phantom Module. Mindways Software.

MIRZAEI, M., ZEINALI, A., RAZMJOO, A. & NAZEMI, M. 2009. On Prediction of the strength levels and failure patterns of human vertebrae using quantitative computed tomography-based finite element method. *Journal of Biomechanics,* 42**,** 1584-1591.

MORGAN, E. & KEAVENY, T. 2001. Dependence of yield strain of human trabecular bone on anatomic site. *Journal of Biomechanics,* 34**,** 569–577.

MORGAN, E. F., BAYRAKTAR, H. H. & KEAVENY, T. M. 2003. Trabecular bone modulus–density relationships depend on anatomic site. *Journal of Biomechanics,* 36**,** 897-904.

MOSEKILDE, L. 1993. Vertebral structure and strengthIn vivo andIn vitro. *Calcified Tissue International,* 53**,** S121-S126.

MOSEKILDE, L., MOSEKILDE, L. & DANIELSEN, C. C. 1987. Biomechanical competence of vertebral trabecular bone in relation to ash density and age in normal individuals. *Bone,* 8**,** 79-85.

NACHEMSON, A. 1960. Lumbar intradiscal pressure. Experimental studies on post-mortem material. *Acta Orthop Scand Suppl,* 43**,** 1-104.

NACHEMSON, A. 1966. The load on lumbar disks in different positions of the body. *Clin Orthop Relat Res.,* 45**,** 107-22.

NATARAJAN, R. N., WILLIAMS, J. R. & ANDERSSON, G. B. J. 2003. Finite element model of a lumbar spinal motion segment to predict circadian variation in stature. *Computers & Structures,* 81**,** 835-842.

NATARAJAN, R. N., WILLIAMS, J. R., LAVENDER, S. A. & ANDERSSON, G. B. J. 2007. Poro-elastic finite element model to predict the failure progression in a lumbar disc due to cyclic loading. *Computers & Structures,* 85**,** 1142-1151.

NEER, R. M., ARNAUD, C. D., ZANCHETTA, J. R., PRINCE, R., GAICH, G. A., REGINSTER, J.-Y., HODSMAN, A. B., ERIKSEN, E. F., ISH-SHALOM, S., GENANT, H. K., WANG, O., MELLSTRÖM, D., OEFJORD, E. S., MARCINOWSKA-SUCHOWIERSKA, E., SALMI, J., MULDER, H., HALSE, J., SAWICKI, A. Z. & MITLAK, B. H. 2001. Effect of Parathyroid Hormone (1-34) on Fractures and Bone Mineral Density in Postmenopausal Women with Osteoporosis. *New England Journal of Medicine,* 344**,** 1434-1441.

NGUYEN, A. M., JOHANNESSEN, W., YODER, J. H., WHEATON, A. J., VRESILOVIC, E. J., BORTHAKUR, A. & ELLIOTT, D. M. 2008. *Noninvasive Quantification of Human Nucleus Pulposus Pressure with Use of T1ρ-Weighted Magnetic Resonance Imaging*.

NIH 2000. Osteoporosis Prevention, Diagnosis, and Therapy. National Institutes of Health Consens Statement.

NJEH, C. F., FUERST, T., HANS, D., BLAKE, G. M. & GENANT, H. K. 1999. Radiation exposure in bone mineral density assessment. *Applied Radiation and Isotopes,* 50**,** 215-236.

NOAILLY, J., LACROIX, D. & PLANELL, J. A. 2005. Finite Element Study of a Novel Intervertebral Disc Substitute. *Spine,* 30**,** 2257-2264 10.1097/01.brs.0000182319.81795.72.

NORDIN, M. & FRANKEL, V. H. 2012. *Basic Biomechanics of the Musculoskeletal System*, Lippincott Williams & Wilkins, a Wolters Kluwer business.

O'NEILL, T. W., FELSENBERG, D., VARLOW, J., COOPER, C., KANIS, J. A. & SILMAN, A. J. 1996. The prevalence of vertebral deformity in European men and women: The

european vertebral osteoporosis study. *Journal of Bone and Mineral Research,* 11**,** 1010-1018.

OBERMAYER-PIETSCH, B. M., MARIN, F., MCCLOSKEY, E. V., HADJI, P., FARRERONS, J., BOONEN, S., AUDRAN, M., BARKER, C., ANASTASILAKIS, A. D., FRASER, W. D. & NICKELSEN, T. 2008. Effects of Two Years of Daily Teriparatide Treatment on BMD in Postmenopausal Women With Severe Osteoporosis With and Without Prior Antiresorptive Treatment. *Journal of Bone and Mineral Research,* 23**,** 1591-1600.

ODGAARD, A., KABEL, J., VAN RIETBERGEN, B., DALSTRA, M. & HUISKES, R. 1997. Fabric and elastic principal directions of cancellous bone are closely related. *Journal of Biomechanics,* 30**,** 487-495.

PAL, G. P. & ROUTAL, R. V. 1986. A study of weight transmission through the cervical and upper thoracic regions of the vertebral column in man. *Journal of anatomy,* 148**,** 245-261.

PFIRRMANN, C., METZDORF, A., ELFERING, A., HODLER, J. & BOOS, N. 2006. Effect of aging and degeneration on disc volume and shape: A quantitative study in asymptomatic volunteers. *J Orthop Res.,* 24**,** 1086-94.

PFIRRMANN, C., METZDORF, A., ZANETTI, M., HODLER, J. & BOOS, N. 2001. Magnetic resonance classification of lumbar intervertebral disc degeneration. *Spine,* 26**,** 1873-8.

POELERT, S., VALSTAR, E., WEINANS, H. & ZADPOOR, A. A. 2013. Patient-specific finite element modeling of bones. *Proceedings of the Institution of Mechanical Engineers, Part H: Journal of Engineering in Medicine,* 227**,** 464-478.

POLIKEIT, A., NOLTE, L. P. & FERGUSON, S. J. 2003. The Effect of Cement Augmentation on the Load Transfer in an Osteoporotic Functional Spinal Unit. *Spine,* 28**,** 991-996.

POLIKEIT, A., NOLTE, L. P. & FERGUSON, S. J. 2004. Simulated influence of osteoporosis and disc degeneration on the load transfer in a lumbar functional spinal unit. *Journal of Biomechanics,* 37**,** 1061–1069.

POLLINTINE, P., DOLAN, P., TOBIAS, J. H. & ADAMS, M. A. 2004a. Intervertebral Disc Degeneration Can Lead to "Stress-Shielding" of the Anterior Vertebral Body: A Cause of Osteoporotic Vertebral Fracture? *Spine,* 29**,** 774-782 10.1097/01.BRS.0000119401.23006.D2.

POLLINTINE, P., PRZYBYLA, A. S., DOLAN, P. & ADAMS, M. A. 2004b. Neural arch load-bearing in old and degenerated spines. *Journal of Biomechanics,* 37**,** 197-204.

POOLE, K. E. S. & COMPSTON, J. E. 2006. *Osteoporosis and its management*.

REGINSTER, J.-Y., MINNE, H., SORENSEN, O., HOOPER, M., ROUX, C., BRANDI, M., LUND, B., ETHGEN, D., PACK, S. & ROUMAGNAC, I. 2000. Randomized trial of the effects of risedronate on vertebral fractures in women with established postmenopausal osteoporosis. *Osteoporosis International,* 11**,** 83-91.

REID, I. R. 2013. Overview of Pathogenesis. *Primer on the Metabolic Bone Diseases and Disorders of Mineral Metabolism.* John Wiley & Sons, Inc.

REILLY, D. T. & BURSTEIN, A. H. 1975. The elastic and ultimate properties of compact bone tissue. *Journal of Biomechanics,* 8**,** 393-405.

RENDERS, G. A. P., MULDER, L., LANGENBACH, G. E. J., VAN RUIJVEN, L. J. & VAN EIJDEN, T. M. G. J. 2008. Biomechanical effect of mineral heterogeneity in trabecular bone. *Journal of Biomechanics,* 41**,** 2793-2798.

RHO, J.-Y., KUHN-SPEARING, L. & ZIOUPOS, P. 1998. Mechanical properties and the hierarchical structure of bone. *Medical Engineering & Physics,* 20**,** 92-102.

ROHLMANN, A., ZANDER, T., SCHMIDT, H., WILKE, H.-J. & BERGMANN, G. 2006. Analysis of the influence of disc degeneration on the mechanical behaviour of a lumbar motion segment using the finite element method. *Journal of Biomechanics,* 39**,** 2484-2490.

ROSS, C. F. 2005. Finite Element Analysis in Vertebrate Biomechanics. *The Anatomical Record Part A,* 283A**,** 253-258.

ROUX, J.-P., WEGRZYN, J., ARLOT, M. E., GUYEN, O., DELMAS, P. D., CHAPURLAT, R. & BOUXSEIN, M. L. 2010. Contribution of Trabecular and Cortical Components to Biomechanical Behavior of Human Vertebrae: An Ex Vivo Study. *Journal of Bone and Mineral Research,* 25**,** 356-361.

RUBERTÉ, L. M., NATARAJAN, R. N. & ANDERSSON, G. B. J. 2009. Influence of single-level lumbar degenerative disc disease on the behavior of the adjacent segments—A finite element model study. *Journal of Biomechanics,* 42**,** 341-348.

SANJEEVI, R., SOMANATHAN, N. & RAMASWAMY, D. 1982. A viscoelastic model for collagen fibers. *Journal of Biomechanics,* 15**,** 181-3.

SATO, K., KIKUCHI, S. & YONEZAWA, T. 1999. In vivo intradiscal pressure measurement in healthy individuals and in patients with ongoing back problems. *Spine,* 24**,** 2468-74.

SCHMIDT, H., HEUER, F., DRUMM, J., KLEZL, Z., CLAES, L. & WILKE, H.-J. 2007a. Application of a calibration method provides more realistic results for a finite element model of a lumbar spinal segment. *Clinical Biomechanics,* 22**,** 377-384.

SCHMIDT, H., HEUER, F., SIMON, U., KETTLER, A., ROHLMANN, A., CLAES, L. & WILKE, H.-J. 2006. Application of a new calibration method for a three-dimensional finite element model of a human lumbar annulus fibrosus. *Clinical Biomechanics,* 21**,** 337-344.

SCHMIDT, H., HEUER, F. & WILKE, H.-J. 2009. Dependency of disc degeneration on shear and tensile strains between annular fiber layers for complex loads. *Medical Engineering & Physics,* 31**,** 642-649.

SCHMIDT, H., KETTLER, A., HEUER, F., SIMON, U., CLAES, L. & WILKE, H. J. 2007b. Intradiscal pressure, shear strain and fiber strain in the intervertebral disc under combined loading. *Journal of Biomechanics,* 39**,** S29.

SCHMIDT, H., KETTLER, A., ROHLMANN, A., CLAES, L. & WILKE, H.-J. 2007c. The risk of disc prolapses with complex loading in different degrees of disc degeneration – A finite element analysis. *Clinical Biomechanics,* 22**,** 988-998.

SCHUIT, S. C. E., VAN DER KLIFT, M., WEEL, A. E. A. M., DE LAET, C. E. D. H., BURGER, H., SEEMAN, E., HOFMAN, A., UITTERLINDEN, A. G., VAN LEEUWEN, J. P. T. M. & POLS, H. A. P. 2004. Fracture incidence and association with bone mineral density in elderly men and women: the Rotterdam Study. *Bone,* 34**,** 195-202.

SHIRAZI-ADL, A., AHMED, A. & SHRIVASTAVA, S. 1986. Mechanical response of a lum-bar motion segment in axial torque alone and combined with compression. *Spine,* 11**,** 914 - 927.

SHIRAZI-ADL, S. A., SHRIVASTAVA, S. C. & AHMED, A. M. 1984. Stress Analysis of the Lumbar Disc-Body Unit in Compression A Three-Dimensional Nonlinear Finite Element Study. *Spine,* 9**,** 120-134.

SILVA MATTHEW J., K. T. M., HAYES WILSON C. 1998. Computed Tomography-Based Finite Element Analysis Predicts Failure Loads and Fracture Patterns

for Vertebral Sections. *Journal of Orthopaedic Research,* 16**,** 300-308.

SIRIS, E. S., CHEN, Y., ABBOTT, T. A. & ET AL. 2004. BOne mineral density thresholds for pharmacological intervention to prevent fractures. *Archives of Internal Medicine,* 164**,** 1108-1112.

SKERRY, T. M. 2008. The response of bone to mechanical loading and disuse: Fundamental principles and influences on osteoblast/osteocyte homeostasis. *Archives of Biochemistry and Biophysics,* 473**,** 117-123.

SMIT, T., ODGAARD, A. & SCHNEIDER, E. 1997. Structure and function of vertebral trabecular bone. *Spine,* 22**,** 2823 - 2833.

SMITH, L. J., NERURKAR, N. L., CHOI, K.-S., HARFE, B. D. & ELLIOTT, D. M. 2011. Degeneration and regeneration of the intervertebral disc: lessons from development. *Disease Models & Mechanisms,* 4**,** 31-41.

SPILKER, R., JAKOBS, D. & SCHULTZ, A. B. 1986. Material constants for a finite element model of the intervertebral disk with a fiber composite annulus. *Journal of Biomechanics,* 108**,** 1-11.

STEVENSON, M., JONES, M. L., DE NIGRIS, E., BREWER, N., DAVIS, S. & OAKLEY, J. 2005. A systematic review and economic evaluation of alendronate, etidronate, risedronate, raloxifene and teriparatide for the prevention and treatment of postmenopausal osteoporosis. *Health Technology Assessment,* 9**,** 160.

STRANGE, D. G. T., FISHER, S. T., BOUGHTON, P. C., KISHEN, T. J. & DIWAN, A. D. 2010. Restoration of compressive loading properties of lumbar discs with a nucleus implant-a finite element analysis study. *The Spine Journal,* 10**,** 602-609.

TANG, B. M. P., ESLICK, G. D., NOWSON, C., SMITH, C. & BENSOUSSAN, A. 2007. Use of calcium or calcium in combination with vitamin D supplementation to prevent fractures and bone loss in people aged 50 years and older: a meta-analysis. *The Lancet,* 370**,** 657-666.

TAWARA, D., SAKAMOTO, J., MURAKAMI, H., KAWAHARA, N., ODA, J. & TOMITA, K. 2010. Mechanical evaluation by patient-specific finite element analyses demonstrates therapeutic effects for osteoporotic vertebrae. *Journal of the Mechanical Behavior of Biomedical Materials,* 3**,** 31-40.

TOTORIBE, K., TAJIMA, N. & CHOSA, E. 1999. A biomechanical study of posterolateral lumbar fusion using a three-dimensional nonlinear finite element method. *Journal of orthopaedic science : official journal of the Japanese Orthopaedic Association,* 4**,** 115-126.

UC, S. 2014. *San Francisco Coordinating Center* [Online]. Available: http://www.coordinatingcenter.ucsf.edu/research/studies.php.

ULRICH, D., VAN RIETBERGEN, B., LAIB, A. & P., R. E. 1999. The Ability of Three-Dimensional Structural Indices to Reflect Mechanical Aspects of Trabecular Bone. *Bone,* 25**,** 55–60.

UMEHARA, S., TADANO, S., ABUMI, K., KATAGIRI, K., KANEDA, K. & UKAI, T. 1996. Effects of Degeneration on the Elastic Modulus Distribution in the Lumbar Intervertebral Disc. *Spine,* 21**,** 811-819.

URBAN, J. P. & ROBERTS, S. 2003. Degeneration of the intervertebral disc. *Arthritis Research & Theraphy,* 5**,** 120-130.

VAN DER KLIFT, M., DE LAET, C. E. D. H., MCCLOSKEY, E. V., HOFMAN, A. & POLS, H. A. P. 2002. The Incidence of Vertebral Fractures in Men and Women: The Rotterdam Study. *Journal of Bone and Mineral Research,* 17**,** 1051-1056.

VILLARRAGA, M. L. & FORD, C. M. 2001. Applications of Bone Mechanics. *In:* COWIN, S. C. (ed.) *Bone Mechanics Handbook.* Second ed.: CRC Press.

WANG, J. L., PARNIANPOUR, M., SHIRAZI-ADL, A., ENGIN, A. E., LI, S. & PATWARDHAN, A. 1997. Development and validation of a viscoelastic finite element model of an L2/L3 motion segment. *Theoretical and Applied Fracture Mechanics,* 28**,** 81-93.

WANG, X., SANYAL, A., CAWTHON, P. M., PALERMO, L., JEKIR, M., CHRISTENSEN, J., ENSRUD, K. E., CUMMINGS, S. R., ORWOLL, E., BLACK, D. M., FOR THE OSTEOPOROTIC FRACTURES IN MEN RESEARCH, G. & KEAVENY, T. M. 2012. Prediction of new clinical vertebral fractures in elderly men using finite element analysis of CT scans. *Journal of Bone and Mineral Research,* 27**,** 808-816.

WASNICH RD 1996. A new, standardized approach to fracture risk interpretation. *Hawaii Medical Journal,* 55**,** 141-143.

WEGRZYN, J., ROUX, J.-P., ARLOT, M. E., BOUTROY, S., VILAYPHIOU, N., GUYEN, O., DELMAS, P. D., CHAPURLAT, R. & BOUXSEIN, M. L. 2010. Role of trabecular microarchitecture and its heterogeneity parameters in the mechanical behavior of ex vivo human L3 vertebrae. *Journal of Bone and Mineral Research,* 25**,** 2324-2331.

WHO 1994. Assessment of fracture risk and its application to screening for postmenopausal osteoporosis. Report of a WHO Study Group.

WIJAYATHUNGA, V., JONES, A. C., OAKLAND, R., FURTADO, N., HALL, R. & WILCOX, R. K. 2008. Development of specimen-specific finite element models of human vertebrae for the analysis of vertebroplasty. *Proc. IMechE J. Engineering in Medicine,* 222**,** 221-228.

WILCOX, R. K. 2007. The influence of material property and morphological parameters on specimen-specific finite element models of porcine vertebral bodies. *Journal of Biomechanics,* 40**,** 669-673.

WILKE, H.-J., ROHLMANN, F., NEIDLINGER-WILKE, C., WERNER, K., CLAES, L. & KETTLER, A. 2006. Validity and interobserver agreement of a new radiographic grading system for intervertebral disc degeneration: Part I. Lumbar spine. *European Spine Journal,* 15**,** 720-730.

WOGNUM, S., HUYGHE, J. & BAAIJENS, F. 2006. Influence of osmotic pressure changes on the opening of existing cracks in 2 intervertebral disc models. *Spine,* 31**,** 1793-8.

WOLFF, J., MAQUET, P. & FURLONG, R. 1986. *The Law of Bone Remodelling*, Springer-Verlag.

WU, H.-C. & YAO, R.-F. 1976. Mechanical behavior of the human annulus fibrosus. *Journal of Biomechanics,* 9**,** 1-7.

YANG, G., KABEL, J., VAN RIETBERGEN, B., ODGAARD, A., HUISKES, R. & COWN, S. 1998. The Anisotropic Hooke's Law for Cancellous Bone and Wood. *Journal of Elasticity,* 53**,** 125-146.

YANG, K. & KING, A. 1984. Mechanism of facet load transmission as a hypothesis for low-back pain. *Spine,* 9**,** 557-65.

YOSIBASH ZOHAR, T. D., TRABELSI NIR 2010. Predicting the yield of the proximal femur using high-order finite-element analysis with inhomogeneous orthotropic material properties. *Philosophical Transactions of The Royal Society A,* 368**,** 2707-2723.

YU, W., GLÜER, C., GRAMPP, S., JERGAS, M., FUERST, T., WU, C., LU, Y., FAN, B. & GENANT, H. 1995. Spinal bone mineral assessment in postmenopausal women: a comparison between dual X-ray absorptiometry and quantitative computed tomography. *Osteoporosis International,* 5**,** 433-9.

ZEINALI, A., HASHEMI-MALAYERI, B. & AKHLAGHPOOR, S. 2010. Noninvasive prediction of vertebral body compressive strength using nonlinear finite element method and an image based technique. *Physica Medica,* 26**,** 88-97.

ZEINALI, A., HASHEMI-MALAYERI, B., AKHLAGHPOOR, S. & NAZEMI, M. 2008. Noninvasive Prediction of Vertebral Body Compressive Strength Using Finite Element Method and An Image Based Technique. *In:* ABU OSMAN, N., IBRAHIM, F., WAN ABAS, W., ABDUL RAHMAN, H. & TING, H.-N. (eds.) *4th Kuala Lumpur International Conference on Biomedical Engineering 2008.* Springer Berlin Heidelberg.

ZHANG, L., YANG, G., WU, L. & YU, B. 2010. The biomechanical effects of osteoporosis vertebral augmentation with cancellous bone granules or bone cement on treated and adjacent non-treated vertebral bodies: A finite element evaluation. *Clinical Biomechanics,* 25**,** 166-172.

ZYSSET, P. K. & CURNIER, A. 1995. An alternative model for anisotropic elasticity based on fabric tensors. *Mechanics of Materials,* 21**,** 243-250.

ZYSSET, P. K. & CURNIER, A. 1996. AN IMPLICIT PROJECTION ALGORITHM FOR SIMULTANEOUS FLOW OF PLASTICITY AND DAMAGE IN STANDARD GENERALIZED MATERIALS. *International Journal for Numerical Methods in Engineering,* 39**,** 3065-3082.

ZYSSET, P. K., GOULET, R. W. & HOLLISTER, S. J. 1998. A Global Relationship Between Trabecular Bone Morphology and Homogenized Elastic Properties. *Journal of Biomechanical Engineering,* 120**,** 640-646.